2021

Interaction of lignin derivatives with polymers, ions and soft surfaces in aqueous systems

Kazzaz, Armin Eraghi

INTERACTION OF LIGNIN DERIVATIVES WITH POLYMERS, IONS AND SOFT SURFACES IN AQUEOUS SYSTEMS

A Thesis Submitted to the
Faculty of Graduate Studies of
Lakehead University

by

Armin Eraghi Kazzaz

Submitted in partial fulfillment of requirements for the degree of

Doctor of Philosophy in Biotechnology

January 2021

Dedication

To my parents and wife for all their support, encouragement and unwavering love

Abstract

Lignin is one of the most abundant biopolymers on earth which has recently gained considerable attention due to its unique potentials to be used in many applications. Many efforts have been made in improving the compatibility and reactivity of lignin for different applications. Although different methods have been suggested to ameliorate lignin properties, there has been a continuous demand for finding effective and new ways of revealing the beneficial uses of this polymer. To address the lack of fundamental understanding of lignin modification pathways in generating lignin-based products, the chemical reactions conducted via grafting functional groups of lignin has been comprehensively reviewed in this thesis. Also, the recent progress on lignin reactions as well as advantages and disadvantage, challenges associated with the product development process, and the reaction procedures have been discussed comprehensively in this work. Also, from the commercial point of view, products such as vanillin and phenol have been commercially available since 1933 and 2015, respectively, with equal or lower prices to their fossil-based counterparts. Lignin-based carbon fiber is also estimated to be produced commercially in 2020-2025. Overall, by reviewing different reactions performed on lignin in this chapter and revealing the possible ones that could be implemented, lignin-based polymers with improved properties could be generated to pave the way to even more commercial products from lignin.

To elucidate the role of the surface chemistry and structure of lignin on its adsorption, the adsorption mechanism of lignin-based sulfonated polymer (lignin-3-sulfopropyl methacrylate (L-S)) was studied on OH, COOH, CH_3, and NH_2 functionalized self-assembled monolayers under different pH, temperature, and salinity and its adsorption mechanism was compared with that of a synthetic-based sulfonated polymer (poly(vinyl alcohol-co-vinyl acetate)-3-sulfopropyl methacrylate (PVA-S)). The information was generated using advanced equipment, such as Quartz crystal microbalance with dissipation (QCM-D), static and dynamic light scattering, and X-ray photoelectron spectroscopy (XPS), which facilitated the correlation between deposition performance and properties of polymers on the functional surfaces. The lower adsorption of lignin-based polymer (L-S) than synthetic-based polymer (PVA-S) was observed onto COOH and OH functionalized surfaces due to its less solubility and limited hydrogen bonding development of L-S than PVA-S. Variations in the temperature, pH, and salt significantly affected the adsorption mechanism of the macromolecules. Through the experimental analyses performed in this chapter by comparing the two bio-based and synthetic polymers, it was obtained that the inherent steric

hindrance of lignin may need to be reduced through chemical modifications such as oxidation and/or depolymerization, to improve its adsorption onto surfaces. Also, since lignin has a folded and compact molecular structure most of its functional groups were not exposed to interact and need to be activated. Overall, by exploring the limitations of lignin in developing different interaction mechanisms compared to a synthetic polymer, certain strategies e.g. chemical modifications could be taken and performed to improve different properties in lignin for desired applications.

In addition, an amphoteric lignin-based polymer was produced in a semi-dry method by polymerizing lignin with sulfonate-containing monomers and grafting lignin with quaternary ammonium groups. By extensively analyzing the effects of modification order and carbon chain length of the grafting reagent through different analytical tools, such as ^{1}H and [2]D ^{1}H COSY NMR, it was found that the reaction order is very critical since the first reaction had more degree of substitution of the functional group than the second one, which would be due to less number of available active sites being remained on lignin for the second reaction. Also, lengthening the carbon chain of the three methylamine lowered the steric hindrance around the carbon atom bearing the leaving group and thus enhanced the reaction yield. The adhesion force and wettability analyses were conducted to understand the behavior of amphoteric lignin and the results were compared with those of cationic or anionic modified lignin with similar molecular weights and charge densities. In oil, amphoteric lignin was wetted well by water, while both cationic and anionic lignin polymers indicated a poor water wettability. In water, the anionic and amphoteric lignin polymers strongly repelled oil droplets. Overall, it was proved that the wetting behavior of the polymer in oil/water mixture depends extensively on the phases and functional groups and thus, amphoteric lignin-based polymer with specific characteristics could be designed experimentally for various oil and water applications.

In a subsequent study, the crosslinked bi-fictionized lignin-based polymer was produced by grafting carboxymethyl and tertiary amine groups onto the lignin backbone. The produced lignin-based polymer was used in evaluating its ability to adsorb both divalent and monovalent salts from saline water. Moreover, it has been found that by increasing the temperature to 75 °C, the produced bi-functional lignin-based polymer released the adsorbed salt into the water due to protonation and deprotonation of carboxy and amine groups, respectively. By using this thermoresponsive behavior of produced polymer, the reusability of this polymer was tested for 15 rounds of adsorption and

desorption. It was observed that the produced lignin-based polymer maintained 70-80 % of its adsorption capacity when reused 15 times. Based on the results, the produced lignin-based polymer was found to have the extra affinity for adsorbing salts from solutions.

Furthermore, the interaction of sulfonated lignin with similar charge densities but different molecular weights with aluminum oxide particles in a colloidal suspension was analyzed. The mechanism and performance of produced flocculants were evaluated under static and dynamic conditions by using techniques, such as zeta potential analysis, focused beam reflectance measurement (FBRM), and vertical scan analyzer. Based on the results, it was found that the higher the molecular weight, the better the lignin-based flocculant since the sulfonated lignin with the highest molecular weight could generate flocs with the most enlarged chord length. The contribution of patching and charge neutralization mechanisms were observed to significantly affect this polymer's performance in flocculating aluminum oxide particles.

The results obtained in this thesis contribute to the knowledge of the chemical modification of lignin and its interaction with salt, solid, and liquid phases. Also, new insights were provided about the applications for lignin-derived polymers in oil-water emulsion systems.

Acknowledgments

Table of Contents

List of Figures:

List of Tables:

Introduction

Polymers and their related products are involved in every aspect of our lives. In the past decade, the rapid progress in the technology and manufacturing has increased attention and efforts in developing polymers for various applications, such as water treatments (i.e., saline/wastewater),[1,2] oil/water separation,[3,4] and polymeric films.[5,6] These efforts have been aimed to produce cost-effective and more efficient materials.

The growing concerns over the rapid petroleum resource consumption coupled with an interest to use eco-friendly materials have triggered more research towards using bio-based polymers such as lignin. Lignin is known as one of the most abundant phenolic polymers on earth with various functional groups including methoxyl, carbonyl, hydroxy, and carboxyl.[7] This polymer could be isolated by using different chemical, physical, physical-chemical, and biological pathways from lignocellulosic biomass. Generally, a vast amount of lignin is produced as a by-product of pulp and paper industries every year.[8]

Lignin has attracted attention to be valorized in various industries due to its low production cost, abundancy, and renewability.[9] Despite the interest in diminishing negative environmental impacts by replacing petroleum-based materials with bio-based ones, lignin has been considered as waste material and only burned and used as an energy source. To date, few lignin-based chemicals have been produced at industrial scales. To further pave the way for the production of lignin derivatives, its limited functional groups and poor interaction with other solid/liquid phases need to be altered extensively.

In the past, different modification pathways have been conducted on lignin, such as phosphorylation,[10] amination,[11,12] carboxyalkylation[13] and sulfomethylation,[14] which have led to the production of either anionic or cationic lignin to make valuable products. According to the lignin structure, modification reactions can occur on aromatic, aliphatic, or both parts.

Amphoteric polymers, by having both cationic and anionic groups, have been reported to have a broader range of applications than single-ionic polymers, thanks to their effectiveness in interacting with other charged materials.[15,16] An amphoteric lignin-based surfactant has been recently produced by grafting quaternary sulfonic acid and ammonium-containing groups onto enzymatically-hydrolyzed lignin.[17] In another study, a pH-responsive polymer was produced from

hydrolyzed lignin by sulfonation and quaternization, and the produced polymer was used for recycling cellulase during the enzymatic hydrolysis of lignocelluloses.[18]

Interaction mechanisms develop between the polymer and adsorbing surface include, but are not limited to, charge neutralization, hydrogen bonding, van der Waals forces, and hydrophobic interactions. Although the mechanisms behind the adsorption of various polymers on different surfaces in contrastingly charged systems have been studied, information on the adsorption in the absence of electrostatic interaction for lignin and PVA based polymers is limited. To address this, two types of branched anionic polymers of poly(vinyl alcohol-co-vinyl acetate)-3-sulfopropyl methacrylate (PVA-S) and lignin-3-sulfopropyl methacrylate (L-S) were produced. To eliminate the effect of molecular weight and charged groups in comparing lignin and PVA, the reaction conditions were controlled to produce polymers with a similar molecular weight and charge density. This will elucidate the role of the structure and surface chemistry of polymers in their adsorption.

Ion exchange polymers have many applications in such as fuel cell,[19-21] water purification,[22,23] and biomedical processing, sensors and actuators, and non-linear optics.[24] As mentioned earlier, several studies were conducted to produce either cationic or anionic polymers by chemical reactions. However, these polymers could adsorb either cationic or anionic components, and their ability to remove salt is limited. Therefore, in this thesis, a multi-charged lignin-based polymer with the capacity of adsorbing both anionic and cationic components of salts from water was proposed to address this issue.

Generally, the flocculation process in the colloid suspensions is significantly affected by the flocculant properties.[25,26] While the impact of charge density and functional groups of linear polymers has been documented in flocculation processes,[27,28] the results cannot be extended to lignin-based flocculants since lignin has a three-dimensional and more complicated structure. Produced lignin derived flocculants can have different molecular weights and charge densities. In some studies, the impact of lignin's charge density on the dispersion of kaolin particles[29] and cement particles were studied.[30] Likewise, the impact of charge density of sulfomethylated lignin on the flocculation of a cationic dye was investigated.[30] However, the impact of the molecular weight of sulfomethylated lignin on its flocculation performance is rather unclear, which is subjected to study.

Chapter one covers the synopsis of the literature pertaining to this Ph.D. thesis work. This chapter contains two primary sections. In the first part, the importance of the current work and general information on the literature related to this work were reviewed. In the second part, the methods employed in the current work were discussed.

Chapter two focuses on the fundamentals associated with the grafting modification of the aliphatic and aromatic hydroxy groups of lignin. In this chapter, the altered reaction pathways on the lignin aliphatic and aromatic parts as well as the recent progress and challenges in lignin grafting reactions were discussed. Also, the disadvantages and advantages associated with each reaction procedure and the product development process were discussed both at the laboratory and industrial scales.

Chapter three describes how the interaction of lignin derivatives, highly branched materials, is different from their synthetic linear equivalents when their molecular weights and charge densities are similar. In this chapter, the adsorbed mass of lignin-based and synthetic-based polymers were analyzed on OH, COOH, CH_3, and NH_2 functionalized surfaces by using QCM-D. This method provides information on their altered adsorption behavior. This chapter provides fundamental insights into quantitative adsorption fundamentals of lignin and synthetic macromolecules. Also, the adsorption was studied under different saline and pH conditions. The results reveal the performance of these sulfonate-based polymers on altered surfaces in different environments and the interaction mechanisms of the adsorption processes on the surfaces. Demonstrating this difference would help establish methods to improve the characteristics of lignin for creating valorized lignin derivatives with desired functionality.

Chapter four discusses the synthesis of amphoteric lignin-based biomaterials. The reactions were conducted in a semi-dry aqueous condition using amino and sulfonic groups via grafting cationic groups and polymerizing with an anionic monomer. This chapter describes the details of synthesis, characterization, and physical properties of the produced amphoteric lignin using anionic and cationic reagents. As various alternatives can be followed to conduct cationic grafting and anionic polymerization, the first aim of this research was to determine the better and more efficient synthetic route for the production of amphoteric lignin-based polymers. Furthermore, the wettability of the produced amphoteric lignin polymers at the interface of oil and water in oil-water mixtures was studied fundamentally.

Chapter five presents the synthesis of reusable crosslinked multi-functional lignin for desalination applications. The polymer has been produced by grafting anionic and cationic monomers and also modifying with crosslinked agents. The produced polymer was analyzed to separate multiple salts (NaCl, KCl, $CaCl_2$, and $MgCl_2$) that exist in saline water. Another advantage of the produced polymer is its reusability since, thanks to its specific grafted monomers, it has a thermoresponsive behavior. Thus, by increasing the temperature, salt desorbs and the polymer could be recovered and reused several times as the adsorbent.

Chapter six substantiates the effect of the molecular weight of sulfomethylated lignin on the flocculation of aluminum oxide particles in the suspension. In this chapter, the aluminum oxide suspension has been used as a model colloidal system to monitor the flocculation performance of sulfomethylated lignin having different molecular weights. The changes in the physicochemical properties of the suspension, as well as the properties of the formed flocs, were monitored and correlated.

Chapter seven states the overall conclusions from the results obtained in this thesis and provides some recommendations for future study.

Objectives

Objectives of this thesis are to:

- Review the current grafting modifications performed on lignin and reveal possible new modifications/applications.
- Reveal and compare the amount and the price of the currently commercially-generated lignin around the world as well as the current and future commercial lignin-based products.
- Produce amphoteric lignin through implementing both cationic and anionic modifications by grafting and polymerization of the softwood kraft lignin.
- Reveal the effect of the carbon chain length of a reagent containing three methylamine on the grafting yield and degree of substitution.
- Reveal the effect of the carbon chain length of the functional group induced to lignin on its hydrophilicity/oleophilicity at the oil/water interface.
- Analyze whether the order of the anionic or cationic modifications affects the properties of the produced amphoteric lignin polymer.

- Introduce a new bio-based and multi-functional polyelectrolyte to be used in a wide range of applications such as oil/water separations and lignin-to-biofuels processing applications.

- Produce an amphoteric polymer under a semi-dry condition, appealing from the industrial perspective.

- Study and compare the interaction mechanisms developed by synthetic and lignin-based sulfonated polymers with hydrophobic, hydrophilic, and charged self-assembled monolayers.

- Reveal the effect of polymer structure (highly branched or linear) and properties on its adsorption onto different functionalized-surfaces.

- Synthesize and characterize crosslinked-multi charged lignin for desalination applications.

- Analyze the reusability of the produced crosslinked-multi charged lignin as a monovalent and divalent salt adsorbent.

- Investigate the effect of the molecular weight of the produced sulfomethylated lignin on the flocculation of aluminum oxide particles.

References

1) Abdelhamid, A. E., & Khalil, A. M. (2019). Polymeric membranes based on cellulose acetate loaded with candle soot nanoparticles for water desalination. *Journal of Macromolecular Science, Part A*, *56*(2), 153-161.

2) Li, M., Zhu, X., Yang, H., Xie, X., Zhu, Y., Xu, G., ... & Li, A. (2020). Treatment of potato starch wastewater by dual natural flocculants of chitosan and poly-glutamic acid. *Journal of Cleaner Production*, 121641.

3) Noor, M. H. M., Ngadi, N., Inuwa, I. M., Opotu, L. A., & Nawawi, M. G. M. (2020). Synthesis and Application of Polyacrylamide Grafted Magnetic Cellulose Flocculant for Palm Oil Wastewater Treatment. *Journal of Environmental Chemical Engineering*, 104014.

4) Guan, Y., Cheng, F., & Pan, Z. (2019). Superwetting polymeric three dimensional (3d) porous materials for oil/water separation: A review. *Polymers*, *11*(5), 806.

5) Umoren, S. A., & Solomon, M. M. (2019). Protective polymeric films for industrial substrates: A critical review on past and recent applications with conducting polymers and polymer composites/nanocomposites. *Progress in Materials Science*, *104*, 380-450.

6) Ito, M. M., Gibbons, A. H., Qin, D., Yamamoto, D., Jiang, H., Yamaguchi, D., & Sivaniah, E. (2019). Structural colour using organized microfibrillation in glassy polymer films. *Nature*, *570*(7761), 363-367.

7) Gosselink, R. J. A., Snijder, M. H. B., Kranenbarg, A., Keijsers, E. R. P., De Jong, E., & Stigsson, L. L. (2004). Characterisation and application of NovaFiber lignin. *Industrial Crops and Products*, *20*(2), 191-203.

8) Kazzaz, A. E., & Fatehi, P. (2020). Technical lignin and its potential modification routes: A mini-review. *Industrial Crops and Products*, *154*, 112732.

9) S.H. Ghaffar and M. Fan, Biomass bioenergy, 2013, 57, 264-279.

10) A.M. Nada, N.F. Kassem and S.H. Mohamed, BioRes., 2008, 3, 538-548.

11) X. Liu, H. Zhu, C. Qin, J. Zhou, J.R. Zhao and S. Wang, BioRes., 2013, 8, 2257-2269.

12) J. Tian, S. Ren, G. Fang, Y. Ma and Q. Ai, BioRes., 2014, 9, 6290-6303.

13) L.H. Gan, M.S. Zhou and X.Q. Qiu, Adv. Mater. Res., 2012, 550, 1293-1298.

14) A.E. Kazzaz, Z.H. Feizi and P. Fatehi, Colloid Polym. Sci., 2018, 296, 1867-1878.

15) H. Kono and R. Kusumoto, React. Funct. Polym., 2014, 82, 111-119.

16) C. Dong, W. Chen and C. Liu, Bioresour. Technol., 2014, 170, 239-247.

17) C. Cai, Y. Bao, X. Zhan, X. Lin, H. Lou, Y. Pang, Y. Qian and X. Qiu, Green Chem., 2019, 21, 1141-1151.

18) C. Cai, X. Zhan, H. Lou, Q. Li, Y. Pang, Y. Qian, H. Zhou and X. Qiu, ACS Sustainable Chem. Eng., 2018, 6, 10679-10686.

19) Agel, E., Bouet, J., & Fauvarque, J. F. (2001). Characterization and use of anionic membranes for alkaline fuel cells. *Journal of Power Sources*, *101*(2), 267-274.

20) Kreuer, K. D., Paddison, S. J., Spohr, E., & Schuster, M. (2004). Transport in proton conductors for fuel-cell applications: simulations, elementary reactions, and phenomenology. *Chemical reviews*, *104*(10), 4637-4678.

21) Jagur-Grodzinski, J. (2007). Polymeric materials for fuel cells: concise review of recent studies. *Polymers for Advanced Technologies*, *18*(10), 785-799.

22) Afonso, M. D., & de Pinho, M. N. (2000). Transport of MgSO4, MgCl2, and Na2SO4 across an amphoteric nanofiltration membrane. Journal of membrane science, 179(1-2), 137-154.

23) Jyothi, M. S., Nayak, V., Padaki, M., Balakrishna, R. G., & Soontarapa, K. (2016). Aminated polysulfone/TiO2 composite membranes for an effective removal of Cr (VI). Chemical Engineering Journal, 283, 1494-1505.

24) Xuan, F., & Liu, J. (2009). Preparation, characterization and application of zwitterionic polymers and membranes: current developments and perspective. Polymer International, 58(12), 1350-1361.

25) Y. I. Chang and K. H. Liu, Colloid Polym, Sci., 2010, 288, 223–231.

26) D. J. Walsh and J. Anderson, Colloid Polym. Sci., 1980, 258, 883–890.

27) W. He, Y. Zhang and P. Fatehi, Colloids Surf. A Physicochem. Eng. Asp., 2016, 503, 19–27.

28) S. Wang, M. K. Konduri, Q. Hou and P. Fatehi, RSC Adv. 2016, 6, 40258–40269.

29) M. K. Konduri and P. Fatehi, Colloids Surf. A Physicochem. Eng. Asp., 2018, 538, 639–650.

30) W. He and P. Fatehi, RSC Adv., 2015, 5, 47031–47039.

Chapter 1. Background and literature review

1.1 Lignocellulosic biomass

Lignocellulosic biomass is the most abundant organic, renewable carbon source on the earth constituting more than 90 % of all plant biomass.[1,2] Lignocellulosic biomass consists of three major components: i.e., lignin (15–30%), cellulose (40–60%), and hemicellulose (10–40%) (Fig. 1.1).[3] Carbohydrate polymers of cellulose and hemicellulose are known as polysaccharides, which are composed of D-Glucose that is linearly connected through β-1,4-glycosidic, and C_5 and C_6 sugars, respectively.[4] Hemicellulose consists of different sugars, e.g., galactose, glucose, and arabinose. The major component of hemicellulose in softwood is mannose, whereas herbaceous plants and hardwood are made mainly of xylose.[1]

The main components in lignocellulosic biomass (lignin, cellulose, and hemicellulose) are associated with each other through chemical and physical interactions. The core of the lignocellulosic matrix is cellulose which is packed into semi-crystalline microfibres.[5] The major interactions between and within cellulose microfibers are van der Waals and hydrogen bonding. The spaces between cellulose fibers are filled with lignin and hemicellulose that act as resin to hold the lignocellulosic matrix together. Lignin properties and its role are discussed more comprehensively in the next section.
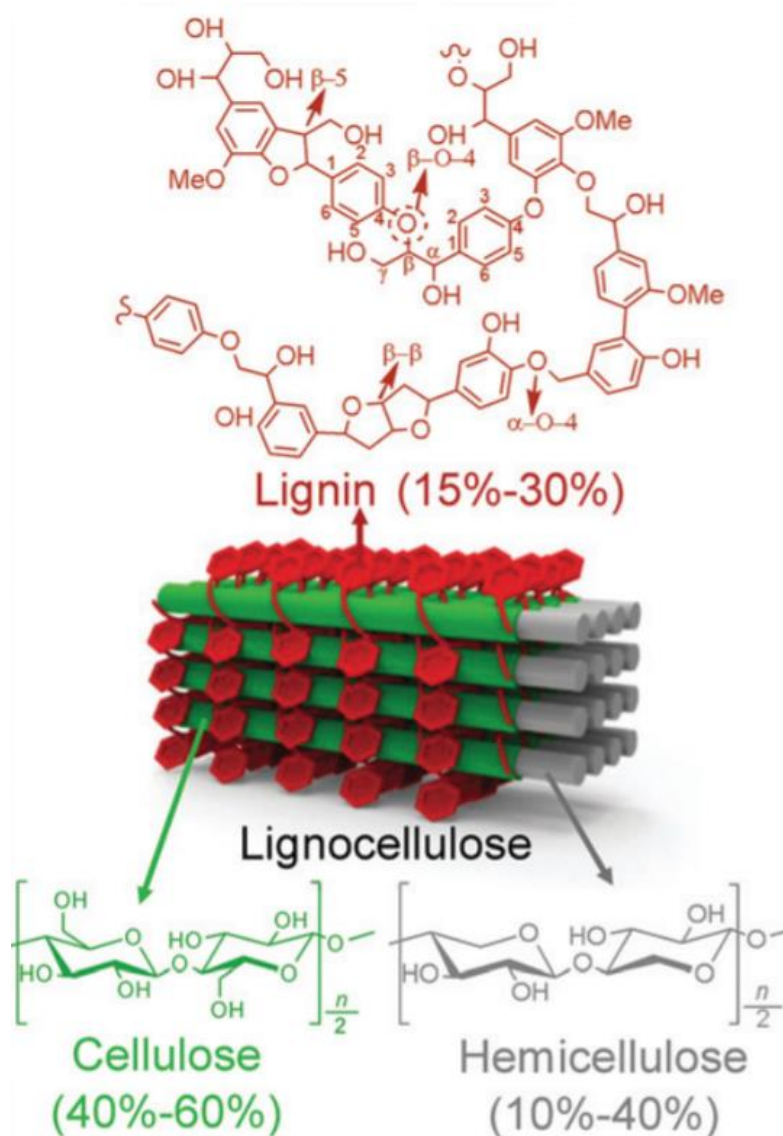
Fig. 1.1. Chemical structure of the main components of lignocellulosic biomass.[1]

1.2 Lignin

In 1819, Augustin Pyramus de Candolle, a Swiss botanist, observed an insoluble fraction of wood after acid treatment, which was mentioned as *'la lignine'* in French derived from the Latin word '*Lignum*' meaning lignin, which the term 'lignin' derived from.[6,7]

Lignin is the key unit of the vascular system in plants. Lignin imparts rigidity and strength to plants and prevents the accessibility of cellulose to microorganisms and enzymes. Lignin and hemicellulose are bound to cellulose fibers by hydrogen bonding, whereas lignin is bound to hemicellulose covalently.[1]

1.2.1 Structure

Based on the current knowledge, lignin is a complex, 3-D cross-linked structure and a recalcitrant aromatic macromolecule. The biosynthesis of lignin polymer is conducted by radical polymerization of phenyl-propanoid building blocks of sinapyl, *p*-coumaryl and coniferyl alcohols. The monomers are linked together by recalcitrant C-C (e.g., β-5 and 5-5´) bonds and labile C-O (β-O-4 and α-O-4) bonds and form the complex lignin structure.[8,9] The β-O-4 is the most dominant linkage in lignin, which in natural lignocellulosic biomass varies from 43% to 65 %. The abundance of β-O-4 bonds may increase to 89% for lignin obtained from plants with bioengineering.[10]

1.2.2 Extraction

Lignin can be isolated from lignocellulosic materials via physical, chemical, biological, physicochemical pretreatment, as presented in Figure 1.2. In the chemical pretreatment, the structure of lignocellulosic materials is disrupted by inorganic or organic substrates and interacts with intra and interpolymer bonds of hemicellulose, cellulose, and lignin. Physical pretreatments includes increases in pressure or temperature which ease biomass destruction. Meanwhile, the combination of physical and chemical pretreatments has the advantage of an increase in the digestibility of biomass. In the biological process, microorganisms and milder conditions are used which makes this procedure one of the most environmentally-friendly processes for biomass degradation. Based on these pretreatment methods, different commercial lignin has been produced, including kraft, lignosulfonate, soda, hydrolyzed lignin, and organosolv. Kraft lignin is the most dominant technology used in pulping industries; thus, kraft lignin has been chosen as the source used in this thesis.[12,13]
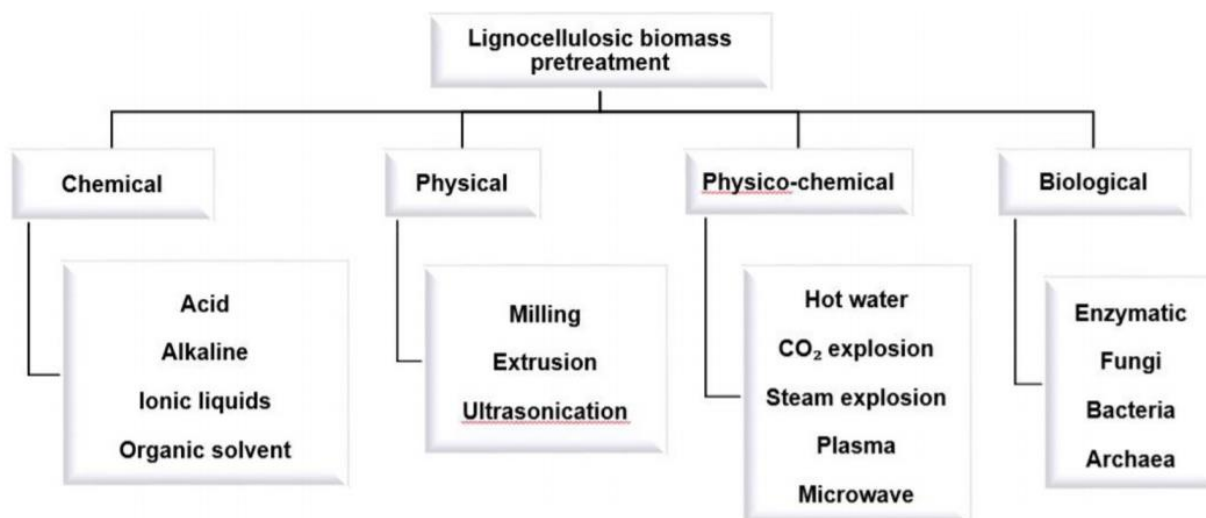
Fig. 1.2 Different pathways to separate lignin from lignocellulosic biomass.[13]

1.3 Research gaps

Modifications are conducted on lignin to improve lignin reactivity and compatibility with other materials for widening its application. Considering the structure of lignin, different modifications can take place on the aromatic and/or aliphatic parts of lignin. While there are review papers available on lignin polymerization,[14] catalytic reactions,[15] depolymerization,[16,17] redox-neutral strategies,[16] and photoredox catalysis,[18] no comprehensive review study has been performed to date to extensively and carefully reveal the fundamentals associated with grafting reactions of lignin. The lack of a comprehensive study on the mentioned topic would further lead to limited scrutiny on the critical industrial applications for lignin. Differentiating the reaction routes that occur on lignin aromatic and aliphatic parts would beget the identification of a suitable pathway to generate value-added lignin-based products with favorable properties for different applications. This comprehensive study is included in this thesis as the second chapter.

Polymers develop different adsorption mechanisms when interacting with different surfaces. These interactions mostly include charge neutralization, hydrogen bonding, and van der Waals forces. While adsorption mechanisms of linear polymers with different oppositely charged surfaces have been studied,[19,20] information on the developed mechanisms by lignin is still limited. Raised from its three-dimensional structure, lignin depicts a distinct interaction behavior in comparison with linear polymers. However, due to the complicated structure of lignin, the interaction mechanisms of lignin derivatives with various functionalized surfaces are still unclear and yet to be discovered.

Identifying such interaction mechanisms could significantly impact its end-used industrial applications. Thus, two anionic polymers of poly(vinyl alcohol-covinyl acetate)-3-sulfopropyl methacrylate (PVA-S) and lignin-3- sulfopropyl methacrylate (L-S), with similar molecular weights and charge densities were generated. The interaction and adsorption of these two polymers were then studied and compared on differently functionalized self-assembled monolayers, which is revealed in the third chapter of this thesis.

The oil/water interface is crucial to be discussed and controlled in different applications, e.g., oil/water separation.[21] When polyelectrolytes interact with hydrophilic/hydrophobic materials, they reconfigure the ionic groups present on their surface which would beget a change in wettability/hydrophilicity of polymers.[22] It is critical to widen the knowledge of oil/water wetting features of newly generated bio-based polymers to pave the way for designing sustainable high performance materials. In the past, there have been efforts on analyzing the performance of single-charged (anionic or cationic) polymers in the improvement of electrostatically induced hydration with a water molecule in oil/water interface,[23] while limited studies have been carried out to investigate the behavior of dual-charged bio-based polymers in the oil/water interface. To address the research gap, the hydration performance of an amphoteric lignin polymer was analyzed at different interfaces to not only shed light on the behavior of the produced lignin-based polymer at the oil/water interface but also to broaden the potential applications of value-added lignin-based polymers in different fields.

Water purification has been a worldwide challenge for decades, as it directly influences the environment and human health. Desalination is required to generate drinkable seawater or produce appropriate water for agriculture to meet the growing demand for usable water. While conventional desalination methods, e.g., evaporation, are applicable, they suffer from costly infrastructure and expensive operational routes.[24,25] Water desalination through microorganism treatments might also be unsuitable due to the generation of secondary pollutions as well as low effectiveness.[26] To address this issue, modified polymers have been used. While some studies have focused on using single-charged polymers for water desalination,[27] the capacity of these generated polymers are limited since they only can adsorb the anionic or cationic component of salts. Also, the high water-solubility of the produced single-charged polymers make their filtration and separation a major challenge. To address this gap, a bio-based insoluble amphoteric polymer was produced and its performance in desalinating water has been studied in the fifth chapter for the first time.

Polymer properties, e.g. charge density and molecular weight can remarkably affect their performance in flocculating particles in colloidal suspensions.[28, 29] While there have been studies on the effect of functional groups and charge density of linear polymers on the flocculation,[30] it is impossible to extend these results to lignin-based flocculants, since lignin has a three-dimensional and more complicated structure. In the literature, some studies have covered the effect of charge density variations on the flocculation/dispersion performance of lignin-based polymers. In one study, the effect of lignin's charge density was analyzed on the dispersion of kaolin particles,[31] while in other studies the influence of the charge density of the sulfomethylated lignin has been investigated on the dispersion of cement particles[32] and the flocculation of cationic dyes.[33] Nevertheless, the influence of the molecular weight of the sulfomethylated lignin has not been covered on its flocculation performance, which is extensively studied and revealed in the sixth chapter of this thesis.

1.4 Modification of lignin

When lignin is used directly for synthesizing other chemicals, the polymeric nature of lignin presents technical limitations, which have enhanced the need for chemical modification. In order to improve lignin's features and properties, different modifications have been conducted in this study.

1.4.1 Methylation

Methylation reaction has been carried out by introducing methyl groups ($-CH_3$) to lignin through nucleophilic aromatic substitution. The methylation reaction had been used to cover phenolic hydroxy groups to study whether the desired reaction occurs on the aliphatic or phenolic hydroxy groups of lignin. By conducting selective lignin methylation, the phenolic hydroxy groups were converted to phenyl methyl ethers, which were less reactive compared to hydroxy groups.[13]

1.4.2 Amination

The amination of lignin introduces amine groups on to lignin through the S_N2 reaction route. Generally, this reaction has been conducted to introduce a cationic charge to lignin. By conducting the amination reaction, the water solubility, molecular weight, and surface activity of lignin increases.

1.4.3 Carboxymethylation

The carboxymethylation reaction of lignin has been conducted by introducing carboxymethyl groups ($-C_2H_3O_2$). The reaction proceeds through the S_N2 mechanism. The carboxymethylation reaction of lignin would occur mostly on its aromatic ring since aromatic hydroxy groups ionize easier than aliphatic hydroxy groups in an alkaline environment. In this thesis, the carboxymethylation of lignin was conducted in order to render lignin negatively charged.

1.4.4 Crosslinking

The crosslinking reaction has been conducted on lignin by using Poly(ethylene glycol) diglycidyl ether under alkaline condition. This reaction was performed to increase the lignin molecular weight by crosslinking different modified lignin polymers to each other.

1.4.5 Sulfomethylation

Negatively charged lignin polymers were produced by introducing sulfonate groups on lignin. This reaction occurs mainly on the *ortho* position of the aromatic ring of lignin. This reaction is conducted by undergoing the S_N2 reaction route.

1.5 Properties and applications of modified lignin

1.5.1 Interaction of modified lignin with Oil/water interface

Oil/water interface has become an important topic of research for different applications such as drug delivery, programmable genes,[34] oil-water separation,[21] and oil-sand.[35] In order to design polymers with better compatibility and performance, the wetting properties of newly fabricated polymers with water and oil need to be widened fundamentally. In chapter three, amphoteric lignin-based polymer was produced and its oil/water interfacial properties were analyzed in different water and oil phases.

1.5.2 Interaction of modified lignin with self-assembled monolayers

In chapter four, the interaction of the modified lignin and a synthetic-based polymer was compared by using self-assembled monolayers (SAMs) having different surface chemistry. The SAM surfaces have been used previously to study the adsorption of polymers such as proteins.[36] Also, different SAMs with various combinations of moieties are used to clarify the contribution of different driving forces for different polymers. In our work, SAMs having different hydrophilicity/hydrophobicity and different signs of charge were used to study the adsorption

mechanisms developed under different conditions of pH and salt by lignin and its synthetic counterpart under different salt and pHs.

1.5.3 Modified lignin as a salt adsorbent

Increasing the high demand for agriculture or drinkable water boosts demand for new technology to use even the seawater to address this issue. In the past, different modifications have been conducted on natural-based polymers and used as adsorbents; however, these studies had focused on modifying polymers either with cationic or anionic groups. This limits the ability of the produced polymer to adsorb and separate both anionic and cationic components (such as salt) from water. In chapter five, cross-linked bi-functional lignin has been produced and used to separate mono and divalent salts from water, while its reusability as an adsorbent has also been analyzed.

1.5.4 Modified lignin as a flocculant for aluminum oxide suspension

The aluminum oxide is used in different industries such as ceramic and mineral processes and has been known for its high thermal stability, surface area, low solubility, and mechanical strength.[37,38] The wastewater produced from these industries contains aluminum oxide which requires treatments. In chapter six, modified lignin samples having the same charge density but different molecular weight were produced and used as flocculants for aluminum oxide suspensions. A fundamental study was also performed on the effect of the lignin-based flocculant molecular weight on the flocculation of particles. The changes in the physicochemical properties of the formed flocs were also studied fundamentally.

1.6 Methodology

1.6.1 Nuclear magnetic resonance spectroscopy (NMR)

The chemical structure of modified and unmodified lignin polymers was elucidated by using nuclear magnetic resonance spectroscopy (NMR).[39] This method relies on the phenomenon that the atomic nuclei of various functional groups resonate differently under a magnetic field and when irradiated with radio waves they are excited. These excited nuclei absorb some energy and subsequently release energy as the nuclei relax back to their original states. The released energy can be scanned and expressed as chemical shifts. These chemical shifts could be considered as fingerprints of chemical structures. The nuclei relaxation time is influenced by the surrounding chemical groups and happens differently based on the type of chemical groups.[40]

1.6.2 Elemental analyzer

An elemental analyzer is a technique used to determine the carbon, sulfur, hydrogen, and nitrogen compositions of polymers.[42] This analysis is conducted under a high-temperature combustion (at 1000 °C) in an oxygen-rich environment and is based on the classical Pregl-Dumas method. The principle includes combustion in a furnace, where, hydrogen is converted to water, carbon to dioxide, sulfur to sulfur dioxide, and nitrogen to nitrogen gas. The reduced combustion gases are analyzed for hydrogen, carbon, nitrogen, and oxygen contents.[43] In this study, the elemental compositions of modified and modified samples were analyzed by the elemental analyzer.

1.6.3 Dynamic light scattering

Dynamic light scattering (DLS) has been conducted in this study to measure the hydrodynamic size of the polymers.[19] The principle of this technique is based on the Brownian movement of particles suspended in a liquid and the speed at which the particles diffuse due to their Brownian motion is measured by recording the rate at which the intensity of the scattered light fluctuates. Bigger particles cause the intensity to fluctuate more slowly than small ones. The time-dependent scattering intensity fluctuations have been measured to determine the translational diffusion coefficient (D), and subsequently the hydrodynamic size of polymers using Stokes-Einstein equation (1.1):[44]

$$R_\text{h} = \frac{KT}{6\pi\eta D} \qquad (1.1)$$

where R_h is the hydrodynamic size (nm), K is Boltzmann constant, T is the temperature (°C), η is solvent viscosity (Pa.s) and D is the diffusion coefficient.

1.6.4 Wettability analysis

The optical tensiometer has been used to determine the wettability of polymers by measuring the contact angle of water or oil droplet on the surface coated with a polymer. In this method, when a liquid droplet is placed on a solid surface, the droplet adheres to the solid surface at an angle formed by the intersection of solid-liquid interface and liquid-vapor interface (Fig. 1.3).

| $\theta = 0°$ complete wetting (spreading) | $\theta < 90°$ good wetting | $\theta = 90°$ wetting | $\theta > 90°$ bad wetting | $\theta = 180°$ no wetting |
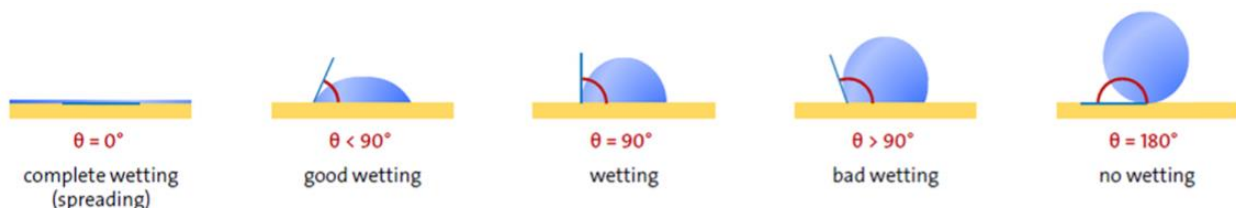
Fig. 1.3 Indicates the different contact angles formed by sessile liquid drops on a solid surface.[45]

1.6.5 Scanning electron microscopy (SEM)

Scanning electron microscopy (SEM) coupled with energy-dispersive X-ray spectroscopy (EDX) has been used to study the morphology of the flocs and produced polymers. In this thesis research, dried samples were coated with gold or carbon under vacuum and analyzed using SEM-EDX technique. In EDX analysis, the specimen (particles) is bombarded with an electron beam. The bombarded electron beam collides with the electrons of the specimen's atoms and knocks out the electrons from the inner shell of atoms to the outer shell. In this process, the void generated in the lower shell is engaged with a higher-energy electron from an outer shell of a specimen atom by releasing energy in the form of X-rays. The atom of every element releases X-rays with unique amounts of energy. Therefore, by measuring the amounts of energy released present in the X-rays during electron beam bombardment, the identity of the sample can be defined.[41]

1.6.6 Zeta potential analysis

The electrokinetic potential of particles in suspension has been measured in this study by using the zeta potential analyzer. In this technique, an applied electric field has been applied across as electrolyte solution. The charged particles suspended in the electrolyte are attracted to the oppositely charged electrode, while viscous force acting on the particles tends to oppose this movement. The particle moves with constant velocity after equilibrium is reached between these opposing forces. The velocity of the particle is called electrophoretic mobility, and based on the Smoluchowski equation (1.2), the zeta potential of particles can be measured.

$$M = \frac{2\varepsilon ZC}{3\eta} \qquad (1.2)$$

where M is electrophoretic mobility (m/s), ε is dielectric constant, Z is zeta potential (mV), C is Smoluchowski constant and η is viscosity of suspension (mPa.s).

1.6.7 Quartz crystal microbalance with dissipation (QCM-D)

Quartz crystal microbalance with dissipation (QCM-D) was used in this study to evaluate the adsorption of produced polymers. The QCM-D is operated by an electric field that induces a standing shear wave to the sensor which resonates between 5 and 20 MHz.[46] Moreover, the sensor is driven at odd integer resonance overtones which leads to measurements that are sensitive to regions at and above the surface of the sensor. Adsorption of substrate yields a decrease in the frequency and an enhancement in the oscillation period (Figure 1.4).[47]
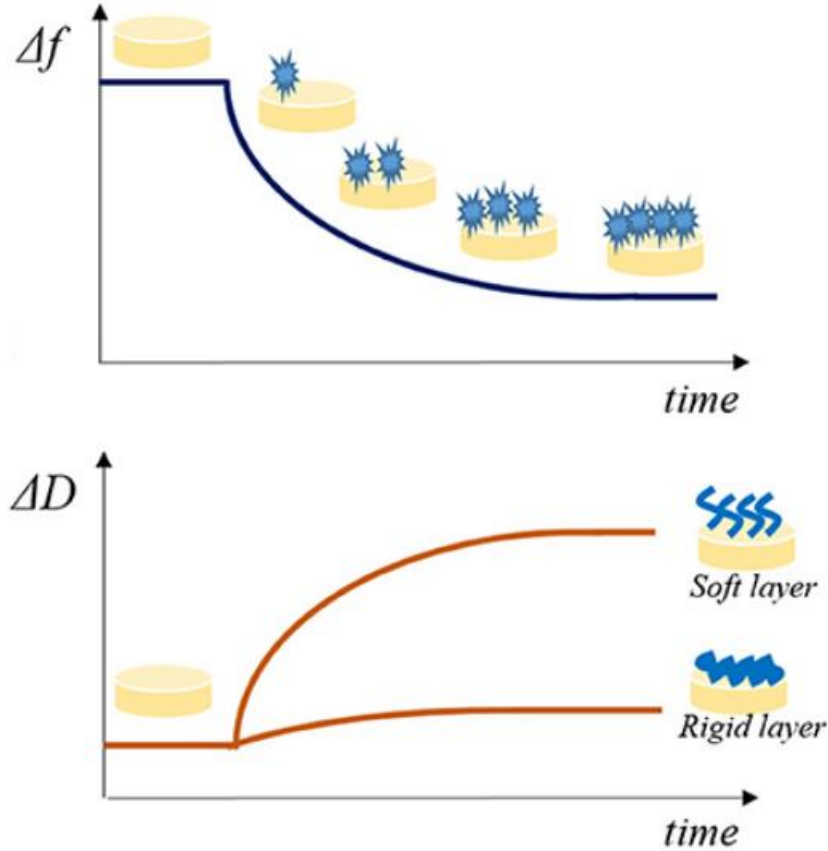
Fig. 1.4 Schematic illustration of QCM-D plots indicating frequency (Δf) and dissipation energy (ΔD) versus time.[48]

The frequency shift magnitude is used to calculate the mass of adsorbed substrate using the Voigt or Sauerbrey viscoelastic models.[49] In the Sauerbrey model, it is assumed the adsorbed mass behave elastically and calculate through equation 1.3:

$$\frac{\Delta f}{n} = \frac{-2\Gamma_s f^2}{A\sqrt{(\mu\rho_q)}} = -C\Gamma_s \qquad (1.3)$$

which Δf is the changes in the frequency, f is the crystal frequency, Γ_s the mass change, n is the overtone number (1, 3, 5, 7, 9, 11, and 13), A is the electrode area, ρ_q is the quartz's density, and μ is the shear modulus. Since constants A, f, ρ_q, and μ are instrument-specific, they all typically reduce to the constant C which is referred to as the sensor mass sensitivity constant value (17.7 ng/ Hz $\times$cm^2) for a 5 MHz quartz crystal sensor.[46]

The changes in the dissipation (D) or energy loss per oscillation is evaluated by the QCM-D instrument using equation 1.4:

$$D = \frac{E_L}{2\pi E_S} \qquad (1.4)$$

18

Where E_L is the energy that is lost over an oscillation cycle and E_S is the total energy that is stored in the sensor. The time scale of the decay reveals the viscoelasticity or rigidity of the adsorbed layer.

1.7 References

1) X. Wu, N. Luo, S. Xie, H. Zhang, Q. Zhang, F. Wang and Y. Wang, Chemical Society Reviews, 2020.

2) S. S. Wong, R. Shu, J. Zhang, H. Liu and N. Yan, Chem. Soc. Rev., 2020, 49, 5510-5560.

3) W. Schutyser, T. Renders, S. Van den Bosch, S. F. Koelewijn, G. T. Beckham and B. F. Sels, Chem. Soc. Rev., 2018, 47, 852–908.

4) D. Klemm, B. Heublein, H. P. Fink and A. Bohn, Angew. Chem., Int. Ed., 2005, 44, 3358–3393.

5) V. B. Agbor, N. Cicek, R. Sparling, A. Berlin and D. B. Levin, Biotechnol. Adv., 2011, 29, 675–685.

6) E. Sjostrom, in Wood Chemistry (Second Edition), ed. E. Sjö̈strö̈m, Academic Press, San Diego, 1993, pp. 71–89, DOI: 10.1016/B978-0-08-092589-9.50008-5.

7) P. M. Visakh, A. P. Mathew and S. Thomas, in Advances in Natural Polymers: Composites and Nanocomposites, ed. S. Thomas, P. M. Visakh and A. P. Mathew, Springer Berlin Heidelberg, Berlin, Heidelberg, 2013, pp. 1–20, DOI: 10.1007/978-3-642-20940-6_1.

8) A. Alber and J. Ehlting, in Advances in Botanical Research, ed. L. Jouanin and C. Lapierre, Academic Press, 2012, vol. 61, pp. 113–143

9) S. Shankar, S. Singh, Shikha, A. Mishra and S. Ram, in Mycodegradation of Lignocelluloses, ed. R. Naraian, Springer International Publishing, Cham, 2019, pp. 119–135, DOI: 10.1007/978-3-030-23834-6_7.

10) L. Shuai, M. T. Amiri, Y. M. Questell-Santiago, F. He´roguel, Y. Li, H. Kim, R. Meilan, C. Chapple, J. Ralph and J. S. Luterbacher, Science, 2016, 354, 329–333.

11) A. E. Kazzaz and P. Fatehi, Ind. Cro.Pro., 2020,154, 112732.

12) D. B. Meneses, G. M. Oca-Vásquez, J. R. Vega-Baudrit, M. Rojas-Álvarez, J. Corrales-Castillo and L. C. Murillo-Araya, Biomass Convers. Biorefin., 2020, 1-18.

13) A. E. Kazzaz, Z. H. Feizi and P. Fatehi, Green Chem., 2019, 21(21), 5714-5752.

14) B. M. Upton and A. M. Kasko, Chem. Rev., 2015, 116, 2275–2306.

15) Z. Sun, B. Fridrich, A. de Santi, A. Elangovan and K. Barta, Chem. Rev., 2018, 118, 614–678.

16) R. Rinaldi, R. Jastrzebski, M. T. Clough, J. Ralph, M. Kennema, P. C. Bruijnincx and B. M. Weckhuysen, Angew. Chem., Int. Ed., 2016, 55, 8164–8215.

17) V. M. Roberts, V. Stein, T. Reiner, A. Lemonidou, X. Li and J. A. Lercher, Chem. – Eur. J., 2011, 17, 5939–5948.

18) J. Zhang, ChemSusChem, 2018, 11, 3071–3080.

19) A. E. Kazzaz, Z. H. Feizi, F. Kong and P. Fatehi, Colloids Surf. A, 2018, 556, 218-226.

20) A. V. Dobrynin, A. Deshkovski and M. Rubinstein, Macromolecules, 2001, 34, 3421-3436.

21) L.H. Gan, M.S. Zhou, X.Q. Qiu, Adv. Mater. Res., 2012, 550, 1293–1298.

22) C. Shi, B. Yan, L. Xie, L. Zhang, J. Wang, A. Takahara and H. Zeng, Chem. Int. Ed., 2016, 55, 15017-15021.

23) I. M. Tucker, J. T. Petkov, C. Jones, J. Penfold, R. K. Thomas, S. E. Rogers and I. Grillo, Langmuir, 20212, 28, 14974-14982.

24) T. M. Missimer and R. G. Maliva, Desalination, 2018, 434, 198-215.

25) A. Nasu, U.S. Patent No. 4,956,157., 1990, Washington, DC: U.S. Patent and Trademark Office.

26) S. I. Abou-Elela, M. M. Kamel and M. E. Fawzy, Desalination, 2010, 250, 1-5.

27) G. M. Geise, B. D. Freeman and D. R. Paul, Polymer, 2010, 51, 5815-5822.

28) Y. I. Chang and K. H. Liu, Colloid Polym, Sci., 2010, 288, 223–231.

29) D. J. Walsh and J. Anderson, Colloid Polym. Sci., 1980, 258, 883–890.

30) S. Wang, M. K. Konduri, Q. Hou and P. Fatehi, RSC Adv. 2016, 6, 40258–40269.

31) M. K. Konduri and P. Fatehi, Colloids Surf. A Physicochem. Eng. Asp., 2018, 538, 639–650.

32) W. He, Y. Zhang and P. Fatehi, Colloids Surf. A Physicochem. Eng. Asp., 2016, 503, 19–27.

33) W. He and P. Fatehi, RSC Adv., 2015, 5, 47031–47039.

34) E.G. Schutt, D.H. Klein, R.M. Mattrey, J.G. Riess, Angew. Chem. Int. Ed., 2003, 42, 3218–3235.

35) A. Natarajan, J. Xie, S. Wang, Q. Liu, J. Masliyah, H. Zeng, Z. Xu, J. Phys. Chem. C., 2011, 115, 16043–16051.

36) S. Huang, Q. Hou, D. Guo, H. Yang, T. Chen, F. Liu and J. Wang, RSC adv., 2017, 7, 39530-39538.

37) M. Wisniewska, S. Chibowski and T. Urban, J Colloid Interface Sci., 2019, 334, 46–152. https://doi.org/10. 1016/j.jcis.2009.03.006

38) T. K. Sheel, P. Poddar, A. B. M. W. Murad, A. J. M. T. Neger and A. M. S. Chowdhury, J Adv Chem Eng., 2016, 6, 1000152. https://doi.org/10.4172/2090-4568. 1000152

39) M. Sarwar Jahan, Z. Liu, H. Wang, A. Saeed and Y. Ni, Cellul. Chem. Technol., 2012, 46, 261-267.

40) N. Hong, S. Zhang, C. Yi and X. Qiu, J. Dispersion Sci. Technol., 2016, 37(3), 415-422.

41) J. Huang, J. Xu, D. Wang, L. Li and X. Guo, Industrial Engineering and Chemistry Research, 2013, 52, 8427-8435.

42) Z. Li and Y. Ge,   J. Braz. Chem. Soc., 2011, 22, 1866-1871.

43) M. Thompson, CHNS elemtal analyzers. AMCTB No 29 , April 2008, http://www.rsc.org/images/CHNS-elemental-analysers-technical-brief-29_tcm18-214833.pdf.

44) M. Kaszuba, D. McKnight, M.T. Connah, F.K. McNeil-Watson and U. Nobbmann, J. Nanopart. Res., 2008, 10, 823-829.

45) M. Grüßer, D. G. Waugh, J. Lawrence, N. Langer and D. Scholz, Langmuir, 2019, 35(38), 12356-12365.

46) K. A. Marx, Biomacromolecules, 2003, 4(5), 1099-1120.

47) E. Niinivaara, M. Faustini, T. Tammelin and E. Kontturi, Langmuir, 2015, 31, 12170-12176.

48) C. Tonda-Turo, I. Carmagnola and G. Ciardelli, Frontiers in bioengineering and biotechnology, 2018, 6, 158.

49) C. Aulin, I. Varga, P. M. Claesson, L. Wågberg and T. Lindström, Langmuir, 2008, 24, 2509-2518.

Chapter 2. Grafting strategies for hydroxy groups of lignin for producing materials

Chemical Engineering Department,
Lakehead University,
955 Oliver Road,
Thunder Bay, Ontario P7B 5E1, Canada

*Corresponding author

2.1 Abstract

Lignin is one of the most abundant biopolymers on Earth and is considered as the primary resource of aromatic compounds. Recently, lignin has attracted attention from scientists and industrialists due to its inherent potential arising from its unique structure, which leads to its possible use in many applications. Many efforts have been made to ameliorate the reactivity and compatibility of lignin in different areas. Although methods have been proposed for endowing lignin with different properties, there continues to be a considerable demand for discovering new and effective ways of unraveling the beneficial uses of this aromatic polymer. Considering the structure of lignin, different grafting modifications can occur on the aliphatic and/or aromatic groups of lignin. To date, there has been a lack of fundamental understanding of the modification pathways of lignin for generating lignin-based products. In this review paper, we discuss comprehensively the chemical reactions that were introduced in the literature for preparing lignin with different features via modifying its phenolic and aliphatic hydroxy groups for altered uses. This review paper critically and comprehensively elaborates on the recent progress in lignin reactions as well as the challenges, advantages and disadvantages associated with the reaction procedures and the product development processes. Furthermore, the research gap in reaction strategies and product development are described throughout this study.

2.2 Introduction

The Lignin is an abundant, natural polymer representing between 15 and 30 wt% of lignocellulosic biomass.[1] This polymer exists in the cellular wall of cellulose fibers and provides structural support against oxidative stresses and microbial attacks for plants.[2–4] Lignin, an amorphous heteropolymer, is insoluble in water and has a limited reactivity.[5,6] It mainly comprises methoxylated phenylpropanoid (guaiacyl and syringyl) subunits that provide lignin with an energy density of 30% higher than that of polysaccharide polymers.[1,7] Lignin can be an alternative product to petroleum feedstocks for producing different chemicals.[8] The availability of lignin in the biosphere exceeds 300 billion tons, with a growth rate of around 20 billion tons every year.[9] However, a small fraction of the extracted lignin is used in the formulation of adhesives,[10] dispersants,[11] surfactants or as antioxidants in rubbers and plastics.[12–14] Thus, there is considerable room for taking greater advantage of the inherent potential of this abundant polymer in various fields.

Based on the types of plants (softwood, hardwood, and nonwood), the amount of each monolignol could be different. Hardwood lignin contains the highest amount of syringyl alcohol among the three classes of lignin with a smaller amount of coniferyl alcohol monolignols. Lignin extracted from softwood resources (also called coniferous or guaiacyl lignin) merely contains coniferyl alcohol monolignols. Meanwhile, lignin from grass (i.e., non-wood lignin) contains all three monolignols while the highest amount of monolignols is uncertain.

Since methoxy groups provide steric hindrance to the aromatic hydroxy groups of monolignol, their amount in monolignol is very critical. This is due to the fact that the enzyme catalyzing monolignol units' polymerization severely attacks the hydroxy groups, which connect monomers to generate a polymer chain. Hence, the overall cross-linking in the lignin structure decreases due to the enhancement in the steric hindrance, which lowers the ability of the aromatic part of lignin to react with other monomers. In addition, considering the internal cross-linking of the lignin structure, hardwood lignin, by virtue of having numerous units of syringyl alcohol monolignol, exhibits minimal internal cross-linking, while, lignin from grasses has more of a cross-linked structure than other lignin classes. It is worth noting that this internal cross-linked structure affects both the lignin molecule and the characteristics of lignin-based materials.[15]

The polymeric nature of lignin presents technical restrictions when used directly for synthesizing with other chemicals, which raises the need for its structural modification. Lignin modification and its use in alternative products has become particularly popular in biorefining processes. Biorefining can be considered as analogous to petroleum refining that is supposed to create many biodegradable, non-toxic and recyclable chemicals from the biomass.[16] In the past, different modification pathways had been conducted on lignin to make it a valuable product. Based on the lignin structure, modification reactions can occur on aromatic, aliphatic, or both parts.

Lignin can be isolated from the spent pulping liquors of sulfite, kraft, organosolv, and soda processes. Among these, sulfite and kraft processes are the two dominant techniques that are commercially utilized in the pulping industry.[17–19] Lignin produced from the kraft process is usually used as a fuel and burned in mills, while lignin generated in the sulfite pulping process is extracted as lignosulfonate. The solubility of kraft lignin is much lower than that of lignosulfonate due to the lack of hydrophilic groups on kraft lignin.[20,21] Nonetheless, kraft lignin possesses some outstanding properties in comparison with other types of lignin, such as a higher phenolic hydroxide group content, which is raised from the cleavage of β-aryl bonds during the pulping

process. Interest on lignosulfonate, on the other hand, has increased because its sulfonic acid groups are attached to its aliphatic part rendering it soluble in water and providing it with the capability of emulsifying and binding properties. There are two commercial techniques called LignoBoost and Lignoforce that utilize acidification for lignin isolation from black liquor with the lignin solid content of 50–60 wt%.[22,23]

Herein, the primary objective of this review is to discuss the fundamentals associated with the modification of the aromatic and aliphatic groups of lignin. Distinguishing the altered reaction pathways on lignin aromatic and aliphatic parts can possibly lead to the identification of an appropriate method for producing lignin-based products with desired properties for altered applications. Furthermore, the challenges and perspectives associated with the modification methods at both laboratory and commercial scale practices are discussed throughout this study. In addition, since reviews are available on the topics of polymerization,[24,25] catalytic reactions,[26,27] depolymerization,[8,24,28,29] redox-neutral strategies,[8] and photoredox catalysis,[30] this study has excluded the discussion on the above-mentioned strategies. Lignin oxidation has also been covered briefly in this study, while more comprehensive information on the oxidation of lignin and its derivatives could be found in the literature.[31–33] However, the graft modifications of lignin have not been studied comprehensively, which further begets the lack of studies on some curtail applications of lignin in industry. This study also excludes discussion on model compounds but provides comprehensive discussion on the modification of industrial lignin as the raw material.

2.3 Alternative methods for modification of phenolic structure of lignin

2.3.1 Phosphorylation

Phosphorus-containing compounds have been widely studied to develop non-toxic and environmentally friendly flame retardants to diminish the production of toxic fumes and smoke during burning and to hamper the combustibility of polymers.[34–36] Phosphorylation of lignin occurs via the addition of a phosphoryl group ($-PO_3$) to a molecule. This reaction proceeds through the S_N2 reaction mechanism (Fig. 2.1). Generally, in an S_N2 reaction, lignin's hydroxy groups, as a nucleophile, attack the carbon atom, an electrophilic center, due to the withdrawal of some electron density by the leaving-group (e.g., bromine, chlorine) from carbon, which makes the carbon partially positive. This leads the nucleophile that is the lone pair of an electron on oxygen (hydroxy of lignin) to attack the partially positive carbon. As the nucleophilic groups of lignin generate a bond with the carbon atom, the bond among the leaving group and the carbon atom breaks,

simultaneously. At the same time, the bond between carbon and the leaving group breaks, which renders the leaving-group negatively-charged. Finally, the hydroxy groups of lignin form a bond with the carbon atom to generate the product. The reaction mentioned above was reported to occur on both aromatic and aliphatic hydroxy groups of lignin.[37,38]
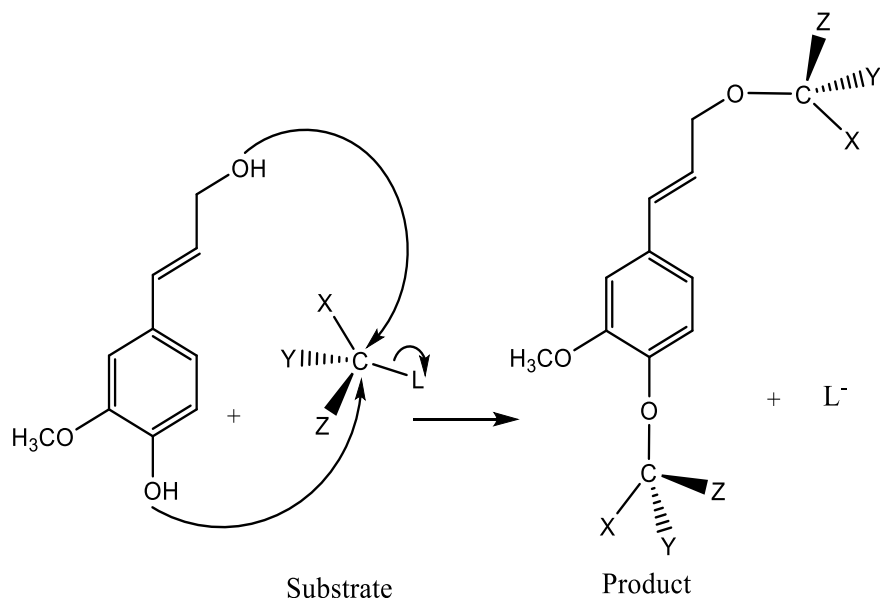
Fig. 2.1. General S_N2 reaction mechanism between lignin and substrate to form a new product and a leaving group (L). Substituents of the reacting carbon (X, Y, and Z) do not interfere with the reaction.[39-43]
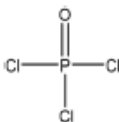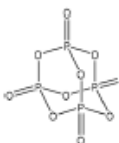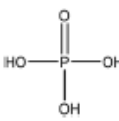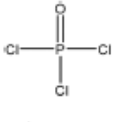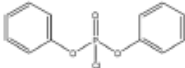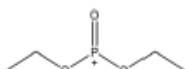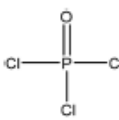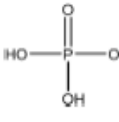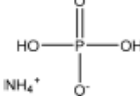
Table 2.1 shows some of the phosphorylation reactions conducted on lignin. Lignin phosphorylation has been carried out under different conditions using various phosphorus reagents, such as phosphorus trihalides, phosphorus oxyhalides, phosphorus thiohalides, phosphorus oxides, and phosphorus sulfides, for instance.[44–47] Tetrahydrofuran,[38,48] pyridine,[39,49] acetonitrile,[47] dimethylformamide, formaldehyde[44,45] and urea[37] were also used as solvents for phosphorylation in different studies. The reaction conditions were reported to occur in the time range of 1–12 h and the temperature range of 25–180 °C.[38,49,50] After the reaction, lignin-based products were reported to be isolated from the reaction media using methanol, diethyl ether and ion exchange processes.[38,47,49,50]

The phosphorylated group on lignin has facilitated its use as a high-performance flame-retardant additive in polyurethane, polybutylene succinate, polypropylene, epoxy and polylactic acid.[39,44–47] The proposed application is attributed to the fact that the phosphorylation of aromatic compounds enhances char formation under fire conditions by acting either in the gas phase or in the condensed

phase via interacting with the polymeric matrix.[38,39,48] Phosphorylated lignin has also been used as a cation exchange resin[49] and a sorbent of metal ions in wastewater treatment processes.[37,49,51] While lignin phosphorylation has certain advantages, some drawbacks, such as long reaction times, use of toxic reagents, e.g., phosphorus oxychloride and phosphorus oxychloride, or toxic solvents, such as dimethyl formaldehyde or dioxane, exist for the phosphorylation of lignin, which may be obstacles for the development of these reaction systems at commercial scales.[52]

Table 2.1. Phosphorylation of lignin.

Lignin source/type	Reaction conditions Time (h)	Temperature (°C)	pH	Reagent	Solvent	Separation	Property improvement	Yield (%)	Application	Ref.
Wheat straw alkali	12	95	3–4		Triethylamine, dimethylformamide	Methanol	Thermal stability	92	Flame retardant	53
Kraft	7–8	20–25	N/A		Tetrahydrofuran	Water	Thermal stability	N/A	Flame retardant	48 and 38
Spruce	1	80	N/A		Urea	Water and HCl	Phosphorus content	96	Sorbent	37
Black liquor	2	115	N/A		Pyridine	N/A	N/A	N/A	Sodium and metal ion adsorbent	51
Kraft	12	N/A	N/A		Pyridine	Water and DMSO	Oxidative stability	N/A	Flame retardant	39
Wheat straw alkali	5	70	5		Dimethylformamide and formaldehyde	Water	Flame retardancy, thermal stability	N/A	Flame retardant	44 and 45
Cotton stalks	2	115	N/A		Pyridine	HCl	Adsorption selectivity, thermal stability	N/A	Heavy metal ion adsorbent	51
Hydrolysis	3–6.5	140–180	N/A		Urea	Water	Thermal stability	70–75	Fire-retardant fillers for epoxy compounds	46
Alkali and an organosolv	15	80	N/A		Acetonitrile	Diethyl ether	Thermal stability	N/A	Flame retardant for polybutylene succinate	47

N/A: not available.

27

2.3.2 Hydroxymethylation

Hydroxymethylation introduces a hydroxymethyl group (–CH$_2$OH) into lignin molecules, which is performed by electrophilic aromatic substitution (Fig. 2.2). Under alkaline conditions, the sigma complex of lignin loses a proton to regain its aromaticity, which makes the oxyanion become protonated. By reacting lignin and formaldehyde in hydroxymethylation, the hydroxymethyl group is introduced into the para and/or ortho position on the aromatic ring of lignin.[54,55] Since this reaction is endothermic, temperature elevation would improve reaction yields.[56]
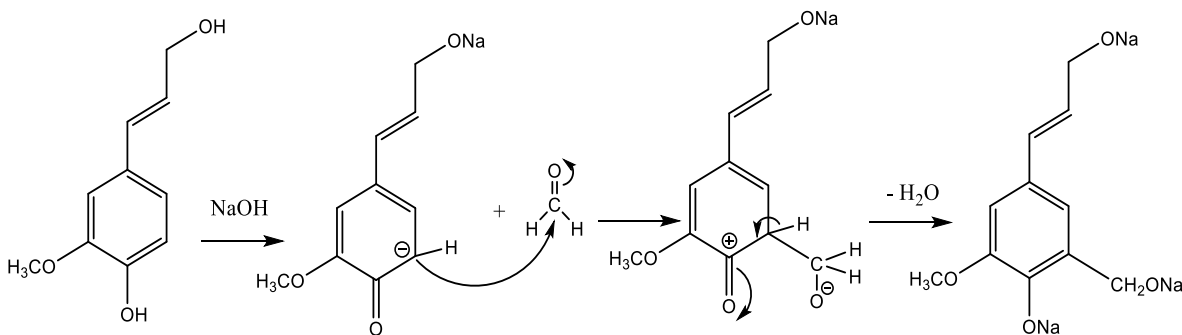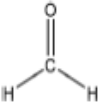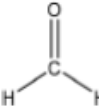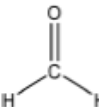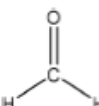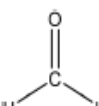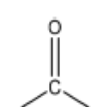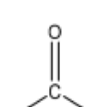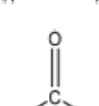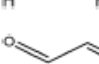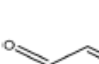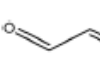
Fig. 2.2. Hydroxymethylation of lignin using formaldehyde.[57]

Table 2.2 shows the results of hydroxymethylation reaction conducted on lignin in the past. In most cases, the reactions were carried out using formaldehyde in alkaline media in the temperature range of 25–90 °C for 2–8 h (or even 72 h) to produce hydroxymethylated lignin. Compared to other reagents, formaldehyde was reported to shorten the reaction time due to its high reactivity. The use of paraformaldehyde in this reaction prolongs the reaction time as it requires the release of formaldehyde monomers at a slower pace in the reaction.[58] It is worth noting that formaldehyde may polymerize by itself in the hydroxymethylation reaction, which is undesirable. The hydroxymethylated lignin was reported to be separated from the reaction media by acidification and washing with acids.[59] It is worth mentioning that hydroxymethylation is one of the most appealing methods used to produce lignin derivatives used for wood adhesive applications. This reaction can also be used prior to sulfonation and amination reactions to attach a methyl group to lignin for the desired reactions.[20,57,61]

Hydroxymethylated lignin is also found to have high antioxidant activity since the phenolic OH groups are remained intact in its structure.[61] Hydroxymethylated lignin has also been reported to be used in polyurethane foam production[62] and as a binder in adhesive applications.[63]

Table 2.2. Hydroxymethylation of lignin.

Lignin source/type	Reaction conditions					Separation	Property improvement	Yield (%)	Application	Ref.
	Time (h)	Temperature (°C)	pH	Solvent	Reagent					
Organosolv	2	40	Alkaline	Water	formaldehyde	Acidification	Reactivity, thermal stability	N/A	N/A	64
Wheat straw, and grass	3	90	10.5	Water	formaldehyde	Acidification and centrifugation	Molecular weight	N/A	N/A	55 and 65
Kraft, and sodium lignosulfonate	0.25–4	50	Alkaline	Water	formaldehyde	N/A	Thermal stability	N/A	Phenolic resin	66
Kraft	72	20–25	12–12.5	Water	formaldehyde	N/A	Cross-linking ability	N/A	Adhesives and resins	54
Wheat straw, and grass	3	90	9.7–9.9	Water	formaldehyde	Acidification and centrifugation	Reactivity	N/A	N/A	67
Calcium lignosulfonate	2	80	11	Water	formaldehyde	N/A	Foaming ability, foam half-life time	N/A	N/A	57
Wheat straw	N/A	55–90	10–10.5	Water	formaldehyde	Acidification and centrifugation	Carbonyl groups, thermal degradation	N/A	As bio-protection in wood and adhesive	68
Alkali	3	60–90	10.5–12	Water	formaldehyde	N/A	Reactivity with resol resin, viscosity	N/A	Phenolic adhesive substitution	69
Softwood alkali	8	60	Alkaline	Water	glyoxal	N/A	Decrease in molecular weight	N/A	Wood adhesive	70
Calcium lignosulfonate	8	58	12–12.5	Water	glyoxal	N/A	N/A	N/A	Wood adhesive	71
Soda bagasse	8	58	12–12.5	Water	glyoxal	N/A	N/A	N/A	Wood adhesive	72

N/A: not available.

2.3.3 Phenolation
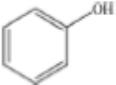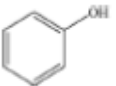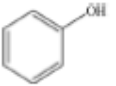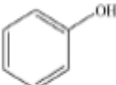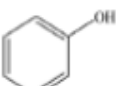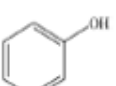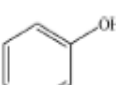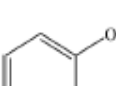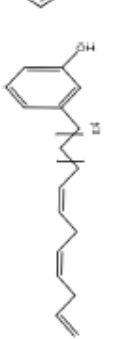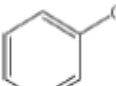
Phenolation is a reaction in which the number of phenolic OH groups of lignin are increased by the addition of phenol to lignin's aliphatic chain.[73,74] This reaction proceeds through S_N2 (Fig. 2.1) or addition reaction.[75] A reduction in lignin's molecular weight could be observed in some cases,

which would be due to the breakage of ether bonds.[76] In general, the phenolation reaction improves the flexibility, tensile strength and glass transition temperature of lignin making it preferable to be used in polyurethane films' production.

Additionally, phenolated lignin has been mostly studied when producing phenol formaldehyde resins, in which lignin is primarily phenolated to react with formaldehyde. Thus, the formaldehyde resins produced with phenolated lignin demonstrated an adequate curing time and viscosity required for panels' production which is comparable to those of commercial resins.[74]

Table 2.3 shows the phenolation reaction carried out on lignin. Generally, lignin is mixed with phenol or cardanol, an alkyl phenol isolated from the liquid shell of cashew nut,[77] mostly in water under harsh acidic conditions at a temperature range of 25–125 °C for 20 min–6 h. Phenolated lignin can be separated from the reaction mixture using filtration and/or washing with water, acetone or ether. Additionally, phenolated lignin used in phenolic resins has been reported to have better mechanical properties than unmodified or hydroxymethylated lignin.[78,79] Nonetheless, the immense amount of sulfuric acid used in lignin phenolation is not economically or environmentally attractive since it requires an expensive recovery process.

Table 2.3. Phenolation of lignin.

| Lignin source/type | Reaction conditions | | | | Solvent | Separation | Property improvement | Yield (%) | Application | Ref. |
	Time (h)	Temperature (°C)	pH	Reagent						
Black liquor	5	60	Acidic		Water	Filtration and water	Ion-exchange capacity	N/A	Making resin	80
Enzymatic hydrolysis	2	110–120	Acidic		Ether	Filtration and water	Molecular weight	100–120	Adhesive	73
Sulfuric acid	6	60	Acidic		Water	Filtration and water	Solubility and reactivity	N/A	N/A	81
Organosolv	1	50–80	N/A		Water	N/A	Curing time	N/A	Resins for particleboard	78
Organosolv	1–2	70–110	Acidic		Acetone and water	Filtration and water	Molecular weight and dispersity	71–96	Thermoset resin	82
Eucalyptus/ acetosolv	1.5	125	Acidic		Water	N/A	Reactivity	N/A	Resin	83
BioChoice, and a pine (softwood) kraft	2	90–110	Acidic		Water	Ether, and filtration	Molecular weight decreased	30–60	Thermosets	75
Sulfuric acid	N/A	20–25	Acidic		Ethanol or water	Acetone, and centrifugation	Light colored	~93–110	Selective phenolation	84
Softwood kraft	N/A	50	Acidic		Water	N/A	Tensile strength, glass transition temperature	20–40	Polyurethane film	77
Beech organosolv	0.33	110	Acidic		Water	N/A	Strength	N/A	Wood veneer and particle board adhesion	85

N/A: not available.

31

2.3.4 Sulfonation

Sulfonation occurs through the substitution of a sulfonate group with lignin's aliphatic hydroxy groups through the addition reaction (Fig. 2.3),[86] rendering lignin negatively charged. This reaction primarily occurs on the carbon of the α position.[87] As an exception, sulfonation with chlorosulfonic acid occurs on the lignin's phenolic ring. Sulfonated lignin has a broad range of applications in various industries such as oil drilling,[88] paper coating,[89] cement and concrete production,[90,91] in ion-exchange,[80] and as a surfactant,[93] binder, and dispersant.[88,93–95] The anti-oxidant and UV absorbent properties of sulfonated lignin have also made this product attractive to be used in flame retardants and sunscreens' production, respectively.[96]
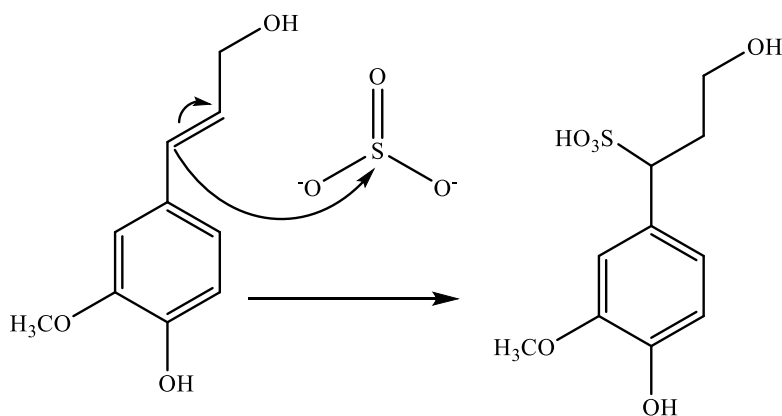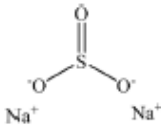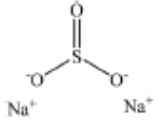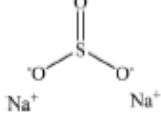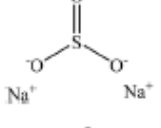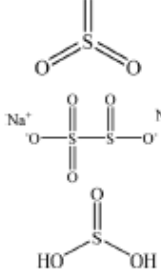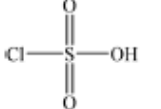
Fig. 2.3. Sulfonation of lignin with sodium sulfite.[97]

Table 2.4 shows sulfonation reactions performed on lignin. The sulfonation of lignin has been reported to be conducted using either sulfur dioxide (SO_2), sulfur trioxide (SO_3), sulfurous acid (H_2SO_3), sodium metabisulfite ($Na_2S_2O_5$), or bi-sulfite (M_2SO_3) (where M can be Ca, Na, H, Mg, K, or their combination) as a reagent. In this reaction, lignin is generally mixed with the reagent mostly in water under either acidic or alkaline conditions in a high-temperature range of 70–180 °C for 0.5 to 4 hours. Thus, the produced lignin samples could be separated and purified using filtration and a dialysis membrane.

Table 2.4. Sulfonation of lignin.

Lignin source/type	Reaction conditions			Reagent	Solvent	Separation	Property improvement	Yield (%)	Application	Ref.
	Time (h)	Temperature (°C)	pH							
Esparto grass	4	140	4–9	(sodium sulfite structure)	Water	Filtration	Solubility	N/A	Plasticizing for cement	91
Washed aqueous slurry	2	140	~7	(sodium sulfite structure)	Water	N/A	Solubility	N/A	Dispersant in dye	95
Kraft	1–5	100–180	Alkaline	(sodium sulfite structure)	Water	Dialyzed	Molecular weight decreased	N/A	N/A	97
Corn stalks	0.5–1	95	Alkaline	(sodium sulfite structure)	Water	N/A	N/A	~70–85	N/A	98
Kraft	1–2	70–120	Acidic	(sulfur trioxide / sodium dithionate / sulfurous acid structures)	Water	N/A	N/A	N/A	Sulfonation of alkali pulp	92
Phenolyzed	1.5	100	Alkaline	(Cl–SO$_2$–OH structure)	Tetrachloroethane	Filtration and water	Ion-exchange capacity	~33–58	Making resin	80

N/A: not available.

2.3.5 Sulfoalkylation
2.3.5.1 Sulfomethylation
Sulfomethylation reaction introduces a methylene sulfonate group mainly into the ortho position of the aromatic ring of lignin.[99] Sulfoalkylation of lignin occurs through the S$_N$2 route as the electrophilic S attacks the carbon in the CH$_2$OH group of lignin while the OH group leaves the molecule (Fig. 2.4). In this case, sodium sulfonate methyl derivatives are formed by the addition of nucleophilic sodium sulfite anions into alkaline media. In this reaction, unsubstituted carbon-5 sites in phenolic units of lignin are the primary targets.[100] Under alkaline conditions, the reaction occurs with equimolar alkali metal sulfite salt and phenolic units.[101] In sulfomethylation,

formaldehyde introduces the methoxy group into lignin, which is the reacting location in the sulfonation reaction with sodium sulfite.[102] Table 2.5 shows the data available on the sulfomethylation of lignin. Generally, the sulfomethylation reaction has been carried out in the pH range of 7–13 at 60–140 °C for 0.5–9 hours. The sulfomethylated lignin can be separated and purified via neutralizing the pH and using membrane dialysis, respectively.[20] Filtration[103,104] and ion exchange resin were also reported as the practical options for purifying the product.[100] In the meantime, sodium thiosulfate is observed to be produced in the side reaction, which is reported to affect the yield of the sulfomethylation reaction adversely. This yield could be enhanced by increasing the temperature from 100 °C to 150 °C.

However, the reactivity of this reaction is rather low and highly depends on the lignin type. In order to improve lignin reactivity toward sulfomethylation, oxidation was reported to be conducted prior to sulfomethylation.[20,101]
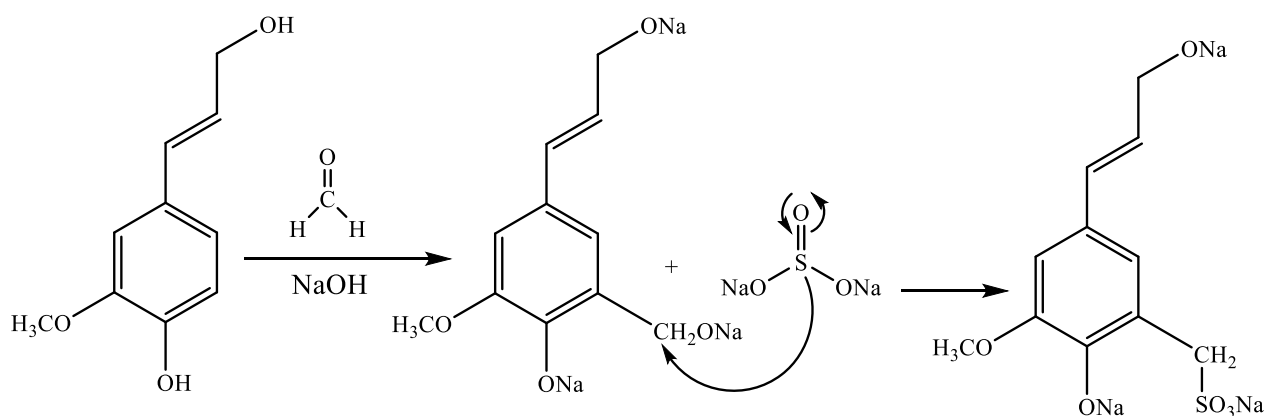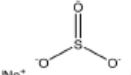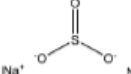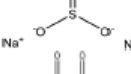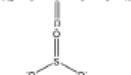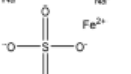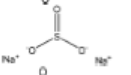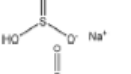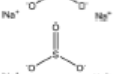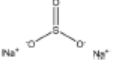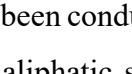
Fig. 2.4. Sulfomethylation of lignin with sodium sulfite.[20,57]

Overall, sulfomethylated lignin has been investigated to have various applications in industry, such as a dispersant for coal–water slurry[21,57] and concrete paste[20,101] or a flocculant for aluminum oxide suspension[105] due to its augmented hydrophilicity and charge density. However, using formaldehyde in sulfomethylation can be considered as the main drawback of this modification pathway since it is toxic, carcinogenic and mutagenic, which raises environmental concerns.

Table 2.5. Sulfomethylation of lignin.

Lignin source/type	Reaction conditions Time (h)	Temperature (°C)	pH	Reagent	Solvent	Separation	Property improvement	Yield (%)	Application	Ref.
Enzymatic hydrolysis	3	95	Alkaline		Formaldehyde	Filtration	Steric energy reduction	N/A	Dispersion for graphite suspension	106
Alkaline, and enzymatic hydrolysis	1–5	80–130	N/A		Formaldehyde	H$_2$SO$_4$	Compressive strength of concrete	~60–90	Dispersant for concrete paste	107
Oxidized	1–3	100	Alkaline		Water and formaldehyde	Membrane dialysis	Molecular weight, charge density	33–38	Flocculant for aluminum oxide suspension	105
Aminated alkaline	2	90	10		Water	Filtration	N/A	N/A	Heavy metal ion removal	109
Oxidized softwood kraft	0.5–4	60–100	7		Water, and formaldehyde	Membrane dialysis	Molecular weight, charge density	N/A	Dispersant for cement	101
Hardwood kraft	1–7	80–140	N/A		Formaldehyde	Membrane dialysis	Molecular weight, charge density	N/A	Dispersant for cement	20
Kraft	3	75	3–4		Formaldehyde, H$_2$O$_2$	Dialyzed	Molecular weight decreased, and lighter color	N/A	N/A	97
Calcium lignosulfonate	2	90	10		Formaldehyde	N/A	N/A	N/A	Dispersant for cement	57
Alkali	5	90	10		Water, and formaldehyde	N/A	Adsorption selectivity, wettability	N/A	Dispersant for coal–water slurry	21
Alkali-corn stalk	2–9	75	9		Formaldehyde	Filtration	N/A	N/A	Dispersant for dye	100
Hydroxymethylated alkali	4	95	13		Formaldehyde	Neutralization and Buchner funnel	Charge density, solubility	N/A	Adsorbent	103
Wheat straw alkali	4	95	N/A		Formaldehyde	Neutralization and Buchner funnel	Charge density	N/A	Dispersion for TiO$_2$	104

N/A: not available.

2.3.5.2 Sulfobutylation

Sulfobutylation reactions have been conducted on lignin by introducing –C$_4$H$_8$–SO$_3$H into hydroxy groups on both aromatic and aliphatic sites, with long alkyl chains using a 1,4-butane sultone reagent. This reaction occurs through the S$_N$2 mechanism with ring-opening under alkaline conditions (Fig. 2.5). The reaction mechanism for sulfobutylation is different from those using conventional sulfomethylation reagents, such as Na$_2$SO$_3$ or Na$_2$S$_2$O$_5$ with formaldehyde. Also, sulfobutylation occurs on both aromatic and aliphatic groups.[109] The sulfobutylation reaction has been reported to enhance the water-solubility of the polymer, which is highly desirable in aqueous based applications. The molecular weight of sulfobutylated lignin was reported to be greater than that of sulfomethylated lignin.[110] The long alkyl chain and sulfonic acid groups of the reagent were reported to play key roles in improving dispersibility performance by developing steric hindrance and electrostatic repulsion.[110]
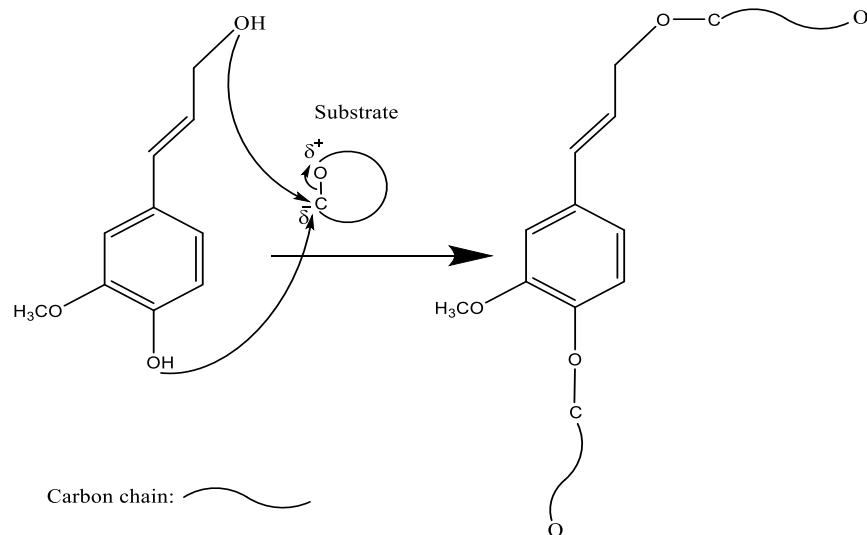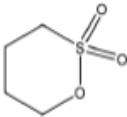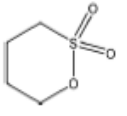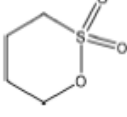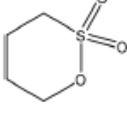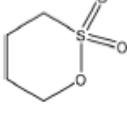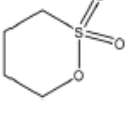
Fig. 2.5. General S_N2 reaction with ring-opening. Electrophilic center (carbon) is partially negatively-charged, and oxygen is partially positively-charged.[109,111,112]

Table 2.6 shows the sulfobutylation reactions conducted on lignin. In general, sulfobutylation was conducted using 1,4- butane sultone at 70 °C for 6–7 hours at pH 12. In order to separate the produced polymer from the reaction media, the ion-exchange resin and dialysis membrane have been used. Sulfobutylated lignin has been used as a dopant and a dispersant for coal–water slurry and carbendazim.[109–111]

Sulfobutylation seems to be a more favorable reaction over sulfomethylation because (1) sulfobutylation needs lower temperature and pressure (Tables 5 and 6), which results in using less expensive and simpler equipment, (2) the use of toxic formaldehyde in sulfomethylation is another downside of this reaction,[109] and (3) sulfomethylation can only occur on the phenolic part of lignin, while sulfobutylation can occur on both aliphatic and aromatic parts. However, the 1,4-butane sultone reagent used in sulfobutylation is substantially more expensive than sulfomethylation reagents (Na_2SO_3, $Na_2S_2O_5$), which may make this modification process expensive.

Table 2.6. Sulfobutylation of lignin.

Lignin source/type	Time (h)	Temperature (°C)	pH	Reagent	Solvent	Separation	Advancement in properties	Yield (%)	Application	Ref.
Alkali	7	70	12	(sultone structure)	Water	Ion-exchange resin	Molecular weight	N/A	As dopant and dispersant	111
Alkali	6	65	12	(sultone structure)	Water	Ion-exchange resin	Molecular weight	N/A	Dispersant for coal–water slurry	109
Eucalyptus kraft	3	70	12	(sultone structure)	Water	Ethanol	Brightness	N/A	Dispersant for dye	113
Alkali	7	70	12	(sultone structure)	Water	Dialysis membrane	Molecular weight	N/A	Dispersant for carbendazim	110
Alkali	7	50	12	(sultone structure)	Water	Filtration and dialysis	Hydrodynamic size	N/A	Aggregation-induced emission	114
Kraft	1–6	50–90	Alkaline	(sultone structure)	Water	Dialyzed	Molecular weight decreased, and lighter color	N/A	N/A	97

N/A: not available.

2.3.6 Carboxyalkylation
2.3.6.1 Carboxymethylation
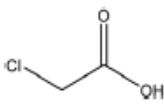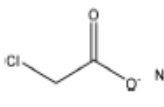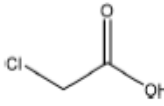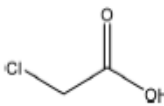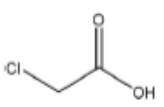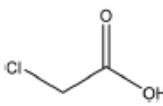
Carboxymethylation is applied to lignin by introducing a carboxymethyl group ($-C_2H_3O_2$) following the S_N2 reaction, as discussed earlier (Fig. 2.1).[40] In the carboxymethylation reaction with sodium chloroacetate, salt (i.e., NaCl) and glycolic acid are observed to be generated as by-products. Since aromatic hydroxy groups ionize easier than aliphatic hydroxy groups in an alkaline environment, the reaction would occur primarily on the aromatic ring.

Table 2.7 shows the lignin carboxymethylation reactions performed in the literature. The carboxymethylation reaction has been carried out by mixing lignin with NaOH followed by sodium chloroacetate or monochloroacetic acid in the time and temperature range of 1–6 h and 30–90 °C,

respectively.[40,115–119] Alternative pathways were considered for purifying the products, such as acidification,[118] membrane dialysis,[40] and washing with ethanol.[116,119,120]

Carboxymethylated lignin has been proposed as an effective dispersant for oil–water emulsions,[109] crude bitumen emulsions,[121] and clay,[40] cement,[116] and graphite suspensions.[122] Carboxymethylated lignin was also used as a stabilizer in kerosene-in-water emulsions[117] and as a foaming agent.[110] The composite of carboxymethylated lignin–tetra ethoxysilane was tested as a packaging and antimicrobial formula as well as in wound dressings. In addition, due to its potential in adsorbing heavy metals, such as nickel and cadmium, this product has been suggested to be used in wastewater treatment and biofilters.[119] Carboxymethylated lignosulfonate was also reported to improve the heat capacity of leather when it was used along with tanning chromium in leather production.[115]

Table 2.7. Carboxymethylation of lignin

| Lignin source/type | Reaction conditions | | | Reagent | Solvent | Separation | Property improvement | Yield (%) | Application | Ref. |
	Time (h)	Temperature (°C)	pH							
Organosolv	3.5	55	N/A	Cl–CH₂–COOH	Ethanol	Filtration	N/A	N/A	Stabilizer in ceramic industries	116
Harwood kraft	1–6	30–70	Alkaline	Cl–CH₂–COO⁻ Na⁺	Water	Membrane dialysis	Charge density, solubility, molecular weight	N/A	Dispersant for clay suspension	40
Kraft	3.5	55	N/A	Cl–CH₂–COOH	Ethanol	Filtration and ethanol	Surface tension	N/A	Stabilizer for oil-in-water emulsions	117
Kraft and organosolv	3.5	55	N/A	Cl–CH₂–COOH	Ethanol	Filtration and HCl	Decrease in heat capacity, and surface tension	90	Stabilizer of crude bitumen	121
Wheat straw alkali	1–3	50–90	N/A	Cl–CH₂–COOH	Water	HCl	N/A	~80	Dispersant	122
Kraft	N/A	N/A	Alkaline	Cl–CH₂–COOH	Water/ ethanol	HCl	Adsorption to fibre-laden	N/A	Stabilizer of fiber-laden foams	120

N/A: not available.

2.3.6.2 Carboxyethylation

Carboxyethylation is the grafting of the –CH$_2$–CH$_2$–COOH group to lignin. Fig. 2.6 shows the mechanism of carboxyethylation of lignin in an alkaline environment. The reaction proceeds through an S$_N$1 mechanism in the basic medium by the substitution of the carboxyethylate group with the aromatic and aliphatic hydroxy groups of lignin. Carboxyethylation of lignin by 2-chloropropionic acid has been proceeded by the dissociation of the carbon–halogen bond, which generates negatively charged chloride ions (as the leaving group) and positively charged carbocation intermediate (on the reagent) in the first stage. In the second stage, the alkoxide ion (of lignin) attacks the planar carbocation and bonds to the reagent. In the meantime, sodium lactate and homopropionic acid polymer could be produced as the byproducts of carboxyethylation with 2-chloropropionic acid. Carboxyethylation of lignin would improve its hydrophilicity and generate a highly charged anionic lignin, which could be a pathway to produce pH sensitive anionic lignin[123] for use as a dispersant and flocculant in industry. This reaction reported to slightly increase the molecular weight of lignin as well.[123]
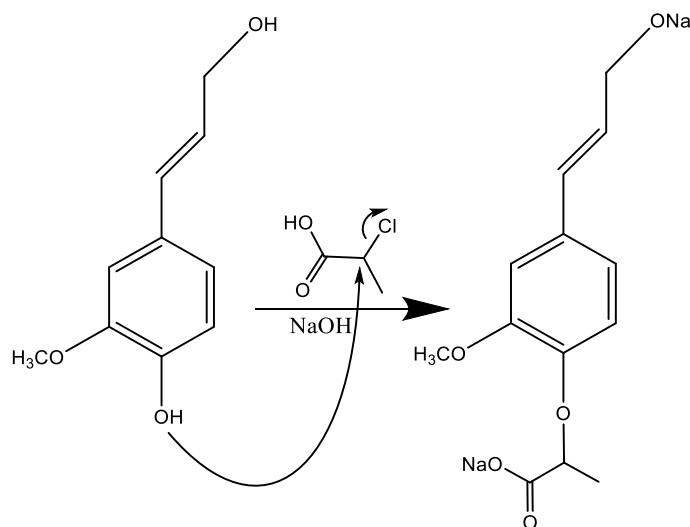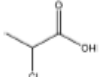
Fig. 2.6. Carboxyethylation of lignin under alkaline conditions by using 2-chloropropionic acid.[123]

In this reaction, lignin can be mixed with 2-chloropropionic acid, the donor of the carboxyethyl group, in a mixture of water and isopropyl alcohol in the basic environment at 60–90 °C for 0.5–2 h (Table 2.8). The production of sodium lactate is the undesired side reaction.[123] Due to the insolubility of the produced lignin in solvents, the reaction mixture can be mixed with ethanol for lignin isolation.[123] Alternatively, membrane dialysis and filtration can be used for isolating the product from the reaction media. In opposition to carboxymethylation reactions, carboxyethylation can occur on both aromatic and aliphatic hydroxy groups of lignin. Therefore, carboxyethylation

may be considered as a more influential modification pathway for lignin than carboxymethylation.[122,123] However, the main drawback of carboxyethylation is the solvent used in the reaction (e.g., isopropyl alcohol), which may not be an attractive pathway to develop green processes for lignin modification.

Table 2.8. Carboxyethylation of lignin.

Lignin source/type	Reaction conditions					Separation	Advancement in properties	Yield (%)	Application	Ref.
	Time (h)	Temperature (°C)	pH	Reagent	Solvent					
Lignosulfonate	0.5–2.0	60–90	Alkaline		Water/isopropyl alcohol	Ethanol/water	Charge density, molecular weight	N/A	Dispersant	123
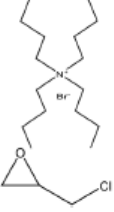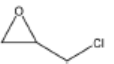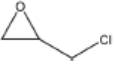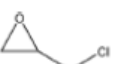
N/A: not available.

2.3.7 Epoxidation

Chemicals possessing amino or hydroxy groups have good reactivity with epoxy groups. Lignin can be rendered lipophilic when it is modified with epoxy containing materials. This reaction facilitates the dissolution of lignin in organic solvents, such as methylene chloride, tetrahydrofuran, acetone, and chloroform for generating value-added products.[124] Epoxy resins are used in a broad variety of applications in electrical and electronic laminates, high-performance composites, industrial coatings, adhesives, paving applications, and feedstock for emulsifiers and detergents.[122,124–126] Epoxidation of lignin proceeds through the S_N2 mechanism as discussed earlier (Fig. 2.1) under alkaline conditions.[112] Epoxidation was reported to occur on the aromatic ring of lignin by the substitution of hydroxy groups with epoxy groups.[61,127] Table 2.9 shows the epoxidation reactions of lignin reported in the literature. In this reaction, lignin is mixed with either di-epoxides, such as polyethylene glycol diglycidyl ether (PEGDGE), with different chain lengths, or epichlorohydrin in an alkaline environment (pH > 12) at 30–90 °C for 1–18 h.[50,112,126–128] The epoxidized lignin product is then isolated by neutralizing the reaction mixture with sodium dihydrogen phosphate (NaH$_2$PO$_4$) and centrifugation. The solid epoxy lignin can then be recrystallized in chloroform for further use.[61–67] Stronger alkalinity could enhance the lignin degradation and produce more phenolic hydroxy groups to react with epichlorohydrin, which increases the reaction yield.[112] In this case, lignin macromolecules will be converted to more of lignin monomers, and then monomers would have a higher tendency to epoxidize. However, using epichlorohydrin has some disadvantages, such as toxicity and limited rheological characteristics associated with the gel-like dispersion.[129,130] Epoxy resins produced by lignin usually have low

40

thermal stability and T_g value over the mercantile ones (i.e., a synthetic bisphenol A). In this regard, the limited number of epoxy rings in lignin prevents the generation of dense crosslinks in cured epoxy systems. Hence, it would be more favorable to produce lignin-based curing agents to be used in generating epoxy systems with efficient performance.[131] Similarly, the epoxy lignin was reported to have antibacterial activity and was mostly resistant to *Bacillus* sp. and *Klebsiella* sp. strains.[61] Nonetheless, the disadvantages associated with lignin-based epoxy resins include low water solubility, slow curing rate, high cost and brittleness.[24,132–135]

Table 2.9. Epoxidation of lignin.

Lignin source/type	Reaction conditions Time (h)	Temperature (°C)	pH	Reagent	Solvent	Separation	Property improvement	Yield (%)	Application	Ref.
Alkaline	5	90	Alkaline		Water	Neutralization and water	Molecular weight	~12	Feedstock for an emulsifier, detergent, and additive	124
Alkali	6	50–80	N/A		Diethanolamine, and formaldehyde	N/A	Thermal stability	N/A	Thermal stable resin	126
Organosolv lignin	3–5	50–90	N/A		Water	Water and filtration	Molecular weight	107–126	Bio-based epoxy resin	125
Wheat straw	2	60	Alkaline		Water	N/A	N/A	N/A	Bio-based epoxy resin	127
Sugarcane bagasse	3–6	70	Alkaline		Water	Neutralization and centrifugation	Antibacterial activity, lower radical scavenging activity	N/A	Natural antibacterial	61
Sarkanda, and wheat straw, Protobind 1000	3–7	50–90	Alkaline		Water	Neutralization and centrifugation	Thermal stability decreased	61–88	Composite formation	67
Alkaline	8	50	N/A		Water	Filtration and ethane/water	Decomposition temperature decreased	37–91	Epoxy resin additive	112
Alkali	3	30	Alkaline		Water	Centrifugation	Viscosity	N/A	Thickener in bio-lubricant	129

N/A: not available.

2.3.8 Oxyalkylation/oxypropylation

Oxyalkylation is a process by which hydroxy groups of lignin are converted to oxyalkylated groups. The oxyalkylation of lignin proceeds through the S_N2 mechanism (Fig. 2.7). In the reaction of cyclic organic carbonates with hydroxy groups of lignin (Fig. 2.7), cyclic carbonate (e.g., propylene carbonate) can react with aliphatic and aromatic hydroxy groups[136] according to two

reaction pathways; aliphatic hydroxy tends to attack the carbonyl carbon atom leading to carbonate linkages, while aromatic hydroxy can attack the alkylene carbon atoms and ether linkage with a subsequent loss of CO_2, which allows the production of polyether polyols with primary and secondary hydroxy groups.[136,137] At temperature lower than 170 °C, the rate of oxyalkylation trend on the aromatic hydroxy groups is higher than that on the aliphatic ones due to the lower nucleophilicity of aliphatic hydroxy groups. At a higher temperature (>170 °C) and in the presence of the basic catalyst (e.g., K_2CO_3), only 0.3% of carbonate linkages could be developed, while etherification of the aliphatic hydroxy groups was found to be favored at high temperatures.[136,138] Oxyalkylation liberates the lignin's hydroxy groups, especially that of the aromatic OH, and induces moieties of ether that presents uniformity, solubility, and reactivity to lignin. In this case, lignin can be converted to a liquid polyol product[139] that could be a potential alternative to replace typical ones in polyurethanes. Among all, oxypropylation is the most popular oxyalkylation reaction, which could be feasible to conduct under both alkaline and acidic conditions, while it was suggested to be more efficient and economically favorable if performed in an alkaline environment.[140]
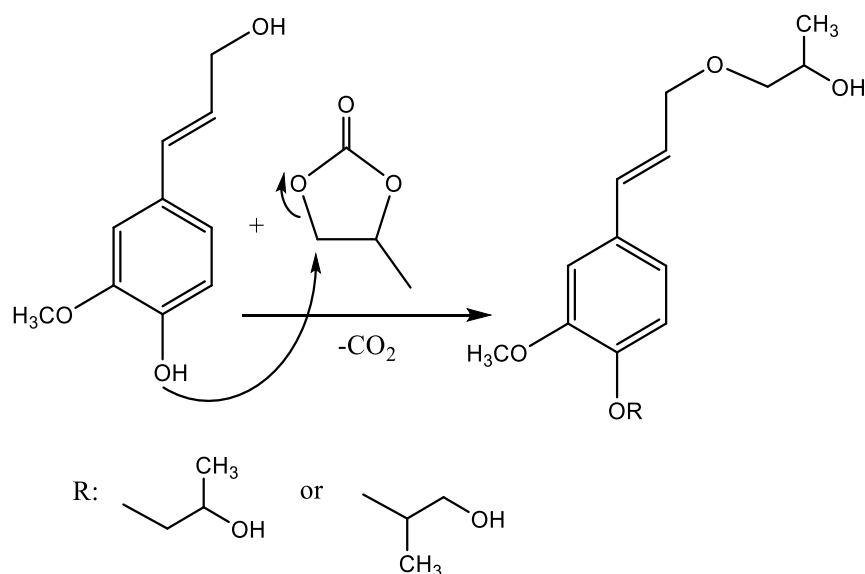
Fig. 2.7. Oxypropylation of lignin by using propylene carbonate.[136]

Table 2.10 shows reports on the oxypropylation of lignin. To produce oxypropylated lignin, lignin is mixed with reagents, such as propylene oxide or propylene carbonate, and NaOH or KOH, and is reacted in the temperature range of 40–285 °C for 4 min to 24 h under atmospheric and pressurized (up to about 40 bar) conditions.[136,138,141,144,150] To extract the product from the reaction

media, the reaction mixture is acidified to pH 2.5, which facilitates the precipitation of oxypropylated lignin.[136,138,141]

Oxypropylated lignin has found application in polyurethane foams.[142,143] It was reported that oxypropylated lignin has remarkably enhanced the mechanical properties of foams compared to commercial polyols.[145] In addition, the produced lignin polyols were suggested to be a valuable substitution for oil-based polyols, which are extensively used in polyester and polyurethane productions.[136–138] However, the use of propylene oxide, which is obtained from oil-based chemicals may be unattractive, as the final product may contain less than 50% lignin.[145] In addition, this reagent is very expensive which makes the reaction unfavorable for commercial purposes. This reaction also suffers from safety concerns due to the high vapor pressure as well as high toxicity, carcinogenicity, and flammability of propylene oxide in the reaction media. Instead, cyclic organic carbonates, such as propylene carbonate, could be used in this reaction to reduce the precautions since it is non-toxic and eco-friendly.[137] Furthermore, high boiling and flash points, as well as low vapor pressure and high solubility make this reagent more attractive than propylene oxide to be used in the oxypropylation of lignin.[136,137,146.]

Table 2.10. Oxyalkylation of lignin.
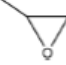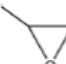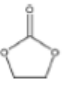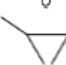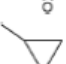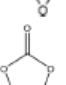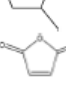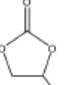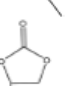
| Lignin source/type | Reaction conditions | | | | | | | | | |
	Time (h)	Temperature (°C)	pH	Reagent	Catalyst/solvent	Separation	Property improvement	Yield (%)	Application	Ref.
Kraft	12	40	Alkaline		Potassium hydroxide	HCl	Molecular weight decreased	N/A	Use in carbon fiber	147
Soda	0.08–0.16	120–140	Alkaline		Potassium hydroxide	N/A	Molecular weight decreased	N/A	Use in polyurethane foam	142
Organosolv, kraft, and oxidized organosolv	0.3–15	140–190	Alkaline		Potassium hydroxide	Vacuum removal	Dimensional stability of the foam	N/A	Use in polyurethane foam	143
Kraft	2	140	Alkaline		Potassium hydroxide	Tartaric acid	Viscosity of the polyester-polyether polyol	N/A	Use in the polyurethane production	148
Sodium lignosulfonate	4	175	Alkaline		Sodium carbonate	Distillation	Darkness, viscosity	N/A	As dispersants for carbon black, as emulsifiers	149
Wheat straw soda	24	70	Alkaline and acidic		Water	Ethyl ether anhydrous	Molecular weight, smother morphology	N/A	As a substitute for polyols in view of polyurethane	140
Kraft, soda, organosolv	~0.58–1.8	169–271	Alkaline		Potassium hydroxide	N/A	Viscosity	N/A	As a substitute for polyols in view of polyurethane	140
Kraft	18	40	Alkaline		Water	HCl	Thermal stability decreased	N/A	Thermoplastic materials	150
Kraft	0.15	150–285	Alkaline		Potassium hydroxide	N/A	Molecular weight decreased	N/A	As a substitute for polyols in view of polyurethane	144
Softwood kraft	18	20–25	Alkaline		Water	N/A	Molecular weight decreased	N/A	N/A	141
Organosolv	3	170	N/A		Methylimidazole, 1,4-dioxane	Acidification and filtration	Molecular weight	N/A	As a substitute for polyols in view of polyurethane and polyesters	136
	21	50								

Table 2.10. (*Contd.*)

| Lignin source/type | Reaction conditions | | | | | | | | | |
	Time (h)	Temperature (°C)	pH	Reagent	Catalyst/solvent	Separation	Property improvement	Yield (%)	Application	Ref.
Beech wood organosolv	0.5–24	100–170	N/A		1,8-Diazabicyclo[5.4.0] undec-7-ene/potassium carbonate	Acidification and filtration	Molecular weight	N/A	Substitution of conventional petroleum-based polyols	137
Beechwood, wheat straw Organosolv	3	170	N/A		1,8-Diazabicyclo[5.4.0] undec-7-ene	Water and filtration	Molecular weight	N/A	Biobased polyols	138
Organosolv	3	170	Alkaline		1,8-Diazabicyclo[5.4.0] undec-7-ene/dimethyl sulfoxide	Acidification	Molecular weight	97–99	Prepolymer for nonisocyanate polyurethanes	151

N/A: not available.

2.3.9 Esterification

Generally, esterification is the conversion of alcohols to esters.[152] The esterification of lignin is performed by nucleophilic substitution (Fig. 2.8). In this reaction, the lone pair electron of the aromatic hydroxy group will attack the carbon of the ester group on the reagent (Fig. 2.8). As a

result, the carboxylic acid group will leave, and hydroxy groups of the aromatic ring are replaced with carbonyl groups.[153] This reaction is feasible using mono- or dicarboxylic acids, their anhydrides, acid chlorides, or via transesterification with carboxylic acid esters. For instance, maleic acid, acetic acid, phthalic acid, fumaric acid, or fatty acids such as oleic acid, lauric acid or their anhydrides, acid chlorides or simple esters can be used in the esterification of lignin.[153–155] Esterification occurs on both aromatic and aliphatic hydroxy groups of lignin but is more favored to occur on the aromatic hydroxy group.[156] The reason for this tendency could be the lower pKa of the aromatic hydroxy groups than the aliphatic counterparts of lignin since the acetylation reagents, e.g., pyridine or imidazole, act as both catalysts and bases accelerating the production of nucleophiles.[157]
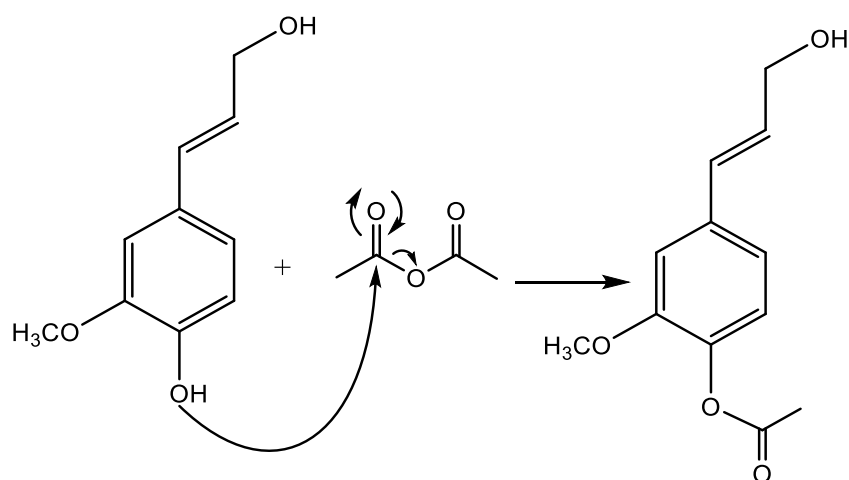
Fig. 2.8. The esterification reaction of lignin with acetic anhydride.[61]

Table 2.11 shows the esterification reaction conducted on lignin. Generally, lignin is mixed with different acid anhydrides (succinic, phthalic, acetic and maleic anhydrides) in solvents, such as pyridine, tetrahydrofuran, dimethylformamide, acetone, dioxin, and 1-methylimidazole, in the temperature range of 25–120 °C for the period of 5 min and 48 h.[143,148–151] After the reaction, acidification or solvent (e.g., acetone, ethanol) addition and membrane dialysis were used as means of the product purification strategy.[153,158,160,161]

Esterification has been commonly used to reduce the hydrophilicity and solvophilicity of lignin, which makes it favorable to be used for composite productions.[162–164] Lignin esterification by butylation, for instance, transforms the alcohol groups to butyl esters and improves lignin miscibility in low-polar solvents, which would facilitate its use in the construction industry.[165–167] Esterifying lignin also enhances its compatibility with plastic blends such as polystyrene,

polyethylene, and poly(3-hydroxybutyrate-co-3-hydroxy valerate) blends.[160,161,168] In addition, esterified kraft lignin was reported to remarkably improve the interfacial tension between the resin and reinforcing flax fibers.[169] Furthermore, lignin esterification increases the thermal mobility of lignin molecules by diminishing the intermolecular interaction, which further leads to a reduction in the glass transition temperature of lignin.[170]

The esterification was reported to improve the morphology of lignin-based materials. For example, carbon fibers made from phthalic anhydride-modified lignin were revealed to have reasonably high micro-scale porosity in comparison with carbon fibers made from unmodified lignin.[158] It is also worth mentioning that the structural properties of carbon fibers produced from lignin depend on the reagent used in the esterification reaction. For instance, lignin with a cyclic anhydride such as succinic, maleic or phthalic may form di-esters, whereas lignin could only form a monoester with acetic anhydride. In addition, the esterification of lignin using phthalic anhydride would render lignin more hydrophobic. Using maleic anhydride, a reagent with a double bond in its structure may increase cross conjugation between lignin's structural units.

These reports also suggested that the esterified lignin could be a green alternative to replace petroleum-based fillers in thermoplastics[159,161,169] as well as being a potential photosensitizer.[171] Esterification has also promoted lignin's application as an oxygen and water-vapor barrier in the packaging.[172] However, esterification was observed to reduce the antioxidant activity of lignin, which may be due to lowering its phenolic hydroxy groups.[61]

Table 2.11. Esterification of lignin.
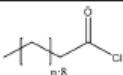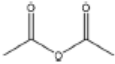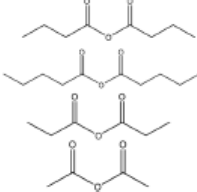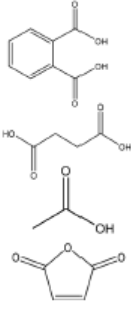
Lignin source/type	Reaction conditions Time (h)	Temperature (°C)	pH	Reagent	Solvent/Catalyst	Separation	Property improvement	Yield (%)	Application	Ref.
Organosolv	2	20	N/A	(acyl chloride structure, n:8)	N,N,1-Dimethylformamide/pyridine	Filtration and ethanol	Hydrophobicity	N/A	As a dispersant and a protective agent	173
Pulp and paper industries	0.6	80	N/A	(acetic anhydride structure)	Pyridine	HCl	Molecular weight	122	Mold lubricant	164
Organosolv	3	100	N/A	(anhydride structures)	Pyridine containing 4-dimethylaminopyridine	Water or diethyl ether	Strength	N/A	Blend with poly(ε-caprolactone)	163
Organosolv	6	70	N/A	(phthalic acid, succinic acid, acetic acid, maleic anhydride structures)	Tetrahydrofuran	Methanol and filtration	Surface area, pore volume	~36–46	Lignin-based carbons	158
Kraft	5	100	N/A	(maleic anhydride structure)	Triphenyl antimony	Acetone	Thermal stability	N/A	N/A	153

Table 2.11. (*Contd.*)
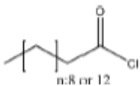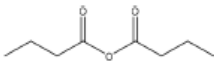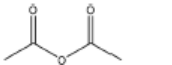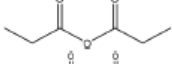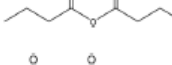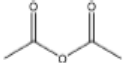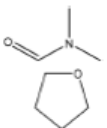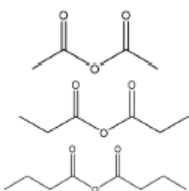
Lignin source/type	Time (h)	Temperature (°C)	pH	Reagent	Solvent/Catalyst	Separation	Property improvement	Yield (%)	Application	Ref.
				Reaction conditions						
Softwood and hardwood kraft	20	20–25	N/A	(acyl chloride, n:8 or 12)	Dimethylformamide	Ethanol, Soxhlet extraction in chloroform	Molecular weight	N/A	Oxygen and water vapor barrier	152
Hardwood and softwood kraft	3	50	N/A	(anhydride)	Acetic, and propionic	Filtration	Molecular weight, reduce water adsorption	88–99	Polyethylene blends	160
Softwood kraft	24	65	N/A	(anhydrides)	1-Methylimidazole	Ethanol and centrifugation	Tensile strength, reduced water adsorption	24	Fillers for thermoplastics	161
		95						29		
		120						46		
Organosolv	1	100	N/A	(acetic anhydride)	Pyridine	N/A	Solubility	~96	N/A	174
Softwood kraft	48	65	N/A	(dimethylformamide, tetrahydrofuran)	Pyridine	Soxhlet extraction using tetrahydrofuran	T_g and melt torque reduced	60–80	Thermoplastic	159
Hardwood kraft	Overnight	20–25	Alkaline	(anhydrides)	Water	Acetone and filtration	Compatibility of lignin	86	Polyethylene blends	168

Table 2.11. (*Contd.*)
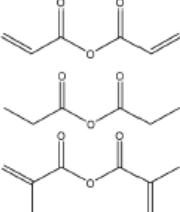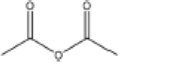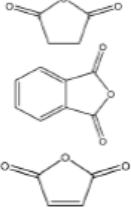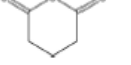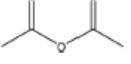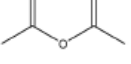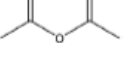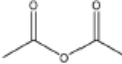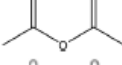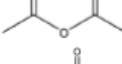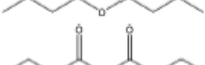
Lignin source/type	Time (h)	Temperature (°C)	pH	Reagent	Solvent/Catalyst	Separation	Property improvement	Yield (%)	Application	Ref.
Hardwood and softwood kraft	Overnight	50	N/A	(structures)	1-Methylimidazole/1,4-dioxane	Ethyl ether	Solubility in non-polar solv, molecular weight	N/A	Use in unsaturated thermosets	169
Enzymatic hydrolysis	1.5	80	N/A	(structure)	4-Dimethylamino pyridine, sodium acetate, and sulfuric acid	Ethanol	N/A	N/A	N/A	155
Kraft	7	60	N/A	(structures)	Acetone	Filtration, water or toluene	Hydrophobicity, molecular weight, thermal stability	N/A	Reinforced wood plastic composites	175
Bagasse	4	90	N/A	(structure)	1-Allyl-3-methylimidazolium chloride	Ethanol	Surface adhesion compatibility	N/A	N/A	132
Sugarcane bagasse	72	20–25	N/A	(structure)	Pyridine	Filtration, water	Radical scavenging index decreased	N/A	Antioxidant	61
Synthetic	48	30	N/A	(structure)	Pyridine	HCl, centrifugation	Secondary cinnamaldehydes prohibited	N/A	N/A	176
Kraft	48	N/A	N/A	(structure)	Pyridine	Methanol	Molecular weight decreased	N/A	Chromatographic eluent	177

Table 2.11. (*Contd.*)

Lignin source/type	Time (h)	Temperature (°C)	pH	Reagent	Solvent/Catalyst	Separation	Property improvement	Yield (%)	Application	Ref.
Alkaline soda	18	20–25	N/A	(structure)	Pyridine	Ethanol, or HCl	Thermal stability decreased	N/A	In polyolefins	157
Organosolv	48	25	N/A	(structure)	Pyridine	Filtration	Solubility in tetrahydrofuran	N/A	Photosensitizers	171
Hardwood	N/A	N/A	N/A	(structure)	Dioxin	N/A	Photodiscoloration behavior under decreased	77	Studying photoyellowing properties	162
Organosolv	3	60	N/A	(structure)	1-Methylimidazole	n-Hexane	Viscosity decreased	N/A	Additive for plasticizing	165
Hardwood kraft	N/A	50	N/A	(structure)	1-Methylimidazole	Ethyl ether	Flexural strength, viscosity	N/A	Resin and flax fibers	156
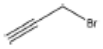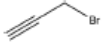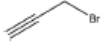
N/A: not available.

2.3.10 Propargylation

Propargylation takes place by adding a propargyl group to a molecule. Lignin propargylation occurs via an S_N2 mechanism, as shown in Fig. 2.1. This reaction occurs only on the phenolic hydroxy groups of lignin since these groups have a higher ionization efficiency compared to aliphatic ones.[41,147]

Table 2.12 shows the propargylation reaction on lignin carried out in the previous studies. In propargylation, lignin is mixed with propargyl containing bromide and NaOH or KOH at 70–90 °C for 1–4 h in an alkaline environment.[41,178] Then, the generated product is separated by acidifying the reaction mixture.[41,178] Lignin propargylation increases the reactivity of lignin in a uniform and modulated way, thus increasing the potential use of the propargylated lignin in carbon fibers.[147,178] According to the US Department of Energy, using propargylated lignin in carbon fibers would reduce the final price of carbon fibers by half.[179] Similarly, propargylated lignin has been reported to be used in transportation applications such as tire production and composite production as the curable thermosetting resin.[178] However, using propargyl bromide can be considered as the main problem of this modification because it is toxic and may cause environmental issues.

Table 2.12. Propargylation of lignin.

| Lignin source/type | Reaction conditions | | | | | Separation | Property improvement | Yield (%) | Application | Ref. |
	Time (h)	Temperature (°C)	pH	Reagent	Solvent					
Kraft	1	90	13.7		Potassium hydroxide	HCl	Molecular weight	N/A	Carbon fiber, tires	178
Paper factory	4	70	Alkaline		Water/ethanol	Filtration	Solubility, thermal properties	98	Resin for composite matrix	180
Softwood kraft	2	75	Alkaline		Water	Acidification	Thermal stability, molecular weight	91–96	To increase thermal stability	41
Methylated softwood kraft	2	75	Alkaline		Water	Acidification	Molecular weight	N/A	Carbon fiber	178

N/A: not available.

2.3.11 Methylation

Methylation reaction is the addition of a methyl group ($-CH_3$) to lignin. The methylation of lignin occurs by nucleophilic aromatic substitution (Fig. 2.9). Under alkaline conditions, the lone pair electron of aromatic hydroxide of lignin attacks the carbon of the methyl group. As a result, hydroxy groups are replaced with a methyl group in lignin. Methylation is considered as an alkylation in which a methyl group is exchanged with a hydrogen atom. This reaction had been used to cover the phenolic hydroxy groups to render lignin hydrophobic, or to analyze whether the

desired reaction tends to occur on the phenolic or aliphatic hydroxy groups of lignin. The selective methylation of lignin's phenolic hydroxy groups converts these groups to phenyl methyl ether, which are remarkably less reactive compared to hydroxy groups.

In addition, a carefully controlled and monitored methylation of lignin may reduce lignin's reactivity, which could provide possibilities for its self-polymerization at high temperatures (above 130 °C).[147] However, this radically initiated self-polymerization of lignin could be inhibited entirely by methylating the phenolic hydroxy groups.[181] In methylation, methyl groups replace only phenolic hydroxy groups due to their remarkably higher (about 80 times) ionization efficiency.[123,141]
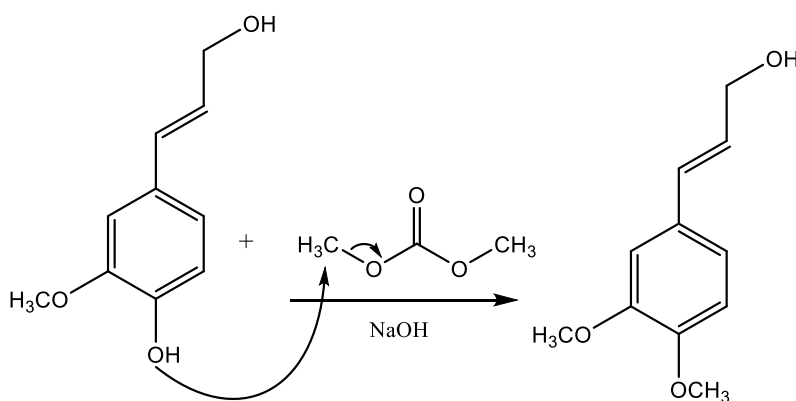
Fig. 2.9. Methylation of lignin by dimethyl carbonate.[181]

Table 2.13 shows the methylation reaction implemented on lignin. In the past, lignin was mixed with dimethyl sulfate, methyl iodide, diazomethane or tetramethylammonium hydroxide in an alkaline medium or it was dissolved in anhydrous N,N-dimethylformamide (DMF) for methylation. The reaction generally occurs at room temperature for 72 h or at 75–150 °C for 2–24 h.[123,141,150,182,183] To collect lignin derivatives, the reaction mixture is acidified, if conducted under the alkaline conditions and purified via filtration, for instance.[123,141] The methylation reduces the glass transition temperature of lignin since most of the intra-molecular hydrogen bonding becomes eliminated in this reaction.[150]

Methylation was reported to enable the use of lignin in thermoplastics and carbon fibers.[141,150] However, methyl iodide and dimethyl sulfate, the most common reagents used for methylation, are very toxic and hazardous, which is the major drawback of this process. One advantage of lignin methylation is that the by-products, methanol and carbon dioxide, could be recycled and reused in the production of dimethyl carbonate.[181,184] Among other reagents, dimethyl carbonate has the

supremacy of safe and straightforward handling since it is not mutagenic or hazardous. However, the chemical reactivity of dimethyl carbonate depends on the temperature in a way that at a temperature higher than 120 °C, it participates in methylation reaction via a base mediated alkyl cleavage nucleophilic substitution mechanism, and at a lower temperature (e.g., 90 °C), it can act as a carboxymethylating agent via a base mediated acyl cleavage nucleophilic substitution mechanism.[181] Therefore, to use dimethyl carbonate as a methylating agent, the reaction temperature needs to be higher than 120 °C, and since this temperature is higher than the dimethyl carbonate's boiling point (90 °C), the reaction has to be carried out in a closed reactor and pressurized system.[181]

Table 2.13. Methylation of lignin.

Lignin source/type	Reaction conditions				Solvent	Separation	Property improvement	Yield (%)	Application	Ref.
	Time (h)	Temperature (°C)	pH	Reagent						
Milled wood	72	20–25	Acidic		Methanol and hydrochloric acid	N/A	N/A	N/A	Mask phenolic hydroxide groups	182
Lignosulfonate	2	80	11–11.5		Water	HCl	Molecular weight	N/A	Mask phenolic hydroxide groups	123
Softwood and hardwood kraft	2, 10	25, 80	Alkaline		N,N-Dimethylformamide	HCl	Molecular weight	N/A	Mask phenolic hydroxide groups	141
Softwood kraft	2–24	120 and 150	Alkaline		Dimethyl sulfoxide	HCl	T_g decreased	N/A	N/A	181
Softwood kraft	2	75	Alkaline		Water	HCl	Molecular weight, T_g	N/A	N/A	150
Softwood kraft	2	75	Alkaline		Water	HCl	N/A	N/A	Carbon fiber	178

N/A: not available.
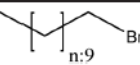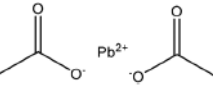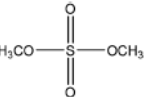
2.3.12. Alkylation

Alkylation introduces an alkyl group ($-C_nH_{2n+1}$) to a lignin macromolecule via the S_N2 mechanism (Fig. 2.1). Lignin can be readily alkylated through nucleophilic substitution on its active aromatic hydroxy groups with an alkyl chain having different chain lengths.[42] It has been reported that the alkylation reaction increases the thermal resistance of lignin while reducing its

hydrophilicity.[42,181,185] Alkylated lignin could be used as a plasticizer in polymer blends.[186] It was also used in polypropylene composites along with synthetic polymers and it was reported to improve the composite's stiffness and storage moduli.[181,185,187]

Table 2.14 shows the alkylation reaction of lignin. In general, bromododecane or lead acetate, as the alkylating agent, can be mixed with lignin at pH 8–12 at 25 or 80 °C for 24–72 h in isopropanol, water, and dioxane as a solvent.[42,185] As a drawback, alkylated lignin could be quite brittle, which might not be favorable in polymer blends.[188]

Table 2.14. Alkylation of lignin.

Lignin source/type	Reaction conditions				Solvent	Separation	Application	Ref.
	Time (h)	Temperature (°C)	pH	Reagent				
Unbleached hardwood kraft	24	80	8–10	(structure, Br, n:9)	Isopropanol	Water	Retardant and toughening agent for polypropylene	185
Pulping industry	N/A	50	N/A	(structure, Pb²⁺)	Distilled water	Filtration, water	Surfactants	42
Kraft	72	20–25	11–12	(structure, H₃CO—S—OCH₃)	Dioxane	Water, centrifuged	Plasticizer	186

N/A: not available.

2.3.13. Halogenation

Halogenation is a method used for introducing a halogen group into the lignin molecule. The halogenation of lignin occurs by electrophilic aromatic substitution. As an example of halogenation, Fig. 2.10 shows the bromination reaction of lignin with bromine in a hydrophilic (polar) protic solvent of acetic acid. Halogenation has been reported to occur on the aromatic ring of lignin since the aromatic hydroxy group could activate the adjacent positions for the electrophoretic attack.[189]
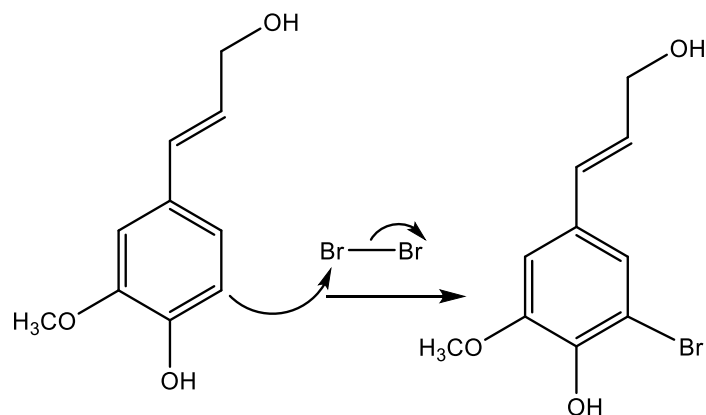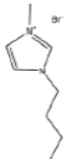
Fig. 2.10. Bromination reaction on lignin by using bromine.[191]

Table 2.15 shows the halogenation reactions of lignin. Typically, lignin is mixed with a halogen (hydrogen bromide, N-bromosuccinimide, and an ionic liquid, liquid chlorine) in the temperature range of 20–164 °C for 1–2 h.[189–191] Halogenated lignin can be precipitated using a mixture of diethyl ether and ethyl acetate.[191]

Bromination of lignin was reported to restrict lignin's agglomeration.[192] Meanwhile, halogenated compounds are intensively used as fungicides, herbicides, insecticides, and precursors in the synthesis of pesticides. They could also be used as intermediates in the synthesis of dyes, agricultural chemicals and pharmaceuticals.[193] As is well-known, the reagents used in halogenation have different levels of reactivity. For example, chlorine and halogen fluorine are the most aggressive reagents compared to bromine[194] due to their high electrophilicity while bromine is a weaker reagent, and iodine is classified as the least reactive reagent of the halogens. It is advised that the chlorination reaction should be carried out with caution due to toxicity issues, which may require additional control. Furthermore, fluorination is mostly used in the production of fluorocarbons.[194] Since halogenated organics are highly toxic, the halogenation process has serious disadvantages, which requires health caution.[195]

Table 2.15. Halogenation of lignin

| Lignin source/type | Reaction conditions | | | | | | | |
	Time (h)	Temperature (°C)	pH	Reagent	Solvent	Separation	Application	Ref.
Hardwood and softwood	2	163–164	N/A	Br–Br	Glacial acetic acid	N/A	N/A	191
Hydrolysis	1	20	N/A	Br–Br	Carbon tetrachloride and water	Water	N/A	190
depolymerized	N/A	20–25	N/A		1-Butyl-3-methylimidazolium bromide	Diethyl ether and ethyl acetate	Surfactant	189

N/A: not available.

2.3.14. Amination

Amination is a simple method for introducing amine groups onto lignin. This reaction occurs through the S_N2 route (Fig. 2.1). Generally, the amination reaction has been applied to lignin with the aim of generating cationic surfactants, slow-release fertilizers, flocculants, heavy metal adsorbents, coagulants, cationic asphalt emulsifiers, curing agents of epoxy resin, anion-exchange resins and retention aids.[108,112,196–201] Lignin amination could enhance the surface activity, water solubility, charge density and molecular weight of lignin.[69,202]

Logically, introducing nitrogen-containing groups into lignin can render lignin an efficient adsorbent for heavy metals. This phenomenon arises since the nitrogen-containing bases tend to chelate with acidic metallic ions.[203,204]

Table 2.16 shows the amination reactions of lignin. Generally, lignin is mixed with amination agents, such as diethylenetriamine, dimethylamine, methylamine, propane diamine, and triethylamine in water or a solvent, such as formaldehyde or dioxane, in the temperature range of 20–90 °C under both acidic and alkaline conditions for 1–17 h. Produced aminated lignin samples can be precipitated via mixing the reaction mixtures with hydrochloric acid, acetone, ethyl acetate or isopropanol.[189] Although inducing amine groups on lignin through amination reaction is selective and straightforward, using the toxic, carcinogenic and mutagenic chemical of formaldehyde in most of the reactions can be unsafe and cause environmental problems.

Table 2.16. Amination of lignin.
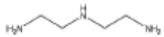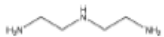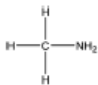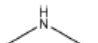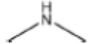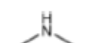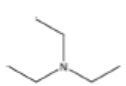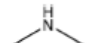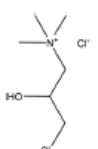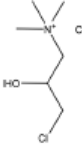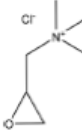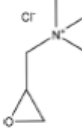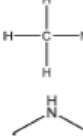
Lignin source/type	Reaction conditions Time (h)	Temperature (°C)	pH	Reagent	Solvent	Separation	Property improvement	Yield (%)	Application	Ref.
Epoxidated	3	80	Alkaline	H_2N–...–NH_2 (diamine)	Formaldehyde	Filtration and water	N/A	N/A	Heavy metal adsorbent	197
Oxidized	5	90	10	H_2N–...–NH_2 (diamine)	Formaldehyde	Filtration	N/A	N/A	Heavy metal adsorbent	60
Alkaline	2–6	40–90	8–13	H–C(H)(H)–NH_2	Water	HCl	Molecular weight, nitrogen content	N/A	Lead removal	108
LignoBoost	4	60	Acetic	dimethylamine	Dioxane, and formaldehyde	Membrane dialysis	Molecular weight, nitrogen content	N/A	Surfactant and slow-release fertilizers	196
Epoxidated	4–6	80	Alkaline	H_2N–R–NH_2	Water	Acetone	Decomposition temperature decreased	N/A	Curing agents of epoxy resin	112
Carboxylated	3	80	Alkaline	dimethylamine	Water	Membrane dialysis	Removing both anionic and cationic dyes	N/A	Flocculant	205
Sulfuric acid treated	4–48	50	Acetic	dimethylamine	Formaldehyde, and dioxane	Ethyl acetate	Solubility	~0.6–63	Retention aid	199
Kraft	1	20–25	N/A	triethylamine	Formaldehyde	Filtration and isopropanol	N/A	97	Coagulant in wastewater	198
Enzymatic hydrolysis	2	20	3	dimethylamine	Formaldehyde, and acetone	Membrane dialysis	Efficiency in higher pH	N/A	Flocculant for anionic azo dyes	201
Sulfonated	4	85	12	quaternary ammonium Cl⁻, HO–, Cl–	Water	Membrane dialysis	Hydrophilicity	N/A	Enhanced the enzymatic hydrolysis of lignocellulose	206

Table 2.16. (*Contd.*)

Lignin source/type	Reaction conditions				Solvent	Separation	Property improvement	Yield (%)	Application	Ref.
	Time (h)	Temperature (°C)	pH	Reagent						
Lignosulfonate	4	85	12		Water	Membrane dialysis	Fluidity	N/A	Clay-tolerance sacrificial agent	207
Softwood kraft	1	70	12.5		Water	Membrane dialysis	Solubility, charge density	N/A	Flocculant for dye removal	208
Hardwood organosolv, and enzymatic hydrolysis	20	60	Alkaline		Water	Dialyzed	Solubility	N/A	Removal of sulfate, kaolin, and humic acid	209
Sulfuric acid treated	4–72	60	N/A		Formaldehyde	Membrane dialysis	Brightness of the paper	78–90	Retention aid in papermaking	200

N/A: not available.

2.3.14 Oxidation

Recently, the oxidation of lignin has become popular because of the extensive need for replacing fossil fuel feedstock with sustainable materials to produce fuels and chemicals. Oxidation occurs through the electron loss of a molecule. In lignin oxidation, the cleavage of C–O bonds occurs leading to the generation of carboxylic acids and aromatic aldehydes.[210] The type of catalyst used in the oxidation reaction is responsible for its low molecular weight reduction or phenolic product generation.[210–212]

It is worth mentioning that the reaction pH plays a critical role in lignin oxidation. In one study,[212] hydrogen peroxide was used to oxidize lignin under both acidic and alkaline conditions. As a result of the reaction under acidic conditions, formic acid and acetic acid were produced as the main components, while no aromatic acids, aldehydes, chromophoric groups, and phenolic components was detected.[212] However, in an alkaline environment, lignin with a high amount of carboxylic acid was produced along with oxalic, formic, acetic, malonic, and succinic, as well as vanillin, syringaldehyde, and chromophoric groups. These chromophoric groups also undergo a ring cleavage reaction and further degradation to form low molecular weight acids. Interestingly,

reactions conducted under strong alkaline conditions proceed at low temperatures of 80–90 °C, while those under acidic conditions need higher temperatures of 130–160 °C.[212] That being said, most of the oxidation reactions have been performed in an alkaline environment since it helps solubilize lignin and accelerates the deprotonation of hydroxy groups.[211,212]

2.3.14.1 Harsh oxidation

In a severe oxidation reaction, the lignin's aromatic ring is destroyed, and acids with low molecular weight are produced.[211] The oxidation reaction depolymerizes lignin via cleavage of C–O and C–C bonds. Comparing these linkages, it is harder to break the linkages in C_α–C_β since the bonding energies in C_α–C_β (264.3–294.2 kJ mol^{-1}) linkages are stronger than those in C_β–O (161.1–247.9 kJ mol^{-1}) linkages.[213–216] Due to the non-polarity and robustness of the C–C bond, its selective cleavage is a challenge.[216] Table 2.17 shows the oxidation reaction on lignin that results in ring opening products. A wide range of reagents were used to oxidize lignin, such as hydrogen peroxide (H_2O_2) (in acidic medium),[212,217] nitrobenzene and copper oxide[218] and oxygen.[197,219–221] The reaction time and temperature have been reported to vary between 2–20 h and 80–160 °C, respectively, while the pressure of the reaction systems is mostly reported to be 10 bar.[212,218]

Lignin oxidation by the aliphatic and aromatic hydroxy groups of lignin leads to the generation of ketones, quinones, aldehydes, vanillin (shown in Table 2.17).[7,222,223] Also, some of the most advanced oxidative routes are used in pulp and paper industries to depolymerize or remove lignin from cellulosic materials.[224,225]

Based on the literature reports,[226,227] a correlation could be found between the resulting product and the oxidative breaking of specific linkage. Fig. 2.11 depicts this correlation under aerobic oxidation conditions. As depicted, the cleavage of the C_α–C_β bond forms phenolic aldehydes, while C_{ph}–C_α bond cleavage leads to the generation of para-quinones and oxirane structures. The cleavage of the lignin aromatic ring also yields the production of muconic acid derivatives.[226,227]

para-quinones
and oxirane

C_{Ph}-C_α
Cleavage

C_α-C_β
Cleavage

Aromatic aldehydes

Ring cleavage

Derivatives of muconic acid

X= OMe
Y= H, OEt, OH
Z= H, OMe
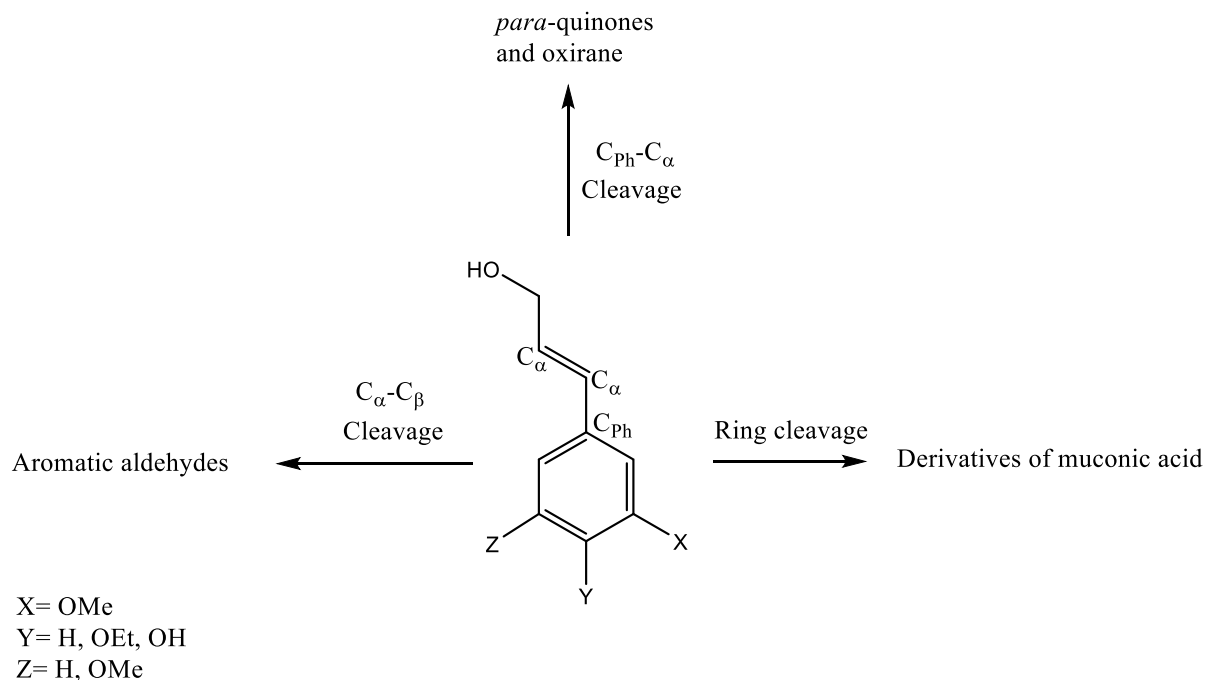
Fig. 2.11. Potential bond cleavage pathways in lignin aerobic oxidation.[226,227]

Meanwhile, aromatic aldehydes, such as vanillin, could be the main product of lignin oxidation.[228] Vanillin is the only mercantile product achieved from lignin through oxidation with a market volume of around 20 000 tonnes per year. Nonetheless, a majority (90%) of the synthetic vanillin used today is oil-based implying a need to improve and develop the lignin-based vanillin production, which is closer in flavor/taste to natural vanilla than vanillin produced from petrochemical guaiacol.[8] However, these oxidation pathways are accompanied by some disadvantages, such as long reaction times and use of toxic catalysts, such as sodium periodate or palladium chloride.[229,230]

Table 2.17. Harsh oxidation reaction on lignin
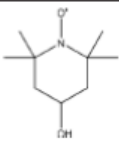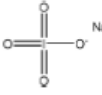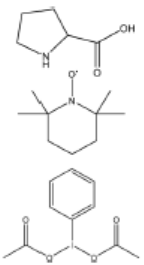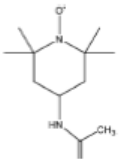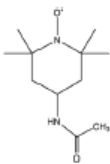
| Lignin source/type | Reaction conditions | | | | Oxygen pressure atm | Solvent | Separation | Remark | Yield (%) | Ref. |
	Time (h)	Temperature (°C)	pH	Catalyst						
Organosolv beech wood	1.5–3	N/A	N/A		1	Water	Ethyl acetate	Formation of quinones and phenol derivatives	N/A	231
Precipitated hardwood	0.08–0.016	95–160	Acidic	HO–OH	N/A	H_2SO_4	H_2SO_4	Formic acid and acetic acid	41	212
Alkali	0.15–2	20	N/A		N/A	Acetic acid	N/A	N/A	N/A	229
Organosolv beech wood	5	20–25	N/A		N/A	Acetonitrile-d3	Filtration	One-pot two-step reaction	N/A	231
Eucalyptus black liquor	2	150–190	Alkaline	Cu^{2+}, Co^{2+}	10–15	Water	N/A	Phenolic compound production	3.5	211
Aspen	12–48	110	Acidic		2	HNO_3, CH_3CN, HCl, water	Evaporation	Two-step reaction	N/A	232

60

Table 2.17. (*Contd.*)

| Lignin source/type | Reaction conditions | | | | | | Separation | Remark | Yield (%) | Ref. |
	Time (h)	Temperature (°C)	pH	Catalyst	Oxygen pressure atm	Solvent				
Curaua fibers and sugar cane bagasse	0.5	55	N/A	O=Cl=O	N/A	CH_3COOH	Centrifuging and water	Lower molecular weight products. Elimination of quinones	N/A	233
Kraft	1	450	N/A	TiO_2, Ta_2O_5–IrO_2	N/A	Ethanol–isopropanol	N/A	Lower molecular weight products	N/A	223
Softwood and hardwood	0.5–12	100	N/A	Polyoxometalate, and HO–OH	N/A	Water	N/A	Vanillin and syringaldehyde	5	7
Softwood and hardwood kraft	0.08–4	90–110	Alkaline	O_2	~5.9–8.8	Water	HCl	Lower molecular weight products	N/A	220
Softwood kraft	0.5	95	Alkaline	Fe^{3+}	~9.8	Water containing Fe^{3+}	H_2SO_4	Lower molecular weight products and vanillin	20	219
Organosolv	40	135	N/A	(HTc) and $V(acac)_3$/Cu$(NO_3)_2 \cdot 3H_2O$	9.8	Pyridine	N/A	Veratraldehyde and veratric acid	22–30	234
Softwood kraft	N/A	150	14	O_2	~9.8	Water	N/A	Vanillin	~3.5–8	235
Softwood	N/A	160	13	$CuSO_4$	~1.9	Water	N/A	Vanillin	N/A	217
Poplar, maple, and maize	28	65	Acetic		2	HNO_3, CH_3CN, HCl	Evaporation	Low-molecular-weight aromatics	N/A	236
Hydrolyzed	N/A	80	Acidic	HO–OH	N/A	Sulfuric acid	Filtration and acidification	Forming soluble fraction of oxidized hydrolyzed lignin	22–78	237
Sugar-cane	N/A	~99.8–139.8	N/A	$PdCl_2$, and γ-alumina	~1.9–9.8	Water	N/A	Aromatic aldehyde	12	221
Soda	10–120	N/A	Acidic	HO–OH	N/A	Water	Filtration	More carboxylic groups rather than ketones or aldehydes	N/A	238

N/A: not available.

2.3.14.2 Mild oxidation

Mild oxidation of lignin introduces carboxylic acid groups into lignin and does not necessarily depolymerize lignin.[239] In this paper, the oxidation that reduced the molecular weight of lignin by less than 10% is considered mild. Undoubtedly, increasing the amount of carboxylate groups in lignin improves its anionicity and hydrophilicity.[211,239] This reaction has been performed by using hydrogen peroxide (in alkaline medium),[57,240] nitrobenzene,[218] metal oxides,[218] and catalysts with oxygen.[211]

Hydrogen peroxide is widely available in pulp mills and is extensively used for bleaching pulp worldwide. As an oxidant, it can also be used for oxidizing lignin to introduce carboxylate groups. It is reported that hydrogen peroxide generally decomposes the phenolate group of lignin, whereas it induces the carboxylate group into lignin.[42,240,241] It was reported that the majority of hydrogen peroxide molecules was utilized for the partial decomposition of the lignin structure by the bond cleavage of lignin's ether bonds.[240]

Fig. 2.12 shows the mild oxidation by using different sources of lignin and oxidizing reagents. Lignin undergoes two different reaction sets in lignin oxidation with hydrogen peroxide;

perhydroxy anions attack nucleophilically while removing lignin chromophores. Meanwhile, free radical species generated by the decomposition of hydrogen peroxide yield oxidative degradation of the phenolic structures of lignin and converts them to carboxylic acid groups.[242] The perhydroxy anion cleaves the side chains of lignin, opens the benzene ring, and produces new compounds, which have carboxylate or chromophore groups.[212,242,243] These groups may undergo the ring cleavage reaction under severe reaction conditions and further degrade to form different low molecular weight compounds, such as oxalic acid, formic acid, and malonic acid.[212]
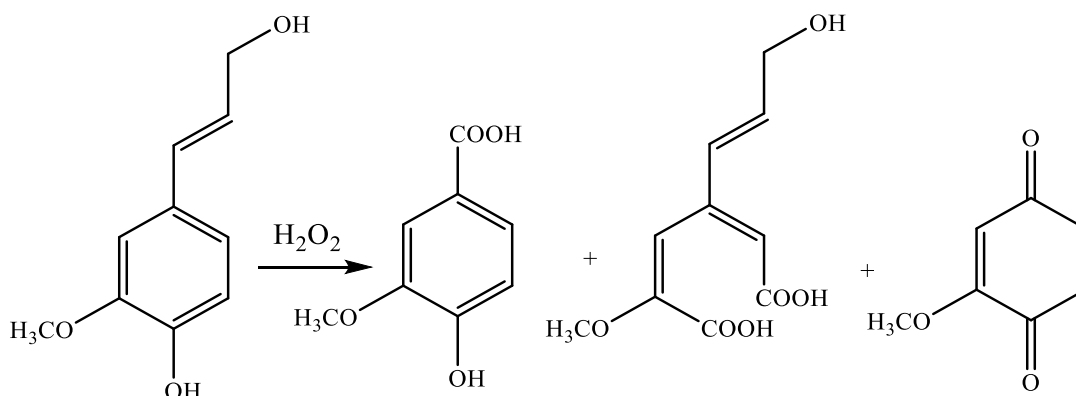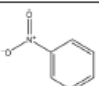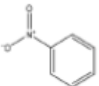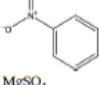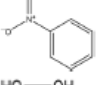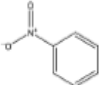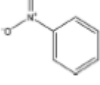
Fig. 2.12. Mild oxidation of lignin by hydrogen peroxide under alkaline condition.[240]

The oxidation of lignin via hydrogen peroxide would promote the solubility and increase the charge density of lignin, and therefore it could be used as an anionic dispersant for kaolin and other suspensions.[240] Employing nitrobenzene to oxidize lignin generates aromatic aldehydes as main products; however, using nitrobenzene have some disadvantages, such as difficulties in recovering the oxidant as well as the complexity of the reaction raised from the formation of phenylhydroxylamine, aniline, and nitrobenzene products, leading to a condensation among them. Also, the respective carboxylic acids produced in mild oxidation have lower yields than in harsh oxidation.[218]

Oxygen, Cu(II), Co(II), and CuO have also been used to oxidize lignin (Table 2.18). Protolignin oxidation with CuO has claimed to have a lower yield compared with nitrobenzene as the oxidant.[218,244,245] Co(II) is a better oxidant than nitrobenzene, as the oxidant recovery is easier and harmful byproducts are not produced in the reaction.[246] Although oxygen (or air) as a catalyst will not contribute significantly to the oxidation cost, it has lower selectivity and produces low molecular weight acids.

Generally, although the mild oxidation pathways could be affordable, they are not effective in significantly altering the hydrophobicity of lignin.[239] Therefore, the lignin-based materials produced in some pulping and biorefining processes may need a stronger oxidizing agent.[42,247]

Table 2.18. Mild oxidation of lignin.

Lignin source/type	Reaction conditions						Separation	Remark	Yield (%)	Ref.
	Time (h)	Temperature (°C)	pH	Catalyst	Oxygen pressure atm	Solvent				
Proto Alkali	2.5	170–180	Alkaline	Nitrobenzene	N/A	Water	N/A	Product ratio depends on the material source	Syringaldehyde 36%, vanillin 15% Syringaldehyde 25%, vanillin 10%	244
Hardwood	N/A	80–160	Alkaline	HO–OH	N/A	Water	N/A	Lower molecular weight products	30–50	212
Calcium lignosulfonate	1.5	80	9	HO–OH	N/A	Water	N/A	Foam height and half-life decreased	N/A	57
Eucalyptus black liquor	2–2.30	150	Alkaline	Cu(II), and Co(II)	10–15	Water	N/A	Lower phenolic aldehyde compared to other lignin oxidants CuO and nitrobenzene	4	211
Eucalyptus black liquor	2–4	170–190	Alkaline	Nitrobenzene	N/A	Water	N/A	Nitrobenzene is more effective than copper(II) oxide	15–18% by using nitrobenzene, 7–8% by using CuO	218
Alkali Thio	2	180	Alkaline	Nitrobenzene	N/A	Water	Filtration	Product ratio depends on the material source	Vanillin 17% Vanillin 6.6%	248
Softwood kraft	1	78–110	Alkaline	MgSO$_4$	2.72	Water	Water	Increase in tensile strength	43–50	249
Proto Alkali	4	160	Alkaline	Nitrobenzene	N/A	Water	N/A	N/A	Vanillin 4% Vanillin 3%	245
Sugar cane, red spruce kraft, and hardwood organosolvent	N/A	20–25	N/A	HO—OH / Re=O	N/A	Acetic acid	Filtration	Increase in carboxylic acid content	98	243
Softwood kraft	1–3	60–100	Alkaline	HO–OH	N/A	Water	Membrane	Decrease in molecular weight, increase in charge density and degree of the carboxylate group. Dispersant for kaolin suspensions	N/A	240
Proto	3	160	Alkaline	Nitrobenzene	N/A	Water	Filtration	Half of lignin combined through C–C linkages	Syringaldehyde 13%, vanillin 8.5%	250
Native Alkali	2	180	Alkaline	Nitrobenzene	8.9	Water	Filtration	N/A	Vanillin 25% Vanillin 14%	251

N/A: not available.
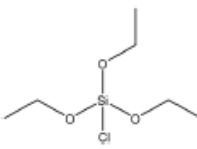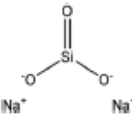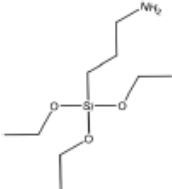
2.3.15 Silylation

Silica can be introduced on both phenolic and aliphatic hydroxy groups of lignin[252] under an S_N2 reaction mechanism (Fig. 2.1). Silica and derivatives of silane have been used as flame retardants. Dissimilar to carbon-based polymers, silicas generate inorganic silica under combustion. Silica residues could hamper fire deployment by restraining mass and heat transfer. Basically, no toxic emissions are produced from the combustion of silicas.[253,254] Hence, silica foams are highly favorable to be used in applications, such as construction building (e.g., acoustic designs). Lignin–silica products have been used as gaskets, sealing materials, metal and organic adsorbents, as well as adsorbents for heavy metal ions and dyes.[43,252,255] They have also been reported as effective

electrochemical sensors, polymer fillers,[252] and biosorbents for removing toxic substances from aqueous solutions.[42,252,255]

Table 2.19 shows the grafting of various silica on lignin. This reaction is generally conducted by introducing reagents including tetraethyl orthosilicate, silicon dioxide, sodium metasilicate, and tetraethoxysilane into lignin in a solvent (pyridine, ethanol, water, and dioxane) environment at 25–35 °C for 1.5 to 24 h. Although the lignin–silica reaction is popular in producing composites, these reactions are associated with drawbacks. For example, the two-step method used to produce lignin/silica composites intensely agglomerates composite particles. Also, the consumption of surfactants and various costly coupling agents in the preparation process of lignin/silica composites makes this process complicated and costly. Thus, there is a need for the expansion of a one-pot method for the lignin/silica composites' preparation, mainly in aqueous media.[256]

Table 2.19. Lignin-silica reaction.

Lignin source/type	Reaction conditions			Reagent	Solvent	Separation	Property improvement	Yield (%)	Application	Ref.
	Time (h)	Temperature (°C)	pH							
Alkali	24	20–25	N/A		Pyridine	Pyridine	Thermal stability, surface area	N/A	Wastewater treatment	43
Magnesium lignosulfonate	1.5	N/A	N/A	O=Si=O	Water	Vacuum evaporator	Thermal stability	N/A	Polymer filler, and metal adsorbent	252
Quaternized alkali	4	35	Alkaline		Ethanol and water	Water	UV-absorption ability, mechanical properties	N/A	Blend with polyurethane films	256
Ultrafiltered LignoBoost kraft	24	N/A	Acetic		Dioxane and water	Ethanol and water	Thermal stability surface area	N/A	Sorbents for organic molecules	255

N/A: not available.

2.4 Modified lignin's characteristics

2.4.1 Hydrophilic lignin

Lignin is known for its complexity due to having hydrophilic groups attached to its hydrophobic rings. Chemical modifications (e.g., carboxyalkylation and sulfoalkylation) would render it more

hydrophilic.[40,100,175] The applications for hydrophilic lignin products can expand extensively to an adsorbent, stabilizer, and dispersant for emulsions, clay suspensions, coal/water slurry, dye suspensions, and cement admixtures. However, it is mostly favored to be used as a dispersant or flocculant for emulsion and suspension systems.

Various reactions render lignin anionic by introducing a negative charge into its backbone, of which carboxyalkylation, sulfoalkylation, and oxidation are the most common ones. The reaction temperature preferred for performing carboxymethylation, carboxyethylation, and sulfobutylation is mostly below 90 °C, but sulfomethylation is generally carried out at higher temperature (Tables 5–8). In addition, sulfobutylation has mostly been performed in a solvent-free environment, which is highly favorable.

Comparing the reaction routes stated above, while both carboxyalkylation and sulfomethylation are conducted in alkaline media, sulfomethylation seems to be less favorable due to several reasons: (1) an oxidation reaction is suggested to perform prior to sulfomethylation to increase the reaction yield, which is unfavorable since it has a dramatic impact on the performance of the sulfomethylation reaction; (2) the use of formaldehyde in sulfomethylation is a major downside due to its toxicity; and (3) the sulfomethylation reaction is a slow reaction that occurs at high temperature. Carboxyethylation and sulfobutylation have more advantages than carboxymethylation and sulfomethylation, since they grant lignin with a higher anionic charge density stemming from the occurrence of the reaction on both aromatic and aliphatic hydroxy groups of lignin.[110,122,123]

Cationic lignin is produced by the addition of a positively charged group to its backbone. While lignin cationization has not been carried out as extensive as the anionization in the past, producing cationic lignin through amination is a wellknown method of cationization, which further fosters its potential use in various applications, e.g., flocculant, adsorbent, surfactant.[108,196–198]

2.4.2 Hydrophobic lignin

Hydrophobic lignin and its derivatives have a strong interaction with other materials in organic solvents,[12] and are almost insoluble in water. Reactions improving the hydrophobicity of lignin include esterification, alkylation, methylation, epoxidation, propylation, and oxypropylation, as they introduce hydrophobic groups into lignin's structure.

In comparing these reaction routes, while all are mostly conducted under alkaline conditions, alkylation and epoxidation benefit from a relatively lower reaction temperature (below 90 °C). On

the other hand, a broad and high reaction temperature range in oxypropylation (40–285 °C) and prolonged reaction time (72 h) in alkylation, as well as in methylation (if conducted at room temperature) might be the drawbacks of some of these modification pathways. In addition, oxypropylation could render lignin more hydrophobic than esterification,[12] which is favorable for some applications, such as foams and composites.

Although the abovementioned reactions improve the hydrophobicity of lignin, each endows lignin with different features; the thermal resistance of lignin was reported to be improved via alkylation, and thus it promotes the application of alkylated lignin as a plasticizer in polymer blends.[42,181] On the other hand, epoxy lignin was reported to have antibacterial activity,[61] while esterified and methylated lignin were both reported to have a lower glass transition temperature than untreated lignin. Therefore, these reactions make products suitable for thermoplastics, plastic blends and carbon fibers.[150,158] However, none of the mentioned reactions are environmentally friendly, as reagents in these reactions are mostly toxic and carcinogenic.

2.5 Applications for modified lignin

Lignin is a polymer with tremendous potential for its use in various industries. Table 2.20 shows the reactions conducted on lignin for specific applications, as well as drawbacks of lignin properties for the desired applications, which were improved through modification reactions. As seen, various reactions have been carried out on lignin to improve its charge density and solubility/hydrophilicity to be used as a dispersant, such as sulfomethylation for coal–water slurry and concrete admixture, sulfobutylation for coal–water slurry and carbendazim, carboxymethylation for oil–water emulsions, crude bitumen emulsion, clay, cement, and graphite suspensions, halogenation for surfactant, animation of cationic surfactants, and cationic asphalt emulsifier productions.

Phosphorylation, hydroxymethylation, and oxypropylation reactions make modified lignin a good alternative for oil-based polyols used in polyester and polyurethane productions through improving lignin properties, such as tensile strength, molecular weight, viscosity, and glass-transition temperature. In addition, phosphorylation, carboxyethylation, amination, silylation, and sulfomethylation make lignin a polyelectrolyte with applications in aqueous systems by enhancing its selectivity and thermal stability.

Phosphorylation, epoxidation, and amination (curing agents of epoxy resin) increase lignin's molecular weight and thermal stability, which further promote lignin's application in the epoxy resin industry. Epoxy resins possess a wide range of applications, such as flooring, electronic laminates, industrial coatings and adhesives and high-performance composites. However, a slow curing rate, limited water solubility, and brittleness are the negative aspects of lignin-based epoxy resins. Lignin-based adhesives could be produced by hydroxymethylation and epoxidation. They could also be applied to mimic lignin antioxidant and anti-bacterial properties.

Miscibility of the polymers is a critical factor in applications such as polymer blends. Although two polymers' miscibility is not favorable entropically, it could be improved if the polymers involved in blending have intermolecular interactions since the negative enthalpy of mixing overcomes the opposite entropy.[257] Using lignin in polymer blends develops a convenient and powerful pathway to produce novel and functional green materials. It should be stated that polar synthetic polymers generate an intermolecular hydrogen bonding with lignin, while non-polar ones generally generate immiscible blends, showing distinct T_g points for two immiscible phases. In the past, lignin had been used in blending with synthetic polymers.[181] Lignin's phenolic hydroxy groups tend to contribute more in forming hydrogen bonds with other polymers in a blend than its aliphatic ones due to the higher acidity of lignin's phenolic hydroxy group.[257] Previously, alkylation, acetylation, methylation, and esterification of lignin have been carried out to increase the compatibility of lignin with various synthetic polymers in polymer blend applications.

Lignin alkylation and acetylation have reported modulating its chemical and thermal reactivities, which further leads to a thermal improvement in a polymer blend. Comparing alkylated and acetylated lignin with the unmodified lignin, it is found that the thermal stability of the polymer blends was improved when modified lignins were used in blends' composition.[185]

Lignin methylation was also observed to impact the thermal stability of the lignin/polyethylene blend, diminishing the degradation temperature of the polyethylene remarkably. Nevertheless, since the lignin's phenolic hydroxy groups become entirely masked through methylation, the tendency to form intermolecular hydrogen bonding in polymer blends can be reduced significantly.[257]

Lignin esterification was also performed to increase lignin compatibility in polymer blends.[163] On the other hand, the esterified lignin's miscibility strongly depends on the carbon numbers presented in the side chain of the ester in that the miscibility improves with an increase in the ester groups'

chain length. However, the esterified lignin's interaction in a polymer blend might be similar to the methylated lignin's interaction due to the masking of the phenolic hydroxy groups via esterification, hindering the hydrogen bonding development.

Table 2.20. Different reactions conducted for desired applications

Application	Shortcomings of lignin	Reaction	Ref.
Dispersant	Charge density	Sulfomethylation	20, 21, 57, 100, 101, 104 and 107
	Solubility/wettability	Sulfonation	95
		Sulfobutylation	109, 110 and 111
		Carboxymethylation	40, 116 and 120–122
		Carboxyethylation	123
		Oxidation	240
		Esterification	173
		Oxyalkylation	149
Surfactant	Hydrophilicity/phobicity	Halogenation	189
	Molecular weight	Sulfonation	92
		Alkylation	42
		Amination	196
Plasticizer	Charge density	Esterification	159 and 175
	Hydrophilicity	Sulfonation	90 and 91
		Oxyalkylation	150
		Esterification	159
		Alkylation	186
Flame-retardant	Thermal and oxidative stability	Phosphorylation	38, 39, 45, 47, 48, 53 and 139
		Lignin–silica	256
Additive in polyurethane	Tensile strength	Phosphorylation	47
	Glass-transition temperature	Phenolation	77
	Molecular weight	Oxypropylation	136–140, 142–144 and 148
	Viscosity		
Adsorbent of metal ions in wastewater treatment	Selectivity	Phosphorylation	49 and 51
	Thermal stability	Lignin–silica	252
		Sulfomethylation	60
		Amination	60 and 197
Flocculant/coagulant	Molecular weight	Sulfomethylation	105
	Charge density	Amination	198, 201, 205, 208 and 209
Epoxy	Thermal stability	Phosphorylation	46
	Molecular weight	Epoxidation	112 and 125
		Amination	112
Adhesive	Viscosity	Hydroxymethylation	54, 66 and 68–72
	Molecular weight	Sulfonation	88 and 93
Anti-oxidant and anti-bacterial	High radical-scavenging activity	Epoxidation	61
		Sulfonation	96
Resin	Thermal stability	Phenolation	78, 80 and 83
	Cross-linking		

2.6. Current and future trends

Lignin has been used as fuel. The price of lignin as fuel varies between 70–150 USD per ton, which is dependent on its moisture content and contaminants.[258] Two technologies have been developed to generate lignin in dried powder forms. Lignoboost™ that has been implemented at Stora Enso, Sweden, with the production capacity of 50 000 ton per year, and Domtar, NC, USA with the production capacity of 25 000 ton per year. Lignoforce™ has also been commercialized at West Fraser Inc, AB, Canada, with the production capacity of 30 t per day. The production of lignin in such quantities will undeniably pave the way to generate lignin derivatives at commercial scales. Table 2.21 shows the addressable markets of lignin-based products. This table also comprises the estimated market values and capacities as well as the price of the lignin or fossil-based products.

As seen, there are products, such as vanillin and phenol, which have been commercially available since 1933 and 2015, respectively, with lower or equal prices to their fossil-based counterparts. Lignin-based carbon fiber is also estimated to be produced commercially in 2020–2025.

Table 2.21. Markets of lignin-based products

Industrial products from lignin	Est. total market value per year (billion dollar)	Est. scale produced per year (lignin-based) (MTon)	Est. lignin-based price ($ per kg)	Est. fossil-based price ($ per kg)	Ref.
Carbon fiber	4.5	N/A	6.5–12	17–26	261 and 262
Phenol	12–15	8	1–1.5	N/A	261–263
Vanillin	0.2	0.016	12	12	261 and 262

N/A: not available.

While the utilization of lignin might seem limited with current technologies, it is anticipated that lignin would be even more available in future due to the production of lignin in commercial processes, such as LignoForce and LignoBoost,[259,260] which can pave the way for its further valorization. Although various modifications have been performed on lignin, there are still some unexplored reactions that could further improve the properties of lignin for different applications. For example, in carboxyalkylation, there is room for carboxypropylation and carboxybutylation of lignin to tune its charge density and hydrophilicity/hydrophobicity. Although sulfomethylation and sulfobutylation reactions have been conducted on lignin, no specific reports have been found in the literature on sulfoethylation and sulfopropylation of lignin, which could be a case of study since different reactions of carboxyalkylation or sulfoalkylation lead to the production of lignin with different properties as they introduce different carbon chain lengths and mimic the hydrophilicity/hydrophobicity of lignin alterably. In the case of oxyalkylation, by far, oxypropylation has been the only reaction carried out on lignin, leaving room for investigating other routes in oxyalkylation.

Generally, the solvent use and recovery impact the operation costs and ultimately the price of lignin derivatives and the environmental footprints of the developed technologies. If solvent use is necessary for lignin modification, the solvent recovery process is an important aspect of the process from finance and environment perspectives. For developing more industrially attractive and environmentally friendly pathways for lignin valorization, non-toxic reagents and chemistry should be discovered. Furthermore, the use of aqueous systems for lignin alteration would help reduce the environmental impacts of any lignin valorization processes.

As mentioned earlier, lignin has been studied in many applications, such as a dispersant, flocculant, adsorbent, and flame retardant (Table 2.20), while biological applications for lignin have been barely touched in the literature. For example, lignin's interaction with organic molecules, such as proteins, antibiotics, bacteria, and viruses could be studied for expanding either lignin-based biomedical applications as well as water and wastewater treatment systems. Using lignin in drug delivery systems, wound dressing, tissue engineering, and pharmaceutical applications could also be investigated. However, proceeding with such applications for lignin requires broad and detailed studies on the toxicity analysis of lignin, which has not been covered extensively as of yet.

2.7 Conclusions

Lignin is the most abundant aromatic polymer in nature, while its utility has been untapped in industry. Thanks to the numerous studies conducted in exploring lignin chemistry and structure over the last few years, the applications of lignin have been growing tremendously. This trend shows the increasing level of enthusiasm and interest of researchers in developing lignin-based applications and more importantly, the replacement of aromatic substances with petrochemical origins. Thus, various modifications have been performed on lignin to alleviate or remove the restrictions in the nature of lignin that limits its applications in industry. Some of these reactions are very promising to improve lignin's reactivity with other materials and compatibility in different environments. This work comprehensively reviewed and compared various modification routes while highlighting the strength and weak points. Despite the reactions mentioned, there is still room for expanding the other possible modification methods. In addition, biological applications of lignin could be studied more extensively to explore further and expand the functionality of this biobased and abundant material. In conclusion, distinguishing the modifications occurring on different parts of lignin, knowing the precise manner of reactions and reaction sites of the modifications, as well as pros and cons of each reaction, can pave the way for understanding and expanding the use of lignin in various processes.

2.8 References

1) L. Shuai, M. T. Amiri, Y.M. Questell-Santiago, F. Heroguel, Y. Li, H. Kim, R. Meilan, C. Chapple, J. Ralph and J. S. Luterbacher, Science., 2016, 354, 329-333.
2) A. Scalbert, C. Morand, Manach and C. Rémésy, Biomed. Pharmacother., 2002, 56, 276-282.

3) G. Janusz, A. Pawlik, J. Sulej, U. Świderska-Burek, A. Jarosz-Wilkołazka and A. Paszczyński, FEMS Microbiol. Rev., 2017, 41, 941-962.

4) J. C. M. S. Moura, C. A. V. Bonine, J. de Oliveira Fernandes Viana, M. C. Dornelas and P. Mazzafera, J. Integr. Plant Biol., 2010, 52, 360-376.

5) J. Perez, J. Munoz-Dorado, T. D. L. R. de la Rubia and J. Martinez, Int. Microbiol., 2002, 5, 53-63.

6) J. Chen, A. Eraghi Kazzaz, N. AlipoorMazandarani, Z. Hosseinpour Feizi. Z and P. Fatehi, Molecules, 2018, 23, 868.

7) G.F.D. Gregorio, R. Prado, C. Vriamont, X. Erdocia, J. Labidi, J. P. Hallett and T. Welton, ACS Sustainable Chem. Eng., 2016, 4, 6031-6036.

8) R. Rinaldi, R. Jastrzebski, M. T. Clough, J. Ralph, M. Kennema, P. C. Bruijnincx and B. M. Weckhuysen, Angew. Chem. Int. Ed., 2016, 55, 8164-8215.

9) M. Alekhina, O. Ershova, A. Ebert, S. Heikkinen and H. Sixta, Ind. Crops Prod., 2015, 66, 220-228.

10) Y. Liu. Y and K. Li, J. Adh. 2006, 82, 593-605.

11) M. Zhou, X. Qiu, D. Yang, H. Lou and X. Ouyang, Fuel Process. Technol., 2007, 88, 375-382.

12) S. Laurichesse and L. Averous, Prog. Polym. Sci., 2014, 39, 1266-1290.

13) V. P. Saraf and W. G. Glasser, J. Appl. Polym. Sci., 1984, 29, 1831-1841.

14) N. Alwadani and P. Fatehi, Car. Res. Con., 2018, 1, 126-138.

15) A.Lourenco and H. Pereira, Lignin: Trends and Applications, InTech, Croatia, 2018.

16) L. Christopher, J. H. Clark and G. A. Kraus, Integrated forest biorefineries, Royal Society of Chemistry, Cambridge, 2012.

17) A. G. Vishtal and A. Kraslawski, BioResources, 2011, 6, 3547-3568.

18) Z. H. Feizi, A. E. Kazzaz, F. Kong and P. Fatehi, Sep. Purif. Technol., 2019, 222, 254-263.

19) D. Tarasov, M. Leitch and P. Fatehi, Biofuels., 2018, 11, 269.

20) M. K. Konduri and P. Fatehi, ACS Sustainable Chem. Eng., 2015, 3, 1172-1182.

21) Y. Qin, D. Yang, W. Guo and X. Qiu, J. Ind. Eng. Chem., 2015, 27, 192-200.

22) M. A. Hubbe, R. Alén, M. Paleologou, M. Kannangara and J. Kihlman, BioResources, 2018, 14, 2300-2351.

23) A. N. Evdokimov, A. V. Kurzin, O. V. Fedorova, P. V. Lukanin, V. G. Kazakov and A. D. Trifonova, Wood Sci. Technol., 2018, 52, 1165-1174.

24) A. M. Upton and A. M. Kasko, Chem. Rev., 2015, 116, 2275-2306.

25) W. Boerjan, J. Ralph and M. Baucher, Annu. Rev. Plant Biol., 2003, 54, 519-546.

26) Z. Sun, B. Fridrich, A. de Santi, A. Elangovan and K. Barta, Chem. Rev., 2018, 118, 614-678.

27) C. Li, X. Zhao, A. Wang, G. W. Huber and T. Zhang, Chem. Rev., 2015, 115, 11559-11624.

28) W. Schutyser, T. Renders, S. Van den Bosch, S. F. Koelewijn, G. T. Beckham and B. F. Sels, Chem. Soc. Rev., 2018, 47, 852-908.

29) V. M. Roberts, V. Stein, T. Reiner, A. Lemonidou, X. Li and J. A. Lercher, Chem. Eur. J., 2011, 17, 5939-5948.

30) J. Zhang, ChemSusChem, 2018, 11, 3071-3080.

31) S. Gharehkhani, Y. Zhang and P. Fatehi, Prog. Energy Combust. Sci., 2019, 72, 59-89.

32) J. Zakzeski, P. C. Bruijnincx, A. L. Jongerius and B. M. Weckhuysen, Chem. Rev., 2010, 110, 3552-3599.

33) S. Gillet, M. Aguedo, L. Petitjean, A. R. C. Morais, A. M. da Costa Lopes, R. M. Lukasik and P. T. Anastas, Green Chem., 2017, 19, 4200-4233.

34) X. Chen, L. Song and Y. Hu, J. Appl. Polym. Sci., 2010, 115, 3332-3338.

35) H. Vothi, Nguyen. C.; Lee. K.; and Kim. J. Polym. Degrad. Stab., 2010, 95, 1092-1098.

36) P. A. Song, L. Xu, Z. Guo, Y. Zhang and Z. Fang, J. Mater. Chem., 2008, 18, 5083-5091.

37) G. L, Bykov, and B. G. Ershov, Russ. J. Appl. Chem., 2010, 83, 316-319.

38) B. Prieur, M. Meub, M. Wittemann, R. Klein, S. Bellayer, G. Fontaine and S. Bourbigot, Polym. Degrad. Stab., 2016, 127, 32-43.

39) G. P. Mendis, S. G. Weiss, M. Korey, C. R. Boardman, M. Dietenberger, J. P. Youngblood and J. A. Howarter, Green Mater., 2016, 4, 1-11.

40) M. K. Konduri. F. Kong and P. Fatehi, Eur. Polym. J., 2015, 70, 371-383.

41) S. Sen, H. Sadeghifar, and D. S. Argyropoulos, Biomacromolecules, 2013, 14, 3399-3408.

42) L. R. Morrow, M. G. DaGue and L. E. Whittington, US Pat., 4 790 382, 1988.

43) R. Saad and J. Hawari, J. Porous Mater., 2013, 20, 227-233.

44) L. Liu, G. Huang, P. Song, Y. Yu and S. Fu, ACS Sustainable Chem. Eng., 2016, 4, 4732-4742.

45) L. Liu, M. Qian, P. A. Song, G. Huang, Y. Yu and S. Fu, ACS Sustainable Chem. Eng., 2016, 4, 2422-2431.

46) A. A Alalykin, R. L. Vesnin and D. A. Kozulin, Russ. J. Appl. Chem., 2011, 84, 1616.

47) L. Ferry, G. Dorez, A. Taguet, B. Otazaghine and J. M. Lopez-Cuesta, Polym. Degrad. Stab., 2015, 113, 135-143.

48) B. Prieur, M. Meub, M. Wittemann, R. Klein, S. Bellayer, G. Fontaine and S. Bourbigot, RSC Adv., 2017, 7, 16866-16877.

49) A. M. Nada, N. F. Kassem and S. H. Mohamed, BioResources, 2008, 3, 538-548.

50) J. Qin, M. Woloctt and J. Zhang, ACS Sustainable Chem. Eng., 2014, 2, 188-193.

51) A. A. M. Nada and M. L. Hassan, J. Appl. Polym. Sci., 2003, 89, 2950-2956.

52) G. B. Quistad, N. Zhang, S. E. Sparks and J. E. Casida, Chem. Res. Toxicol., 2000, 13, 652-657.

53) Y. Yu, S. Fu, P. A. Song, X. Luo, Y. Jin, F. Lu and J. Ye, Polym. Degrad. Stab., 2012, 97, 541-546.

54) Clarke. M. R.; Dolenko. A. J. U.S. Patent. 4.113.675. 1978.

55) A. M. Capraru, V. I. Popa, T. Malutan and G. Lisa, Cellulose Chem. Technol., 2009, 43, 409-418.

56) R. Goncalves and P. Benar, Bioresour. Technol., 2001, 79, 103-111.

57) Y. X. Pang, X. Q. Qiu, D. J. Yang and H. M. Lou, Colloids Surf. A., 2008, 312, 154-159.

58) X. L. Liu, Y. H. Liao, Z. J. Wu, L. F. Cun, X. M. Zhang, W. C. Yuan, J. Org. Chem., 2010, 75, 4872-4875.

59) T. Malutan, R. Nicu, V. I. Popa, BioResources, 2007, 3, 13-20.

60) Y. Ge, Z. Li, Y. Kong, Q. Song and K. Wang, J. Ind. Eng. Chem., 2014, 20, 4429-4436.

61) R. Kaur, S. K. Uppal and P. Sharma, Sugar Tech., 2017, 19, 675-680.

62) R. V. Gadhave, P. A. Mahanwar and P. T. Gadekar, Open J. Polym. Chem., 2018, 8, 1.

63) S. Pietarinen, O. Ringena, K. Eskelinen and S. Valkonen, US Pat., 9 464 219, 2016.

64) P. Benar, A. R. Gonçalves, D. Mandelli and U. Schuchardt, Bioresour. Technol., 1999, 68, 11-16.

65) A.M. Capraru, E. Ungureanu, L. Trinca, T. Malutan and V. I. Popa, Cellul. Chem. Technol., 2012, 46, 589-597.

66) M. E. Taverna, F. Felissia. F, M. C. Area. M, D. A. Estenoz and V. V. Nicolau, J. Appl. Polym. Sci., 2019, 47712.

67) T. Malutan, R. Nicu and V. I. Popa, BioResources, 2008, 3, 1371-13767.

68) E. Ungureanu, O. Ungureanu. A. M. Capraru and V. I. Popa, Cellul. Chem. Technol., 2009, 43, 263.

69) X. Wang, Y. Zhang, C. Hao, F. Feng, H. Yin and N. Si, Ind. Eng. Chem. Res., 2014, 53, 6585-6592.

70) A.Ang, Z. Ashaari, E. S. Bakar and. N. A. Ibrahim, BioResources, 2015, 10, 4795-4810.

71) N. E. E. Mansouri, A. Pizzi and J. Salvado, J. Appl. Polym. Sci., 2007, 103, 1690-1699.

72) H. Younesi-Kordkheili and A. Pizzi, J. Adh., 2017, 14, 1120-1130.

73) F. Zhang, X. Jiang, J. Lin, G. Zhao, H. M. Chang and H. Jameel, New J. Chem., 2019, 43, 2238-2246.

74) A.Effendi, H. Gerhauser and A. V. Bridgwater, Renewable Sustainable Energy Rev., 2008, 12, 2092-2116.

75) X. Jiang, J. Liu, X. Du, Z. Hu, H. M. Chang and H. Jameel, ACS Sustainable Chem. Eng., 2018, 6, 5504-5512.

76) L. Hu, H. Pan, Y. Zhou and M. Zhang, BioResources, 2011, 6, 3515-3525.

77) T. T. M. Tan, Polym. int., 1996, 41, 13-16.

78) N. S. Cetin and N. Özmen, Int. J. Adhes. Adhes., 2002, 22, 477-480.

79) N. S. Cetin and N. Özmen, Int. J. Adhes. Adhes., 2002, 22, 481-486.

80) S. Kamel, Int. J. Polym. Mater., 2005, 55, 283-291.

81) Y. Matsushita and S. Yasuda, Bioresour. Technol., 2005, 96, 465-470.

82) J. Podschun, B. Saake and R. Lehnen, Eur. Polym. J., 2015, 67, 1-11.

83) G. Vazquez, J. Gonzalez, S. Freire and G. Antorrena, Bioresour. Technol., 1997, 60, 191-198.

84) M. Funaoka, M. Matsubara, N. Seki and S. Fukatsu, Biotechnol. Bioeng., 1995, 46, 545-552.

85) J. Podschun, A. Stücker, R. I. Buchholz, M. Heitmann, A. Schreiber, B. Saake and R. Lehnen, Ind. Eng. Chem. Res., 2016, 55, 5231-5237.

86) E. Rojo, M. S. Peresin, W. W. Sampson, I. C. Hoeger, J. Vartiainen, J. Laine and O. J. Rojas, Green Chem., 2015, 17, 1853-1866.

87) D. Fengel and G. Wegener, Wood: chemistry. ultrastructure. Reaction, Walter de Gruyter, New York, 2011.

88) I. Chiwetelu, V. Hornof, G. H. Neale, and A. E. George, Can. J. Chem. Eng., 1994, 72, 534-540.

89) G. Telysheva, T. Dizhbite, E. Paegle, A. Shapatin and I. Demidov, J. Appl. Polym. Sci., 2001, 82, 1013-1020.

90) A. Macias and S. Goni, Mater. J., 1999, 96, 40-46.

91) Kamoun, A. Jelidi and M. Chaabouni, Cem. Concr. Res., 2003, 33, 995-1003.

92) W. L. Ng, D. Rana, G. H. Neale and V. Hornof, J. Appl. Polym. Sci., 2003, 88, 860-865.

93) R. Chen and Q. Wu, J. Appl. Polym. Sci., 1994, 52, 437-443.

94) T. Aro and P. Fatehi, ChemSusChem, 2017, 10, 1861-1877.

95) P. Dilling, US Pat., 4 546 173, 1985.

96) S. E. Lebo Jr, J. D. Gargulak and T. J. McNally, Encycl. Polym. Sci. Technol., 2002, DOI: 10.1002/0471440264.pst179.

97) H. Zhang, Y. Bai, W. Zhou and F. Chen, Int. J. Biol. Macromol., 2017, 97, 201-208.

98) A. J. Latibari, M. Roohnia, A. Tajdini, F. Darvishqadima and M. Moradbak, J. Appl. Che. Res., 2008, 2, 34-44.

99) P. Dilling, US Pat., 4 732 572. 1988.

100)   H. Wu, F. Chen, Q. Feng and X. Yue, BioResources, 2012, 7, 2742-2751.

101)   W. He and P. Fatehi, RSC Adv., 2015, 5, 47031-47039.

102)   P. Dilling, US Pat., 4 670 482. 1987.

103)   Yang, Y. Chang, X. Wu, X. Qiu and H. Lou, RSC Adv., 2014, 4, 53855-53863.

104)   H. Zhou, Y. Chang, X. Wu, D. Yang and X. Qiu, ACS Sustainable Chem. Eng., 2015, 3, 518-523.

105)   A. E. Kazzaz, Z. H. Feizi and P. Fatehi, Colloid Polym. Sci., 2018, 296, 1867-1878.

106)   A. Zhang, D. Yang, H. Wang, Y, Qian, J. Huang, L. Yu and X. Qiu, ACS Sustainable Chem., 2018, 7, 1120-1128.

107)   A. Huang, J. Ma, W. Zhang, G. Huang and Q. Yong, Polymers, 2018, 10, 841.

108)   Y. Ge, Q. Song and Z. Li, J. Ind. Eng. Chem., 2015, 23, 228-234.

109)   X. Qiu, W. Zeng, W. Liang, Y. Xue, N. Hong, Y. Li. J. Dispersion Sci. Technol., 2016, 37, 472-478.

110)   1X. Qiu, W. Zeng. W. Yu, Y. Xue, Y. Pang, X. Li and Y. Li, ACS Sustainable Chem. Eng., 2015, 3, 1551-1557.

111)   Y. Li, Y. Wu, W. Zeng, Y. Li L. Xu, X. Qiu, W. Huang, ACS Sustainable Chem. Eng., 2016, 4, 2004-2011.

112) H. Pan, G. Sun and T. Zhao, Int. J. Biol. Macromol., 2013, 59, 221-226.

113) H. Zhang, B. Yu, W. Zhou, X. Liu and F. Chen, Int. J. Biol. Macromol., 2018, 109, 1232-1238.

114) Y. Xue, X. Qiu, Y. Wu, Y. Qian, M. Zhou, Y. Deng and Y. Li, Polym. Chem., 2016, 7, 3502-3508.

115) V. I. Chursin, Russ. J. Appl. Chem., 2010, 83, 312-315.

116) M. Cerrutti, C. S. de Souza, A. Castellan, R. Ruggiero and E. Frollini, Ind. Crops Prod., 2012, 36, 108-115.

117) S. Li, J. A. Willoughby and O. J. Rojas, ChemSusChem., 2016, 9, 2460-2469.

118) W. Lange, W. Schweers, Wood Sci. Technol., 1980, 14, 1-7.

119) K. Shweta and H. Jha, Bioresources Bioprocess, 2016, 3, 31.

120) S. Li, W. Xiang, M. Jarvinen, T. Lappalainen, K. Salminen, O. J. Rojas, ACS Appl. Mater. Interfaces., 2016, 8, 19827-19835.

121) S. Li, D. Ogunkoya,T. Fang, J. Willoughby andO. J. Rojas, J. Colloid Interface Sci., 2016, 482, 27-38.

122) L. H. Gan, M. S. Zhou and X. Q. Qiu, Adv. Mater. Res., 2012, 550, 1293-1298

123) K. Bahrpaima and P. Fatehi, ChemSusChem., 2018, 11, 2967-2980.

124) Chen, M. Zhu, M. Li, Y. Fan, R. C. Sun, Biotechnol. Biofuels., 2016, 9, 87.

125) F. Ferdosian, Z. Yuan, M. Anderson and C. C. Xu, J. Sci. Technol. For. Prod. Processes., 2012, 2, 11-15.

126) N. Ding, X. Wang, Y. Tian, L. Yang, H. Chen and Z. Wang, Polym. Eng. Sci., 2014, 54, 2777-2784.

127) G. H. Delmas, B. Benjelloun-Mlayah, Y. L. Bigot and M. Delmas, J. Appl. Polym. Sci., 2013, 127, 1863-1872.

128) Y. Nonaka, B. Tomita and Y. Hatano, Holzforschung, 1997, 51, 183-187.

129) Cortes-Trivino, C. Valencia, M. Delgado and J. Franco, Polymers., 2018, 10, 670.

130) A. L. Brocas, G. Cendejas, S. Caillol, A. Deffieux and S. Carlotti, J. Polym. Sci. Part A: Polym. Chem., 2011, 49, 2677-2684.

131) S. Nikafshar, O. Zabihi, Y. Moradi, M. Ahmadi, S. Amiri and M. Naebe, Polymers, 2017, 9, 266.

132) S. Wang, S. Ma, C. Xu, Y. Liu, J. Dai, Z. Wang and J. Zhu, Macromolecules, 2017, 50, 1892-1901.

133) K. Hofmann and W. G. Glasser, J. Adh., 1993, 40, 229-241.

134) T. A. Khan, J. H. Lee, and H. J. Kim, Lignocellulose for Future Bioeconomy, Elsevier, Amsterdam, 2019.

135) Q. Yin, W. Yang, C. Sun and M. Di, BioResources, 2012, 7, 5737-5748.

136) Kuhnel, J. Podschun, B. Saake and R. Lehnen, Holzforschung., 2015, 69, 531-538.

137) Kuhnel, B. Saake and R. Lehnen, React. Funct. Polym., 2017, 120, 83-91.

138) Kuhnel, B. Saake and R. Lehnen, Ind. Crops Prod., 2017, 101, 75-83.

139) A. Cateto, M. F. Barreiro, A. E. Rodrigues and M. N. Belgacem, Ind. Eng. Chem. Res., 2009, 48, 2583-2589.

140) B. Ahvazi, O. Wojciechowicz, T. M. Ton-That and J. Hawari, J. Agric. Food Chem., 2011, 59, 10505-10516.

141) H. Sadeghifar, C. Cui and D. S. Argyropoulos, Ind. Eng. Chem. Res., 2012, 51, 16713-16720.

142) B. Berrima, G. E. R. A. R. D. Mortha, S. A. M. I Boufi, E. E. Aloui and M. N. Belgacem, Cellul. Chem. Technol, 2016, 50, 941-950.

143) H. Nadji, C. Bruzzèse, M. N. Belgacem, A. Benaboura and A. Gandini, Macromol. Mater. Eng., 2005, 290, 1009-1016.

144) Y. Li and A. J. Ragauskas, J. Wood Chem. Technol., 2012, 32, 210-224.

145) A. Arbenz and L. Averous, RSC Adv., 2014, 4, 61564- 61572.

146) J. Busch, J. Am. Coll. Toxicol., 1987, 6, 23-51.

147) S. Argyropoulos, US Pat., 61 601 181. 2012.

148) W. G. Glasser and O. H. H. Hsu, US Pat., 4 017 474. 1977.

149) L. T. Monson and W. J. Dickson, US Pat., 2 854 444. 1958.

150) C. Cui, H. Sadeghifar, S. Sen and D. S. Argyropoulos, BioResources, 2013, 8, 864-886.

151) I, Kühnel, B. Saake and R. Lehnen, Macromol. Chem. Phys., 2018, 219, 613.

152) M. Wanga, Z. Wanga, Z. Sun and H. Jiang, React. Kinet. Catal. Lett., 2005, 84, 223-228.

153) J. Lisperguer, C. Nunez, P. Perez-Guerrero, J. Chil. Chem. Soc., 2013, 58, 1937-1940.

154) N, Blank, I. Schober, P. R. Von Rohr and T. Voitl, US Pat., 13 257 733. 2010.

155) X. Zhao, Y. Zhang, L. Wie, H. Hu, Z. Huang, M. Yang, A. Huang, J. Wua and Z. Fenga, RSC Adv., 2017, 7, 52382- 52390.

156) L. Li, Y. Hu and F. Cheng, BioResources, 2015, 10, 3181-3196.

157) P. Buono, A. Duval, P. Verge, L. Averous and Y. Habibi, ACS Sustainable Chem. Eng., 2016, 4, 5212-5222.

158) S. Chatterjee, A. Clingenpeel, A. McKenna, O. Rios and A. Johs, Rsc Adv., 2014, 4, 4743-4753.

159) K. A. Koivu, H. Sadeghifar, P. A. Nousiainen, D. S. Argyropoulos, J. Sipilä, ACS Sustainable Chem. Eng., 2016, 4, 5238-5247.

160) L. Dehne, C. V. Babarro, B. Saake, K. U. Schwarz, Ind. Crops Prod., 2016, 86, 320-328.

161) S. Luo, J. Cao and A. G. McDonald, Ind. Crops Prod., 2017, 97, 281-291.

162) Y. Pu and A. J. Ragauskas, Can. J. Chem., 2005, 83, 2132-2139.

163) Y. Teramoto, S. H. Lee and T. Endo, Polym. J., 2009, 41, 219.

164) H. F. Lewis and F. E. Brauns, US Pat., 2 429 102. 1947.

165) R. Ding, H. Wu, M. Thunga, N. Bowler and M. R.; Kessler, Carbon, 2016, 100, 126-136.

166) W. G. Glasser and R. K. Jain, Holzforschung, 1993, 47, 225-233.

167) M. Thunga, K. Chen, D. Grewell and M. R. Kessler, Carbon, 2014, 68, 159-166.

168) L. Dehne, C. Vila, B. Saake and K. U. Schwarz, J. Appl. Polym. Sci., 2017, DOI: 10.1002/APP.44582.

169) W. Thielemans and R. P. Wool, Composites. Part A., 2004, 35, 327-338.

170) J. H. Lora and W. G. Glasser, J. Polym. Environ., 2002, 10, 39-48.

171) Marchand, C. A. Calliste, R. M. Williams, C. McLure, S. Leroy-Lhez and N. Villandier, ChemistrySelect., 2018, 3, 5512-5516.

172) L. Hult, K. Koivu, J. Asikkala, J. Ropponen, P. Wrigstedt, J. Sipilä and K. Poppius-Levlin, Holzforschung, 2013, 67, 899-905.

173) O. Gordobil, R. Herrera, R. Llano-Ponte and J. Labidi, Prog. Org. Coat., 2017, 103, 143-151.

174) N. Cachet, S. Camy, B. Benjelloun-Mlayah, J. S. Condoret, M. Delmas, Ind. Crops Prod., 2014, 58, 287-297.

175) Y. Chen, N. M. Stark, Z. Cai, C. R. Frihart, L. F. Lorenz, R. E. Ibach, BioResources, 2014, 9, 5488-5500.

176) T. Sonoda, T. Ona, H. Yokoi, Y. Ishida, H. Ohtani and S. Tsuge, Anal. Chem., 2001, 73, 5429-5435.

177) N. E. Mansouri and J. Salvadó, Ind. Crops Prod., 2006, 24, 8-16.

178) Sadeghifar, S. Sen and S. V. Patil, ACS Sustainable Chem. Eng., 2016, 4, 5230-5237.

179) D. A. Baker and T. G. Rials, J. Appl. Polym. Sci., 2013, 130, 713-728.

180) M. Wang and L. Yang, J. Polym. Environ., 2012, 20, 783-787.

181) S. Sen, S. Patil and D. S. Argyropoulos, Green Chem., 2015, 17, 1077-1087.

182) K. Iiyama and R. Pant, Wood Sci. Technol., 1988, 22, 167-175.

183) D. E. McKinney, D. M. Carson, D. J. Clifford, R. D. Minard and P. G. Hatcher, J. Anal. Appl. Pyrolysis., 1995, 34, 41-46.

184) D. Delledonne, F. Rivetti and U. Romano, J. Organomet. Chem., 1995, 488, 15-19.

185) Chen, H. Dai, X. Dong, J. Yang and M. Zhong, Polym. Compos., 2011, 32, 1019-1025.

186) S. Sarkanen and Y. Li, US Pat., 6 172 204. 2001.

187) M. Tajvidi, R. H. Falk and J. C. Hermanson, J. Appl. Polym. Sci., 2006, 101, 4341-4349.

188) Y. Li and S. Sarkanen, Macromolecules, 2002, 35, 9707-9715.

189) A. Sequeiros, L. Serrano and J. Labidi, J. Chem. Technol. Biotechnol., 2016, 91, 1809-1815.

190) N. N. Shorygina and L. I. Kolotova, Russ. Chem. Bull., 1953, 2, 505-508.

191) S. C. Puri, S. M. Anand and C. K. Atal, Indian J. Chem., 1985, 16, 294-295.

192) W. Zhao, L. P. Xiao, G. Song, R. C. Sun, L. He, S. Singh and G. Cheng, Green Chem., 2017, 19, 3272-3281.

193) A. Longoria, R. Tinoco and R. Vázquez-Duhalt, Chemosphere, 2008, 72, 485-490.

194) J. G. Speight, Environmental organic chemistry for engineers, Butterworth-Heinemann, Oxford, 2016.

195) D. N. S. Hon, Chemical modification of lignocellulosic materials. CRC Press: New York, 1995.

196) X. Du, J. Li, and M. E. Lindstrom, Ind. Crops Prod., 2014, 52, 729-735.

197) X. Liu, H. Zhu, C. Qin, J. Zhou, J. R. Zhao, S. Wang, BioResources., 2013, 8, 2257-2269.

198) Dong, W. Peng, L. N. Lewis, US Pat., 9 181 405. 2013.

199) Y. Matsushita and S. Yasuda, J. Wood Sci., 2003, 49, 166-171.

200) Y. Matsushita, A. Iwatsuki, S. Yasuda, J. Wood Sci., 2004, 50, 540-544.

201) R, Fang, X. Cheng and X. Xu, Bioresour. Technol., 2010, 101, 7323-7329.

202) Ruihua, Y. Bingchao, D. Zheng and B. Wang, J. Mater. Sci., 2012, 47, 845-851.

203) Harmita, K. G. Karthikeyan and X. Pan, Bioresour. Technol., 2009, 100, 6183-6191.

204) Aguado, J. M. Arsuaga, A. Arencibia, M. Lindo and V. Gascón, J. Hazard. Mater., 2009, 163, 213-221.

205) Tian, S. Ren, G. Fang, Y. Ma and Q. Ai, BioResources, 2014, 9, 6290-6303.

206) C. Cai, X. Zhan, M. Zeng. H. Lou, Y. Pang, J. Yang and X. Qiu, Green Chem., 2017, 19, 5479-5487.

207) T. Zheng, D. Zheng, X. Li, C.Cai, H. Lou, W. Liu and X. Qiu, ACS Sustainable Chem. Eng., 2017, 5, 7743-7750.

208) F. Kong, K. Parhiala, S. Wang and P. Fatehi, Eur. Polym. J., 2015, 67, 335-345.

209) R. Wahlstrom, A. Kalliola, J. Heikkinen, H. Kyllonen and T. Tamminen, Ind. Crops Prod., 2017, 104, 188-194.

210) C. Cheng, J. Wang, D. Shen, J. Xue, S. Guan, S. Gu and K. Luo, Polymers., 2017, 9, 240.

211) J. C. Villar, A, Caperos and F. Garcia-Ochoa, Wood Sci. Technol., 2001, 35, 245-255.

212) Q. Xiang and Y. Y. Lee, Appl. Biochem. Biotechnol., 2000, 84, 153-162.

213) J. M. Chan, S. Bauer, H. Sorek, S. Sreekumar, K. Wang and F. D. Toste, Acs Catal., 2013, 3, 1369-1377.

214) S. K. Hanson, R. Wu,L. A. P. Silks, Angew. Chem., 2012, 124, 3466-3469.

215) S. Son and F. D. Toste, Angew. Chem. Int. Ed., 2010, 49, 3791-3794.

216) Wang, J. Lu, X. Zhang, L. Li, H. Li, N. Luo and F.Wang, ACS Catal., 2016, 6, 6086-6090.

217) V. E. Tarabanko, N. A. Fomova, B. N. Kuznetsov, N. M. Ivanchenko and A. V. Kudryashev, Reaction Kinetics and Catalysis Letters., 1995, 55, 161-170.

218) J. C. Villar, A. Caperos and F. García-Ochoa, React. Kinet. Catal. Lett., 1997, 17, 259-285.

219) Tong, Y. Matsumoto and G. Meshitsuka, J. Wood Sci., 2000, 46, 371-375.

220) S. Rovio, S. Kuitunen, T. Ohra-aho, S. Alakurtti, A. Kalliola and T. Tamminen, Holzforschung., 2011, 65, 575-585.

221) F. G. Sales, C. A. M. Abreu and J. A. F. R. Pereira, Braz. J. Chem. Eng., 2004, 21, 211-218.

222) T. A. D. Nguyen, A. M. Wright, J. S. Page, G. Wu and T. W. Hayton, Inorg. chem., 2014, 53, 11377-11387.

223)   Tian, J. Wen, D. MacDonald, R. M. Asmussen and A. Chen, Electrochem. Commun., 2010, 12, 527-530.

224)   C. Zhu, W. Ding, T. Shen, C. Tang, C. Sun, S. Xu and H. Ying, ChemSusChem., 2015, 8, 1768-1778.

225)   R. Behling, S. Valange and G. Chatel, Green Chem., 2016, 18, 1839-1854.

226)   Gierer, Wood Sci. Technol., 1986, 20, 1-33.

227)   R. Ma, Y. Xu and X. Zhang, ChemSusChem, 2015, 8, 24-51

228)   R. Prado, A. Brandt, X. Erdocia, J. Hallet, T. Welton and J. Labidi, Green Chem., 2016, 18, 834-841.

229)   Marton, S. C. Charleston and E. Adler, US Pat., 3 071 570. 1963.

230)   T. Okamoto, H. Takeda, T. Funabiki, M. Takatani and R. Hamada, React. Kinet. Catal. Lett., 1996, 58, 237-242.

231)   S. Dabral, H. Wotruba, J. G. Hernández and C. Bolm, ACS Sustainable Chem. Eng., 2018, 6, 3242-3254.

232)   A. Rahimi, A. Ulbrich, J. J. Coon and S. S. Stahl, Nature, 2014, 515, 249.

233)   W. Hoareau, W. G. Trindade, B. Siegmund, A. Castellan and E. Frollini, Polym. Degrad. Stab., 2004, 86, 567-576.

234)   Mottweiler, M. Puche, C. Räuber, T. Schmidt, P. Concepción, A. Corma and C. Bolm, ChemSusChem., 2016, 8, 2106-2113.

235)   J. D. Araújo, C. A. Grande and A.E. Rodrigues, Chem. Eng. Res. Des., 2010, 88, 1024-1032.

236)   A. Das, A. Rahimi, A. Ulbrich, M. Alherech, A. H. Motagamwala, A. Bhalla and B. E. Dale, ACS Sustainable Chem. Eng., 2018, 6, 3367-3374.

237)   E. I. Evstigneyev, O. S. Yuzikhin,A. A. Gurinov, A. Y. Ivanov, T. O. Artamonova, M. A. Khodorkovskiy and A. V. Vasilyev, J. Wood Chem. Technol., 2016, 36, 259-269.

238)   A. Mancera, V. Fierro, A. Pizzi, S. Dumarçay, P. Gérardin, J. Velásquez and A. Celzard, Polym. Degrad. Stab, 2010, 95, 470-476.

239)   R. L. Couch, J. T. Price and P. Fatehi, ACS Sustainable Chem. Eng., 2016, 4, 1954-1962.

240)   W. He, W. Gao and P. Fatehi, ACS Sustainable Chem. Eng., 2017, 5, 10597-10605.

241)   J. J. Meister, J. Macromol. Sci. Polym. Rev., 2002, 42, 235-289.

242) Y. Sun, M. Fenster, A. Yu, R. M. Berry and D. S. Argyropoulos, Can. J. Chem., 1999, 77, 667-675.

243) C. Crestini, P. Pro, V. Neri and R. Saladino, Bioorg. Med. Chem., 2005, 13, 2569-2578.

244) R. Kavanagh and J. M. Pepper, Can. J. Chem., 1955, 33, 24-30.

245) S. Kagawa, Japan Tappi J., 1970, 24, 424-428.

246) Y. Sang, B. Wang, Q. Wang, G. Zhao and P. Guo, Sci. Rep., 2014, 4, 6321.

247) N. Alam and T. G. Van De Ven, J. Sci. Technol. For. Prod. Processes., 2014, 4, 22-26.

248) D. E. Bland, G. Ho and W.E. Cohen, Aust. J. Chem., 1950, 3, 642-648.

249) R. Yang, L. Lucia, A. J. Ragauskas, H. Jameel, J. Wood Chem. Technol., 2003, 23, 13-29.

250) T. Higuchi, J. Biochem., 1985, 45 675-685.

251) J. C. Pew, J. Am. Chem. Soc., 1955, 77, 2831-2833.

252) L. Klapiszewski, J. Zdarta, T. Szatkowski, M. Wysokowski, M. Nowacka, K. Szwarc-Rzepka and T. Jesionowski, Open Chem., 2014, 12, 719-735.

253) S. Hamdani, C. Longuet, D. Perrin, J. M. Lopez-cuesta, F. Ganachaud, Polym. Degrad. Stab., 2009, 94, 465-495.

254) J. Zhang, E. Fleury, Y. Chen and M. A. Brook, RSC Adv., 2015, 5, 103907-103914.

255) T. Budnyak, S. Aminzadeh, I. Pylypchuk, A. Riazanova, V. Tertykh, M Lindström and O. Sevastyanova, Nanomaterials., 2018, 8, 950.

256) W. Xiong, X. Qiu, D. Yang, R. Zhong, Y. Qian, Y. Li and H. Wang, Chem. Eng. J., 2017, 326, 803-810.

257) J. F. Kadla and S. Kubo, Composites. Part A., 2004, 35, 395-400.

258) P. Bruijnincx, B. Weckhuysen, G. J. Gruter and E. EngelenSmeets, Lignin valorisation: The importance of a full value chain approach, Utrecht University, Google Books, 2016.

259) L. Kouisni, A. Gagné, K. Maki, P. Holt-Hindle and M. Paleologou, ACS Sustainable Chem. Eng., 2016, 4, 5152-5159.

260) J. Kihlman, Nord. Pulp Pap. Res. J., 2016, 31, 573-582.

261) 261 M. Abraham, Encyclopedia of sustainable technologies. Elsevier, Cambridge, 2017.

262) N, Smolarski, Frost & Sullivan, https://www.greenmaterials.fr/wp-content/uploads/2013/01/High-value-Opportunities-for-Lignin-Unlocking-its-Potential-Market-Insights.pdf, (accessed August 2019).

263) LigniMATCH online, https://www.gmv.gu.se/digitalAssets/1448/1448662_roadmap.pdf, (accessed August 2019).

Chapter 3. Interaction of synthetic and lignin-based sulfonated polymers with hydrophilic, hydrophobic, and charged self-assembled monolayers

Adapted from: Armin Eraghi Kazzaz, Pedram Fatehi*

Biorefining Research Institute,
Green Processes Research Centre,
Chemical Engineering Department,
Lakehead University,
955 Oliver Road,
Thunder Bay, ON, Canada, P7B5E1

*Corresponding author

3.1 Abstract

There is a need to understand the role of polymer structure on its interaction with surfaces to produce effective functional surfaces. In this work, we produced two anionic polymers of lignin-3-sulfopropyl methacrylate (L-S) and poly(vinyl alcohol-*co*-vinyl acetate)-3-sulfopropyl methacrylate (PVA-S) with similar charge densities and molecular weights. On the gold-coated surface, we deposited self-assembled monolayers (SAM) bearing different terminal moieties namely, hydroxy, carboxyl, methyl, and amine groups of alkanethiols. This study highlighted the difference between the interaction of L-S and PVA-S and functionalized self-assembled surfaces. The information was generated using advanced tools, such as an X-ray photoelectron spectroscopy (XPS), and a quartz crystal microbalance with dissipation (QCM-D), which facilitated the correlation development between polymer properties and deposition performance on the functionalized surfaces. The higher deposition of PVA-S than L-S onto OH and COOH surfaces was observed due to its greater hydrogen bonding development and higher solubility. The solubility and structure of PVA-S were also beneficial for its higher adsorption than L-S onto CH_3 and NH_2 surfaces. However, the variation in pH, temperature, and salt significantly affected the adsorption of the macromolecules.

Keywords: Lignin, PVA, adsorption, XPS, QCM, colloid

3.2 Introduction

Polymeric films are ubiquitous in applications ranging from automobiles to constructions. The majority of polymer films are multilayer polymeric materials with varied functionalities. To generate multilayer films, the interaction of polymers with different surfaces is critical. Polymer adsorption on different surfaces and at the solid/water interface can happen as a result of hydrophobic, hydrogen-bonding, and electrostatic interactions between polymer segments and surfaces. Polymer adsorption is influenced by the properties of the polymer and the interaction between the polymer, surface, and solvent. In this context, the difference in the structure of the polymer, e.g., linear or three-dimensional, has shown to have a crucial impact on the adsorption behavior of the polymer on surfaces.[1,2]

Poly(vinyl alcohol-*co*-vinyl acetate) (PVA) has been known as an odorless, whitish or creamy, nontoxic, biocompatible, thermostable linear synthetic polymer used widely in different

applications. PVA polymer is used vastly in textile, papermaking, coating industry, 3D printing, optical gas and humidity sensors, emission sensors for vehicles and oral drug delivery, and solar cells.[3-7] PVA, by having a linear structure,[2] has been functionalized with anionic and cationic monomers to improve its adsorption on fibrous pulp and broaden its application as adhesives and emulsifiers.[6,8]

Lignin, an abundant phenolic polymer, is one of the alternatives to petroleum feedstocks,[9] which recently attracted tremendous attention and applications.[10-15] Lignin, by having a complex three-dimensional structure, has been reported to show a distinct interaction behavior compared to linear polymeric materials.[16-17] However, as lignin has a complicated structure, the interaction mechanisms of lignin derivatives with different functionalized surfaces are still unclear. Revealing these mechanisms is believed to highly affect its end-used applications in wastewater treatment, surface coating, and biological applications, for instance.

Polymers could adsorb following altered mechanisms.[18-20] Thus, interaction mechanisms between the polymer and adsorbing surface include, but are not limited to, charge interaction, hydrogen bonding, van der Waals forces, and hydrophobic interactions. Although the mechanisms behind adsorption of various polymers on different surfaces in contrastingly charged systems have been studied, information on the adsorption in the absence of electrostatic interaction for lignin and PVA based polymers is limited. To address this, two types of branched anionic polymers of poly(vinyl alcohol-*co*-vinyl acetate)-3-sulfopropyl methacrylate (PVA-S) and lignin-3-sulfopropyl methacrylate (L-S) were produced. To eliminate the effect of molecular weight and charged group in comparing lignin and PVA, the reaction condition was controlled to produce polymers with a similar molecular weight and charge density. This will elucidate the role of the structure and surface chemistry of polymers in adsorption.

Self-assembled monolayers (SAMs), having different surface chemistries, were used to study the adsorption of polymers and the adsorption kinetics.[21-24] These surfaces are extensively used in electrochemical sensors[25] and also as model surfaces to study the adsorption of polymers, such as proteins.[26] Various SAMs with various combinations of moieties can be used to elucidate the different contributions of the driving force for polymer adsorption.[23] In studying the interaction of a polymer with SAM surfaces, it was found that polyelectrolytes and the surface with like-charges showed interaction and adsorption.[23] In other words, although these systems had an interaction barrier of electrostatic origins, the adsorption of the polymer was fast.[23] In another study, the

adhesion forces between a hydrophobic surface (CH$_3$-SAM) with alkaline lignin was analyzed and revealed the importance of hydrophobic interaction between the CH$_3$ surface and in non-modified lignin.[24] As another objective of this work, the comparison of lignin and poly(vinyl alcohol-*co*-vinyl acetate) adsorption on different SAM surfaces could provide insights into the impact of polymer properties on the adsorption performance of polymers on altered surfaces. To the best of the authors' knowledge, the interaction of sulfonated PVA and lignin-based compounds on SAMs have not been studied.

In the present study, the adsorbed amount of PVA-S and L-S on OH, COOH, CH$_3$, and NH$_2$ functionalized surfaces were studied for the first time using QCM-D to provide information on their altered adsorption behavior. The selected SAM surfaces carried distinct terminal functional groups relevant to the surfaces used in different industries such as surface coatings, mining, pharmaceutical, and cosmetics.[4,7,9] Also, conducting adsorption studies under different saline and pH conditions would reveal the performance of these sulfonate-based polymers on altered surfaces in different environments and the interaction mechanisms of the adsorption processes on the surfaces.

The main goal of this paper was to identify how the interaction of lignin derivatives, *i.e.*, highly branched materials, is different from their synthetic linear equivalents when their molecular weights and charge densities are similar. This paper provides fundamental insights into quantitative adsorption fundamentals of lignin and synthetic macromolecules. Demonstrating this difference would help establish methods to improve the characteristics of lignin for creating valorized lignin derivatives with desired functionality.

3.3 Experimental section

3.3.1 Materials

In this work, 11-mercapto-1-undecanol (-OH, 97%), 12-mercaptododecanoic acid (-COOH, 96%), 1-dodecanethiol (-CH$_3$, ≥98%), ammonium hydroxide, 6-amino-1-hexanethiol hydrochloride (-NH$_2$), vinyl acetate (99%), 3-trimethylsilyl-(2,2,3,3-D$_4$)-propionic acid sodium salt (TMSP) (99.8 %), hydrochloric acid (37 %), sodium hydroxide (99.0 %), poly diallyl dimethylammonium chloride (PDADMAC) with the molecular weight of 100-200 kg/mol, potassium chloride (KCl), D$_2$O (with the isotopic purity of 99.8 %), 3-sulfopropyl methacrylate potassium salt (98 %) (S), sodium persulfate (Na$_2$S$_2$O$_8$), sodium chloride (99%), ethanol (99.8 %), methanol (99.8 %) and dimethyl sulfoxide-d6 ([D$_6$]DMSO)(99.9 %), and hydrogen peroxide (30 wt. %) were all

purchased from Sigma-Aldrich company. Cellulose acetate membrane with the molecular weight cut-off of 1,000 g/mol was purchased from Spectrum Labs. Inc., USA. Also, softwood kraft lignin (L) was produced via the LignoForce technology of FPInnovations in Thunder Bay, ON, and received as a raw material. High-performance liquid chromatography grade water was produced using a Milli-Q water purifier with the resistivity of less than 18 MΩ/cm and used throughout this work. AT-cut gold-coated piezoelectric quartz crystal sensors (5 MHz resonant frequency) were purchased from Biolin Scientific Inc. Nylon filters with a pore size of 0.22 μm were purchased from the Celltreat Scientific company. Additionally, all of the chemicals utilized in this work were of analytical grades.

3.3.2 Synthesis of L-S and PVA-S Polymers

Softwood kraft lignin (L) was polymerized with 3-sulfopropyl methacrylate potassium salt (S) based on the methodology described in a previous study.[25] The reaction was conducted at a molar ratio of 1.2 S/L, 10 wt.% HCl, 90 wt.% of the water in the presence of 1.5 wt.% of potassium persulfate (as initiator) at 80 °C for 90 min. The produced polymer was purified with membrane dialysis for three days to remove any unreacted monomers, and the purified lignin-3-sulfopropyl methacrylate sample was denoted as L-S.

In another set of reactions, vinyl acetate was used, instead of lignin, in polymerizing with 3-sulfopropyl methacrylate potassium salt (S). The reaction was conducted by using vinyl acetate (VA) and S in a molar ratio of 0.5 S/VA, 10 % NaOH, 9/1 v/v of methanol/water in the presence of 1.5 wt.% of potassium persulfate (as initiator) at 80 °C for 90 min.[6,28] The produced polymer was precipitated by methanol precipitation and centrifugation at 3500 rpm for 10 min and then purified using membrane dialysis for three days. The poly (vinyl alcohol-*co*-vinyl acetate)-3-sulfopropyl methacrylate sample was donated as PVA-S. Polymeric solutions were prepared in the concentration of 1 g/L for different analyses in this study.

3.3.3 Static and Dynamic Light Scattering

The light scattering analysis of produced L-S and PVA-S polymers were performed by a static light scattering instrument, Brookhaven BI-200SM, equipped with a goniometer. The laser polarized light was set at 633 nm.[29] The cell was set at different temperatures ranging from 15 to 65 °C. The samples were passed through a 0.22 μm diameter porous filter. The second virial coefficient (A_2), and the average radius of gyration (R_g) were obtained from the concentration dependence and slope of the angle based on Zimm plot equation (3.1), respectively:[30-32]

$$\frac{Kc}{\Delta R_\theta} = \frac{1}{Mw}\left[1 + \frac{16\pi n^2}{3\lambda^2} R_g^2 \sin^2\left(\frac{\theta}{2}\right)\right] + 2A_2c \quad (3.1)$$

where $K = 4\pi^2 n^2 (dn/dC)^2 / N_A \lambda^4$

with A_2 is the second viral coefficient, θ is the measurement angle, n is the refractive index of the liquid medium, R_g is the radius of gyration, N_A is Avogadro's number, λ is the laser wavelength (633 nm), and ΔR_θ is the excess Rayleigh ratio [$\Delta R_\theta = R_\theta$(solution)$-R_\theta$(solvent)], respectively.

The hydrodynamic radius (R_h) was determined using a dynamic light scattering (DLS) instrument, NanoBrook, ZetaPALS, Brookhaven Instruments Corp., USA, which was equipped with a 35 mW power laser ($\lambda = 637$ nm, wavelength). Measurements were made at 90° at different temperatures (15-65 °C), and sample solutions were filtered using 0.2 μm pore size filters for light scattering measurements. The hydrodynamic radius (R_h) was measured based on the diffusion coefficient (D) by using the Stoke-Einstein equation (3.2):[25,33,34]

$$R_h = \frac{K_B T}{6\pi\eta_s D} \quad (3.2)$$

where η_s, K_B, T are the viscosity of the solvent, Boltzmann constant, and the absolute temperature, respectively.

Differential refractometry (DR) technique was used to determine the macromolecular solutions' specific refractive index increments (dn/dc). It is essential to measure the dn/dc precisely to obtain an accurate M_w value. The refractive index increment of each polymer solution (dn/dc) was measured using a Brookhaven BI-DNDC instrument. Although many studies have reported dn/dc values for homopolymers, limited reports are found on the dn/dc values for heteropolymers.[29,35]

The second virial coefficient (A_2), the average radius of gyration (R_g), hydrodynamic radius (R_h), and refractive index increments (dn/dc) were conducted three times and the average values were reported.

3.3.4 Characterization

The charge density of samples was determined with a Particle Charge Detector (PCD 04, BTG Mütek GmbH) using a 0.005 mol/L PDADMAC or 0.005 mol/L PVSK solution as the titrant, as explained elsewhere.[14,36] The elemental analysis of the polymers was performed using an elemental analyzer (Vario EL Cube, Elemental Analyzer, Germany) as explained in detail elsewhere.[37] The molecular weight of PVA-S and L-S polymers was measured by a gel permeation chromatography (GPC, Malvern GPCmax VE2001 with multi-detectors) after treating the samples at different pH values (4.0, 6.7, and 11.0) for 12 h and purifying the samples using membrane

dialysis for 3 days.[38] The details of this analysis can be found in the supplementary information file.

The phenolic hydroxy and carboxylate group contents of L and L-S samples were determined using an automatic potentiometric titrator (785 DMP Titrino, Metrohm, Switzerland) with the HCl standard solution as a titrant (more information can be found in the supplementary information).

The contact angle of water-air ($\theta_{W/A}$) of PVA-S and L-S polymers at different pH were conducted using Theta Lite contact angle analyzer (Biolin Scientific, Finland) associated with a camera-based on our previous experiment.[25] PVA-S and L-S were coated on glass slides using a spin coater (WS-650, Laurell Technologies Corp) and dried overnight. Then, the contact angle of 1.5 µL of a droplet on coated surfaces was determined.

The structure of L, PVA-S, and L-S was analyzed by a ^{1}H NMR spectroscopy with 32 scans. Samples were dissolved in D_2O or $[D_6]$DMSO and stirred until fully dissolved (i.e., for 12 h).[9,39] Trimethylsilyl propionic acid (TMSP) was used as the internal standard.[40] More information about this experiment is available in the supplementary information file.

The zeta potential of lignin (L), L-S, and PVA-S polymers were analyzed using a NanoBrook Zeta PALS (Brookhaven Instruments Corp, USA) at pH ranging from 3.0 to 11.0. The analysis was performed three times, and the average values were reported in this study.

3.3.5 Self-Assembled Monolayers (SAM)s Preparation

In the QCM-D measurements, AT-cut piezoelectric quartz crystals (Biolin Scientific Inc), which were covered with gold and had a fundamental frequency of 5 MHz, were used. The crystals were modified according to the procedure described by Hedin et al.[41] The surfaces were initially cleaned for 10 min in a UV/ozone chamber, which was followed by immersing in a 1:1:6 mixture of hydrogen peroxide (25%), ammonium hydroxide (25%), and Milli-Q water for 8 min at 78 °C. To obtain chemically well-defined and electrically inert SAM surfaces, the crystals were immersed overnight (>15 h) in 20 mL of 2 mM of alkanethiol solution in degassed ethanol (99.8 %) and an amber bottle, and stirred at 50 rpm and 25 °C in a water bath. Then, 11-Mercapto-1-undecanol (-OH), 1-dodecanethiol (-CH), 12-mercaptododecanoic acid (-COOH), and 6-amino-1-hexanethiol hydrochloride (-NH$_2$) chemicals were used to form hydroxy (OH), methyl (CH$_3$), (COOH) and (NH$_2$) terminated SAMs on the surfaces, respectively. The thiol group of n-alkanethiols bonds to Au surfaces by metal-sulfur bonds (*i.e.*, chemisorption) and forms close-packed SAMs (*i.e.*, self-assembled monolayers), which leaves -OH, -COOH, CH$_3$, and NH$_2$ (*i.e.*, the other end of the

functional groups) available on the surface.[23,41] To remove excess thiols from the treated surfaces, the surfaces were washed and ultrasonicated in ethanol five times, each time for 5 min. The SAM surfaces were dried under N_2 gas.

3.3.6 SAM Characterization

Theta Lite Contact Angle analyzer (Biolin Scientific, Finland) associated with a camera was employed to quantitatively analyze the wettability of the Au surfaces before and after SAM deposition. The contact angle analysis of water droplets (1.5 µL) on the bare and modified QCM sensors was conducted using the sessile drop method based on Young's equation with three independent measurements. The values of the water contact angle were evaluated for the four types of SAM are reported in Table 3.2 and are consistent with reports in the literature.[23,42,43]

The X-ray photoelectron spectroscopy (XPS) measurements were performed on the bare and SAM-coated sensors by using a Kratos Axis Supra with a monochromatic Al Kα radiation (1486.6 eV) with 1mm spot diameter at a base pressure of about 3×10^{-10} mbar and 20 eV pass energy. Based on the surface plane, the take-off angle for the detected photoelectrons was adjusted to 60°. For energy referencing, spectra were calibrated to the C1 line peak at 284.6 eV.[44] Data analysis and peak fitting were conducted using ESCApe software (V1.2.0.1325). The thickness of SAM-terminated surfaces on Au substrates was estimated by means of the attenuation of the Au4f signal using the following equation (3.3):

$$I = I_0 \cdot \exp\left[-\frac{d}{\lambda \, sin\theta}\right] \quad (3.3)$$

where I and I_0 are the average intensities of the Au4f$_{5/2}$ and Au4f$_{7/2}$ peaks, attenuated by SAM and the bare gold surface, respectively. θ is the photoelectron take-off angle, λ is the effective attenuation length of the photoelectron, and d is the film thickness.[44,45] The theoretical length values of SAM molecules used in this work have been attained from computational modeling Avogadro software (V1.2.0) (written in C++ (Qt) with General Public License) and force field model of MMFF94 (designed by Merck).

3.3.7 Quartz Crystal Microbalance with Dissipation (QCM-D)

The detailed description of the QCM-D technique has been explained by Li et al.[46] and Pensini et al.[47] The adsorption studies of L-S and PVA-S were conducted on the above mentioned SAM-coated gold sensors by using a QCM-D, E1, 401, instrument (Q-Sense Inc., Gothenburg, Sweden). A peristaltic pump was used to pump solutions at the flow rate of 0.15 mL/min through the chamber of the QCM instrument. The temperature was set to room temperature (25 °C) for all

experiments. The adsorption experiment was initially conducted with a buffer solution of the desired aqueous pH and electrolytes, until achieving a baseline signal in the analysis. Then, the adsorption experiment was initiated by replacing the buffer solution with L-S or PVA-S polymer solutions with the same pH and electrolyte concentration. After reaching saturation in adsorption, the solutions were changed to the buffer solutions for removing unadsorbed components from the SAM coated surfaces. The solutions were degassed prior to the experiment. This analysis was conducted at different salt concentrations (1-1000 mM) and pH (3.0-11.0) with PVA-S and L-S solutions. It is worth noting that the PVA-S, L-S, and buffer solutions had the same pH and salinity in all experiments.

In this analysis, Sauerbrey and Voigt equations were used to evaluate the properties of the adsorbed layers and analyze the changes in the adsorbed mass on the sensor (more information is available in the supplementary information). The Sauerbrey equation was used when $\Delta D \leq 1 \times 10^{-6}$, which would be an indication of an elastic and rigid layer. However, data points were fitted into the Voigt model for layers with the higher dissipation using three harmonic overtones of 5, 7, and 9 of the Q-Tools software. The 9th overtone was used for the better representation of data (details available in the supplementary information). Also, the fluid density and viscosity were considered to be 0.99 g/cm^3 and 1.05 mPa, respectively. The error bars related to the adsorbed mass present the standard deviation of the repeated experiments.

3.4 Results and discussion

3.4.1 Characterization of Produced Polymers

The ^{1}H-NMR spectra of the produced samples are depicted in Figures S3.1 and S3.2. The appearance of a new peak at 0.96 and 1.10 ppm is assigned to the methyl group of S monomer in the ^{1}H-NMR spectra.[25,48,49] The three peaks at 4.7, 4.5, and 4.2 ppm are assigned to the proton in the (OH) group of PVA (Figure S3.2).[39,50] The peak at 1.97 ppm is also assigned to the methyl (CH$_3$) group of PVA.[39,51] More information could be found in the supplementary information. The results in Figures S3.1 and S3.2 confirm the successful production of L-S and PVA-S. Also, FTIR analysis was performed on the obtained polymers and the spectroscopy, as well as the peak data, are shown in Figure S3.3 and Table S3.1 in the supplementary information file, respectively. The results of this analysis also confirmed the successful polymerization and the production of L-S and PVA-S. In addition, the reaction yield for the production of L-S (65.32 %) was measured to be lower than the reaction yield for the production of PVA-S (74.21 %). The properties of produced

polymers are shown in Table 3.1. Based on the elemental analysis (Table 3.1), L (unmodified lignin), L-S, and PVA-S had 0.76, 8.03, and 8.17 wt. % sulfur element, respectively, and no traceable nitrogen. The charge density (CD) of L, L-S, and PVA-S were -0.85, -3.17, and -3.20 meq/g, respectively, which would indicate that the amount of introduced sulfur content to polyvinyl acetate and lignin was equal. The GPC analysis demonstrated the molecular weight of 1.8×10^4, 11.4×10^4, and 11.3×10^4 g/mol for L, L-S, and PVA-S, respectively. Since the adsorption of the produced polymers is going to be analyzed on different surfaces at different pH, it is crucial to analyze the stability of the polymers at different pH. To do so, the molecular weight analysis was performed using GPC for the samples pretreated in both acidic and alkaline pH for 12 h. As seen in Table S3.2, compared to neutral pH, the PVA-S, and L-S samples showed 7.6-8.9, and 4.0-0.2 % reduction in their molecular weights, respectively. These results reveal that both polymers are relatively stable over the examined pH range. The charge of produced polymers at various pH was determined through zeta potential analysis and presented in Figure S3.4 in the supplementary information file. By changing the pH, the zeta potential of L was changed from about -7.5 to -17.6 mV. The zeta potential increment was observed more drastically for both PVA-S and L-S polymers than L, which could be due to their sulfonate groups.

Table 3.1. Chemical properties of produced polymers

Samples name	L	L-S	PVA-S
Nitrogen content,^{a} wt%	$<0.09^b$	$<0.09^b$	$<0.09^b$
Sulfur content,^{a} wt%	0.76	8.03	8.17
Charge density,^{a} µeq. g^{-1}	-0.85	-3.17	-3.20
Carboxylate content,^{a} mmol g^{-1}	0.17	0.16	—
Phenolic hydroxyl group content,^{a} mmol g^{-1}	1.86	0.18	—
M_w (GPC), g mol^{-1}	1.8×10^4	11.4×10^4	11.3×10^4
M_n (GPC), g mol^{-1}	0.48×10^4	6.38×10^4	6.05×10^4
dn/dc,^{a} mL g^{-1}	0.1320	0.1601	0.0660
Reaction yield, %	100	65.32	74.21

^{a} Error was <0.05%. ^{b} Method sensitivity <0.09.

3.4.2 Characterization of Self-Assembled Monolayers (SAM)

A series of SAM-modified surfaces were produced by reacting thiols with different end groups on the QCM sensor. Figure 3.1 demonstrates the X-ray photoelectron spectroscopy (XPS) of SAM with -OH, -NH$_2$, -CH$_3$, and -COOH end groups on the sensors. The presence of a peak at 162 eV is attributed to the Au-S energy binding, which indicates the successful modification of Au with SAMs.
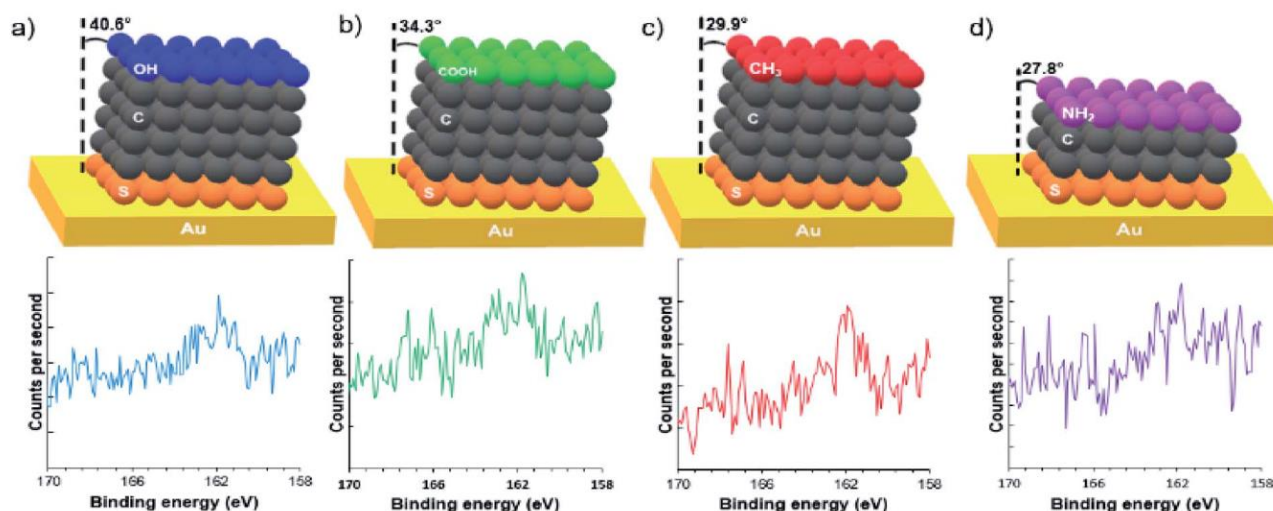
Figure 3.1. SAMs with different terminated groups on gold: XPS S 2p spectra of (a) –OH, (b) –COOH, (c) –CH$_3$, and (d) –NH$_2$.

Table S3.3 (in the supplementary information file) includes the relative atomic concentrations of SAM-modified surfaces (C, O, S, and N), which confirms the successful formation of SAM. The excess amount of O in -CH$_3$ could be attributed to the atmospheric contamination. In the case of -NH$_2$ modified surface, the excess amount of O could be attributed to the atmospheric contamination (3.8 %) and partial oxidation of the S-Au bond to sulfonate (7.3%). The S$_{2p}$ level of -OH, -COOH, -CH$_3$, and -NH$_2$ SAM-terminated surfaces were studied, and it has been found that the partial oxidation of -SH to sulfonate happened only in NH$_2$ terminated SAM, which could be attributed to the HCl used to stabilize amino compound.[52]

Table 3.2 demonstrates the properties of the four types of SAMs. The sessile drop method was used to measure the deionized water contact angle on SAM coated sensors.[42,43] The water contact angle of the gold sensor was $75 \pm 2°$. The contact angle of -OH, -COOH, -CH$_3$, and -NH$_2$ surfaces were measured to be <10°, 30°, 110°, and 41°, respectively. At neutral pH (pH 6.7), -OH and -CH$_3$ carry no charges while -NH$_2$ is positively charged and -COOH is negatively charged.[53] The contact angle measurements of SAM films suggested that the surface coated with the -CH$_3$ group was highly hydrophobic, while the surfaces coated with -OH, -COOH, and -NH$_2$ groups were wettable. SAMs functionalized with -OH could be considered as super-hydrophilic as the water droplet spread on the SAM surface (a contact angle of <10°). According to the literature, the contact angle for -OH functionalized SAM was reported to be as low as 9.5° [23,52] and as high as 40-50°.[54,55] The monolayer surface containing OH has been reported to be unstable.[56] The rate of

94

contact angle variation was also revealed to be dependent on temperature. Also, freshly prepared surfaces were suggested to be used for more credibility of this analysis, which was performed accordingly in this work. These SAMs (-CH$_3$, -OH, -COOH, and -NH$_2$) were well characterized and used extensively as model surfaces.[57,58]

Table 3.2. Used SAMs and their properties

Surface	Chemical formula	SAMs name	Water contact angle, °	Features	Charge at pH 6.7	Theoretical length, Å	Thickness, Å	Tilt angle, °
OH	HS(CH$_2$)$_{11}$OH	11-Mercapto-1-undecanol	<10	Hydrophilic	Neutral	17.1	12.97	40.6
COOH	HS(CH$_2$)$_{11}$COOH	12-Mercaptododecanoic acid	30 ± 3	Hydrophilic	–	18.3	15.11	34.3
CH$_3$	HS(CH$_2$)$_{11}$CH$_3$	1-Dodecanethiol	110 ± 2	Hydrophobic	Neutral	17.3	15.00	29.9
NH$_2$	HS(CH$_2$)$_6$NH$_2$·HCl	6-Amino-1-hexanethiol hydrochloride	41 ± 1	Hydrophilic	+	10.8	9.55	27.8

The theoretical lengths of SAMs were obtained from computational modeling, Avogadro software (V1.2.0), are reported in Table 3.2. By considering the estimated values achieved from the Au4f (Figure S3.5) attenuation analysis, the SAMs show an atilt angle in the range of 27.8-40.6° for the surface (Table 3.2 and Figure S3.5). If SAMs were to be defective, isolated domains would have been formed on the surfaces, which would have further resulted in single molecules to generate a lying-down configuration.[52] Thus, our results reveal a defect-free and tightly packed SAMs. In other words, all SAMs had significant high-packing densities while exhibiting differential end groups.[52,58]

Also, to analyze the interaction of SAM surfaces with water molecules, water adsorption on different SAM surfaces was conducted at different temperatures (Figures S3.6-S3.9) and pH (Figures S3.10-S3.13). Based on the obtained results, no significant difference (i.e., within 10%) was observed between SAM surfaces. This indicates that the chemically modified SAM surfaces are stable under the examined conditions. Also, these conditions (different temperatures and pH) showed no specific effect on the swelling of SAMs (Figures S3.6-S3.13).

3.4.3 Measurements of the Hydrodynamic Radius (R_h), the Radius of Gyration (R_g), and Second Virial Coefficient ($A2$)

Figure 3.2a depicts the hydrodynamic radius, R_h, of PVA-S, and L-S in pure water. As it can be seen, the R_h of L-S increased by increasing the temperature from 15 to 65 °C. The increase in the overall size of L-S with temperature enhancement could be due to more hydration of lignin structure at a higher temperature. In the case of PVA-S, the insignificant change in the R_h might be attributed to the dehydration of PVA-S caused by polyvinyl acetate chains at a high temperature. Similar behavior was reported for poly(ethylene oxide) in water.[59,60] Figure 3.2b depicts the radius

of gyration, R_g, defined as the root mean square distance of a particle's components from its center of mass. As it is seen, enhancing the temperature drastically increased the R_g of L-S, while it did not significantly affect the R_g of PVA-S. It is worth mentioning that R_g is sensitive to the refractive index distribution (mass distribution), while R_h is sensitive to hydrodynamics.[33] It is well established that the ratio of R_g/R_h is a characteristic parameter related to the conformation of polymer chains in solutions. The values of R_g/R_h for uniform hard-sphere, random coil, and rod-like structures have been reported to be 0.778, 1.78, and ≥ 2, respectively.[61-64] In the case of L-S, both R_g/R_h and R_g have increased with increasing the temperature. At 15 °C, the R_g/R_h ratio for L-S was about 0.77, while the R_g/R_h ratio increased to about 1.27 at 65 °C, revealing that the L-S present a swollen structure.[32] An increment in the R_g/R_h ratio for L-S in the range of 0.77 to 1.27 (from 15 to 65 °C) is in agreement with the intermediate structure from a hard-sphere to a looser structure due to the water swelling effect.[65] The respective R_g/R_h ratio of PVA-S changed from ~0.60 at 15 °C to ~0.76 at 65 °C. Thus, the spherical shape of the PVA-S polymer was insignificantly altered via temperature alteration. The higher R_g/R_h ratio at a high temperature also ascribed to the dehydration of PVA-S.[66]
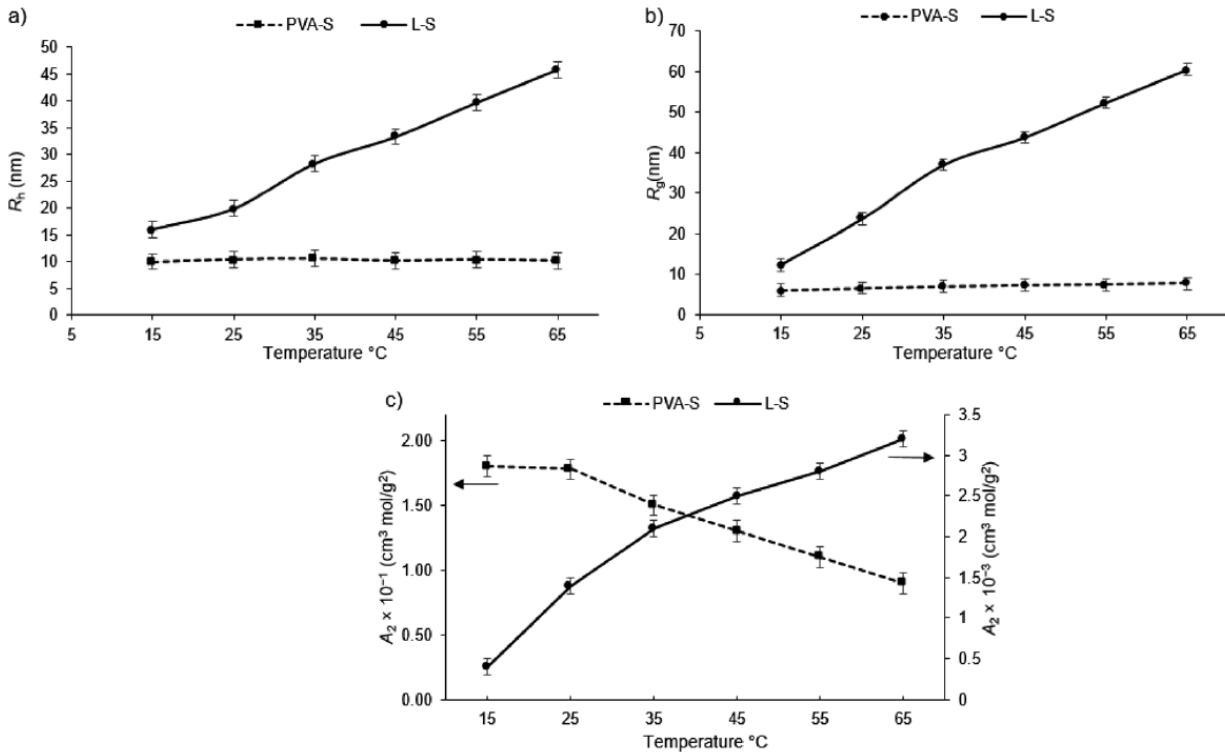
Figure 3.2. Temperature dependence of (a) hydrodynamic radius (R_h), (b) radius of gyration (R_g), and (c) second virial coefficient (A_2) of PVA-S and L-S polymers.

Figure 3.2c indicates the second virial coefficient (A_2) of the polymers, which signifies the polymer-solvent interactions. A low value of A_2 means strong interactions among solute particles, indicating that the solute is in a poor solvent, which means that the polymers are partially or completely insoluble in the solvent. The magnitude of A_2 values denotes the strength of such interactions. The variation in A_2 with temperature depends on the hydrophilic/hydrophobic structure of polymers.[67-69] Based on Figure 3.2c, the A_2 value for L-S polymer increases as the temperature rises from 15 to 65 °C, implying that high temperature improved the interaction of L-S polymer and water. The high interactions between polymer segments could lead to a more compact structure with the hard-sphere configuration at low temperature, while the more efficient interaction between L-S and water loosened the structure of L-S polymer at a higher temperature, which is supported by results depicted in Figure 3.2a and 3.2b. In the case of PVA-S (Figure 3.2c), A_2 values decreased by increasing the temperature implying that water has become a poor solvent for this polymer at a higher temperature. Similar behavior has been reported for poly(vinyl alcohol).[70-71] As reported in the literature, the PVA macromolecule chain becomes dehydrated above critical solution temperature (25 °C in our case).[72-73]

The lower solubility of L-S than PVA-S, based on the second virial coefficient (A_2), could be due to two reasons: its aromatic structure,[74,75] and, its pK_a value (phenolic groups) dropping at higher temperatures and leading to an increase in its solubility.[76,77]

3.4.4 Effect of Temperature on the Adsorption of L-S and PVA-S on SAMs
3.4.4.1 Adsorption on -OH Functionalized Surface

Figure 3.3 illustrates the adsorption analysis of L-S and PVA-S on OH-functionalized surface at different temperatures of 25 °C, 35 °C, and 45 °C (raw data is available in the supplementary information in Figures S3.14-S3.15). Based on these results (Figure 3.3a), limited adsorption was observed for L-S on the OH functionalized surface. Also, increasing the temperature did not improve the adsorption. Although the R_g and R_h of L-S increased with respect to temperature increment (Figures 2a and 2b), they could not improve the development of hydrogen bonding between L-S polymer and OH-functionalized surface. Also, enhancing the temperature decreased the adsorption of PVA-S on the OH-functionalized surface, which might be due to a decrease in its solubility at higher temperatures (Figure 3.2c).
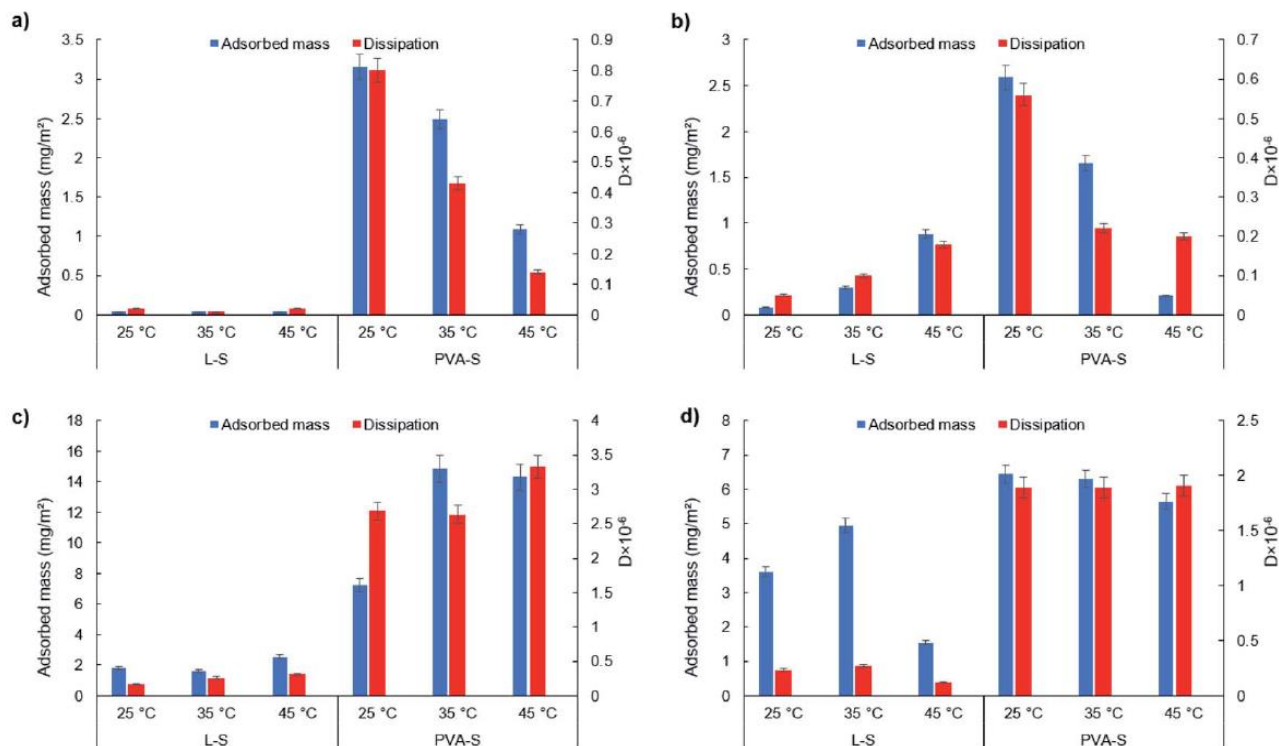
Figure 3.3. Adsorbed mass and dissipation of L-S and PVA-S on (a) OH, (b) COOH, (c) CH$_3$, and (d) NH$_2$ functionalized surfaces at different temperatures.

3.4.4.2 Adsorption on -COOH Functionalized Surface

Figure 3.3b shows the adsorption of L-S and PVA-S on COOH-functionalized surfaces at different temperatures (in the range of 25-45 °C) (raw data is shown in the supplementary information in Figures S3.16-S3.17). The adsorption of L-S on the COOH-functionalized surface was improved marginally by increasing the temperature. At room temperature, the carboxylate group exists in its deprotonated (-COO$^-$) form. By increasing the temperature, the carboxylate group becomes protonated (-COOH),[78] resulting in a decrease in the negative charge density of the surface. This phenomenon paves the way for hydrophilic interactions of L-S with the surface to become more dominant than electrostatic attraction. However, it should be noted that even at a higher temperature (45 °C), the adsorption amount of L-S does not increase significantly, which is a clear indication of the limited adsorption of L-S on the -COOH-functionalized surface (Figure 3.3b). The adsorbed amount of PVA-S is observed to decrease sharply from 2.59 mg/m^2 at 25 °C to 0.21 mg/m^2 at 45 °C. As explained earlier, the solubility of PVA-S was reduced at higher temperatures (Figure 3.2c), and thus its driving force for adsorption dropped. By increasing the temperature, the interaction between hydrophilic groups of PVA-S would decrease. The reason for this could be

the denser structure of PVA at higher temperatures, which would result in dehydration in the structure of PVA[72] and a lower adsorption amount on the -OH functionalized surface. On the other hand, by lowering the hydrogen bonding capability of PVA-S, more hydrophobic parts of PVA-S (i.e., CH) would be exposed and interact with -CH$_3$ functionalized surface.

3.4.4.3 Adsorption on -CH$_3$-Functionalized Surface

Figure 3.3c indicates the adsorption of polymers on the -CH$_3$-functionalized surface at different temperatures (in the range of 25-45 °C) (the raw data is presented in the supplementary information in Figures S3.18-S3.19). According to Figure 3.3c, the L-S adsorption was increased by enhancing the temperature. As the R_g and R_h values for L-S were increased by the temperature increment, its hydrophobic features were more exposed (Figure 3.2), promoting its interaction and thus adsorption on the hydrophobic surface (i.e., -CH$_3$-functionalized surface). Also, the adsorption of PVA-S on this surface (Figure 3.3c) increased in general, which might be attributed to its solubility reduction at a higher temperature (Figure 3.2c).

3.4.4.4 Adsorption on -NH$_2$-Functionalized Surface

Figure 3.3d indicates the adsorption of L-S and PVA-S on the NH$_2$-functionalized surface (the raw data is demonstrated in the supplementary information in Figures S3.20-S3.21). As seen, the highest adsorption of L-S was achieved at 35 °C. Increasing the adsorption from 25 to 35 °C could be due to the improvement in lignin solubility at higher temperatures (Figure 3.2c). In the case of PVA-S (Figure 3.3d) and L-S at higher than 35 °C, by increasing the temperature, the adsorption of PVA-S on the NH$_2$-functionalized surface decreased gradually. This reduction in the adsorption for both L-S and PVA-S polymers could be due to the weakening of electrostatic interaction between negatively charged polymers and the positively charged surface at higher temperatures.[78] Overall, comparing the adsorption of L-S on the NH$_2$ (Figure 3.3d) and CH$_3$ (Figure 3.3c) surfaces, the higher adsorption of L-S was found on the NH$_2$-functionalized surfaces. This implies that the electrostatic interaction could be more dominant than hydrophobic interactions for L-S. In other words, temperature increment could improve the electrostatic interaction development of L-S with surfaces more than its hydrophobic interaction. The similar trend observed for PVA-S adsorption on -NH$_2$ and -CH$_3$ functionalized surfaces could indicate that the electrostatic attraction and hydrophobic interaction were both playing important roles in PVA-S adsorption onto the functionalized surfaces. In addition, comparing L-S and PVA-S, the highest adsorption capacity of L-S (4.95 mg/m^2) was achieved at 35 °C on -NH$_2$ functionalized surface (Figure 3.3d).

Meanwhile, the highest adsorption amount of PVA-S (14.83 mg/m^2) was obtained at 35 °C on the -CH$_3$ functionalized surface (Figure 3.3c). The unmodified lignin (L) polymer contains different functional groups of phenolic hydroxy (1.86 mmol/g (Table 3.1)), carboxylate (0.17 mmol/g (Table 3.1)), carbonyl, and methoxy groups, which could provide the macromolecule with hydrogen bonding capability. However, the rigid and three-dimensional structure of lignin,[11] would limit the chance of available functional groups on L-S to interact with the solid surfaces containing -OH and COOH groups and lead the sites on lignin to prefer developing hydrogen bonds with the solution rather than the surfaces.

3.4.5 Effect of pH on the Adsorption of L-S and PVA-S on SAMs
3.4.5.1 Adsorption on -OH-Functionalized Surface

Representative experimental traces for the QCM adsorption analysis of L-S and PVA-S on OH-functionalized surface are shown in Figure 3.4 under three different pH of 3.0, 6.8, and 11.0, while the raw data is presented in the supplementary information file in Figures S3.22-S3.23. As it is seen in Figure 3.4a, L-S limitedly adsorbed on this surface at all pH ranges, which might reveal that L-S was incapable of developing noticeable hydrogen bonding with this surface in all pH.[79,80] On the other hand, it is seen that PVA-S could adsorb on the OH-functionalized surface more than L-S at all pH, while having the most adsorption at pH 3.0, and the least at pH 11.0. This indicates a stronger electrostatic interaction of PVA-S with the surfaces (results shown in Figures S3.22), since variations in the pH affect the charge of polymers, begetting an attraction or a repulsion in the electrostatic interaction.[81] Moreover, not only the hydrophilicity of PVA-S is higher that L-S (Table S3.4), but PVA-S is also more soluble (Figure 3.2c), which can adsorb more water.
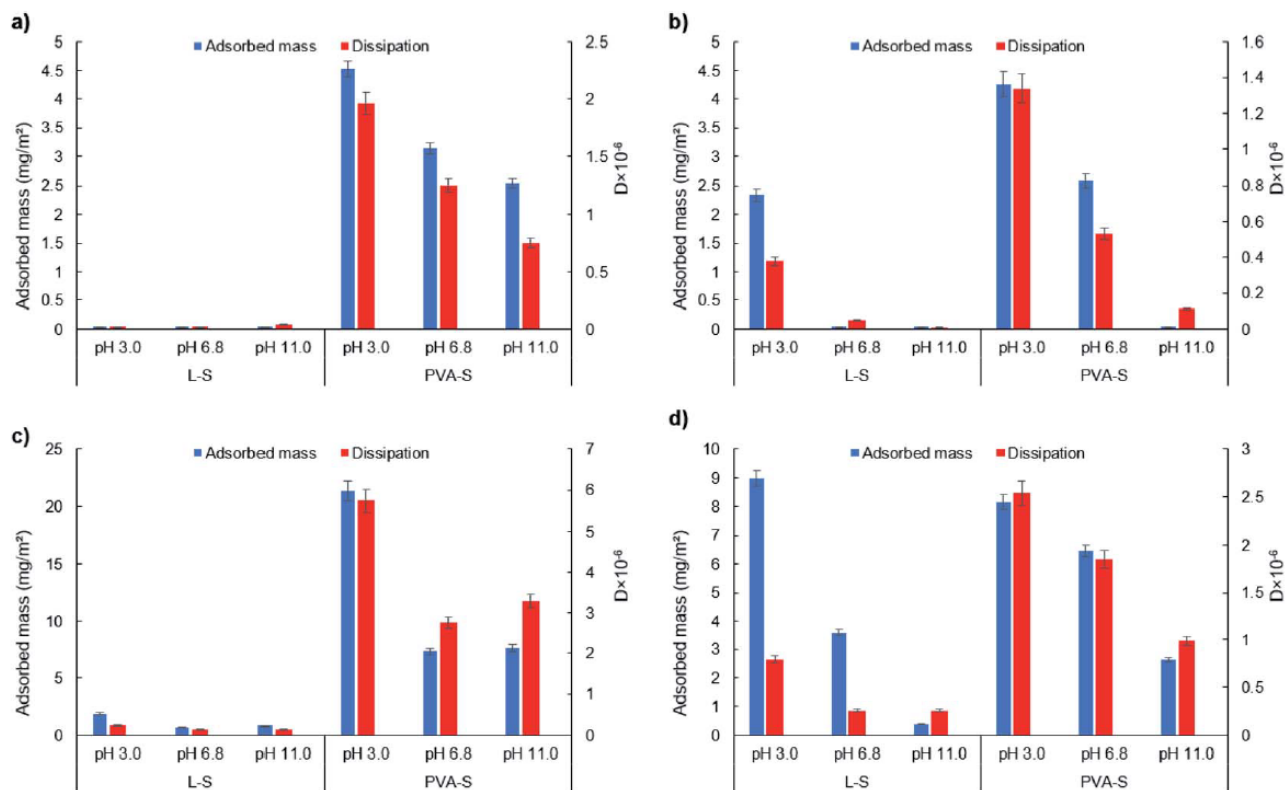
Figure 3.4. Adsorbed mass and dissipation of L-S and PVA-S on (a) OH, (b) COOH, (c) CH₃, and (d) NH₂ functionalized surfaces at different pH.

It is worth noting that the steric hindrance of lignin could also adversely affect its adsorption to the surfaces.[82] Also, since the OH groups of lignin are substituted with S groups after the polymerization reaction, less free hydroxy groups are left on lignin to develop hydrogen bonding interaction. While in the polymerization of PVA, the S groups do not replace the OH groups, leaving more hydroxy groups available on PVA-S to interact through hydrogen bonding with OH-functionalized surface. The higher adsorption of PVA-S than L-S (Figures S3.22-S3.23) increased the dissipation on the sensor.

3.4.5.2 Adsorption on -COOH-Functionalized Surface

Figure 3.4b includes the adsorption of L-S and PVA-S on the -COOH-functionalized surface at different pH, while the raw data is depicted in the supplementary information in Figures S3.24-S3.25. As seen, L-S adsorption to the surface was higher at pH 3.0, and it decreased by the pH elevation. At pH 3.0, L-S could develop a hydrophilic interaction with -COOH through its functional groups. However, this interaction diminishes due to the repulsion force resulted from the higher negativity of the -COOH surface at higher pH. The incapability of L-S in hydrogen

101

bonding development is once more observable due to its minimal adsorption to the surface, which was discussed earlier.[79,80]

A similar trend of reduction in the PVA-S adsorption to -COOH surface was observed by increasing the pH, which is due to the enhancement in the repulsion force between the polymer and the surface. While electrostatic interactions play a critical role in the adsorption of like-charged polymers (i.e., electrostatic repulsion), the interesting PVA-S adsorption on the negatively charged -COOH surface indicates the sensible development of nonelectrostatic interactions between PVA-S and COOH surface (e.g., van der Waals and hydrogen bonding).

3.4.5.3 Adsorption on -CH₃-Functionalized Surface

Figure 3.4c also reveals the adsorption of L-S and PVA-S polymers on the -CH₃ functionalized surface, while the raw data is presented in the supplementary information file in Figure S3.26-S3.27. As seen, the adsorbed mass of L-S onto the surface was reduced at all pH. This interaction reveals that L-S has adsorbed on the -CH₃ functionalized surface via a nonelectrostatic interaction (hydrophobic interaction), which is hypothesized to develop through its aromatic units. It has also been reported that by increasing the pH, the diffuse layer potential for CH₃ becomes negative, which leads to a reduction in the adsorption amount of negatively charged polyacrylate (PAA) and polystyrene sulfonate (PSS) on this surface.[23] Similar results were obtained for the adsorption of PVA-S on -CH₃ as a function of pH.

It is seen that L-S showed less hydrophobic interaction than PVA-S with the CH₃ functionalized surface at all pH studied. This might be because of the linear structure of PVA-S, which facilitates the hydrophobic interaction of PVA-S with the surface, while the three-dimensional structure of L-S prohibits the hydrophobic interaction of the aromatic core of lignin with CH₃ (*i.e.*, steric hindrance).

3.4.5.4 Adsorption on -NH₂-Functionalized Surface

The adsorption of the polymers on the positively charged -NH₂ functionalized surface is also included in Figure 3.4d, while the raw data is shown in the supplementary information file in Figures S3.28-S3.29. As seen, a sharp and fast decrease in the adsorbed mass of L-S onto -NH₂ surface is observed, which reveals a strong electrostatic attraction of this polymer with the surface at pH 3.0, since this surface bears ionized groups at this pH and appears in the form of NH_3^+. It has also been reported that in the oppositely charged systems, adsorption kinetics are very fast.[83,84] The polymer adsorption was reduced by increasing the pH, which might be due to the accumulation

of a larger amount of hydroxy ions at the NH_2/water interface. This leads to a reduction in the positivity of the surface, less electrostatic interaction with the polymer, and thus less adsorption.[23] Also, a similar trend of adsorption was observed for PVA-S as a function of pH. Comparing the adsorption of L-S on NH_2 and CH_3 (Figure 3.4) surfaces, the higher adsorption of L-S was observed on the NH_2 surface.

3.4.5.5 Overall Performance at Different pH

The results in Figures 4 suggest that L-S illustrated significantly different adsorption mechanisms than did PVA-S at different pH values. At pH 3.0, the maximum adsorption of L-S was observed on the NH_2 surface, while the highest adsorption of PVA-S was observed on the CH_3 surface. The monotonical decrease in the adsorption of L-S and PVA-S was observed with increasing the pH for almost all surfaces. The decrease in the adsorption was mainly reported to be attributed to the decrease in the magnitude of the diffuse-layer potential when this potential is contrary to that of the adsorbed polymer.[23,83,85] This effect is due to the reduction in the attraction force and subsequently enhanced repulsion force at the solid/water interface between the deposited polymers.[83,86] Also, the smaller changes in dissipation values of L-S than PVA-S were observed for almost all surfaces at different pH, which might be due to its lower adsorption to SAMs (Figures S3.22-S3.29).

Furthermore, increasing the pH (from 3.0 to 11.0) led to the enhancement in the hydrodynamic radius (R_h) of L-S and PVA-S polymers, and this change was more sensible for L-S (Figure S3.30), which can be due to its better solubility at higher pH. According to the contact angle analysis (Table S3.4), PVA-S was more hydrophilic than L-S at all pH. This means that PVA-S could trap more water in its structure, which might lead to more changes in the adsorbed mass upon its adsorption to SAM surfaces. Although these two polymers have the same amount of sulfonate groups, their structural difference[1] led to their altered interactions with varied surfaces. Also, its linear structure[2] favored the adsorption of PVA-S on the functionalized surfaces.

In general, the maximum adsorption amount of L-S (8.99 mg/m^2) was attained at pH 3.0 on the -NH_2 functionalized surface. Meanwhile, the highest adsorption amount of PVA-S (21.33 mg/m^2) was obtained at pH 3.0 on -CH_3 functionalized surface.

3.4.6 Effect of Salt Concentration on the Adsorption of L-S and PVA-S on SAMs

The adsorption of L-S and PVA-S on different functionalized surfaces at equilibrium is shown in Figures 5 and 6 (the original data is provided as Figure S3.31-S3.34 in the supplementary

information file). In saline systems, the long-range electrostatic double-layer interactions between the polymers and surfaces become remarkably small while the nonelectrostatic forces come into action.[23] By increasing the salt concentration, the adsorption of L-S polymer increased on all surfaces (Figure 3.5a). These results suggest that nonelectrostatic forces played a role in the adsorption of L-S on carboxyl and hydroxy-coated surfaces. The more significant change for OH and COOH might be due to nonelectrostatic forces becoming relatively important compared to electrostatic interaction in salty systems.
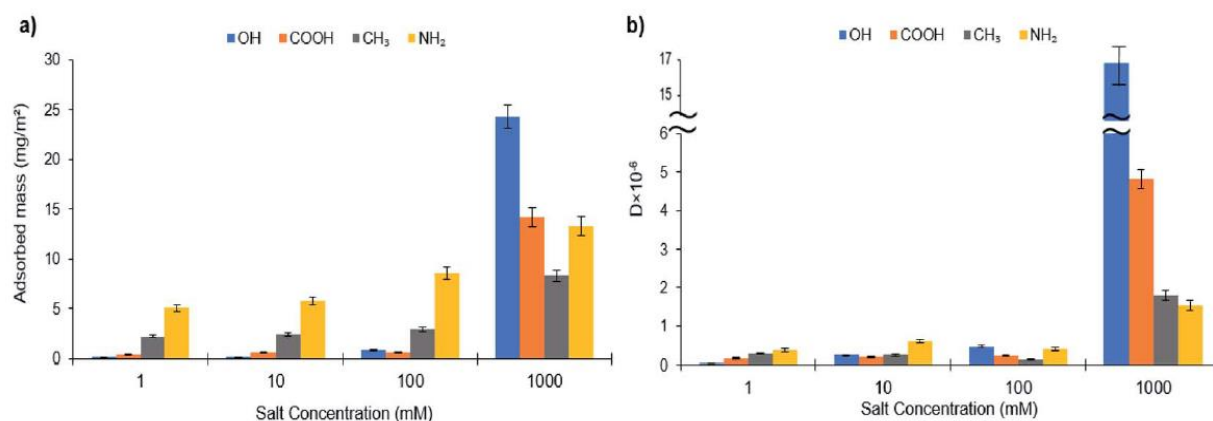
Figure 3.5. (a) Adsorbed mass and (b) dissipation of L-S on SAMs of different surfaces at different salt concentrations.

Figure 3.5b illustrates the dissipation changes on different alkanethiol surfaces. It is seen that the increase in the salt concentration (from 1 mM to 1000 mM) elevated the dissipation of L-S polymer on the -OH surface while depicting the maximum dissipation (16.48×10^6) at 1000 mM of salt concentration (Figure 3.5b). Other surfaces also showed an increase in their dissipation when salt concentration increased from 100 mM to 1000 mM. This increase in dissipation might be raised by two phenomena; an increase in the adsorption of L-S on the surfaces and adaptation of an extended configuration in salty systems (Figure S3.32), which might be due to screening of the intramolecular interactions in the L-S.[87] Increasing the salt concentration affected the hydrodynamic radius (R_h) of the polymer due to electrostatic shielding and attraction between sulfonate groups of L-S and cations available from salt. In this case, the R_h increment was observed to be more in L-S than in PVA-S (Figure S3.35). The addition of salt would increase the attraction between adjacent polymer cores by eliminating the electrostatic interaction and exposing the hydrophobic sites of the polymer. This would lead to more L-S particles to aggregate and thus

enhance L-S adsorption onto surfaces. Similar behaviour was observed for the self-aggregation of CNC (cellulose nanocrystals) at 160 mM KCl.[88]

Figure 3.6 depicts the adsorbed mass and dissipation of PVA-S adsorption on different functionalized surfaces as a function of salt concentration. If electrostatic interactions between the polymer and oppositely charged substrates were dominant, there would be a cutoff of adsorption with increased ionic strength, above which the adsorption would be decreased. Normally, the cutoff is abrupted when there are only electrostatic interactions deriving the adsorption.[86,89-91] The adsorption of PVA-S polymer decreased on the -OH surface, while it was increased on -COOH, -CH$_3$, and -NH$_2$ modified surfaces (Figure 3.6a). Compared to the results obtained from different surfaces, having constant adsorption indicates that nonelectrostatic forces dominated (rather than electrostatic interactions) when the polymer was not ionized.[23] Also, a decrease in the adsorption of PVA-S on the -OH surface in the saline system has been reported in other studies.[23,92] The fast adsorption kinetics (Figure S3.33) seen on positively charged NH$_2$ terminated thiolates were observed to be unaffected by increasing the ionic strength (Figure 3.6). This could be due to the electrostatic attraction force, which is always favorable and fast.[88,92,93]
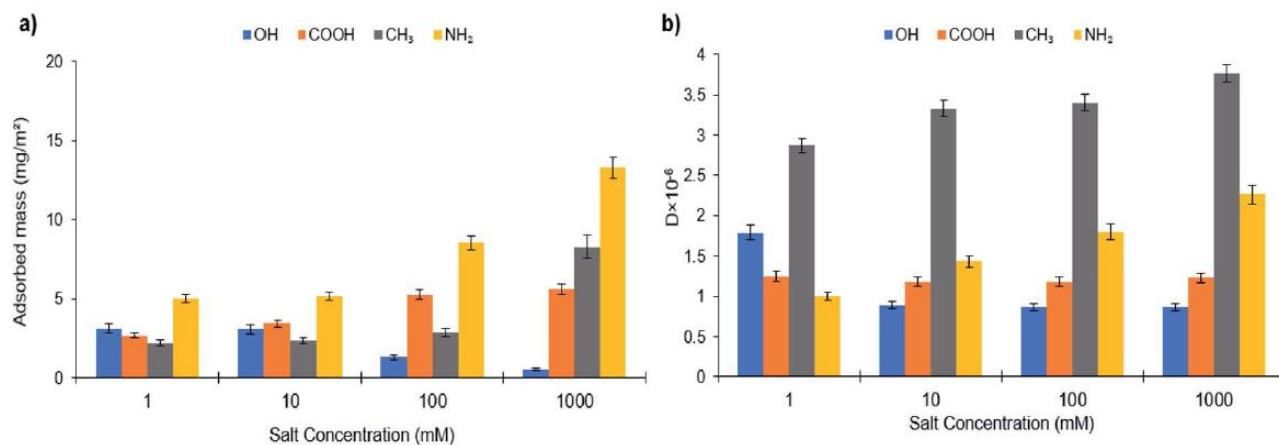
Figure 3.6. (a) Adsorbed mass and (b) dissipation of PVA-S on SAMs of different chemistry at different salt concentrations.

In contrast, the adsorption kinetics for liked-charged systems (PVA-S and L-S on -COOH SAMs) was slow while a late saturation was attained (Figures S3.32-3.33). Salt reduced the kinetic barrier between like-charged polymers and surfaces, further favoring the adsorption.[21,23] The noticeable change in the adsorbed mass of the -CH$_3$ surface indicates that the hydrophobic interaction

developed between the acetate group of the PVA-S and the surface, while all charges on the polymer were screened. The adsorbed mass was increased marginally for PVA-S on amine-rich monolayers by enhancing the ionic strength, which could be related to the higher adsorption of counterions from the solution, suppressing the polymer adsorption to this surface (Figure 3.6). Also, as mentioned earlier, the R_h of L-S and PVA-S increased as a result of an augment in salinity (Figure S3.35). This might be because increasing ionic strength causes the inter and intra-chain repulsion to develop a looser manner and expand polymer chains. These changes in the conformation of polymers lead to more sights become available for the interaction, which might have contributed to the increased adsorption of these polymers on most surfaces (Figures 5 and 6). Polymerized kraft lignin-acrylic acid (KL-AA) with a molecular weight of 7.4×10^5 g/mol was reported to have R_h value of 25.2 nm in salt-free solution.[95] Moreover, the same behavior has been reported in the literature for poly(potassium-2-sulfopropylmethacrylate) by the addition of salt.[96] In salinity, the highest adsorption amount for L-S polymer (24.32 mg/m^2) was attained at 1000 mM of salt concentration on the -OH functionalized surface. Meanwhile, the maximum adsorption of PVA-S (13.3 mg/m^2) was achieved at 1000 mM on the -NH$_2$ surface.

Figure 3.6b shows the dissipation changes on different alkanethiol surfaces with PVA-S adsorption concerning the ionic strength. It can be seen that the reduction in dissipation could be due to the decrease in the adsorption amount. In the case of -COOH, although the adsorbed mass was increased by the salt addition, the reduction in the dissipation could be due to PVA-S adopting a more compact structure, which was generated from nonelectrostatic forces in saline systems. In the case of -OH, -CH$_3$ and -NH$_2$ surfaces, the dissipation value was changed proportionally to the adsorption of PVA-S on these surfaces.

3.4.7 Application

OH-coated surfaces interact with other materials, such as organic dyes polyesters,[97] fatty acids, and alkyd resins.[98] These surfaces are generally used in wastewater treatments, polymer blends, attachment of antibodies, and crystal engineering.[9,99] The adsorption of L-S was less significant than PVA-S. This may make PVA-S a more effective coating material. Considering the temperature, salt, and pH variations, the results suggest that increasing the temperature, salt, and pH have an adverse impact on the adsorption of PVA-S onto the OH-functionalized surface.

For COOH coated surfaces that interact with other materials, such as proteins, surfactants, antigen detection,[100,101] PVA-S showed to be a more effective adsorbent than L-S, but its effectiveness was significantly affected by pH and temperature (Figures 3 and 4).

For CH$_3$ coated surfaces that interact with other materials, such as surfactants or surface-active agents,[102] and have applications such as self-cleaning, anti-fogging, and anti-corrosion,[103] PVA-S showed to be a better candidate. The temperature analysis showed the limited impact of PVA-S adsorption onto this surface. Also, the pH analysis confirmed that at acidic pH, hydrophobic interaction of both PVA-S and L-S polymers with the surface is more significant. The salinity analysis confirmed that a higher salt concentration (1000 mM) could increase the adsorption for both PVA-S and L-S polymers.

In NH$_2$ coated surfaces that interact with other materials, such as heavy metal, and have applications as flocculants, adsorbents, and dispersants, PVA-S observed to be a better candidate. The temperature analysis showed the limited impact of temperature variation on PVA-S adsorption and adverse effect on L-S adsorption. Also, the pH analysis confirmed that alkaline pH has a negative impact on the adsorption for both PVA-S and L-S polymers. The salt analysis confirmed that increasing the salt increases the adsorption for both PVA-S and L-S polymers.

Also, the contact angle analysis confirmed that PVA-S is more hydrophilic than the L-S polymer. Based on the second virial coefficient (A_2) obtained from static light scattering, increasing the temperature adversely impacted the water solubility of PVA-S, while increasing that of L-S. Based on the hydrodynamic radius obtained from dynamic light scattering, pH enhancement has a more impact on the L-S polymer than PVA-S. On the other hand, PVA-S showed sensitivity to temperature, pH, and salt. Although the L-S adsorption was more limited, it was insensitive to temperature. Therefore, L-S could be used in applications that are sensitive to temperature but do not require a high level of adsorption. Also, the adsorption of L-S showed improvement by increasing the salt concentration. This demonstrates the ability of lignin in developing different interaction mechanisms with different functionalized surfaces over PVA-S in saline systems. Thus, the contribution of nonelectrostatic forces seems to be more significant in the L-S polymer, illustrating practically an irreversible adsorption onto all surfaces, and its adsorption to the surfaces even when the electrostatic barrier exists. Therefore, it could be revealed that in applications that contain salts, e.g. wastewater treatment,[15] additives for composites,[104] lignin could be a better candidate to be used than PVA-S.

3.4.8 Future Trend

Understanding the interaction of sulfonated lignin and PVA would help advance scenarios to improve the properties of lignin for generating super functional lignin derivatives. The analysis in this paper reveals that the inherent steric hindrance of lignin may need to be reduced, via depolymerization, oxidation, for instance, for elevating its adsorption on surfaces. Furthermore, raised from its folded and compact molecular structure, most of the functional groups on lignin were not exposed but need to be activated. The larger R_h of lignin and its improved adsorption performance is evidence for the importance of reducing the steric hindrance of lignin for its improved properties. Alternatively, lignin can be decorated with more functional groups to boost its interaction with surfaces. For example, a combination of sulfonation, carboxylation, and polymerization may induce lignin with desired properties.

3.5 Conclusions

There has not been any systematic study in the literature on evaluating the performance of synthetic and lignin-based polymers having a similar charge density and molecular weight on well-defined self-assembled monolayers. In this study, we synthesized two types of anionic polymers of lignin-3-sulfopropyl methacrylate (L-S), and poly (vinyl alcohol-*co*-vinyl acetate)-3-sulfopropyl methacrylate (PVA-S) with similar charge densities and molecular weights. The R_h and R_g of PVA-S were smaller than those of L-S, while it had a larger A_2. The A_2 of PVA-S decreased with augment in the temperature whereas it enhanced for L-S, which was in agreement with the more compact structure of PVA-S. On the OH surface, PVA-S was adsorbed more than L-S, which could be due to the limited hydrogen bonding. Also, temperature, salt, and pH variations adversely affected the adsorption of PVA-S onto this surface. Although PVA-S was a more effective adsorbent on the COOH coated surface due to its higher solubility, pH and temperature were observed to remarkably impact its adsorption performance. The adsorption of both polymers was also increased with salinity enhancement on the COOH-surface. For the CH_3 coated surface, although the PVA-S was observed to be a better candidate than L-S, increasing the temperature enhanced the L-S adsorption onto this surface due to more exposure of its hydrophobic parts. Interestingly, under acidic conditions, the hydrophobic interaction of both PVA-S and L-S polymers with the surface was increased. PVA-S also adsorbed more onto NH_2 coated surface than L-S due to its solubility and polymer structure. The temperature was more significantly affected the L-S adsorption onto this surface than did PVA-S, while the similar negative impact of the increase in

the pH was observed for the adsorption of both polymers onto this surface. Also, in saline systems, L-S adsorption was improved more significantly compared to PVA-S. Overall, the maximum adsorption of L-S and PVA-S polymers were observed on -OH functionalized surface at 1000 mM salt (24.32 mg/m^2) and on -CH$_3$ functionalized surface at pH 3.0 (21.33 mg/m^2), respectively.

3.6 References

1) E. R. Van der Hage, M. M. Mulder and J. J. Boon, J. Anal. Appl. Pyrolysis, 1993, 25, 149-183.
2) F. Wang, P. Chandler, R. Oszust, E. Sowell, Z. Graham, W. Ardito and X. Hu, J. Therm. Anal. Calorim., 2017, 127, 923-929.
3) S. Jie, Y. Li, B. Jie, Z. Chu-shu, L. Shao-fang, Z. Feng and Y. Qing-li, Rsc Adv., 2013, 3, 10619-10622.
4) A. Veerabhadraiah, S. Ramakrishna, G. Angadi, M. Venkatram, V. K. Ananthapadmanabha, K. N. M. H. NarayanaRao and K. Munishamaiah, Appl. Nanosci., 2017, 7, 355-363.
5) J. A. Gidigbi, S. A. Osemeahon, A. M. Ngoshe and A. Babanyaya, IJRIAR, 2019, 3, 231-244.
6) T. Moritani and J. Yamauchi, Polymer, 1998, 39, 559-572.
7) S. Ur-Rehman, M. Noman, A. D. Khan, A. Saboor, M. S. Ahmad and H. U. Khan, Optik, 2020, 202, 163591.
8) T. Moritani and J. Yamauchi, Polymer, 1998, 39, 553-557.
9) A. E. Kazzaz, Z. H. Feizi and P. Fatehi, Green Chem., 2019, 21, 5714-5752.
10) M. Moradipour, E. K. Chase, M. A. Khan, S. O. Asare, B. C. Lynn, S. E. Rankin, and B. L. Knutson, Colloids Surf. B., 2020, 111028.
11) X. Luo, A. Mohanty and M. Misra, Ind. Crops Prod., 2013, 47, 13-19..
12) Z. H. Feizi, A. E. Kazzaz, F. Kong and P. Fatehi, Sep. Purif. Technol., 2019, 222, 254-263.
13) A. E. Kazzaz, and P. Fatehi, Ind. Crops Prod., 2020, 154, 112732.
14) A. E. Kazzaz, Z. H. Feizi and P. Fatehi, Colloid Polym. Sci., 2018, 296, 1867-1878.
15) J. Chen, A. E. Kazzaz, N. AlipoorMazandarani, Z. H. Feizi and P. Fatehi, Molecules, 2018, 23, 868.
16) R. Vanholme, B. Demedts, K. Morreel, J. Ralph and W. Boerjan, Plant physiol., 2010, 153, 895-905.
17) T. M. Garver and P. T. Callaghan, Macromolecules,1991, 24, 420-430.
18) S. L. Clark and P. T. Hammond, Langmuir, 2000, 16, 10206-10214.
19) X. Jiang, C. Ortiz and P. T. Hammond, Langmuir, 2002, 18, 1131-1143.
20) Friedsam, A. D. C. Bécares, U. Jonas, M. Seitz and H. E. Gaub, New J. Phys., 2004, 6, 9.
21) P. Maroni, F. J. M. Ruiz-Cabello and A. Tiraferri, Soft Matter, 2014, 10, 9220-9225.
22) H. Eto, N. Soga, H. G. Franquelim, P. Glock, A. Khmelinskaia, L. Kai and P. Schwille, ACS Appl. Mater. Interfaces, 2019, 11, 21372-21380.
23) P. Maroni, F. J. Montes Ruiz-Cabello, C. Cardoso and A. Tiraferri, Langmuir, 2015, 31, 6045-6054.
24) Y. Song, J. Park, C. Lim and D. W. Lee, ACS Sustainable Chem. Eng., 2020, 8, 362-371.
25) A. E. Kazzaz and P. Fatehi, J. Colloid Interface Sci., 2020, 561, 231-243.
26) J. J. Gooding, F. Mearns, W. Yang and J. Liu, Electroanalysis, 2003, 15, 81-96.

27) S. Huang, Q. Hou, D. Guo, H. Yang, T. Chen, F. Liu and J. Wang, RSC adv., 2017, 7, 39530-39538.

28) C. K. Haweel and S. H. Ammar, J. Chem. Pet. Eng., 2008, 9, 15-21.

29) S. Contreras, A. R. Gaspar, A. Guerra, L. A. Lucia and D. S. Argyropoulos, Biomacromolecules, 2008, 9, 3362-3369.

30) S. M. Munzert, G. Schwarz and D. G. Kurth, RSC adv., 2016, 6, 15441-15450.

31) F. C. Giacomelli, I. C. Riegel, C. L. Petzhold, N. P. da Silveira and P. Štěpánek, Langmuir, 2008, 25, 731-738.

32) P. Dimitrov, M. Jamróz-Piegza, B. Trzebicka and A. Dworak, Polymer, 2007, 48, 1866-1874.

33) H. Hussain, B. H. Tan, G. L. Seah, Y. Liu, C. B. He and T. P. Davis, Langmuir, 2010, 26, 11763-11773.

34) C. L. Berhaut, D. Lemordant, P. Porion, L. Timperman, G. Schmidt and M. Anouti, RSC adv., 2019, 9, 4599-4608.

35) A, Ishikubo, J. Mays and M. Tirrell, Ind. Eng. Chem. Res., 2008, 47, 6426-6433.

36) Z. H. Feizi and P. Fatehi, Cellulose, 2020, 27, 3759–3772.

37) M. K. Konduri, F. Kong and P. Fatehi, Eur. Polym. J,. 2015, 70, 371-383.

38) A. E. Kazzaz, Z. H. Feizi, F. Kong and P. Fatehi, Colloids Surf. A, 2018, 556, 218-226.

39) C. J. Huang, F. S. Shieu, W. P. Hsieh and T. C. Chang, J. Appl. Polym. Sci., 2006, 100, 1457-1464.

40) P. Maes, Y. B. Monakhova, T. Kuballa, H. Reusch and D. W. Lachenmeier, J. Agric. Food Chem., 2012, 60, 2778-2784.

41) J. Hedin, J. E. Löfroth and M. Nydén, Langmuir, 2007, 23, 6148-6155.

42) H. Wang, S. Chen, L. Li and S. Jiang, Langmuir, 2005, 21, 2633-2636.

43) M. L. Wallwork, D. A. Smith, J. Zhang, J. Kirkham and C. Robinson, Langmuir, 2001, 17, 1126-1131.

44) L. Herrer, V. Sebastian, S. Martín, A. González-Orive, F. Pérez-Murano, P. J. Low and P. Cea, Nanoscale, 2017, 9, 13281-13290.

45) C. D. Bain and G. M. Whitesides, J. Phys. Chem., 1989, 93, 1670-1673.

46) Q. Li, R. Yuan and Y. Li, J. Appl. Polym. Sci., 2013, 128, 206-215.

47) E. Pensini, C. M. Yip, D. O'Carroll and B. E. Sleep, J. Colloid Interface Sci., 2013, 402, 58-67.

48) G. Masci, D. Bontempo, N. Tiso, M. Diociaiuti, L. Mannina, D. Capitani and V. Crescenzi, Macromolecules, 2004, 37, 4464-4473.

49) Y. Xu, A. Walther and A. H. Müller, Macromol. Rapid Commun., 2010, 31, 1462-1466.

50) I. Korbag and S. Mohamed Saleh, Int. J. Environ. Stud., 2016, 73, 226-235.

51) H. Lee, M. F. Rubner and R. E. Cohen, Coating, US Pat., 2012, 13 215 869.

52) R. Hajiraissi, M. Hanke, Y. Yang, B. Duderija, A. Gonzalez Orive, G. Grundmeier, A. Keller, Langmuir, 2018, 34, 3517-3524.

53) H. T. Phan, S. Bartelt-Hunt, K. B. Rodenhausen, M. Schubert and J. C. Bartz, PloS one, 2015, 10, e0141282.

54) J. A. Jones, L. A. Qin, H. Meyerson, I. K. Kwon, T. Matsuda and J. M. Anderson, J. Biomed. Mater. Res., Part A., 2008, 86, 261-268.

55) J. Li, T. Guan, C. Hao, L. Li, and Y. Zhang, J. Chem (Hindawi), 2015, 10.

56) S. D. Evans, R. Sharma, and A. Ulman, Langmuir, 1991 7, 156-161.

57) K. S. Chong, S. Sun and G. J. Leggett, Langmuir, 2005, 21, 3903-3909.

58) J. C. Love, L. A. Estroff, J. K. Kriebel, R. G. Nuzzo and G. M. Whitesides, Chem. Rev., 2005, 105, 1103-1170.

59) H. Hussain, K. Busse and J. Kressler, Macromol. Chem. Phys., 2003, 204, 936-946.

60) C. Booth and D. Attwood, Macromol. Rapid Commun., 2000, 21, 501-527.

61) Y. Kawata, S. Kozuka and S. I. Yusa, Langmuir, 2018, 35, 1458-1464.

62) K. Huber, S. Bantle, P. Lutz and W. Burchard, Macromolecules, 1985, 18, 1461-1467.

63) T. Konishi, T. Yoshizaki and H. Yamakawa, Macromolecules, 1991, 24, 5614-5622.

64) H. Hussain, K. Y. Mya and C. He, Langmuir, 2008, 24, 13279-13286.

65) J. H. Yao, K. Y. Mya, X. Li, M. Parameswaran, Q. H. Xu, K. P. Loh and Z. K. Chen, J. Phys. Chem. B, 2008, 112, 749-755.

66) H. Hussain, B. H. Tan, C. S. Gudipati, Y. Liu, C. B. He and T. P. Davis, J. Polym. Sci.; Part A: Polym. Chem., 2008, 46, 5604-5615.

67) T. Liu, Z. Zhou, C. Wu, B. Chu, D. K. Schneider and V. M. Nace, J. Phys. Chem. B, 1997, 101, 8808-8815.

68) B. Jeong, Y. H. Bae and S. W. Kim, Colloids Surf., B, 1999, 16, 185-193.

69) E. Castro, S. Barbosa, J. Juarez, P. Taboada, I. A. Katime and V. Mosquera, J. Phys. Chem. B, 2008, 112, 5296-5304.

70) A. A. Tager, A. A. Anikeyeva, L. V. Adamova, V. M. Andreyeva, T. A. Kuz'mina and M. V. Tsilipotkina, Polym. Sci. USSR, 1971, 13, 751-758.

71) V. T. Matsuo and H. Inagaki, Chem. Phys., 1962, 53, 130-144.

72) J. Liu, C. Detrembleur, M. Hurtgen, A. Debuigne, M. C. De Pauw-Gillet, S. Mornet and C. Jérôme, Polym. Chem., 2014, 5, 5289-5299.

73) N. A. Cortez-Lemus and A. Licea-Claverie, Polymers, 2018, 10, 20.

74) J. P. Inwood, L. Pakzad and P. Fatehi, 2018, 13, 53-70.

75) A. N. Evdokimov, A. V. Kurzin, O. V. Fedorova, P. V. Lukanin, V. G. Kazakov and A. D. Trifonova, Wood Sci. Technol., 2018, 52, 1165-1174.

76) M. Norgren and B. Lindström, Holzforschung, 2000, 54, 519-527.

77) W. Zhu and H. Theliander, BioResources, 2015, 10, 1696-1714.

78) R. Ou, H. Zhang, J. Wei, S. Kim, L. Wan, N. S. Nguyen and H. Wang, Adv. Mater., 2018, 30, 1802767.

79) R. K. Sharma, J. B. Wooten, V. L. Baliga, X. Lin, W. G. Chan and M. R. Hajaligol, Fuel, 2004, 83, 1469-1482.

80) A. A. M. Nada, M. A. Yousef, K. A. Shaffei and A.M. Salah, Polym. Degrad. Stab., 1998, 62, 157-163.

81) A. D. Phan and T. X. Hoang, Chem. Phys. Lett., 2019, 730, 84-88.

82) X. Zhang, Z. Zhao, G. Ran, Y. Liu, S. Liu, B. Zhou and Z. Wang, Powder technol., 2013, 246, 664-668.

83) I. Popa, B. P. Cahill, P. Maroni, G. Papastavrou and M. Borkovec, J. Colloid Interface Sci., 2007, 309, 28-35.

84) M. Porus, P. Maroni and M. Borkovec, Langmuir, 2012, 28, 5642-5651.

85) Bauer, H. Buchhammer, A. Fuchs, W. Jaeger, E. Killmann, K. Lunkwitz, R. Rehmet and S. Schwarz, Colloids Surf. A, 1999, 156, 291-305.

86) I. Szilagyi, G. Trefalt, A. Tiraferri, P. Maroni and M. Borkovec, Soft Matter, 2014, 10, 2479-2502.

87) A. Sweity, W. Ying, M. S. Ali-Shtayeh, F. Yang, A. Bick, G. Oron and M. Herzberg, Water research, 2011, 45, 6430-6440.

88) T. Phan-Xuan, A. Thuresson, M. Skepö, A. Labrador, R. Bordes and A. Matic, Cellulose, 2016, 23, 3653-3663.

89) M. Jiang, I. Popa, P. Maroni and M. Borkovec, Colloids Surf. A, 2010, 360, 20-25.

90) J. Forsman, Langmuir, 2012, 28, 5138-5150.

91) Xie, T. Nylander, L. Piculell, S. Utsel, L. Wågberg, T. Åkesson and J. Forsman, Langmuir, 2013, 29, 12421-12431.

92) S. J. De Carvalho, R. Metzler and A. G. Cherstvy, Phys. Chem. Chem. Phys., 2014, 16, 15539-15550.

93) N. Hansupalak, and M. M. Santore, Langmuir, 2003, 19, 7423-7426.

94) N. G. Hoogeveen, M. A. C. Stuart and G. J. Fleer, J. Colloid Interface Sci., 1996, 182, 133-145.

95) F. Kong, S. Wang, W. Gao and P. Fatehi, RSC adv., 2018, 8, 12322-12336.

96) D. J. Liaw and C. C. Huang, J. Appl. Polym. Sci., 1997, 63, 175-185.

97) K. J. D. MacKenzie, Woodhead Publ., 2015, 777-805.

98) D. H. Solomon and J. J. Hopwood, J. Appl. Polym. Sci., 1966, 10, 981-991.

99) D. Andrews, G. Scholes and G. Wiederrecht, Academic Press 2010.

100)   P. K. Ajikumar, J. K. Ng, Y. C. Tang, J. Y. Lee, G. Stephanopoulos and H. P. Too, Langmuir, 2007, 23, 5670-5677.

101)   M. Gasser, B. Rothen-Rutishauser, H. F. Krug, P. Gehr, M. Nelle, B. Yan and P. Wick, J. Nanobiotechnol., 2010, 8, 31.

102)   S. Jawaid and A. K. Boufi, HPS, Woodhead Publ., 2017.

103)   M. K. Meena, B. K. Tudu, A. Kumar and B. Bhushan, Philos. Trans. R. Soc., 2020, 378, 20190446.

104)   C. Salas, O. J. Rojas, L. A. Lucia, M. A. Hubbe and J. Genzer, ACS Appl. Mater. Interfaces, 2013, 5, 199-206.

3.7 Appendix A. Supplementary material

Electronic Supplementary Information

Interaction of Synthetic and Lignin-based Sulfonated Polymers with Hydrophilic, Hydrophobic, and Charged Self-Assembled Monolayers

Armin Eraghi Kazzaz and Pedram Fatehi*

Biorefining Research Institute, Green Processes Research Centre and Chemical Engineering Department, Lakehead University, 955 Oliver Road, Thunder Bay, ON, Canada, P7B5E1

* Corresponding author

Supporting methods

Gel Permeation Chromatography (GPC)

In this set of experiments, 40 mg of pretreated (under different pH) PVA-A and L-S samples were dissolved in 10 mL of 0.1 mol/L of NaNO$_3$ solution and filtered using a 0.2 µm nylon filter and used for molecular weight analysis. The eluent of the system was 0.1 M sodium nitrate solution with a flow rate of 0.7 mL/min in the GPC. The refractometer (RI) and differential pressure (DP) detectors were used to determine the molecular weight of the samples. All measurements were conducted with respect to standard polyethylene oxide.

Phenolic hydroxy and carboxylate group analysis

The phenolic hydroxy and carboxylate group contents were determined according to eq. S3.1 and eq. S3.2, respectively:

$$\text{Phenolic hydroxy group (mmol/g)} = \frac{\left(\left(\text{EP}'_2 - \text{EP}'_1\right) - \left(\text{EP}_2 - \text{EP}_1\right)\right) \times C}{m} \qquad (S3.1)$$

$$\text{Carboxylate group (mmol/g)} = \frac{\left(\left(\text{EP}'_3 - \text{EP}'_2\right) - \left(\text{EP}_3 - \text{EP}_2\right)\right) \times C}{m} \qquad (S3.2)$$

where C is the concentration of HCl (mol/L) as a titrant, m is the dried weight of the polymer used in the analysis. EP$'_1$, EP$'_2$, and EP$'_3$ are the used volumes of HCl solution (mL) at the first, second, and third end points when the S-L sample was titrated. EP$_1$, EP$_2$, and EP$_3$ are the consumed volumes of HCl solution (mL) at the first, second, and third end points, respectively, when titrating the control sample (blank solution).

^{1}H NMR and FTIR spectroscopy

In this experiment, 1 mg of TMSP and 25-40 mg of the samples were dissolved in 500 μL of D_2O or $[D_6]DMSO$ for 12 h at 50 °C in a water bath shaker at 150 rpm.[1,2]

The FTIR experiment was carried out by using ~0.1 g of freeze-dried polymer samples. Then, 32 scans of each sample with a 4 cm^{-1} resolution and the spectra range of 700 to 4000 cm^{-1} were recorded.

Quartz crystal microbalance with dissipation (QCM-D)

Senses were cleaned by using the following procedure. The gold sensors were cleaned with a mixture of 1:1:5 of H_2O_2 (30%): NH_3 (25%): Milli-Q water for 7 min at 60 °C, rinsed with Milli-Q water and then dried nitrogen gas. The sensors were further cleaned by UV/ozone (digital UV ozone system, PSD Series, NOVASCAN) and treated for 10 min. Hereafter, they were rinsed with Milli-Q water and dried with nitrogen gas.

The adsorbed wet mass per unit based on the Sauerbrey model is calculated following eq. (S3.3):

$$\Delta m_{sauerbrey} = -\frac{C\Delta f}{n} \qquad (S3.3)$$

where Δm and Δf are adsorbed mass and frequency changes, respectively. C is a constant value (0.177 mg/m^2 Hz for 5 MHz AT-cut quartz crystal sensor), n is the measurement overtone used.

Supporting results

^1H NMR spectroscopy

In Figure S3.1, the peak at 7.42-5.99 ppm is attributed to the aromatic protons, the peak at 4.5-3.05 and 3.6-3.2 ppm are ascribed to the methoxy group protons of lignin's, and methylene protons in the β-β structure, respectively. The peaks appearing at 4.7, and 0.0 ppm are assigned to D_2O, and TMSP (3-trimethylsilyl-(2,2,3,3-D_4)-propionic acid sodium salt), respectively.[2-4] In Figure S3.2, the peaks at 2.52, and 3.5 ppm are associated with $[D_6]DMSO$ and H_2O.[5]
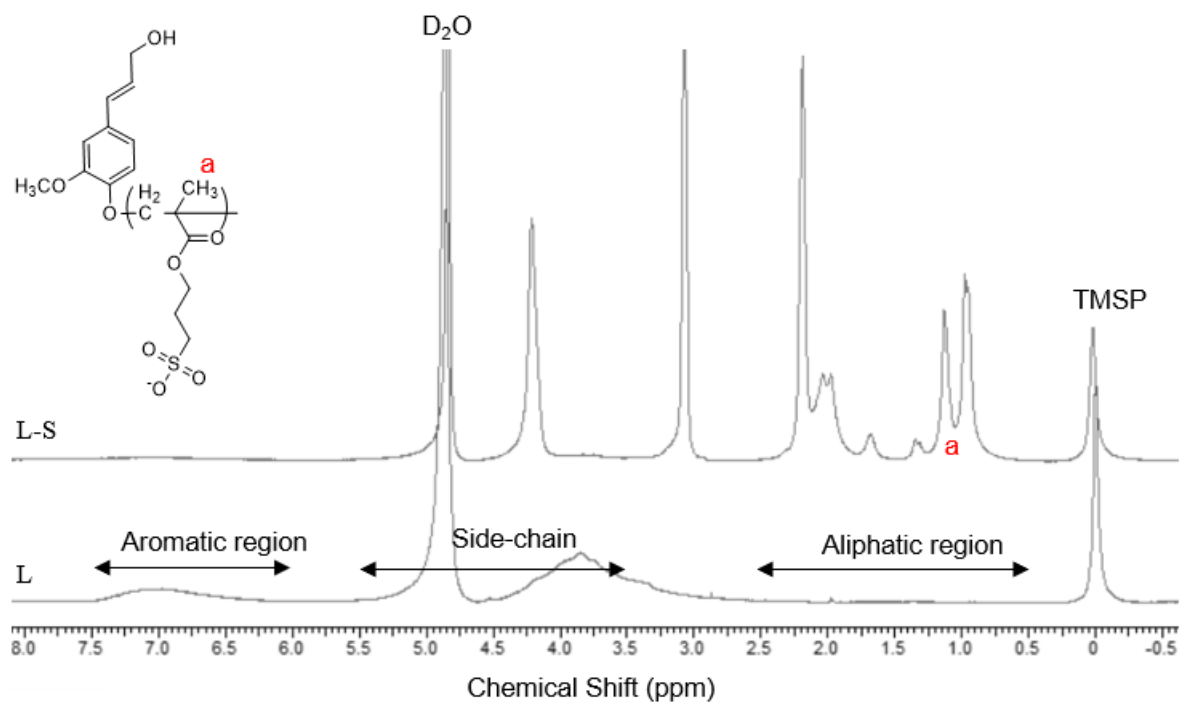
Figure S3.1. ^{1}H NMR spectrum of L, and L-S in D_2O, at 25 °C.
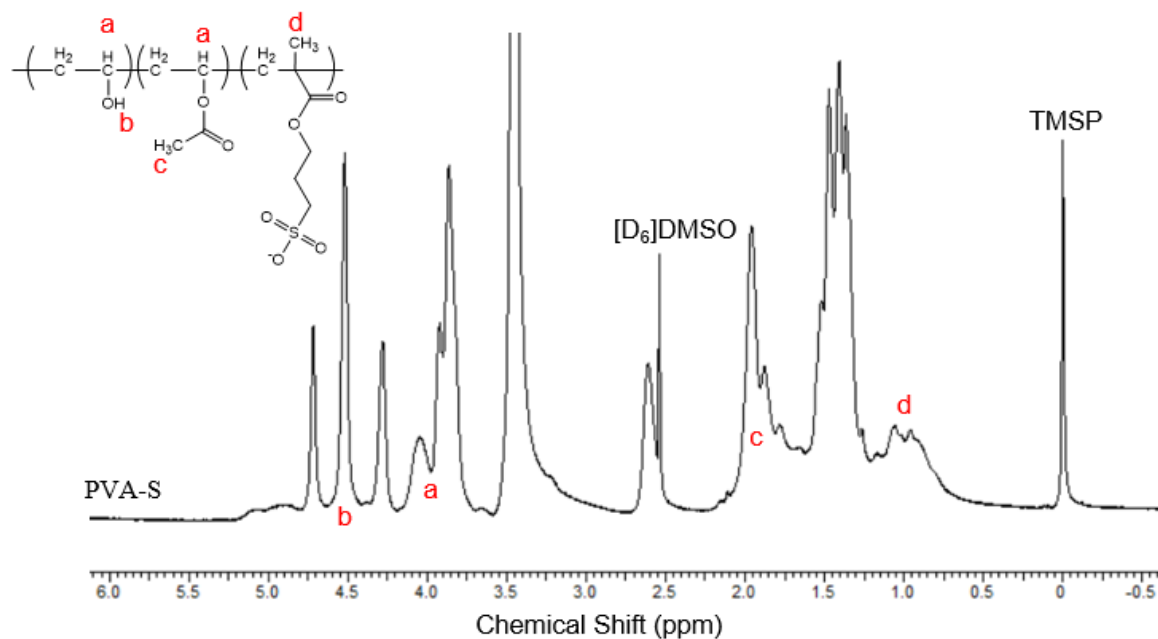
Figure S3.2. ^{1}H NMR spectrum PVA-S in [D_6]DMSO, at 25 °C.

FTIR Spectroscopy

115
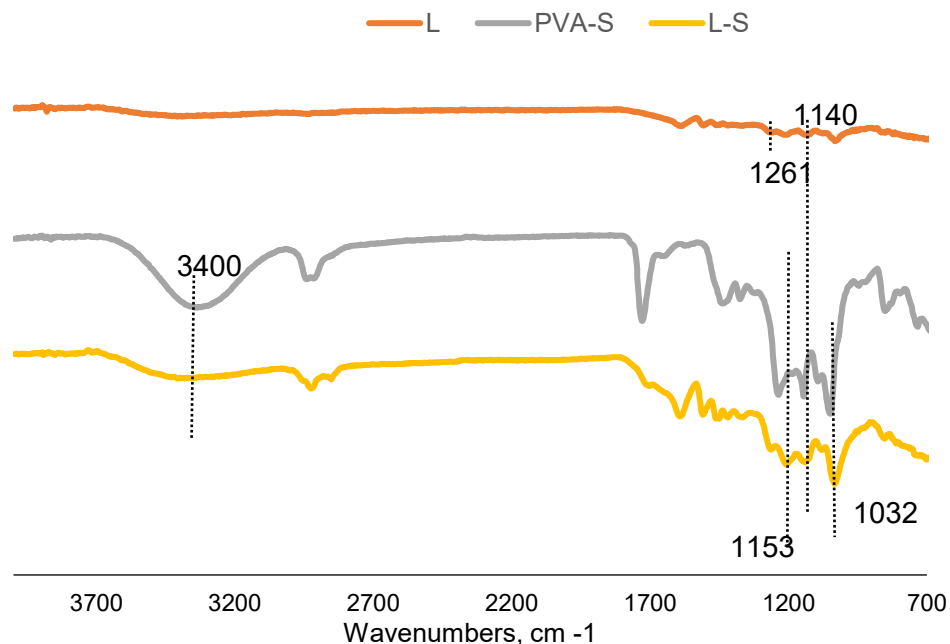
Figure S3.3. FTIR spectra of L, PVA-S, and L-S samples, at 25 °C.

Table S3.1. Assignment of the adsorption in FTIR spectra.

Entry	Band position (cm^{-1})	Assignment	References
1	1261	The C-O stretch of guaiacyl unit	2,6,7
2	1140	The C-H stretch of guaiacyl unit	2,7,8
3	3400	O-H stretching absorption in the phenolic and aliphatic parts of lignin	6
4	1032	C-O-C bond illustrating the ether linkages between the polymer and anionic monomer	6,9
5	1140+-20	The S=O stretch of the sulfonate group	10,11
6	1750-1711	C=O stretch of ester	1,5
7	3000-2800	C-H stretching vibration of ester	1

Gel permeation chromatography (GPC)

116

Table S3.2. PVA-S, and L-S molecular weight analysis by GPC after incubation for 12 h and dialysis.

pH	PVA-S molecular weight (g/mol)	L-S molecular weight (g/mol)
4.0	104,500	111,200
6.7	113,100	114,700
11.0	103,000	114,500

Zeta potential analysis
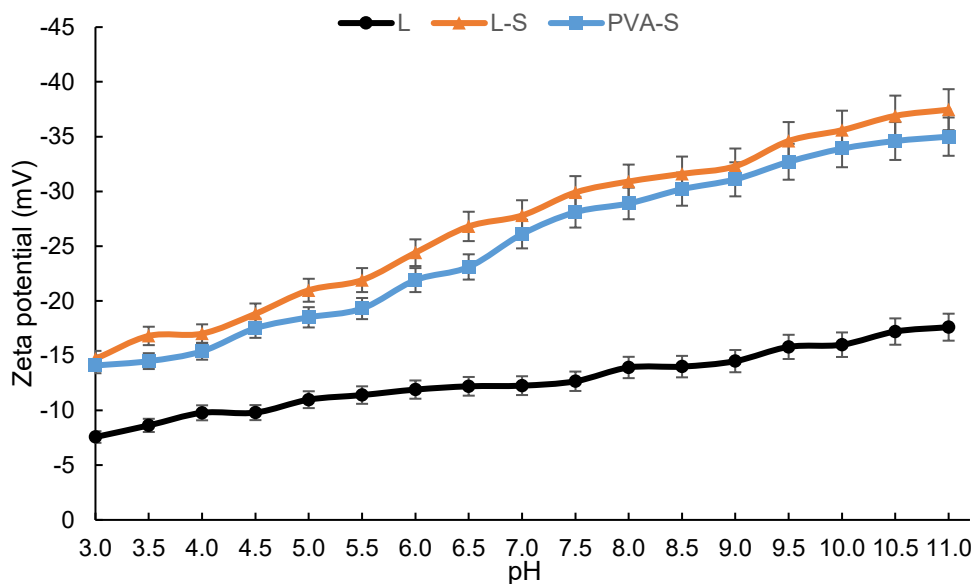
Figure S3.4. The zeta potential analysis of L, L-S, and PVA-S samples under different pH at 25 °C.

X-ray photoelectron spectroscopy (XPS)

Table S3.3. Surface composition of the SAM-terminated surfaces.

Chemical formula	SAMs name	Atomic percentage (at.%)			
		N	C	O	S
$HS(CH_2)_{11}OH$	11-mercapto-1-undecanol	-	82.6	13.1	4.3
$HS(CH_2)_{11}COOH$	12-mercaptododecanoic acid	-	78.4	18.5	3.1
$HS(CH_2)_{11}CH_3$	1-dodecanethiol	-	91.6	3.8	4.6
$HS(CH_2)_6NH_2\ HCl$	6-amino-1-hexanethiol hydrochloride	5.6	78.7	11.1	4.6
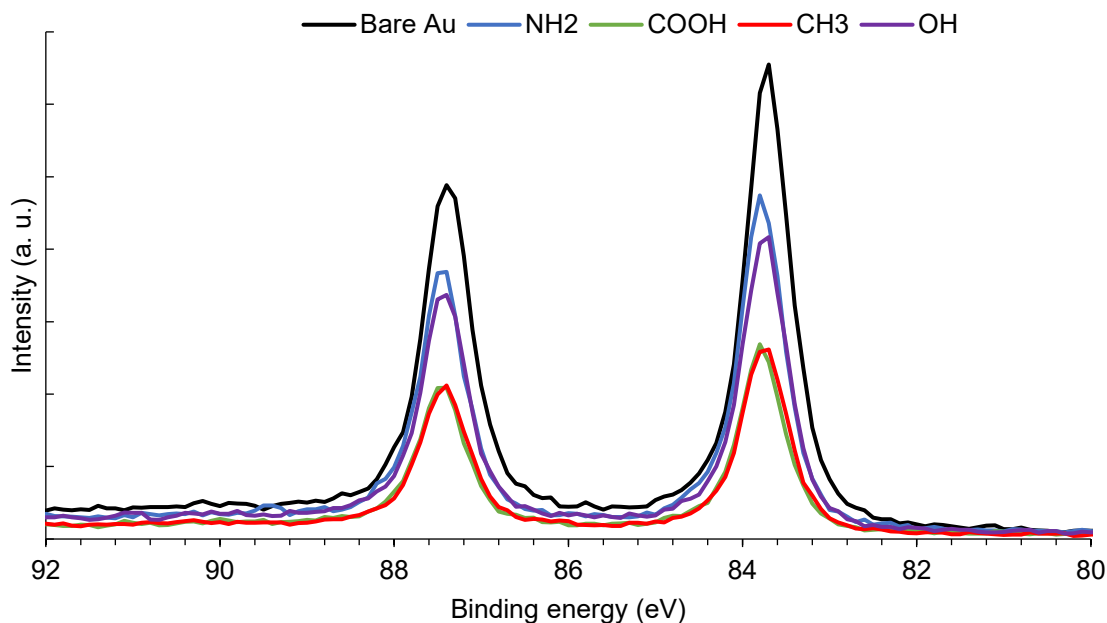
Figure S3.5. XPS high-resolution spectra in the Au4f region for a bare gold (as reference), and different terminated SAMs on Au.

Water adsorption at a different temperature on different SAM surfaces

Adsorption on -OH-functionalized surface
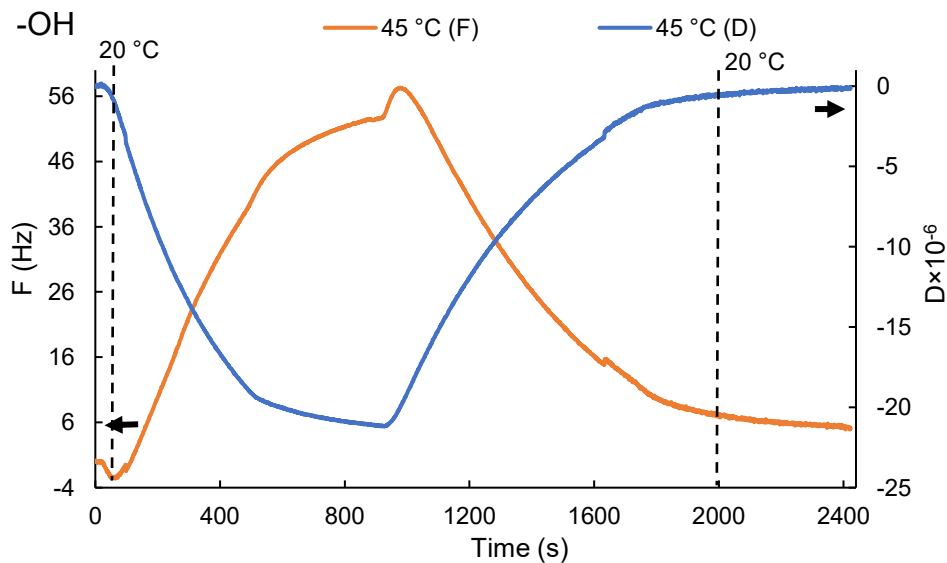
Figure S3.6. Frequency and dissipation changes of the 9th overtone of water adsorption on the -OH-functionalized surface at different temperatures.

Adsorption on -COOH-functionalized surface
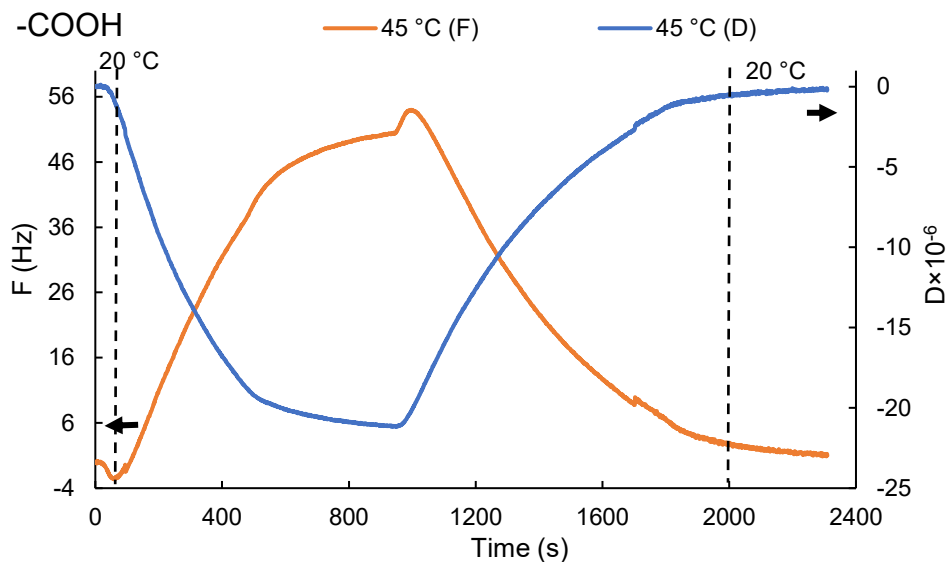
Figure S3.7. Frequency and dissipation changes of the 9th overtone of water adsorption on the -COOH-functionalized surface at different temperatures.

Adsorption on -CH₃-functionalized surface
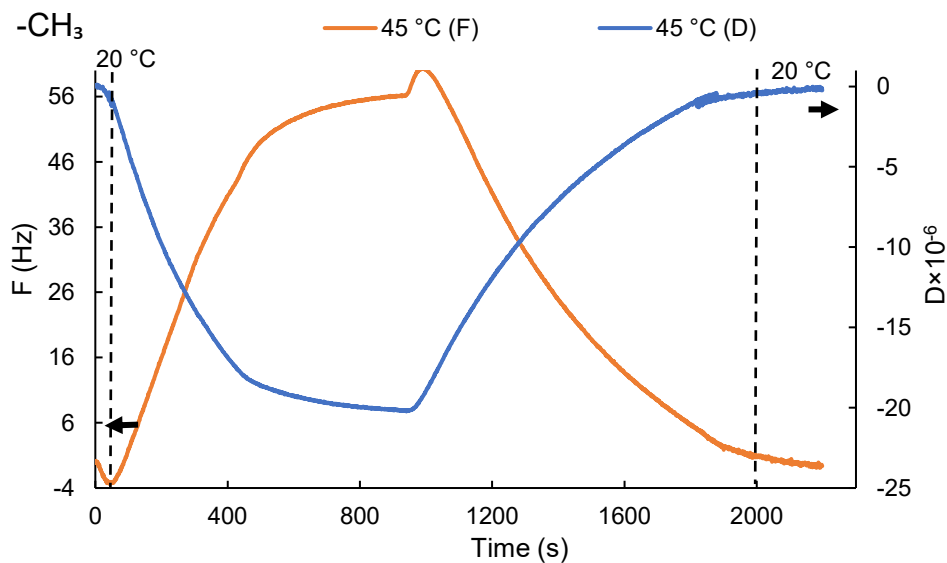
Figure S3.8. Frequency and dissipation changes of the 9th overtone of water adsorption on the -CH₃-functionalized surface at different temperatures.

Adsorption on -NH₂-functionalized surface
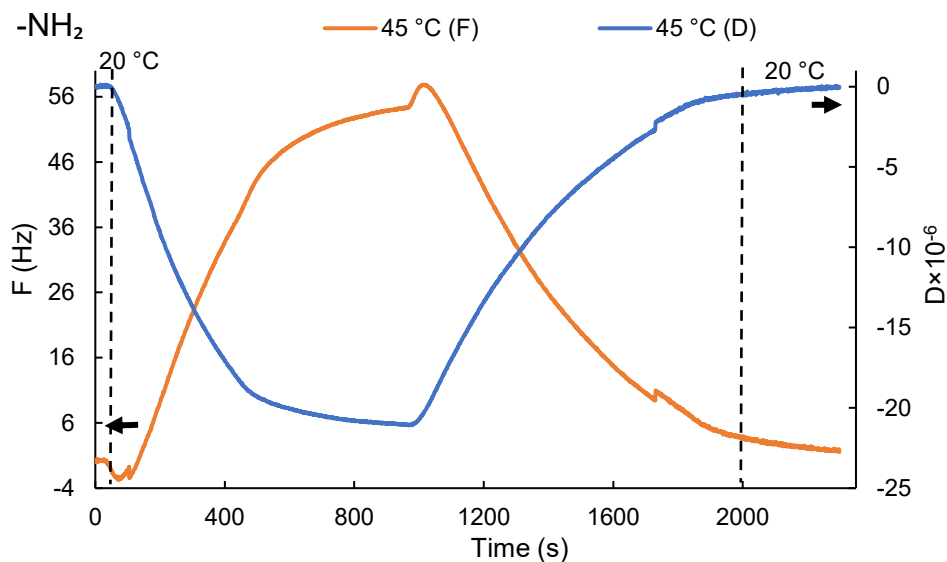
Figure S3.9. Frequency and dissipation changes of the 9th overtone of water adsorption on the -NH$_2$-functionalized surface at different temperatures.

Water adsorption at different pH on different SAM surfaces

Adsorption on -OH-functionalized surface
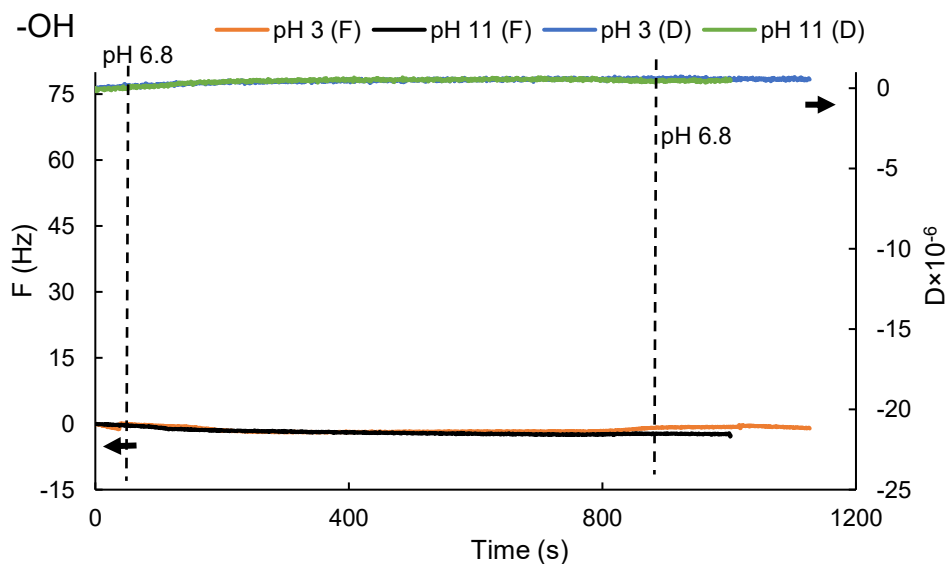
Figure S3.10. Frequency and dissipation changes of the 9th overtone of water adsorption on the -OH-functionalized surface at pH.

Adsorption on -COOH-functionalized surface
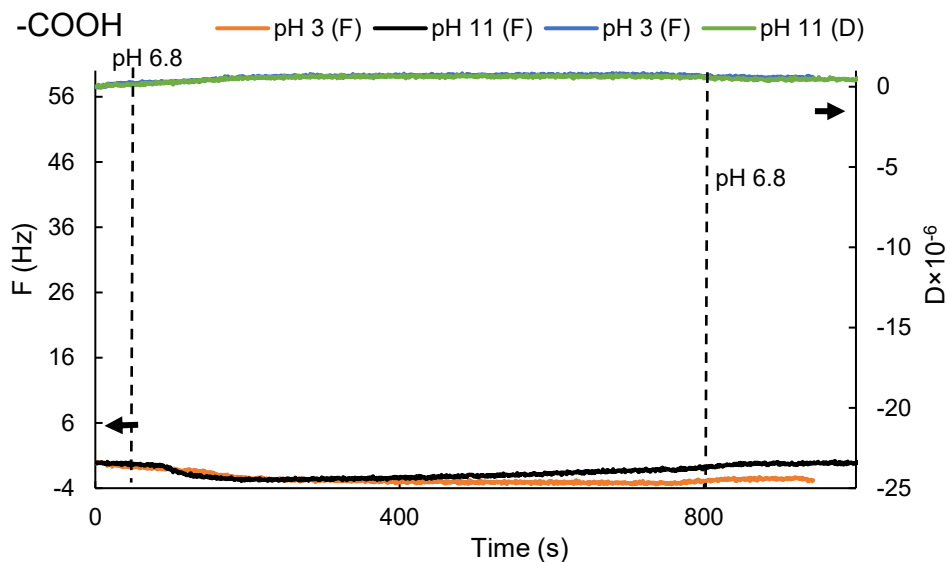
Figure S3.11. Frequency and dissipation changes of the 9th overtone of water adsorption on the -COOH-functionalized surface at pH.

Adsorption on -CH$_3$-functionalized surface
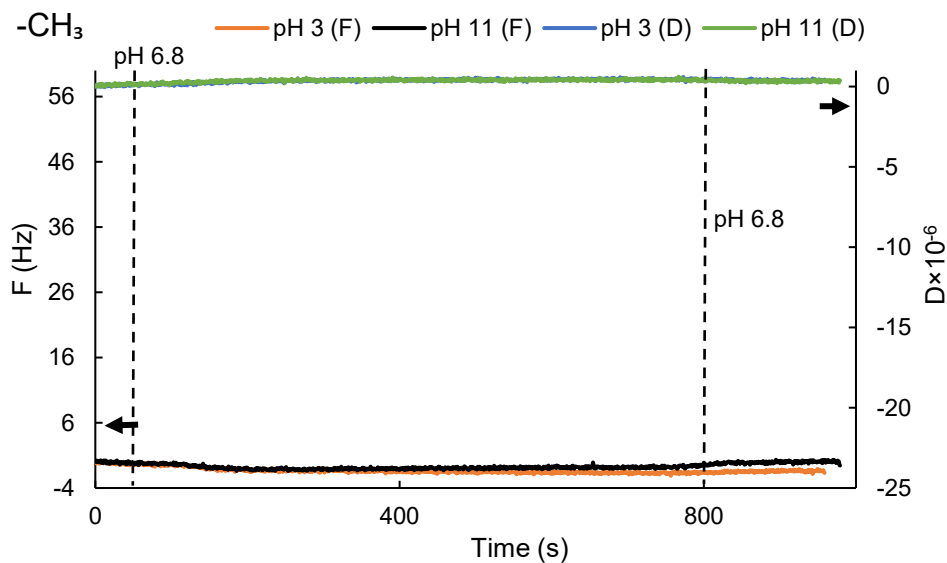
Figure S3.12. Frequency and dissipation changes of the 9th overtone of water adsorption on the -CH$_3$-functionalized surface at pH.

Adsorption on -NH$_2$-functionalized surface
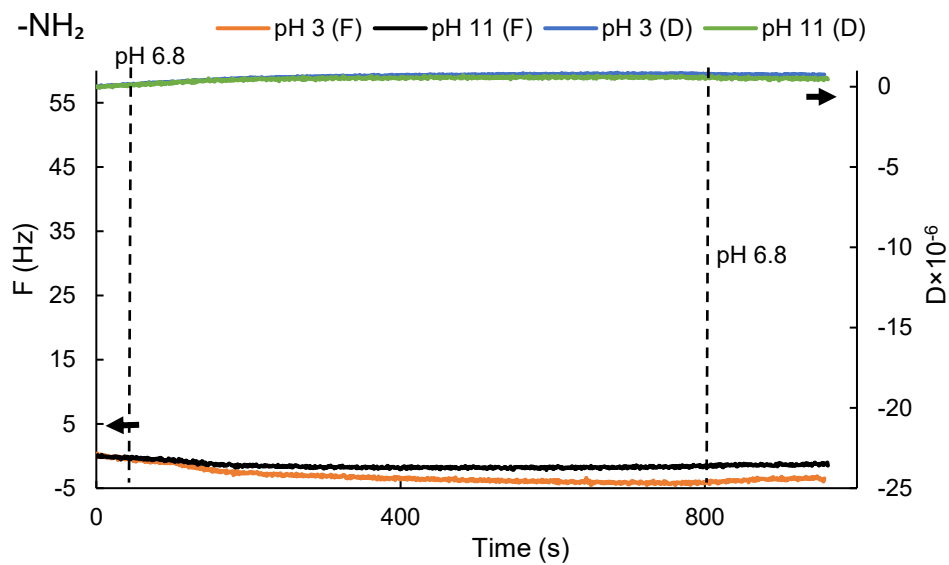
Figure S3.13. Frequency and dissipation changes of the 9th overtone of water adsorption on the -NH$_2$-functionalized surface at pH.

Effect of temperature on the adsorption of L-S, and PVA-S on SAMs

Adsorption on -OH-functionalized surface

a) -OH

b) -OH
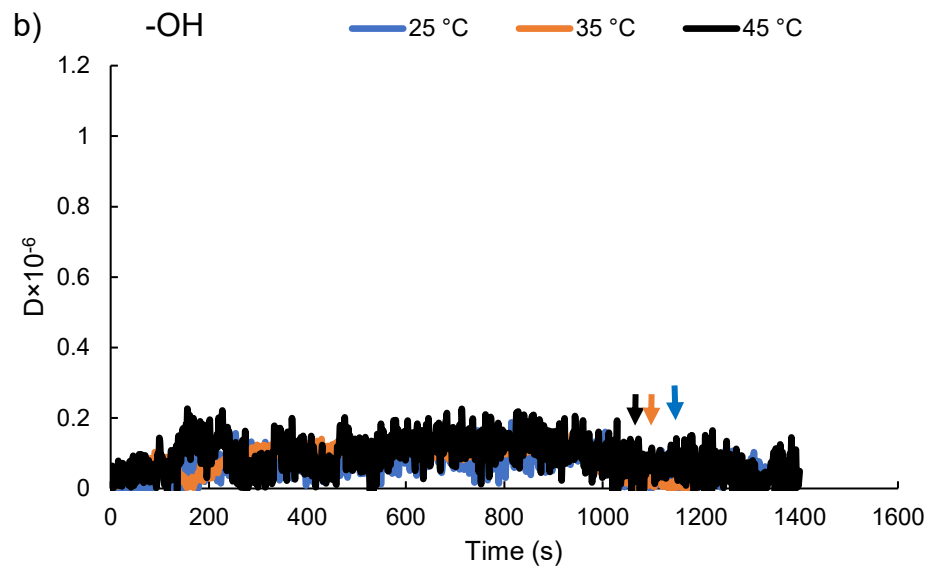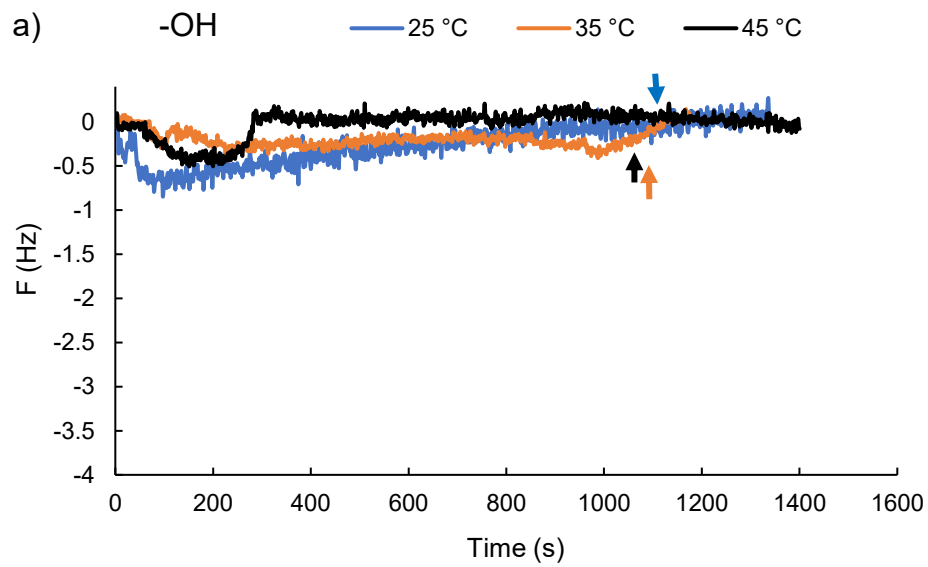
Figure S3.14. a) frequency b) dissipation changes of the 9th overtone of the adsorption of L-S polymer on the -OH-functionalized surface at different temperatures (arrows indicate buffer rinsing).
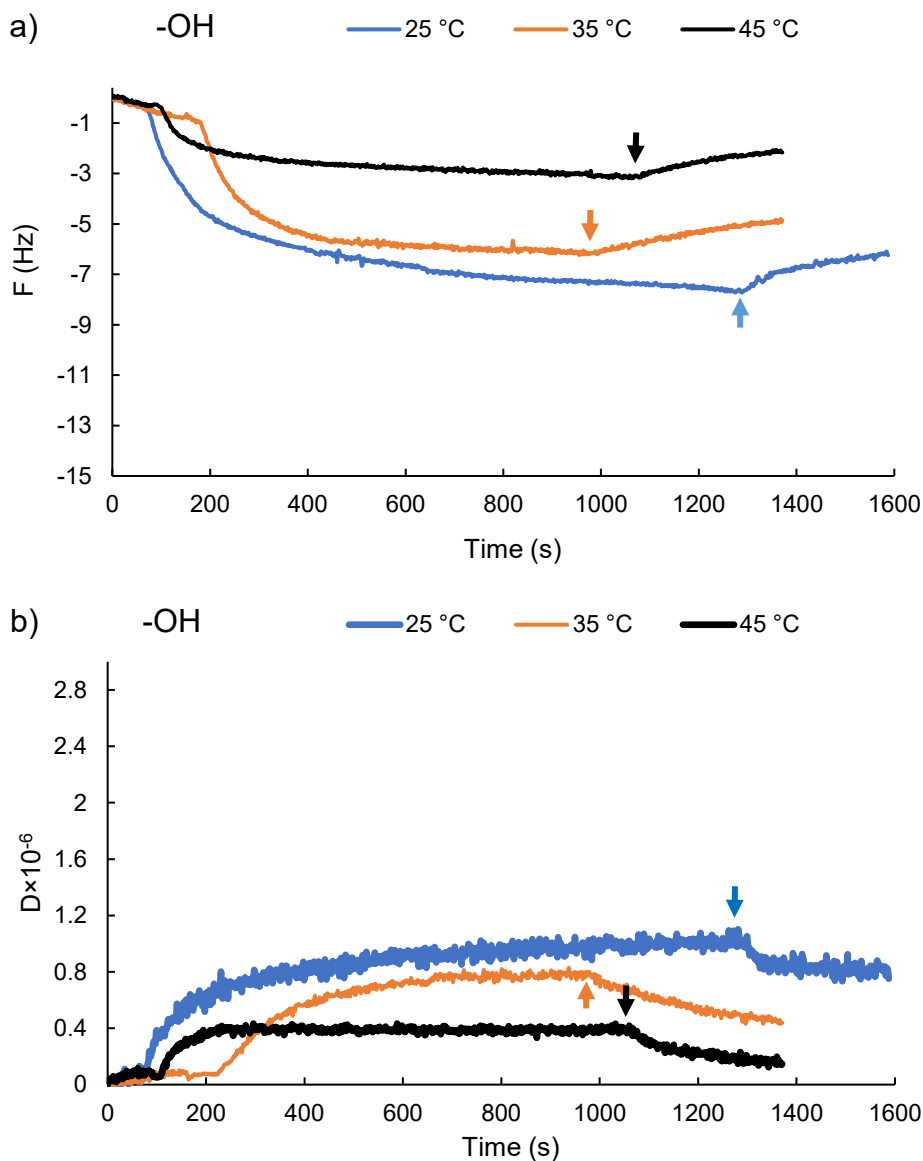
Figure S3.15. a) frequency b) dissipation changes of the 9th overtone of the adsorption of PVA-S polymer on the -OH-functionalized surface at different temperatures (arrows indicate buffer rinsing).

Adsorption on -COOH-functionalized surface

a) -COOH   — 25 °C   — 35 °C   — 45 °C

b) -COOH   — 25 °C   — 35 °C   — 45 °C
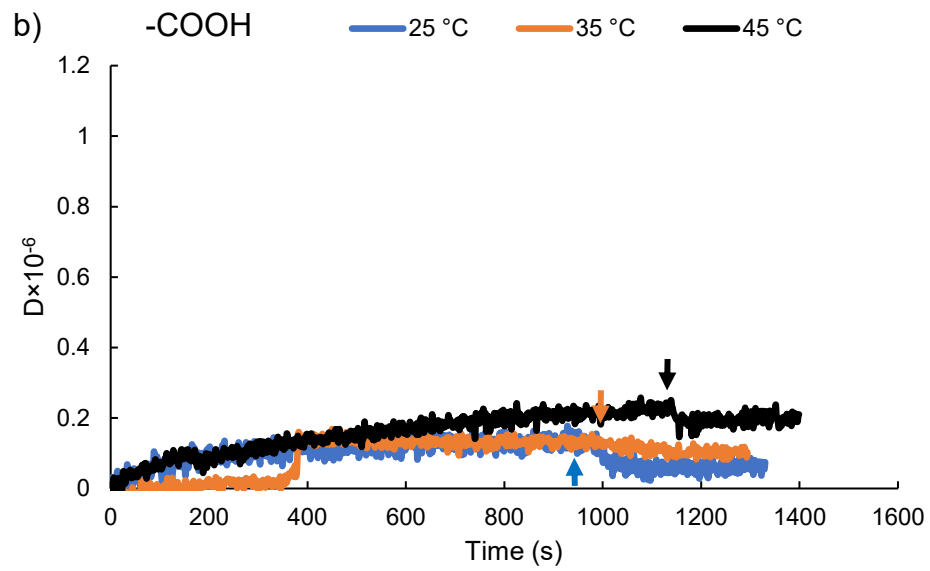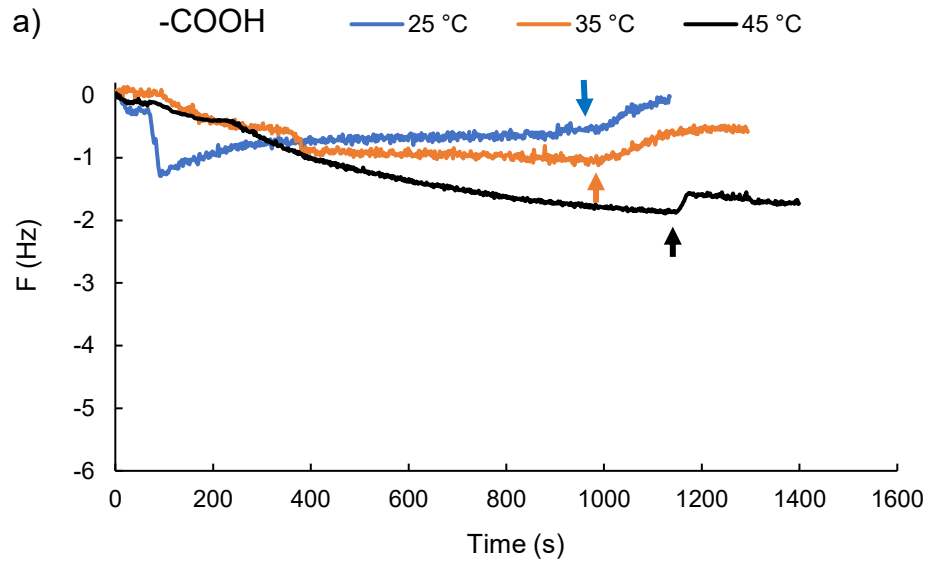
Figure S3.16. a) frequency b) dissipation changes of the 9th overtone of the adsorption of L-S polymer on the -COOH-functionalized surface at different temperatures (arrows indicate buffer rinsing).
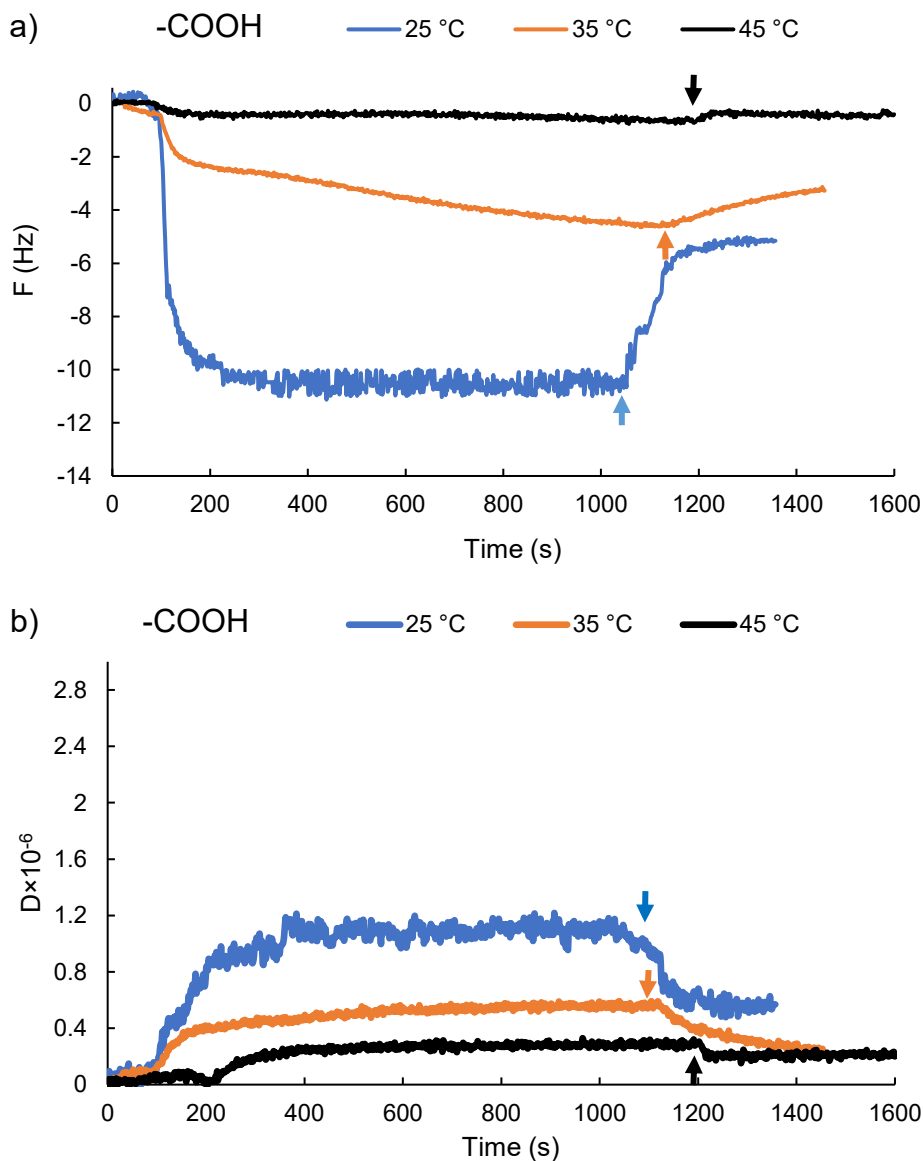
Figure S3.17. a) frequency b) dissipation changes of the 9th overtone of the adsorption of PVA-S polymer on the -COOH-functionalized surface at different temperatures (arrows indicate buffer rinsing).

Adsorption on -CH₃-functionalized surface

a) -CH₃ — 25 °C — 35 °C — 45 °C

b) -CH₃ — 25 °C — 35 °C — 45 °C
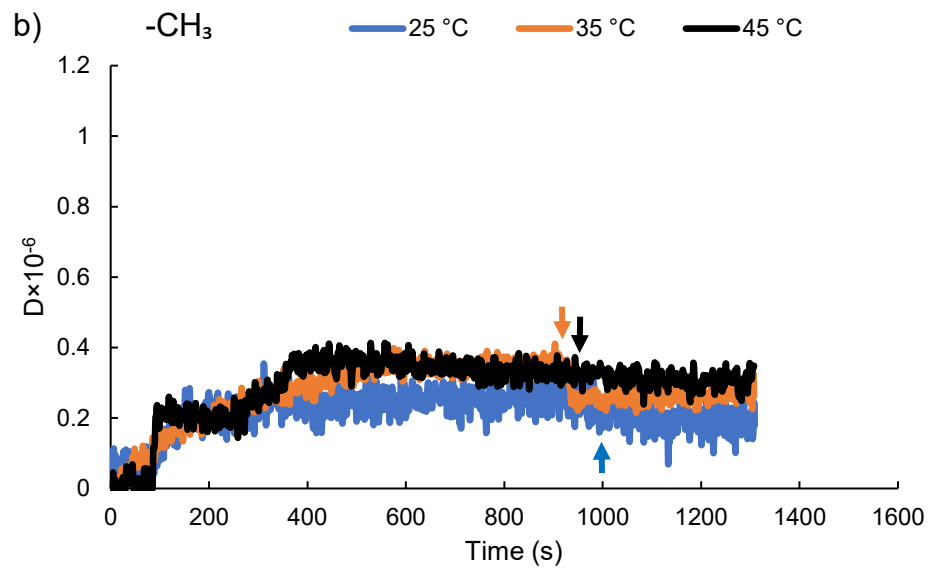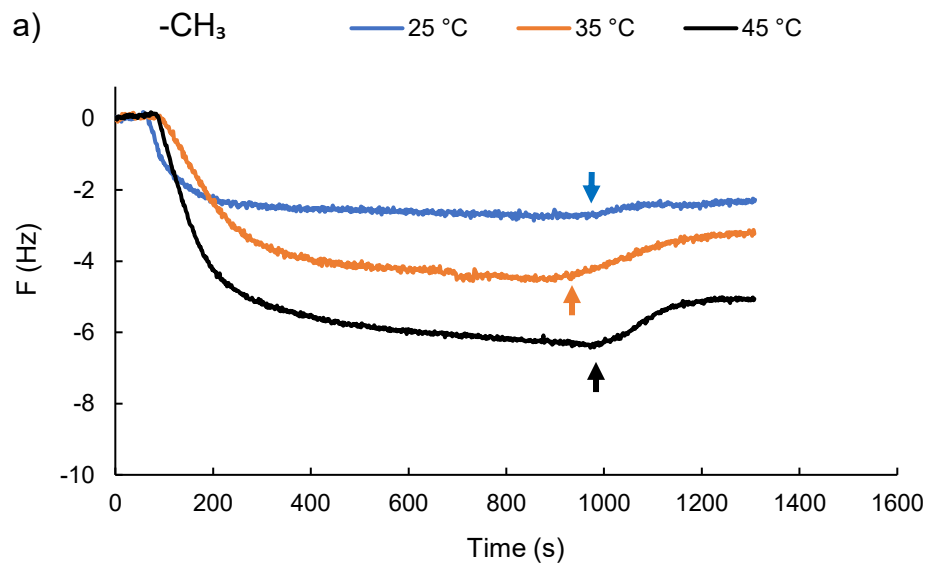
Figure S3.18. a) frequency b) dissipation changes of the 9th overtone of the adsorption of L-S polymer on the -CH$_3$-functionalized surface at different temperatures (arrows indicate buffer rinsing).
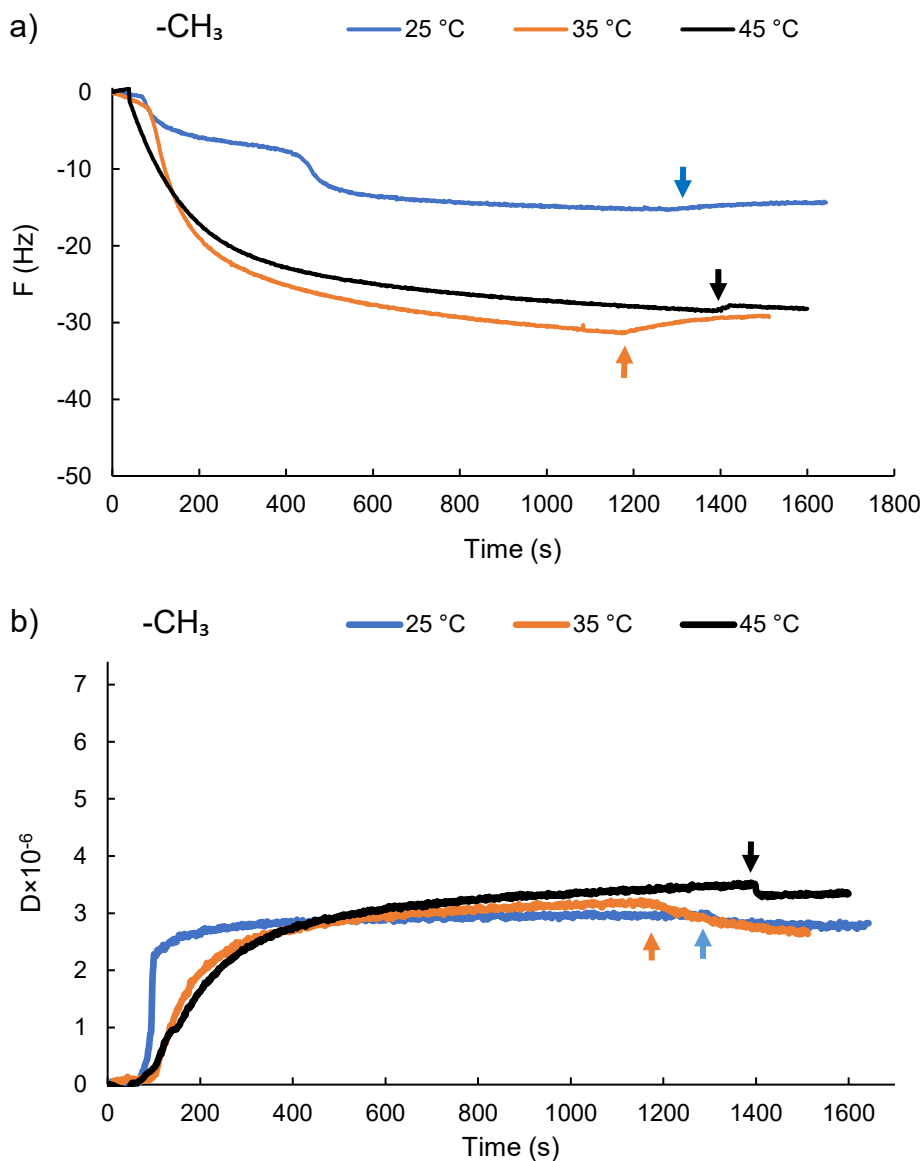
Figure S3.19. a) frequency b) dissipation changes of the 9th overtone of the adsorption of PVA-S polymer on the -CH$_3$-functionalized surface at different temperatures (arrows indicate buffer rinsing).

Adsorption on -NH$_2$-functionalized surface

a) -NH₂ ── 25 °C ── 35 °C ── 45 °C

b) -NH₂ ── 25 °C ── 35 °C ── 45 °C
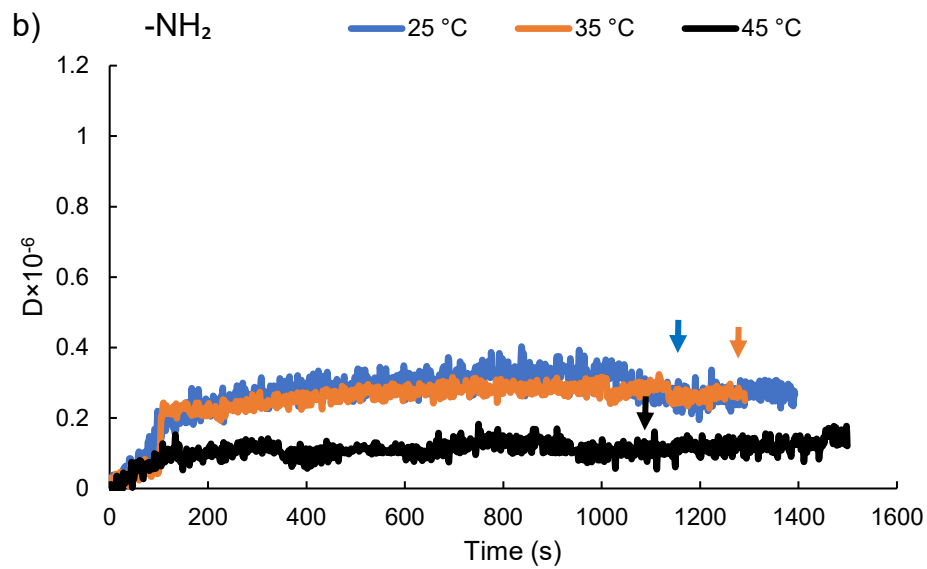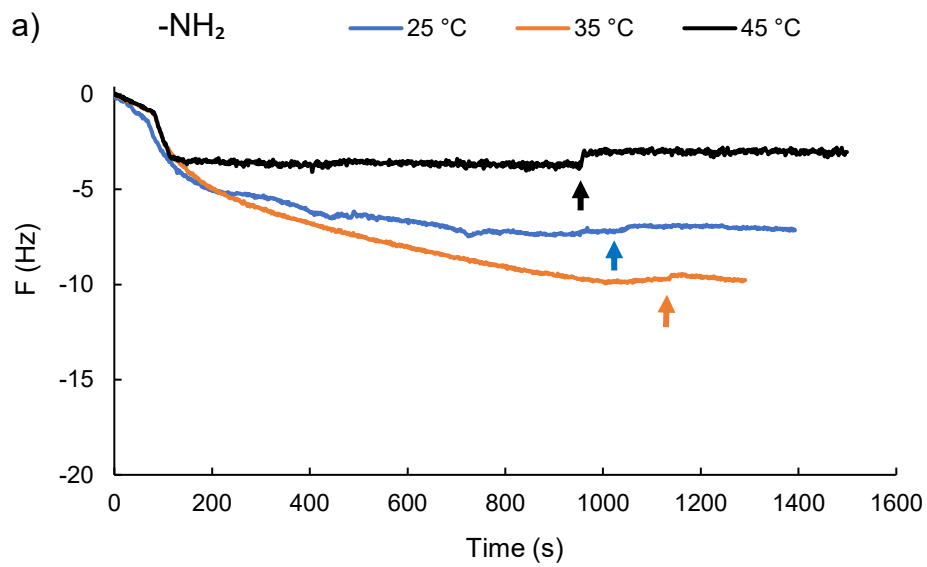
Figure S3.20. a) frequency b) dissipation changes of the 9th overtone of the adsorption of L-S polymer on the -NH$_2$-functionalized surface at different temperatures (arrows indicate buffer rinsing).
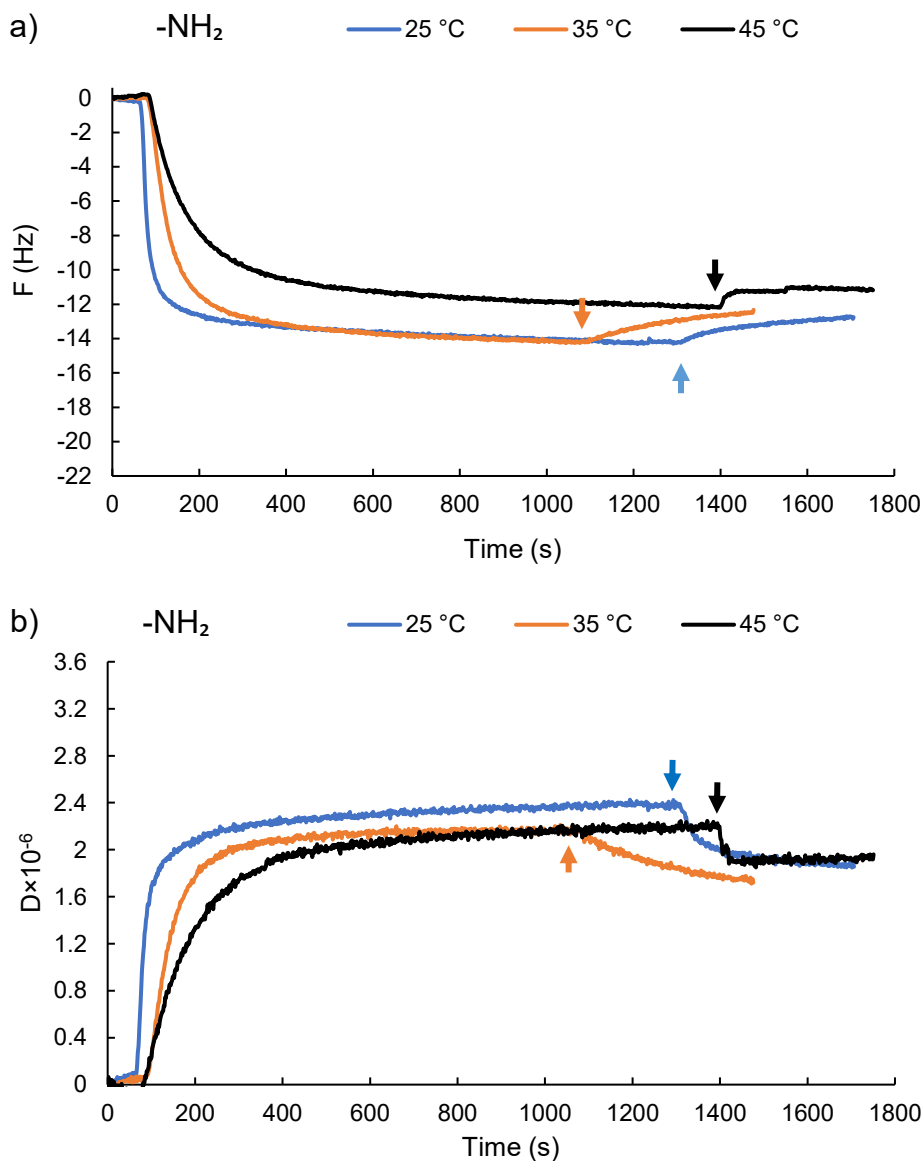
Figure S3.21. a) frequency b) dissipation changes of the 9th overtone of the adsorption of PVA-S polymer on the -NH$_2$-functionalized surface at different temperatures (arrows indicate buffer rinsing).

Effect of pH on the adsorption of L-S, and PVA-S on SAMs

Adsorption on -OH-functionalized surface

a) -OH   pH 3.0 pH 6.8 pH 11.0

b) -OH   pH 3.0 pH 6.8 pH 11.0

131
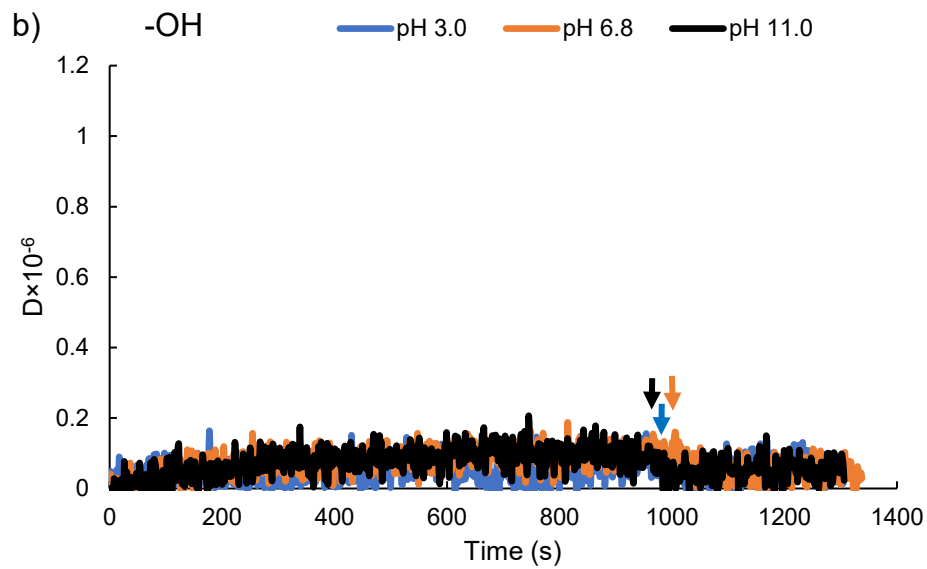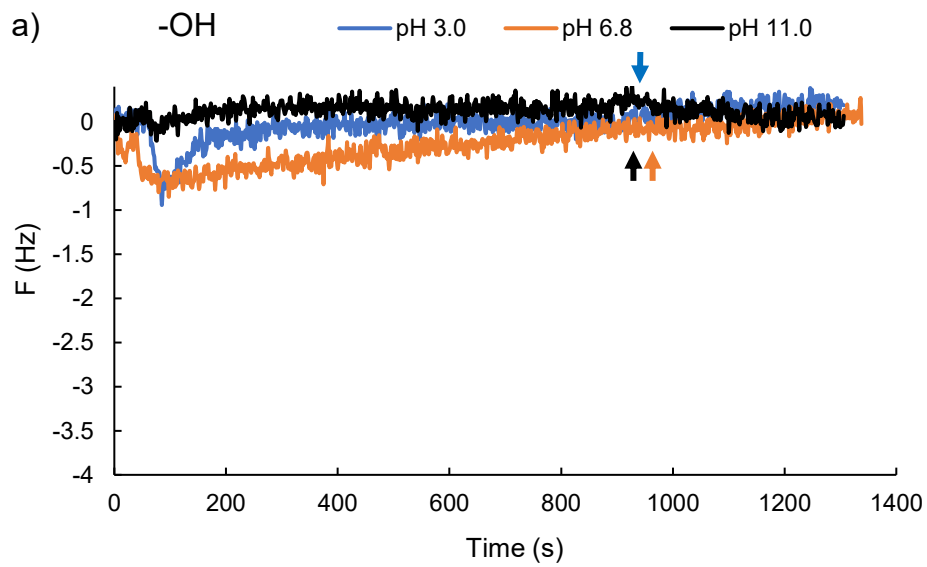
Figure S3.22. a) frequency b) dissipation changes of the 9th overtone of the adsorption of L-S polymer on the -OH-functionalized surface at different pH (arrows indicate buffer rinsing).

a) -OH

b) -OH
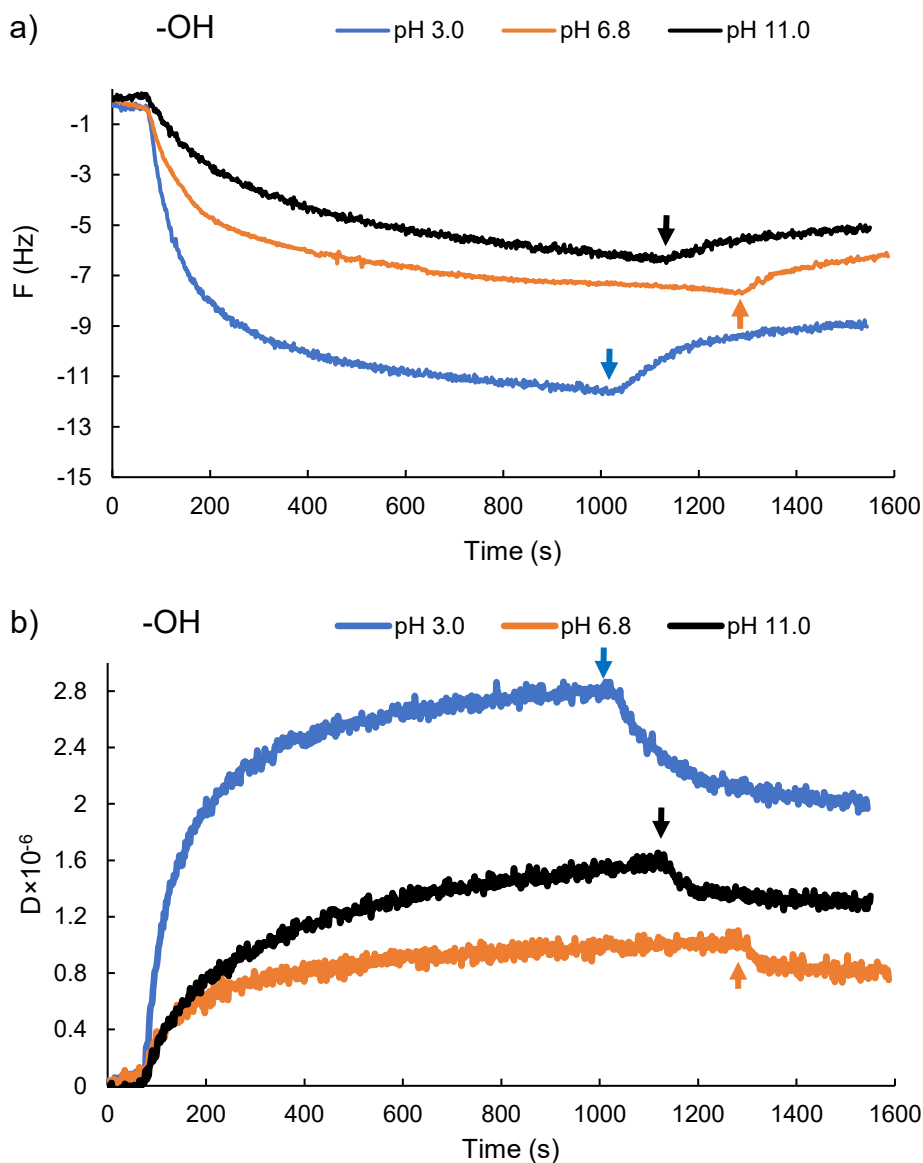
Figure S3.23. a) frequency b) dissipation changes of the 9th overtone of the adsorption of PVA-S polymer on the -OH-functionalized surface at different pH (arrows indicate buffer rinsing).

Table S3.4. Contact angle of water-air ($\theta_{W/A}$) interfaces of PVA-S, and L-S polymers at different pH.

pH	PVA-S	L-S
3.0	11°±0.5	38°±0.5

132

| 6.7 | 12°±1 | 17°±1 |
| 11.0 | 10°±1 | 15°±0.5 |

Adsorption on -COOH-functionalized surface

a) -COOH ⎯ pH 3.0 ⎯ pH 6.8 ⎯ pH 11.0

b) -COOH ⎯ pH 3.0 ⎯ pH 6.8 ⎯ pH 11.0
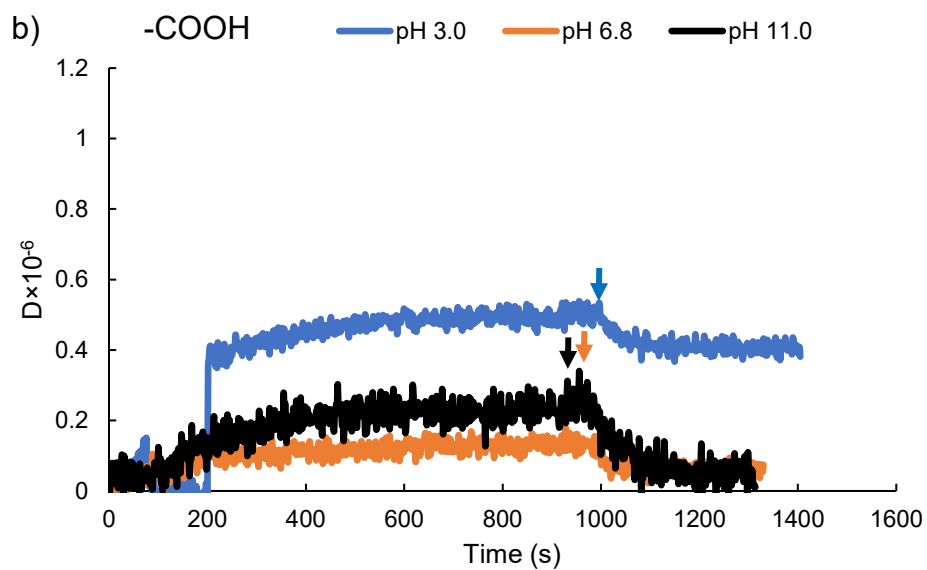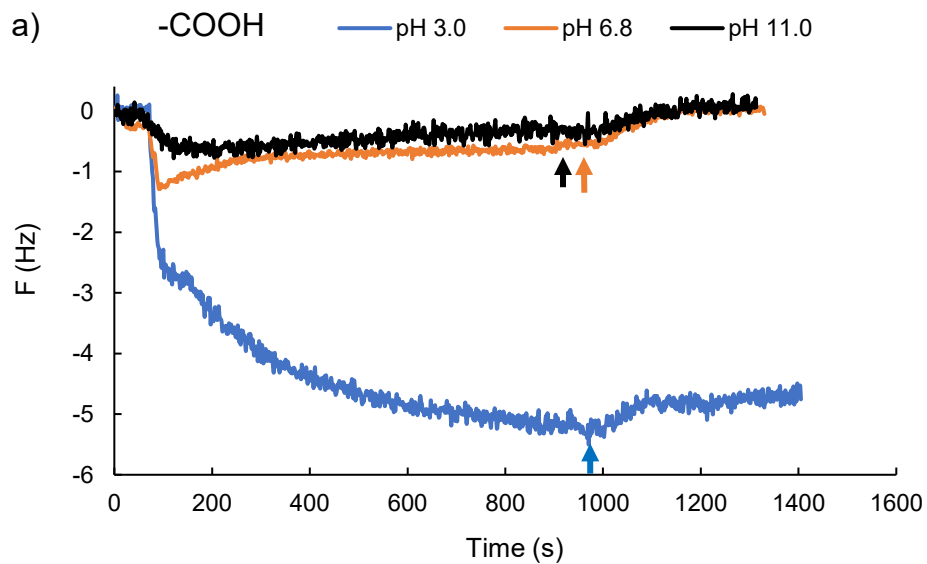
Figure S3.24. a) frequency b) dissipation changes of the 9th overtone of the adsorption of L-S polymer on the -COOH-functionalized surface at different pH (arrows indicate buffer rinsing).
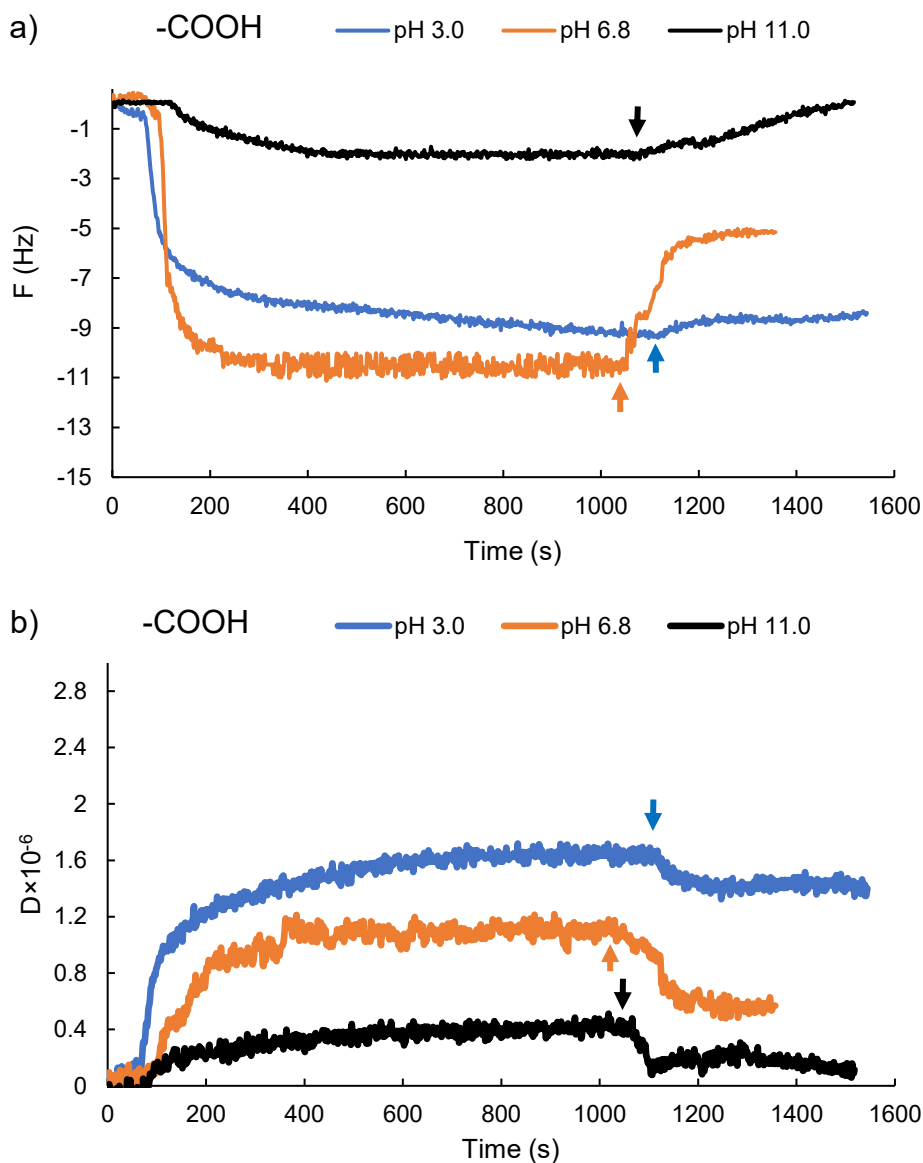
Figure S3.25. a) frequency b) dissipation changes of the 9th overtone of the adsorption of PVA-S polymer on the -COOH-functionalized surface at different pH (arrows indicate buffer rinsing).

Adsorption on -CH$_3$-functionalized surface
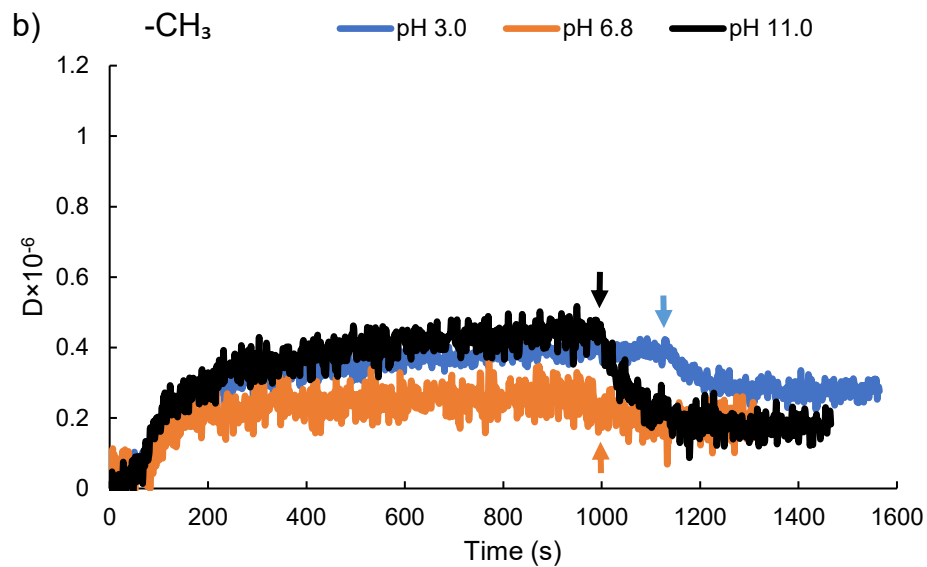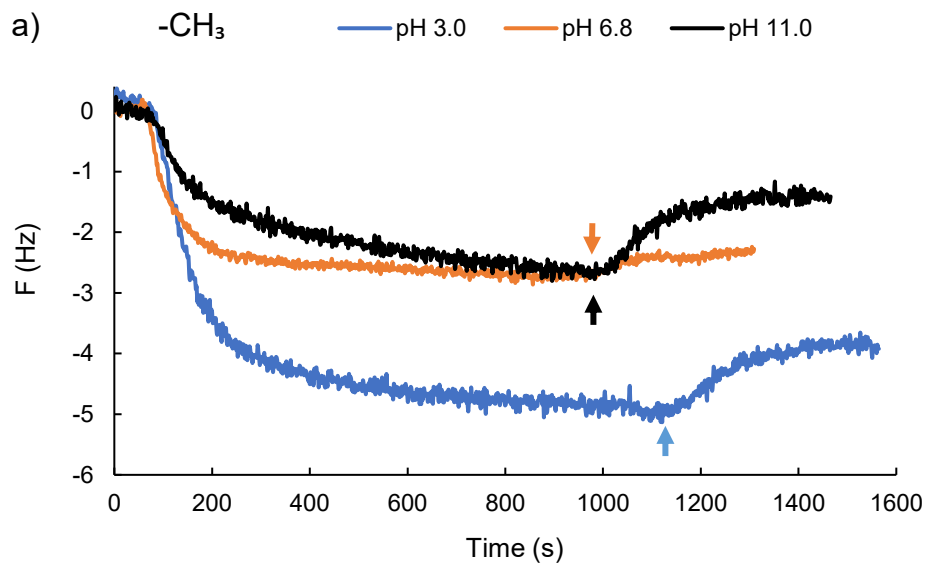
Figure S3.26. a) frequency b) dissipation changes of the 9th overtone of the adsorption of L-S polymer on the -CH$_3$-functionalized surface at different pH (arrows indicate buffer rinsing).
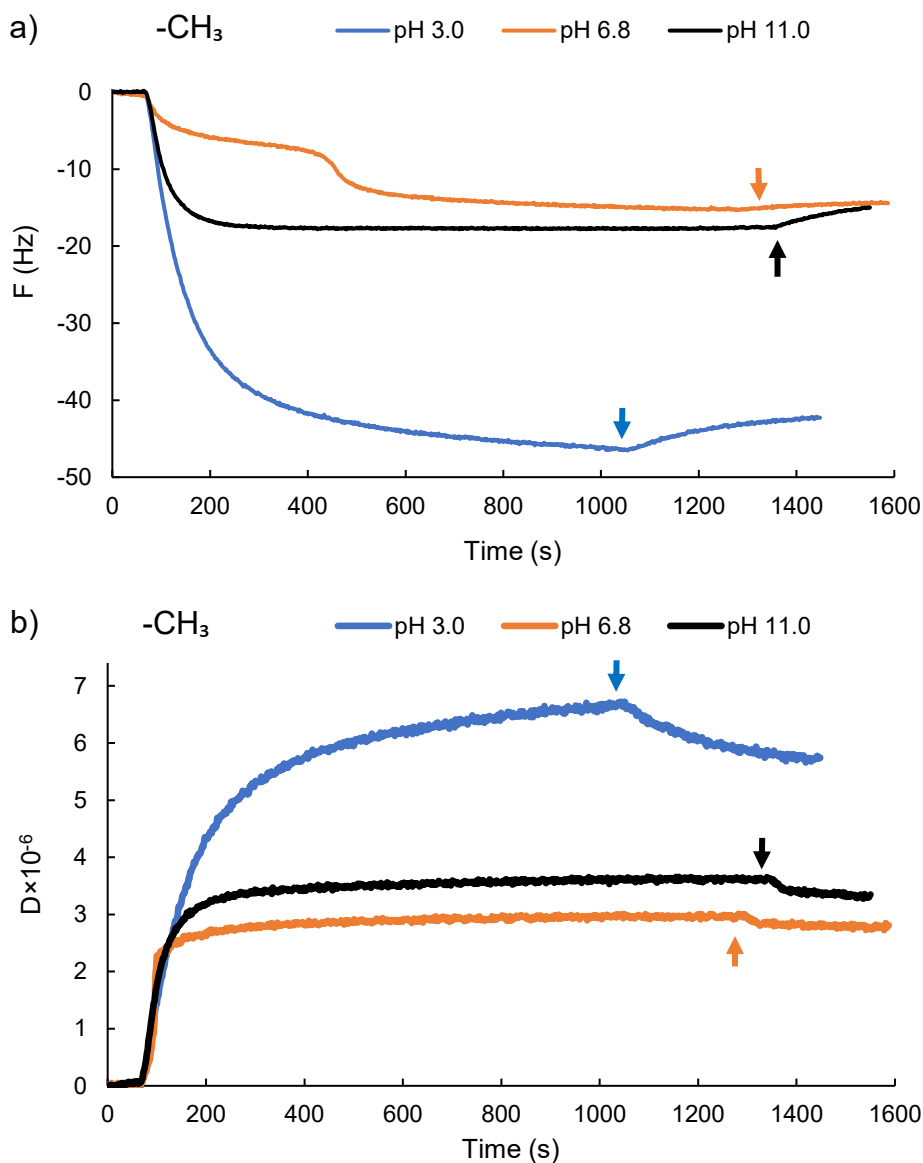
Figure S3.27. a) frequency b) dissipation changes of the 9th overtone of the adsorption of PVA-S polymer on the -CH$_3$-functionalized surface at different pH (arrows indicate buffer rinsing).

Adsorption on -NH$_2$-functionalized surface
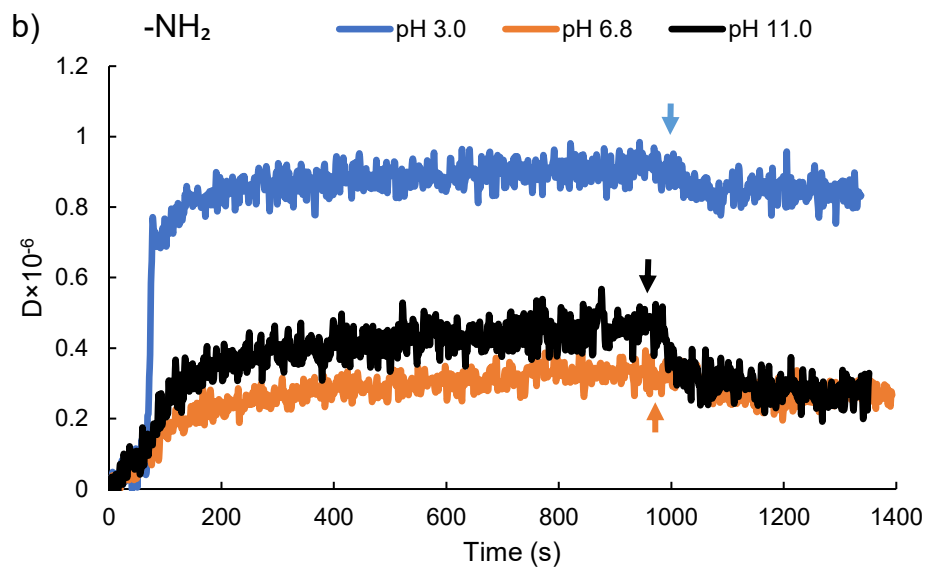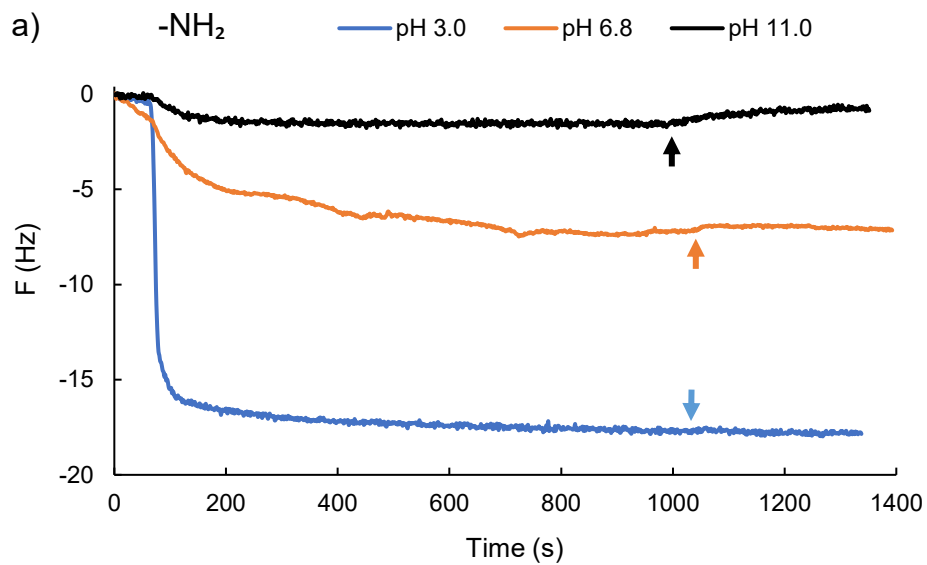
Figure S3.28. a) frequency b) dissipation changes of the 9th overtone of the adsorption of L-S polymer on the -NH$_2$-functionalized surface at different pH (arrows indicate buffer rinsing).
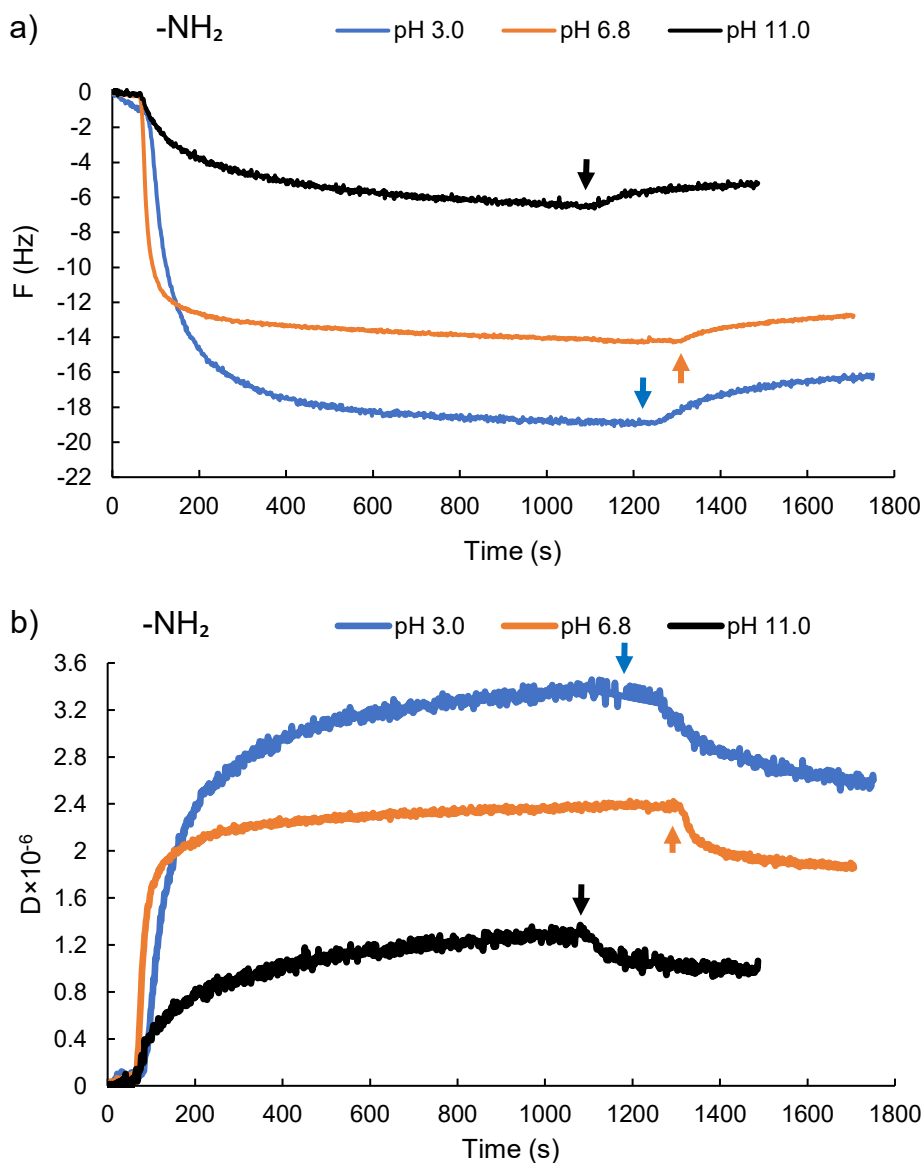
Figure S3.29. a) frequency b) dissipation changes of the 9th overtone of the adsorption of PVA-S polymer on the -NH$_2$-functionalized surface at different pH (arrows indicate buffer rinsing).

Effect of pH on the hydrodynamic radius (R_h) of L-S, and PVA-S
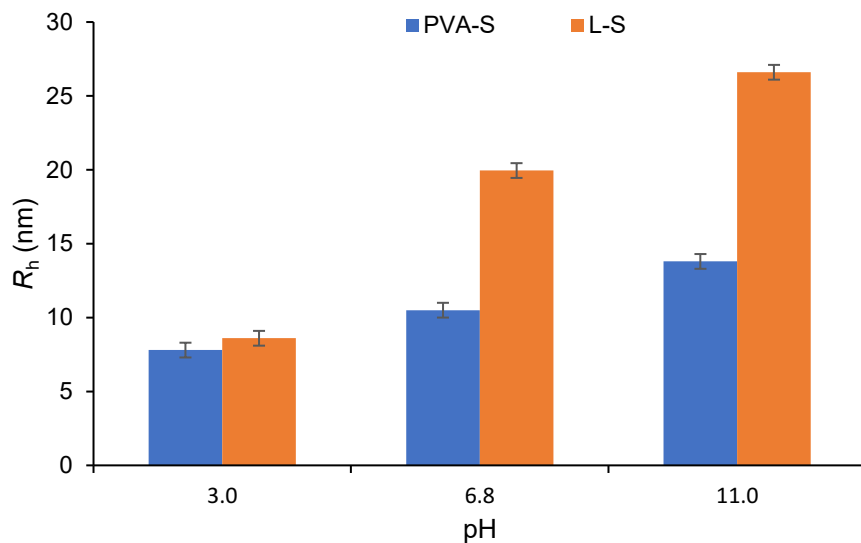
Figure S3.30. R_h as the function of pH for L-S, and PVA-S polymers

Effect of salt concentration on the adsorption of L-S and PVA-S on SAMs
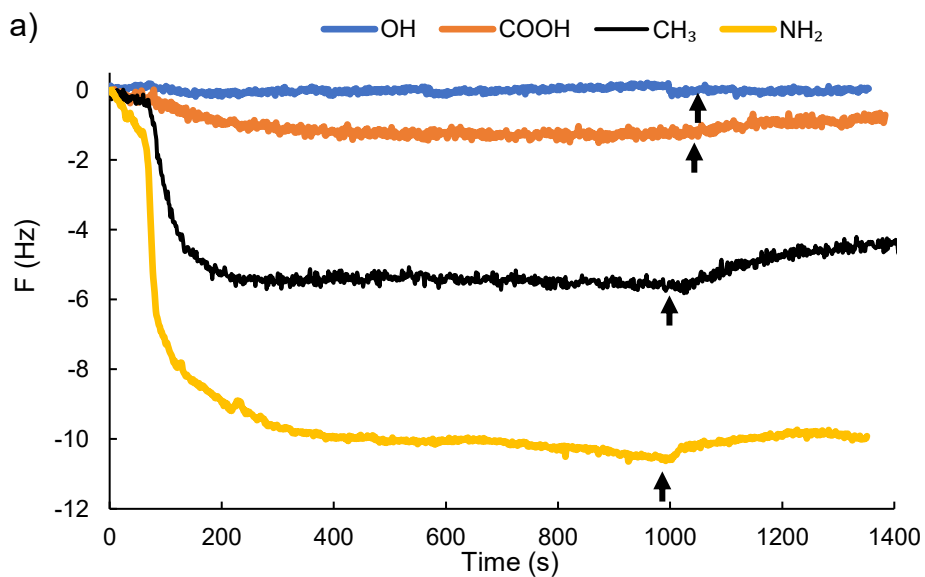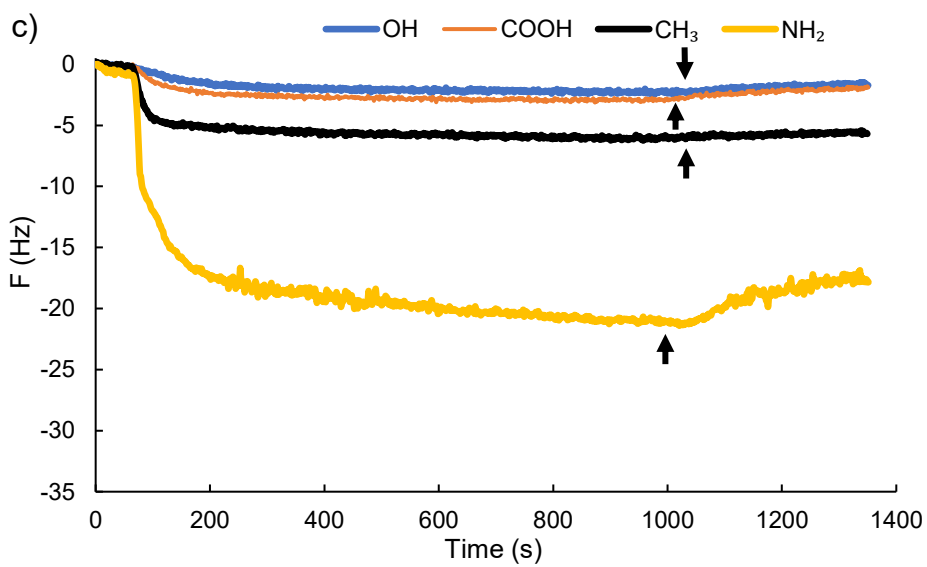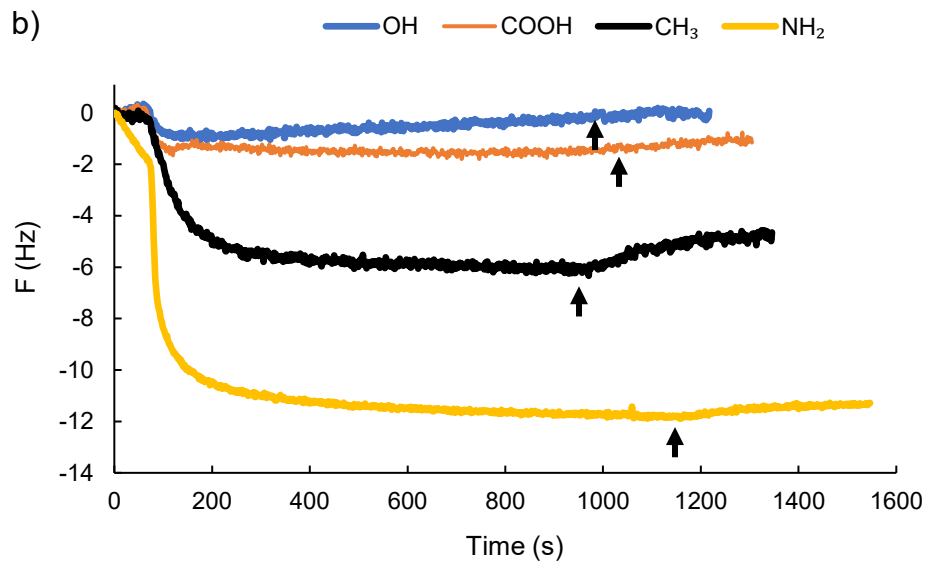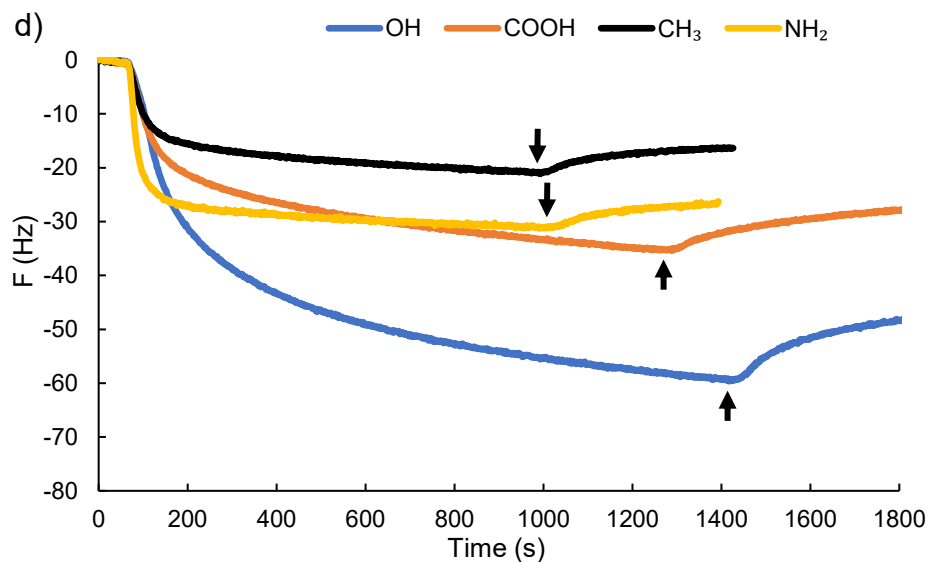
Figure S3.31. Frequency changes of L-S on SAMs of different chemistry at different salt concentrations of a) 1 mM, b) 10 mM, c) 100 mM, and d) 1000 mM (arrows indicate buffer rinsing).
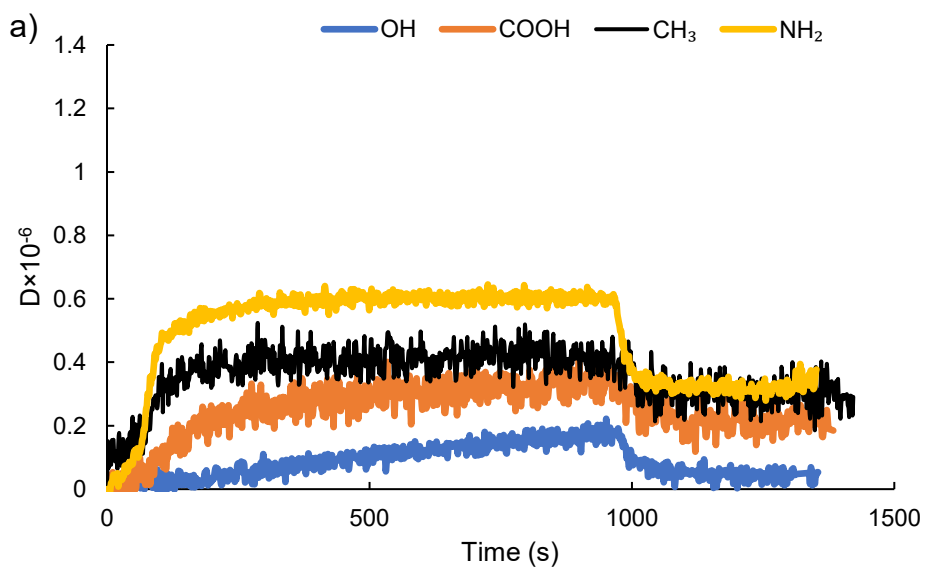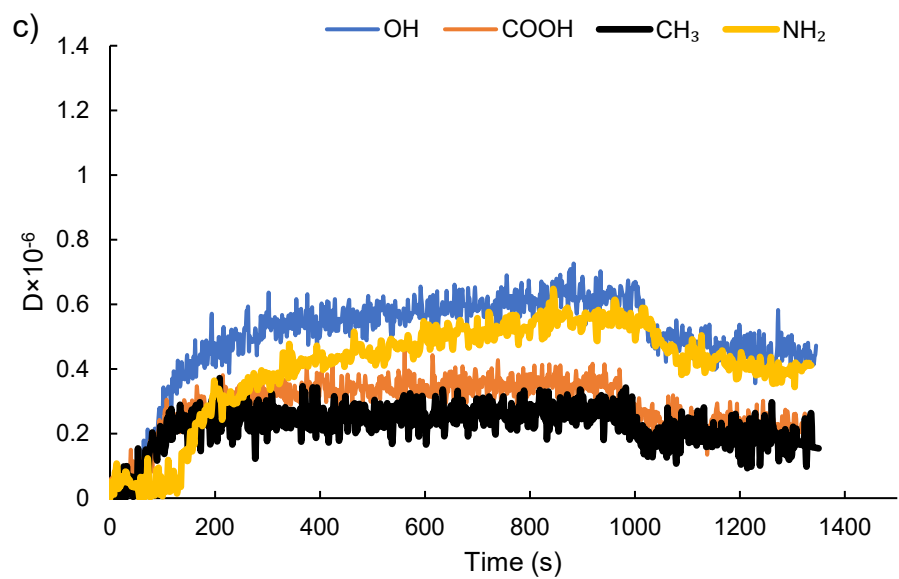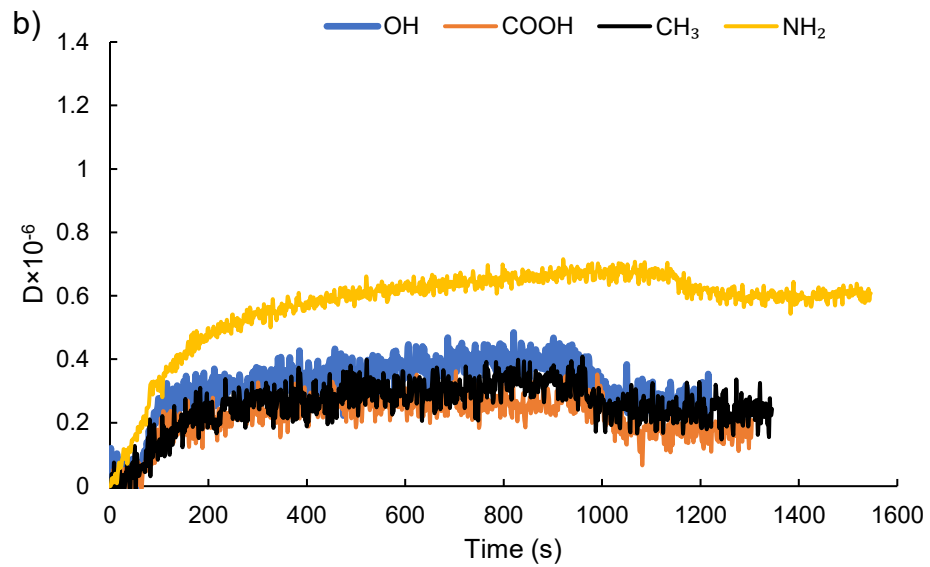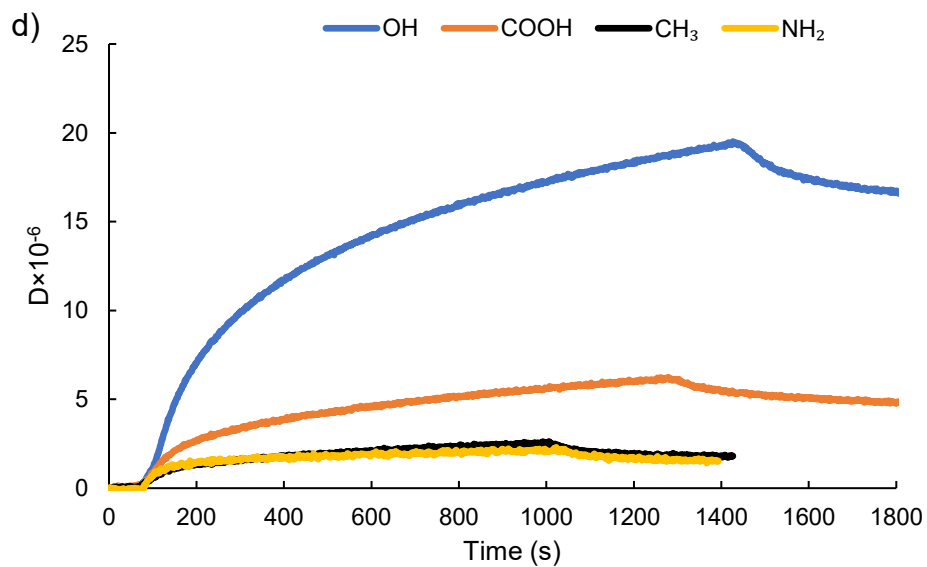
Figure S3.32. Dissipation changes of L-S on SAMs of different chemistry at different salt concentrations of a) 1 mM, b) 10 mM, c) 100 mM, and d) 1000 mM.

143

b)

c)

144
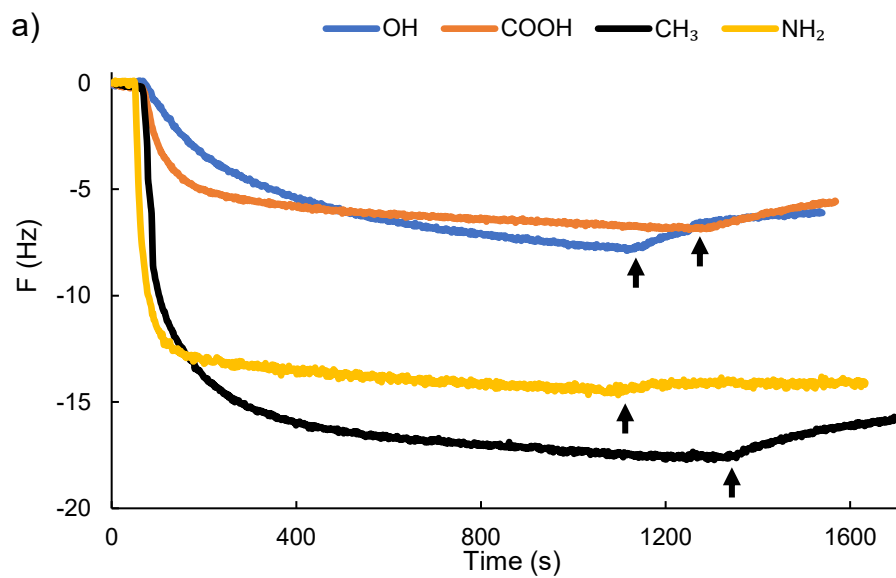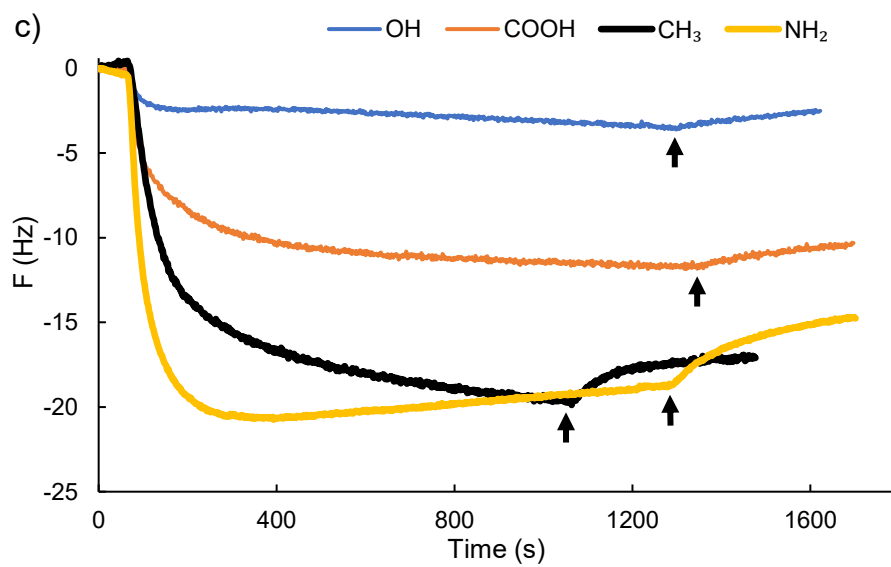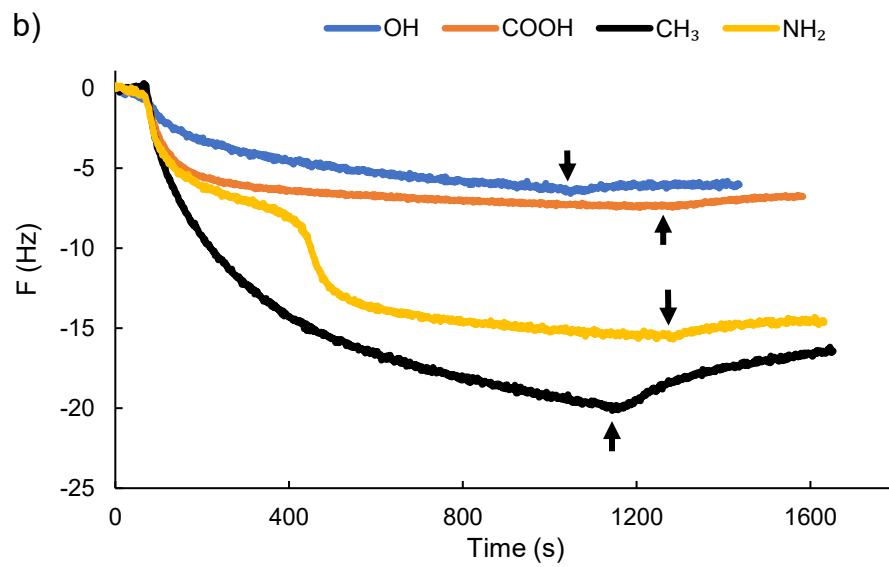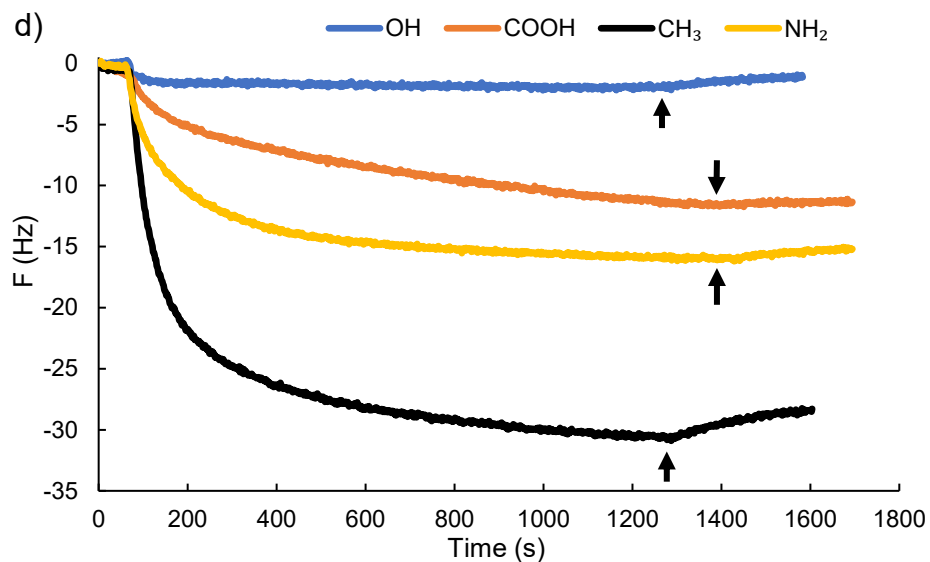
Figure S3.33. Frequency changes of PVA-S on SAMs of different chemistry at different salt concentrations of a) 1 mM, b) 10 mM, c) 100 mM, and d) 1000 mM (arrows indicate buffer rinsing).
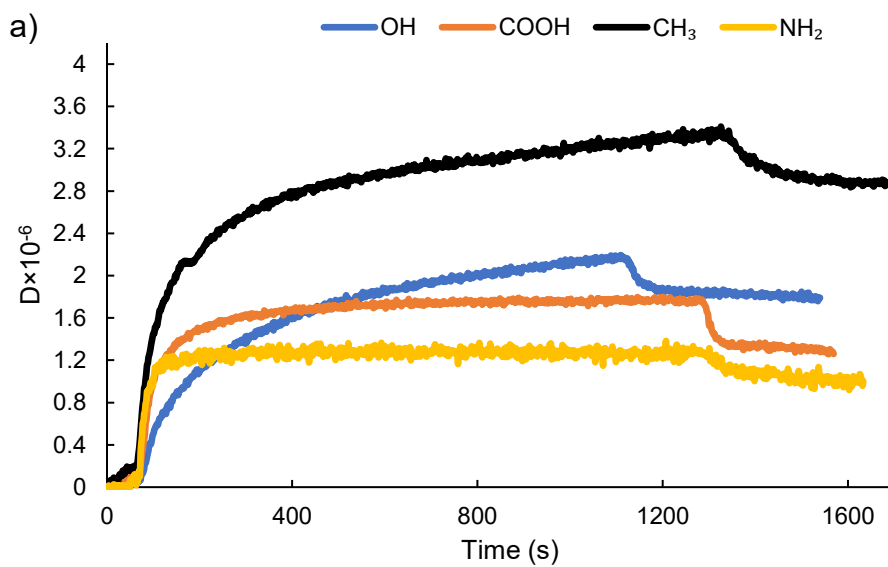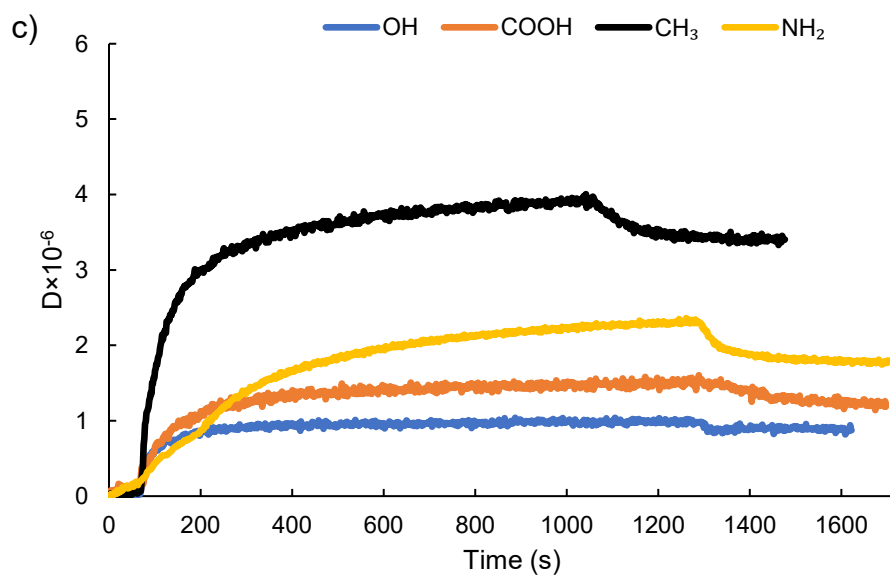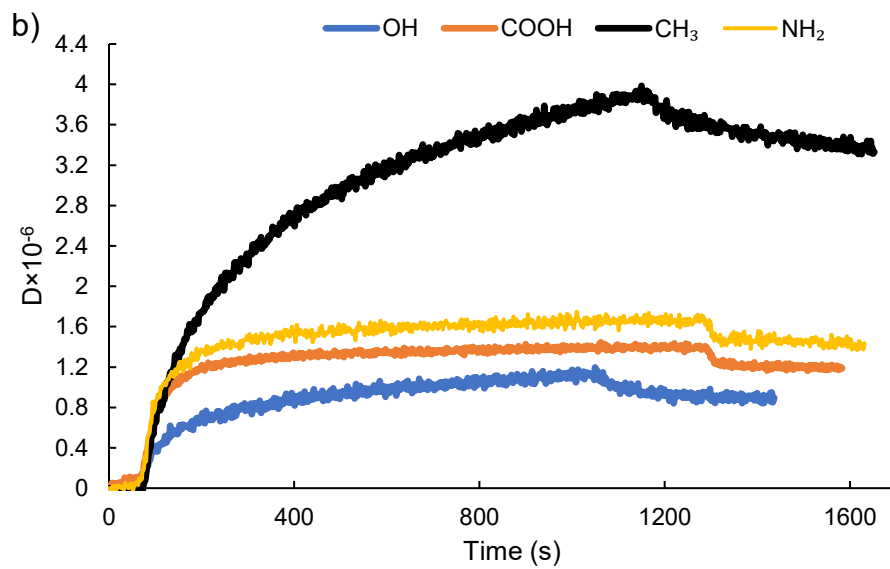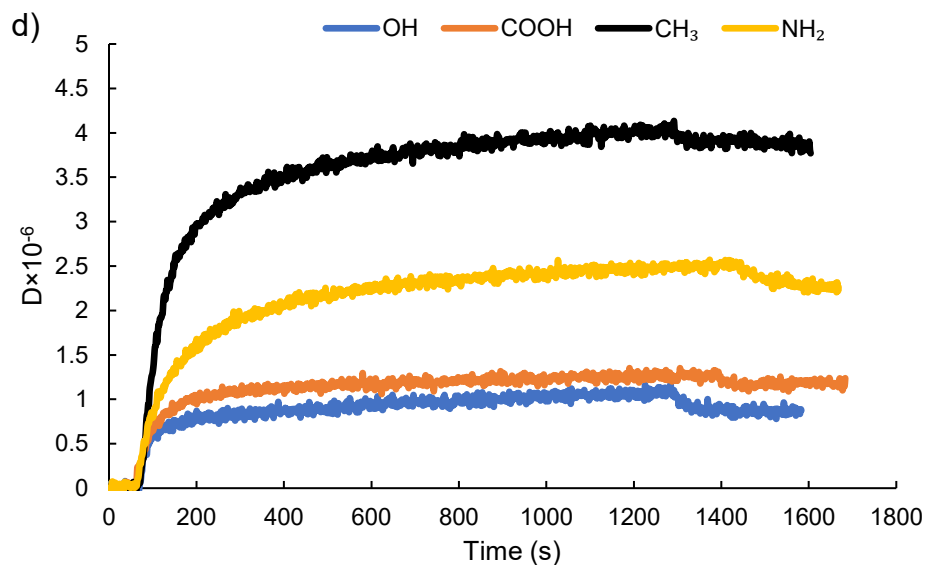
Figure S3.34. Dissipation changes of PVA-S on SAMs of different chemistry at different salt concentrations of a) 1 mM, b) 10 mM, c) 100 mM, and d) 1000 mM.

Effect of salt concentration on the hydrodynamic radius (R_h) of L-S, and PVA-S
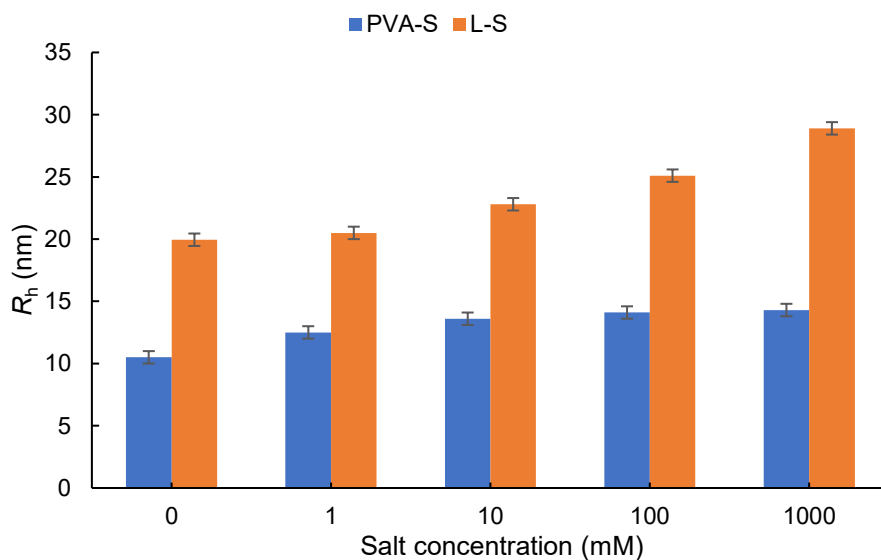
Figure S3.35. R_h as the function of salt concentration for L-S, and PVA-S polymers

References

1. C. J. Huang, F. S. Shieu, W. P. Hsieh and T. C Chang, *J. Appl. Polym. Sci.*, 2006, 100, 1457-1464.

2. A. E. Kazzaz and P. Fatehi, *J. Colloid Interface Sci.*, 2020, 561, 231-243.

3. T. Rashid, C. F. Kait, I. Regupathi and T. Murugesan, *Ind. Crops Prod.*, 2016, 84, 284-293.

4. Y. C. Sun, J. L. Wen, F. Xu and R. C. Sun, *Sci. Res. Essays*, 2010, 5, 3850-3864.

5. I. Korbag and S. Mohamed Saleh, *Int. J. Environ. Stud.*, 2016, 73, 226-235.

6. F. Kong, K. Parhiala, S. Wang and P. Fatehi, *Eur. Polym. J.*, 2015, 67, 335-345.

7. N. E. El Mansouri and J. Salvado, *Ind. Crops Prod.*, 2006, 24, 8-16.

8. S. Zhou, L. Liu, B. Wang, F. Xu and R. Sun, *Process Biochem.*, 2012, 47, 1799-1806.

9. A. Casas, M. V. Alonso, M. Oliet, E. Rojo and F. Rodríguez, *J. Chem. Technol. Biotechnol.*, 2012, 87, 472-480.

10. M. Bouraada, M. S. Ouali and L. C. de Menorval, *J. Saudi Chem. Soc.*, 2016, 20, 397-404.

11. C. A. Barbosa, P. M. Dias, A. M. D. C. Ferreira and V. R. Constantino, *Appl. Clay Sci.*, 2005, 28, 147-158.

Chapter 4. Fabrication of amphoteric lignin and its hydrophilicity/oleophilicity at oil/water interface

Adapted from: Armin Eraghi Kazzaz, Pedram Fatehi*[a]

Green Processes Research Centre and
Chemical Engineering Department,
Lakehead University,
955 Oliver Road,
Thunder Bay, ON P7B5E1, Canada

*Corresponding author

4.1 Abstract

Amphoteric polymers have tremendous applications in colloidal systems. Despite the enormous availability of lignin, the generation of amphoteric lignin polymer has yet to be discovered. In this work, amphoteric lignin was synthesized in an industrially attractive aqueous system via integrating the advantages of grafting quaternary ammonium groups onto lignin and polymerizing lignin with sulfonate containing monomers. The order of the reactions seemed to change the properties of the amphoteric lignin significantly, which was confirmed by ^{1}H and 2D^{1}H COSY NMR analysis. In this research, the behavior of carbon chain length of the reagent containing the cationic group in inducing amphoteric lignin with superior properties was comprehensively discussed. The wettability and adhesion force analyses were performed to understand the impact of amphoteric lignin at the interface of a water/oil mixture. With the help of the contact angle and adhesion force measurements, the superior properties of the amphoteric lignin to those of only anionic or cationic modified lignin were determined. In water, the amphoteric and anionic lignin polymers strongly repelled oil droplets. In oil, both anionic and cationic lignin polymers showed poor water wettability, while the amphoteric lignin was wetted well by water. This paper discusses the fundamental mechanisms associated with the altered behavior of these lignin-based polymers at different interfaces.

Keywords: Amphoteric lignin, Colloid, COSY NMR, Adhesion force, Oil/water interface

4.2 Introduction

The involvement of polymer technology is continuously increasing in various applications, such as wastewater treatment,[1] drilling fluid,[2] oil/water separation,[3] and leather manufacturing.[4] This is because the demand for more efficient, cost-effective, and environmentally friendly biopolymers is enhancing in today's world.

Lignin is arguably one of the most abundant phenolic polymers on the planet, and it is intensively produced as a by-product in the pulp industry.[5,6] Being one of the main components of biomass, lignin possesses a complex and three-dimensional structure with various functional groups. Lignin is eco-friendly and abundant, and it has a low production cost, which makes lignin an attractive substrate to be used in various industries.[6,7] However, lignin has limited functional groups and poor interaction with other materials, restricting its application in industry.

150

Various modifications have been conducted on lignin to improve its functionality, such as phosphorylation,[8] amination,[9,10] carboxyalkylation[11] and sulfomethylation,[12] which have led to the production of either anionic or cationic lignin. By having both cationic and anionic groups, the amphoteric polymers are reported to have a broader range of application than single-ionic polymers, thanks to their remarkable solubility and effectiveness in interacting with other materials.[13,14] An amphoteric lignin-based surfactant has been recently produced by grafting quaternary ammonium and sulfonic acid-containing groups onto enzymatically-hydrolyzed lignin.[15] In another study, a pH-responsive carrier was produced from hydrolyzed lignin by quaternization and sulfonation, and the product was used for recycling cellulase during the enzymatic hydrolysis of lignocelluloses.[16] In this study, as the first objective, we aimed to produce amphoteric lignin by conducting both cationic and anionic modifications via grafting and polymerization of softwood kraft lignin to intro-duce a new bio-based, multi-functional polyelectrolyte applicable to a wide range of uses, e.g., oil/water separations and lignin-to-biofuels processing applications.

To produce an amphoteric lignin-based polymer, the selection of monomers is of extreme importance, as they define the proper-ties of the fabricated polymer. The characteristics of grafting groups have been reported to substantially impact the features of the grafted polymers. For example, cationic deacetylated chitosan was synthesized using pentyl and propyl trimethyl ammonium bromides.[17] It was revealed that the polymer with a longer carbon chain (e.g., pentyl) demonstrated a higher level of interaction with the cell membrane. Another example is carboxyalkylation and sulfoalkylation of lignin. Carboxyethylation occurs on both aliphatic and aromatic groups, while carboxymethylation happens primarily on the aromatic site.[11,18] In the case of sulfomethylation, it occurs on the phenolic site of lignin, while sulfobutyration occurs on both aliphatic and aromatic components,[11,19,20] which implies that the structure of the reagent matters in producing modified lignin with altered structures and functionality (e.g., molecular weight and charge density). As the second objective of this work, two different cationic polymers with short and long carbon chains were selected for grafting on lignin, which sheds light on the effect of the chain length of grafting group on the properties of lignin.

To add sulfonate groups to lignin, there is an option of exploiting grafting or polymerization. Herein, we chose polymerization with sulfopropyl methacrylate due to its highly hydrophilic sulfonate group and little to no pH dependency.[21] In addition, the bridging interaction of the

extended chain of polymerized lignin could facilitate the wettability of the lignin polymer in an oil/water medium.[22] Lignin featured with charged groups is expected to be wetted by water easily, since its ionic groups would be able to bind with water molecules via intense hydration that can be induced by electrostatic interaction.

Oil/water interface has attracted practical and fundamental interests due to its importance in various applications such as oil-sand extraction,[23] programmable genes, drug delivery,[24,25] and oil/water separation.[11] Polyelectrolytes reconfigure their surface ionic groups upon contact with a hydrophobic mate-rial, such as oil. This would lead to an alteration in wettability/hydrophilicity of the polymer.[22] To design materials with high performance and sustainability in various fields, knowledge of the oil and water wetting properties of the newly fabricated polymers should be widened fundamentally. Herein, we analyzed the water/oil wetting properties of the produced amphoteric lignin.

Although several polymers with anionic or cationic charges have been developed with features to enhance electrostatically induced hydration with a water molecule in oil/water interface, amphoteric lignin would demonstrate a dual functionality and unique feature. The third objective of this work was to study the behavior of amphoteric lignin in different interfaces to further expand the fundamental understanding of lignin-based amphoteric polymer in various media for identifying potential applications.

We initially synthesized the amphoteric lignin-based biomaterial in a semi-dry aqueous condition using amino and sulfonic groups via grafting cationic groups and polymerizing with an anionic monomer. This paper describes the details of synthesis, characterization, and physical properties of the produced amphoteric lignin using anionic and cationic reagents. As various alternatives can be followed to conduct cationic grafting and anionic polymerization, the first aim of this research was to determine the better and more efficient synthetic route for the production of amphoteric lignin-based polymers. Furthermore, the wettability of the produced amphoteric lignin polymers at the interface of oil and water in oil-water mixtures was studied fundamentally.

4.3 Material and methods

4.3.1 Materials

Softwood kraft lignin (L) was received from a mill in Alberta, Canada. In addition, (3-bromopropyl)trimethylammonium bromide (97%) (3T), (5-bromopentyl)trimethylammonium bromide(97%) (5T), 3-sulfopropyl methacrylate potassium salt (98%)

(S),polydiallyldimethylammonium chloride (PDADMAC) with the molecular weight of 100–200 kg/mol, D2O (with the isotopic purity of 99.8%), potassium polyvinyl sulfate (PVSK), 3-trimethylsilyl-(2,2,3,3-D4)-propionic acid sodium salt (TMSP) (99.8%), sodium persulfate (Na2S2O8), sodium hydroxide (99.0%), hydrochloric acid(37%), dimethyl sulfate (98.0%), dimethyl sulfoxide-d6 ([D6]DMSO)(99.9%), and ethanol (99.1%) were all obtained from Sigma-Aldrich Company. Toluene was purchased from Caledon Laboratories Ltd., Canada. Dialysis membrane with the molecular weight cut-off of1,000 g/mol was supplied from Thermo Fisher Scientific Inc., USA. Nylon filters with an opening size of 0.45lm were obtained from the Canada-wide company, Canada. All of the chemicals utilized in this work were of analytical grades.

4.3.2 Methylation of lignin

Lignin was methylated following the procedure described by Kong et al.[26] Methylation was conducted to mask the phenolic-OH of lignin to understand if any of the grafting and polymerization reaction would occur on the aliphatic OH of lignin. The detail of the methylation reaction is available in supporting information.

4.3.3 Grafting of lignin with a cationic monomer

The grafting reactions were performed in semi-dry (30–50 wt. % water content) and wet (92 wt. % water content) aqueous conditions in the presence of NaOH (1–2.5 M).[27]

Synthesis and optimization of lignin-(3-bromopropyl)trimethylammonium bromide (L-3T), and lignin-(5-bromopentyl)trimethylammonium bromide (L-5T) were carried out in an alkaline environment at 25 °C for 4 h, and the detail results are available in Table S4.1 in the supplementary material. Lignin was treated with NaOH at pH 11 for 0.5 h, which activated lignin's hydroxy groups and paved the way for grafting 3T or 5T onto lignin. Afterward, the activated lignin was reacted with 3T or 5T with different ratios of 0.5–2 mol/mol of 3T or 5T/L in a water bath at 60–90 °C for 30–120 min.

Another set of cationization reactions were conducted by using methylated lignin (ML) with 3T and 5T reagents. Methylated lignin-(3-bromopropyl)trimethylammonium bromide (ML-3T)and methylated lignin-(5-bromopentyl)trimethylammonium bromide (ML-5T) were produced by reacting 3T or 5T reagents in the same manner as stated above. Electrostatic potential map of cationic monomers has been plotted by using the Avogadro software (http://avogadro.openmolecules.net/).

4.3.4 Polymerization of lignin with an anionic monomer

The reactions were conducted in semi-dry aqueous (30–50 wt. % water content) and wet (92 wt. % water content) conditions in the presence of HCl (10–16 wt. %).[27] Synthesis and optimization steps for producing lignin-3-sulfopropyl methacrylate (L-S) polymers with S monomer (Table S4.2) were the molar ratio of 0.5–2 S/L,10–16 wt. % of HCl (550mL) and desired amount of deionized water to make a 30–92 wt. % concentration. Then, the suspension was deoxygenated by purging with nitrogen gas for 15 min. Potassium persulfate (1–2.5 wt. %) was then added to the mixture as the initiator. Afterward, samples were placed in a water bath, and the reaction was conducted at 60–90 °C for 30–120 min.

Another set of anionic polymerization was conducted by using methylated lignin (ML) and S monomer. To produce methylatedlignin-3-sulfopropyl methacrylate (ML-S), S and ML were reacted at the 1.0 mol/mol ratio in the presence of 1.5 wt. % of potassium persulfate at 80 °C for 30 min using 14 % HCl (550mL), and deionized water was added to make the water content of the mixture 30 wt. % of the total mass.

4.3.5 Purification steps for produced polymers

The produced grafted and polymerized lignin samples were purified following methods outlined in the literature.[28-30] The details of this method are available in the supporting information.

4.3.6 Amphoteric lignin production

There are alternatives, such as grafting lignin with anionic or cationic groups, polymerizing with anionic or cationic monomer, or using grafting and polymerization together to produce amphoteric polymers. In this work, the cationization of lignin with(3-bromopropyl) trimethylammonium bromide (3T) and (5-bromopentyl)trimethylammonium bromide (5T) and polymerization with 3-sulfopropyl methacrylate potassium salt (S) were per-formed together for producing amphoteric lignin, as the positively charged amine (N) group of trimethylamine and negatively charged sulfonate group (S) contribute to its amphoteric characteristics. The reactions were optimized as the details are available in Table S4.1 in supporting information.

Two different scenarios were followed for amphoteric lignin production (information is available in Table S4.3): 1) the cationic polymer of L-3T or L-5T was polymerized by the anionic monomer of S in 1.0 mol/mol ratio of S/L-3T or S/L-5T in the presence of 1.5 wt. % of potassium persulfate at 80 °C for 30 min in 14 % HCl (550mL) and 30 wt. % of water; these samples were denoted as L3T-S, and L5T-S, respectively. 2) the anionic L-S was grafted by cationic monomers of 3T and

154

5T in 1.0 mol/mol ratio of 3T/L-S or5T/L-S at 90 °C for 90 min using NaOH (2.5 M, 550mL) and 30 wt. % of water content. These samples were denoted as LS-3T and LS-5T, respectively.

4.3.7 Production of control samples

Four different control samples were produced (details available in Table S4.3): 1) unmodified lignin (L) was used without further treatments; 2) lignin 1 (L1), which was treated following the steps of cationization, purification, and drying in the absence of 3T and 5T reagents; 3) lignin 2 (L2), which was produced following the steps of polymerization, purification, and drying in the absence of S monomer; 4) lignin 3 (L3) was produced following all steps pointed out in cationization, anionization, purification and drying in the absence of reagents.

4.3.8 Characterization of polymers

The charge density of samples was determined with a Particle Charge Detector (PCD 04, BTG Mütek GmbH) using a 0.005 mol/LPDADMAC or 0.005 mol/L of PVSK solution as the titrant as explained elsewhere.[31]

The elemental analysis of the polymers was performed using an elemental analyzer (Vario EL Cube, Elemental Analyzer, Germany) as described in detail elsewhere.[32] The degree of substitution (DS) and grafting ratio (GR) for cationic and anionic samples were calculated based on Eqs.(4.1) and (4.2), respectively:

$$Degree\ of\ substitution\ (DS)\ (mol/mol) = \frac{180 \times N}{1400 - R \times N} \quad (4.1)$$

where 180 is the molecular weight (g/mol) unit of lignin,[26] R is the molar mass of propyl trimethylammonium group and pentyl trimethylammonium, which are 101.19 and 129.25 g/mol, respectively, and 1400 stands for 100 times of the nitrogen atomic mass.

$$Grafting\ ratio\ (GR)(wt.\%) = \frac{\frac{S_1 - S_2}{32} \times Mw}{100 - (\frac{S_1 - S_2}{32} \times Mw)} \times 100 \quad (4.2)$$

Where S_1 is the sulfur content of lignin, and S_2 is the sulfur content of anionically polymerized lignin samples with S monomer (wt. %), and M_w is the molecular weight of 3-sulfopropyl methacrylate, which is 246.32 g/mol.

4.3.9 Experimental design by Taguchi

A total of 16 runs of the reaction were conducted based on Taguchi orthogonal design (L16) to determine the optimum condition to produce L-3T, L-5T, and L-S polymers (Table S4.2, and S3 in supporting information). In these reactions, the attachment of amine and sulfonate groups to L directly affected the charge density (CD) and grafting ratio (GR) or degree of substitution (DS) of

lignin samples; these parameters were chosen to be considered in determining the maximum reaction efficiency of L-3T, L-5T,and L-S polymers.

The K_i values for each factor were calculated from the mean off our sets of CD and DS or GR results for each level listed in Table S4.4 and S4.5 (supporting information), in which i (1, 2, 3, and 4) is the number of levels. The range value (R) for each factor is determined from the difference between the maximum and minimum K_i values for that factor, and it depicts the effect of variables on the CD, DS or GR results. The high R factor means that the element has a strong impact on the results.[18]

4.3.10 Weight-average molecular weight (M_w) and hydrodynamic radius (R_h) analysis

Static light scattering (SLS) and dynamic light scattering (DLS)analyses were carried out to monitor the weight-average molecular weight (M_w) and hydrodynamic radius (R_h) of lignin samples using Brookhaven BI-200SM instrument equipped with a goniometer. The R_h and M_w measurements were performed following the procedure outlined in Kawata et al.,[30] and Cravillon et al.,[34] respectively (more information is available in supporting information). Mean diffusion coefficients of produced polymers were calculated based on the Stokes-Einstein equation according to previous reports.[12,35,36]

4.3.11 Zeta potential analysis

The isoelectric point (IEP) of lignin and produced amphoteric polymers were analyzed using a NanoBrook Zeta PALS (Brookhaven Instruments Corp, USA) at pH ranging from 2 to 12. The analysis was performed three times, and the average values were reported in this study.[31,37,38]

4.3.12 ¹H NMR, 2D ¹H COSY, and FTIR spectroscopy

The structure of lignin and produced amphoteric lignin polymers were analyzed by ¹H NMR spectroscopy with 16 scans. Lignin samples were dissolved in D_2O or $DMSO[D_6]/D_2O$ (9:1 v/v) and stirred until fully dissolved (i.e., for 12 h). Trimethylsilyl propionic acid (TMSP) was used as the internal standard.[39] More information about this experiment is available in supporting information. The 2D ¹H COSY analysis of L-3T, L-S, and LS-3T was carried out in D_2O. Both ¹H NMR and 2D ¹H COSY were conducted using the INOVA-500 MHz instrument (Varian, USA).The FTIR (Fourier-transform infrared spectroscopy) analysis of lignin samples was carried out to monitor the molecular finger-print of the samples by using Bruker Tensor 37 instrument (Germany, ATR accessory) and the detail of this analysis is available in supporting information of this work.[40,41]

4.3.13 Wettability analysis

Theta Lite contact angle analyzer (Biolin Scientific, Finland) associated with a camera was used for static wettability analysis.[42] Lignin samples (at 1 wt. % concentration) were coated on glass slides using a spin coater (WS-650, Laurell Technologies Corp) and dried overnight. Afterward, 3mL of water or oil was used to measure the contact angle of water-air ($\theta_{W/A}$), water-oil ($\theta_{W/O}$), and oil–water ($\theta_{O/W}$) in oil or water medium as described in detail in supporting information.[43] The oil phase used in this study was toluene.

4.3.14 Adhesion force measurement

The adhesion force is equal to the force needed to detach a liquid (oil or water) droplet from a surface.[44] In this work, the adhesion force between oil or water droplet and the glass surface coated with the amphoteric L5T-S, the anionic L-S, and the cationic L-5T lignin samples in water or oil medium was measured by using an Attention force tensiometer (Sigma 700 Tensiometer, Finland). Platinum-iridium probe with the micro-roughened surface was used to measure the adhesion force. To measure the adhesion force, the drop-loaded probe was lowered until the droplet (oil or water, 3 μL) attached to the coated surface. Afterward, the probe was lifted with a velocity of 5 μm/s, and the measured adhesion force was recorded.[44,45]

4.4 Results and discussion

4.4.1 Behavior of lignin in control experiments

Elemental analysis for control samples confirmed that L(unmodified lignin), L1 (control sample of grafting reactions), L2 (control sample of the polymerization reaction), and L3 (control sample of the amphoteric lignin production) had 1.13, 1.14, 1.14,and 1.13 wt. % sulfur content, respectively, and no traceable nitrogen. The charge density (CD) of L, L1, L2, and L3 were -1.51, -1.60, -1.59, and -1.61 meq/g, respectively, which is in harmony with their sulfur content. L, L1, L2, and L3 had the molecular weight of 18,030, 29,000, 31,100, and 56,300 g/mol, respectively. The higher M_w of L1, L2, and L3 than L could be due to lignin condensation in alkaline and/or acidic condition as well as the collection of higher molecular weight lignin while performing dialysis.[26,46] Since L3 underwent both alkaline and acidic environments for the reaction and two-time membrane dialysis (i.e., lignin polymers with low molecular weights were removed twice), it had a higher M_w than other control lignin samples.

4.4.2 Grafted lignin and polymerized lignin selection

Fig. S4.1 (supporting information) shows the grafting of propyltrimethylammonium or pentyltrimethylammonium monomers onto lignin. Softwood kraft lignin (L) consists mainly of

guaiacyl units,[47] which is shown in this figure. S_N2 reaction route is the primary pathway for grafting the cationic agent onto lignin (Fig. S4.1). In this reaction, the nucleophile attacks the primary alkyl halide while Br leaves to form a bromide anion. Then, the hydroxy group of lignin replaces the bromine group. Fig. S4.2 (supporting information) presents the creation of sulfate radicals, homopolymerization of vinyl monomers, and the polymerization scheme of anionic lignin polymer (i.e., L-S). Also, the analysis on methylated lignin confirmed that the cationic grafting reactions indeed occurred on the aliphatic OH of lignin, implying the chance for grafting cationic groups on phenolic and aliphatic OH of unmethylated lignin. Also, anionic polymerization did not occur on the methylated lignin, suggesting the selective polymerization of 3-sulfopropyl methacrylate potassium salt (S) on only the phenolic OH of lignin (NMR results in Fig. S4.3).

Table S4.1 (in supporting information) lists the reaction conditions, charge density (CD) and degree of substitution (DS) for lignin-(3-bromopropyl)trimethylammonium bromide (L-3T), and lignin-(5-bromopentyl)trimethylammonium bromide (L-5T) samples. Among 16 experiments for L-3T, and 16 experiments for L-5T, the highest DS and CD were obtained for experiment No. 12 for both monomers based on Taguchi orthogonal design with the highest DS of 0.19 mol/mol and 0.33 mol/mol for L-3T and L-5T, respectively. Since the maximum DS for both polymers was achieved under the same reaction conditions, the higher DS for L-5T could presumably be attributed to the difference in the carbon chain of the cationic reagent, which will be discussed later. For anionically polymerized lignin samples (Table S4.2), among 16 experiments, the highest CD and grafting ratio (GR) of -2.56 meq/g and 124.7 mol % were obtained for experiment No.10 based on Taguchi orthogonal design, respectively. The optimized conditions for producing cationic, anionic, and amphoteric lignin are available in Table S4.3 in supplementary materials.

Statistical analysis was carried out to find out the significant levels of different factors (based on K_i and R values) affecting the CD and GR or DS (Table S4.4 for cationic samples and Table S4.5 for anionic polymers in supporting information). The reaction conditions of experiments No. 12 for cationic L-3T and L-5T monomers(Table S4.1) and No.17 for anionic L-S monomer (Table S4.2) have been considered for producing amphoteric lignin-based products with the best properties in this study (more information could be found in supporting information).

The carbon chain length attached to lignin have been found to affect the hydrophilic/hydrophobic behavior of the polymer in aqueous systems and is reported to have practical applications in producing efficient surfactants and dispersants, as well as in amphoteric polymers for enhanced

oil recovery.[48-51] Therefore, the effect of carbon chain length of the cationic monomer was studied in this work. The electrostatic potential maps of 3T and 5T monomers (Fig. 4.1) show the effect of steric hindrance around the carbon atom bearing the leaving group for 3T and 5T reagents, which further facilitates the departure of Br. Under the same reaction conditions with lignin, lengthening a carbon chain of the reagent (5T vs. 3T) reduces the configuration hindrance on Br atom, leading the reagent to have higher replacement tendency (ascribed as GR in this work) (Fig. 4.1). Therefore, by lowering the steric hindrance via increasing the chain length, the reactivity of the reagent could be enhanced in an S_N2 reaction.
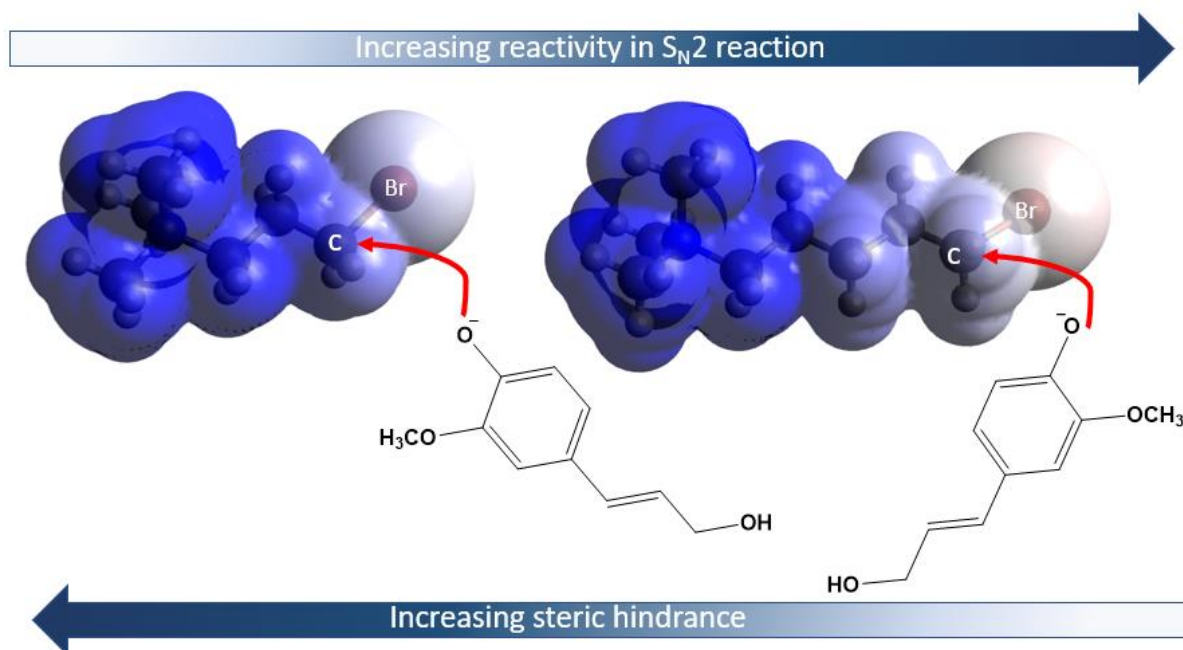
Fig. 4.1. Electrostatic potential maps of 3T and 5T. The figure shows the effect of steric hindrance around the carbon bearing the leaving group (using the Avogadro software (http://avogadro.openmolecules.net/).

4.4.2.1 Properties of amphoteric lignin-based polymers

Four amphoteric lignin-based polymers have been produced in this work as L3T-S, L5T-S, LS-3T, and LS-5T and their proposed chemical structures are shown in Fig. 4.2. The difference among these polymers is that cationization was carried out before anionization for L3T-S and L5T-S, while anionization was conducted before the cationization for LS-3T and LS-5T. In other words, cationization and anionization reactions were performed in different orders to track whether the order of the reactions would result in different contents of sulfonate and amine groups on the amphoteric lignin.
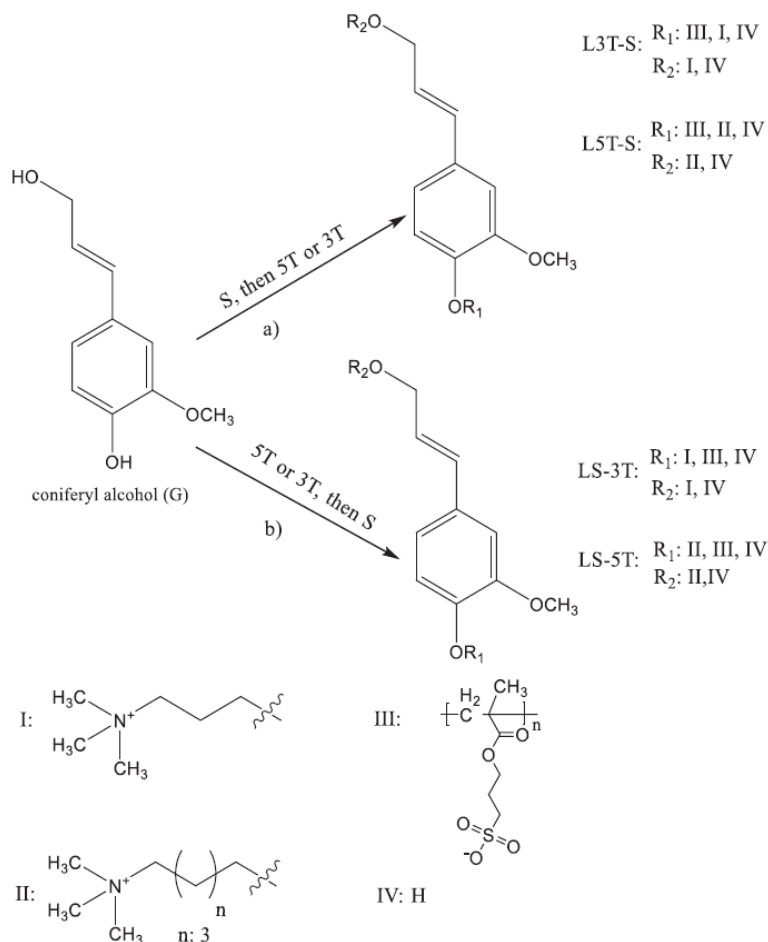
Fig. 4.2. The chemical scheme of amphoteric lignin-based polymers, a) anionic polymerization carried out before cationization, b) cationization carried out before anionic polymerization. The coniferyl alcohol (G unit) starting material represents lignin in this figure.

The chemical properties of the produced polymers are listed in Table 4.1. Among the alternatives, the route that included anionic polymerization reaction first and then cationization led to a lignin polymer with a higher sulfonate content than the other options. For example, for LS-3T (i.e., anionization prior to cationization), the added sulfonate and amine groups after reactions were 7.5 and 1.0 wt. %, respectively. However, for L3T-S (i.e., cationization before anionization), the grafted sulfonate and amine groups were1.3 and 5.9 wt. %, respectively. The higher amount of sulfonate group is due to the larger number of the sulfur-containing group attached to lignin via polymerization reaction, which consists of repeating units of sulfopropyl methacrylate. As stated earlier, the polymerization of lignin proceeded only on the phenolic OH for L-S production, leaving the aliphatic OH for its cationization reaction in the subsequent step. However, as cationization was not selective, it occurred on both aliphatic and phenolic OH for L-5Tand L-3T

production, which reduced the chance of polymerization on the phenolic OH in the subsequent stage, as it was already occupied by the cationic monomers in the first step of the reaction. To conclude, the order of the cationization and anionic polymerization was found to be critical on the functional groups' substitution due to the selectivity of reaction chemistry of grafting and polymerization of different hydroxy groups on lignin.

The yield of produced cationic polymers was 34 and 43 % for L-3T and L-5T, respectively. Based on the earlier discussion, a 5T reagent with a lower steric hindrance would have a higher degree of substitution than the 3T reagent. Moreover, the reaction yield of L-S production was 65 %, which was significantly higher than the reaction yield for producing cationic lignin. This could be attributed to its higher grafting ratio compared with the cationization reaction (Table 4.1). The overall reaction yield for amphoteric polymers of L3T-S, L5T-S, LS-3T, and LS-5T was 21, 25, 43, and 50 %, respectively. The difference in the yield could be attributed to the order of the reactions, which would affect the number of the available active sites on lignin and the degree of substitution of different reagents.

Table 4.1. Chemical properties of produced polymers.

Samples name	L	L-3T	L-5T	L3T-S[1]	L5T-S[1]	L-S	LS-3T[2]	LS-5T[2]
Nitrogen content[3] wt%	<0.09[4]	1.34	2.08	1.33	2.07	<0.09[4]	1.01	1.78
Sulfur content[3] wt%	1.16	1.14	1.18	7.11	6.99	8.67	8.66	8.66
Nitrogen content degree of substitution (mol/mol)	<0.09[4]	0.19	0.33	0.19	0.33	<0.09[4]	0.14	0.27
Sulfur content grafting ratio (wt. %)	Negligible	Negligible	Negligible	85.2	82.1	137.1	137.0	137.0
Total mass (S)/mass (N)	–	0.85	0.56	5.34	3.37	–	8.57	4.86
IEP	< 2	10.2 ± 0.3	11.2 ± 0.3	2.6 ± 0.4	4.2 ± 0.2	≪ 2	2.6 ± 0.4	3.8 ± 0.2
Hydrodynamic radius (R_h) (nm)	1.5	9.5	10.9	24.6	26.6	19.9	28.7	31.0
Mean diffusion coefficient (cm^2/s) × 10^{-7}	28.2	5.1	4.5	2.0	1.8	2.4	1.7	1.6
Weight-average molecular weight (M_w) (g/mol)	18,030	32,600	35,900	73,000	75,900	52,100	81,000	83,700
Reaction Yield %	100	34	43	21	25	65	43	50

[1] Cationization was conducted before anionic polymerization.
[2] Anionic polymerization was conducted before cationization.
[3] Error was <5%.
[4] Method sensitivity < 0.09.

Table 4.1 also classifies the physical properties of the produced polymers. IEP (determined from zeta potential analysis at various pH) reflects the charge property of the polymers that depends strongly on the composition of ionic groups of polymers. The IEP of L and produced modified samples were obtained based on Fig. S4.4 in the supporting materials. IEP is a key parameter to be considered in determining applications for polymers such as flocculants.[52] The IEP of L measured to be in a low pH due to its sulfonate group. Because of the effective grafting of positively charged propyltrimethylammonium or pentyltrimethylammonium groups to the lignin backbone, the IEP of L-3T and L-5T polymers were 10.2 and 11.2, respectively. The slightly higher IEP of L-5T could stem from its higher grafting ratio (Table 4.1). On the other hand, the

161

IEP of L-S sample was measured to be lower than that of L, which is due to the introduction of more sulfonate groups to lignin backbone via polymerization. For the amphoteric samples, the IEP of L3T-S, L5T-S, LS-3T, and LS-5T polymers were 2.6, 4.2. 2.6, and 3.8, respectively. Among all amphoteric samples, L5T-S, having higher aminate groups and lower sulfur groups, had the highest IEP while LS-3T, with a higher sulfonate group content and more moderate amine content, had the lowest IEP. The results postulated that amphoteric lignin polymers with varied IEP could be designed using similar chemicals but following different procedures.

The hydrodynamic radius (R_h) of the polymers is also depicted in Table 4.1. As seen, R_h for L, L-3T, L-5T, and L-S were 1.5, 9.5,10.9, and 19.9 nm, respectively. This shows that the modifications have made lignin with a more branched and stretched structure.[53,55] Slightly higher R_h in L-5T may be attributed to the larger carbon chain of its cationic monomer compared to that of L-3T. R_h was further increased in amphoteric polymers to 24.6, 26.6, 28.7,and 31.0 nm for L3T-S, L5T-S, LS-3T, and LS-5T, respectively. Higher R_h for LS-5T might be due to the higher GR of S containing group, which would lead to a longer branched chain in the amphoteric polymer.[33] Based on R_h changes, the mean diffusion coefficient of lignin polymers was determined following the Stokes-Einstein equation, which would provide information about the average mobility of the polymers (Table 4.1).[56,57] The Brownian movement of polymers can be affected by the type and concentration of ions in solutions.[38,39] As can be seen in Table 4.1, lignin with a lower R_h has the highest diffusion coefficient of 28.20×10^{-7} (cm^2/s). By adding cationic and anionic charges to the lignin structure, the diffusion coefficient has decreased as L-3T, L-5T, and L-S have diffusion coefficients of 5.15, 4.50, and 2.47×10^{-7} (cm^2/s), respectively (Table 4.1). L-5Tshowed a lower diffusion coefficient than L-3T through having a longer chain in its cationic monomer. The diffusion coefficient of amphoteric polymers, L3T-S, L5T-S, LS-3T, and LS-5T were 2.00, 1.85, 1.71, and 1.58×10^{-7} (cm^2/s), respectively. Since the diffusion coefficient not only depends on the size of the polymer but also in how it is influenced by the attachment of different monomers,[58] the produced amphoteric lignin polymers have lower diffusion coefficients compared to lignin as they are more branched in structure.

The molecular weight analysis of the polymers is also depicted in Table 4.1. As seen, the molecular weight of lignin was measured to be 18,030 g/mol. The cationization reaction had increased its molecular weight to 32,600 and 35,900 g/mol for L-3T and L-5T, respectively. The higher molecular weight of L-5T is due to the higher GR and longer carbon chain of the 5T group attached

to lignin. On the other hand, the L-S resulting from the anionic polymerization reaction has the molecular weight of 52,100 g/mol, which is attributed to its polymerization with the sulfur-containing monomers. In the case of the produced amphoteric polymers, the molecular weight of L3T-S, L5T-S, LS-3T, and LS-5T was 73,000, 75,900, 81,000, and 83,700 g/mol, respectively. These results relate positively with obtained GR and R_h values (Table 4.1). In one study, the amphoteric starch polymer was produced by using hydroxymethyldimethylamine and a higher molecular weight was reported for the produced amphoteric polymer compared to unmodified starch, which resulted from its higher viscosity.[59] It is established that a high molecular weight polymer with a longer chain has a higher viscosity than allow molecular weight polymer with a shorter chain at the same concentration.[60]

4.4.2.2 ^{1}H NMR, 2D ^{1}H COSY, and FTIR spectroscopy

^{1}H NMR spectroscopy analysis was carried out to confirm the structure of the produced lignin, and the spectra are depicted Fig.3. As seen in the spectrum of lignin (L), the peak at 8.5 ppm is attributed to the phenolic protons of the unsubstituted lignin, and the peak at 7.42–5.99 ppm is related to the aromatic protons. The peak at 4.5–3.05 ppm is attributed to the protons of the methoxy group of lignin, and the peak at 3.6–3.2 ppm is assigned to the methylene protons in the β-β structure. The peak at 3.3–1.75 ppm is related to the protons of the aliphatic group of lignin and peaks appearing at 4.7, and 0.0 ppm are assigned to D_2O and TMSP (3-trimethylsilyl-(2,2,3,3-D_4)-propionic acid sodium salt), respectively.[61-65]

In Figs. 3 and 4, the peak at 3.3 ppm corresponds to trimethylamine ($-N^+(CH_3)_3$), and the peak at 3.6–3.86 ppm stands for methylene groups connected to the ammonium group and ester carbon.[62,66,67] The peak at 2.18 ppm corresponds to the methylene protons $CH_2CH_2CH_2N^+(CH_3)_3$ of propyltrimethylammonium, and the peak at 2.05 ppm stands for the methylene protons (CH_2-$CH_2CH_2CH_2CH_2N^+(CH_3)_3$) of pentyltrimethylammonium.[17] The peak at 4.2, 2.2, and 3.1 ppm are assigned to the three methylene groups linking ester bond and sulfonate group of S containing group. Moreover, the peak at 0.96 and 1.10 ppm are assigned to the methyl group of S.[68,69] Also, grafting of 3T, 5T, and S monomers onto lignin was confirmed by FTIR spectroscopy. More information can be found in supporting information in Fig. S4.5 and Table S4.6.
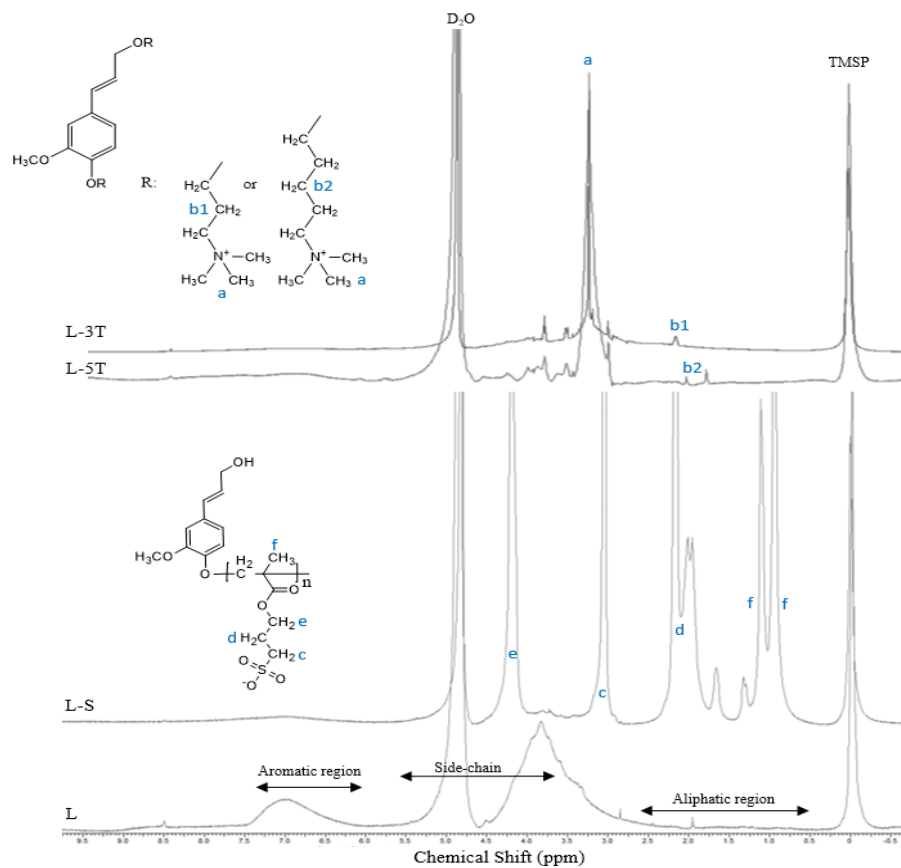
Fig. 4.3. ^{1}H NMR spectra of L, L-S, L-5T, and L-3T in D$_2$O at 25 °C.
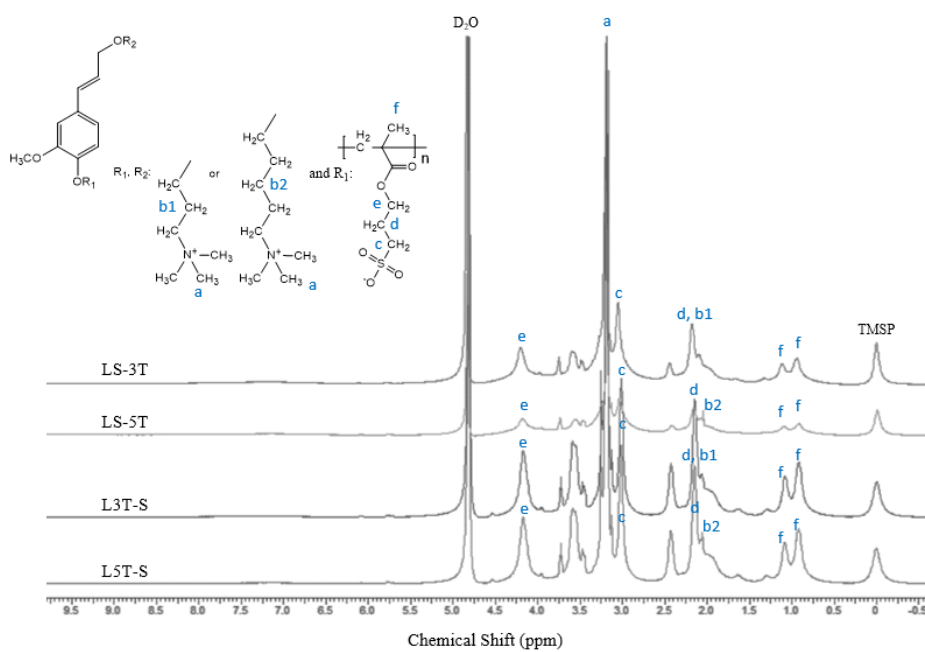
Fig. 4.4. ^{1}H NMR spectra of produced amphoteric samples in D_2O at 25 °C.

As seen in Fig. 4.4, the peaks at 2.18 and 2.2 ppm, which correspond to the methylene protons of propyltrimethylammonium and a three-methyl group of 3- sulfopropyl methacrylate, respectively, overlap in the ^{1}H NMR spectrum. Therefore, 2D^{1}H COSY spectroscopy analysis was conducted to confirm precisely the attachment of trimethylammonium and 3-sulfopropyl methacrylate groups to the backbone of lignin (Fig. 4.5). The 2D ^{1}H COSY spectrum of lignin (L) prior to functionalization can be found in supporting information (Fig. S4.6) for comparison. As seen in Fig. 4.5, the peak of D_2O was observed at around F1 = F2 = 4.7 ppm. Three peaks at {F1 = 2.18, F2 = 3.86 ppm}, {F1 = 2.18, F2 = 3.6 ppm} and {F1 = 2.18, F2 = 2.18 ppm} demonstrate that the methylene group connected to the trimethylammonium. These peaks confirm the existence of propyltrimetylammonium in amphoteric polymers of LS-3T and L3T-S.

a)

b)

c)
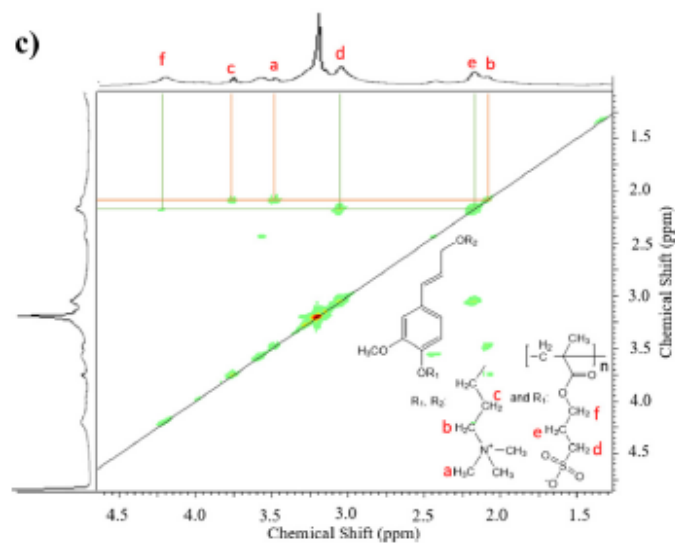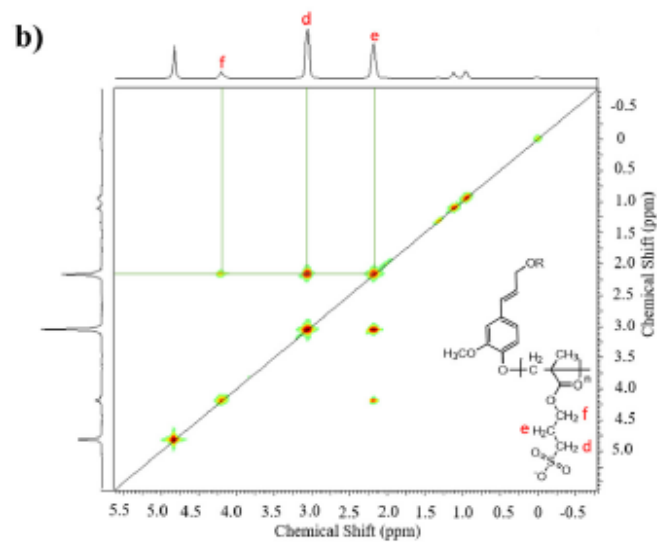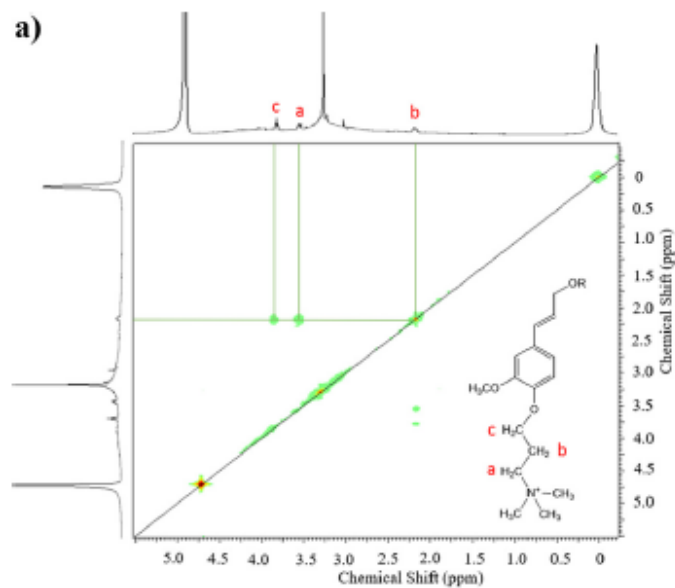
Fig. 4.5. 2D ^{1}H COSY spectroscopy in D$_2$O a) L-3T, b) L-S, and c) LS-3T in D$_2$O.

4.4.2.3 Surface wettability

The wettability of produced polymers was first investigated via contact angle analysis in water–air ($\theta_{W/A}$) interface. The oil-air, water–air, and oil–water tension were 27.5, 73, and 51.4 mN/m, respectively.[70,71] As shown in Table S4.6 (supporting information), the contact angle ($\theta_{W/A}$) for L, L-3T, and L-5T were measured to be 38°, 28°, and 32°, respectively. Thus, the hydrophilicity of L was increased via grafting cationic reagents on it, which is attributed to the addition of charged groups that improve the wettability.[72] Although the L-5T had a larger DS (0.33 mol/mol) than L-3T (0.19 mol/mol), its higher contact angle could be attributed to the longer carbon chain of the pentyltrimethylammonium group, which would induce less hydrophilicity than L-3T to a lignin polymer (Table S4.7).The amphoteric samples of L3T-S, L5T-S, LS-3T, and LS-5Tshowed a $\theta_{W/A}$ of < 6°, 6°, 11°, and 12° (Table S4.7). The higher wettability of these samples compared to single-ionic lignin is due to the presence of both cationic and anionic hydrophilic groups on lignin. Specifically, the addition of S and N groups enhanced the interaction of lignin with water due to an increase in the hydrogen bonding. This implies that these polymers can adapt themselves to different external conditions and may be able to keep their chains in stretched conformation.[17]

The anionic L-S2 (experiment number 2 in Table S4.2), cationic L-5T and amphoteric L5T-S had all similar amounts of sulfonate and amine groups and thus were chosen for further wettability analysis in oil in air ($\theta_{O/A}$), water in air ($\theta_{W/A}$), oil in water ($\theta_{O/W}$), and water in oil ($\theta_{W/O}$) systems (Fig. 4.6). The measured ($\theta_{W/A}$) revealed that the L-S2 and amphoteric L5T-S could easily be wetted by water in the air, exhibiting $\theta_{W/A}$ of 15°and 6°, respectively, while the cationic L-5T indicated a higher degree ($\theta_{W/A}$ of 32°).The oil drop in water $\theta_{O/W}$ contact angle of these three samples was conducted in water to establish their oil wettability. It has been found that all three polymers could be readily wetted by oil in the air (with a contact angle of less than 14°) (first column of Fig. 4.6), showing good lipophilicity of the samples. Interestingly, immersing the sample in water showed distinct oil wetting behaviors. The oil drop was strongly repelled by the amphoteric L5T-Sand anionic L-S2, showing very large $\theta_{O/W}$ of 125°, and 120°, respectively. The $\theta_{O/W}$ for cationic L-5T was lower (90°), which is attributed to the hydrophobic three methyl groups of L-5T.[22,58] Immersing these three samples in oil at the measured water contact angle $\theta_{W/O}$ (last column of Fig. 4.6) shows that both anionic L-S2 and cationic L-5T polymers had poor water wettability with a $\theta_{W/O}$ of 55°and 76°, respectively, while only the amphotericL5T-S polymer could

167

remain well wetted by water ($\theta_{W/O}$ of 19°).The lower wettability of L-5T than L-S2 proposed that the cationic quaternary amine groups (on L-5T) were less hydrated than the anionic sulfonate (SO_3^-) moieties of the L-S2. The relatively weak hydrophilicity of L-5T may also be associated with the presence of the three methyl groups on its quaternary amine group.[22,73,74] Meanwhile, the amphoteric polymer demonstrated higher wettability and could adapt better to water in oil medium by having both groups.
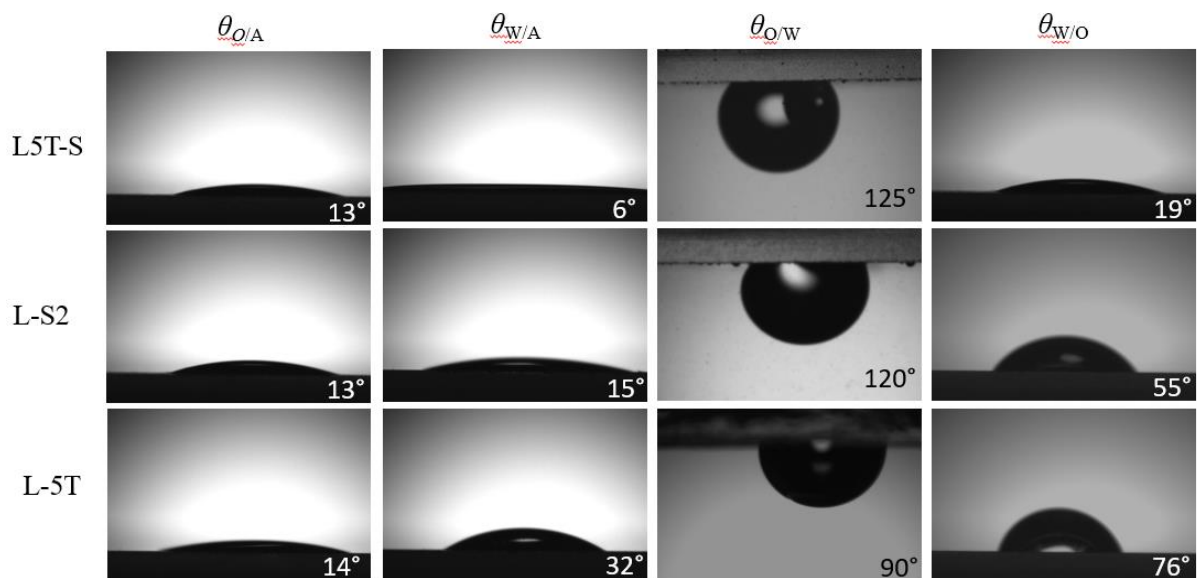
Fig. 4.6. Contact angle images of oil-air ($\theta_{O/A}$), water-air ($\theta_{W/A}$), oil in water ($\theta_{O/W}$), and water in oil ($\theta_{W/O}$) interfaces of amphoteric L5T-S, anionic L-S2, and cationic L-5T polymers.

4.4.2.4 Adhesion force measurement

The water/oil wettability of a polymer in oil/water is governed mainly by the interactive forces between the polymer and the surrounding medium. As an instance, the oil wettability of a substrate in water is governed by two different forces; a strong attraction between the oil droplet and the surface would lead to the depletion of water from the surface (i.e., oil wetting the surface). On the other hand, the repulsion force would remarkably hinder the substrate surface from wetting by oil and further oil fouling.[22] Thus, a quantitative evaluation was carried out to monitor the interaction forces among the amphoteric lignin polymer and water or oil to further explore the intrinsic wetting mechanism of the lignin polymers at oil/water interface.

Fig. 4.7 shows the adhesion force between the water droplet and polymer-coated glass with a driving velocity of 5 µm/s in the oil medium. In all three cases, the water droplets were found to readily attach onto surfaces (as a positive adhesion force and a peak were observed in Fig. 4.7A-

C and are depicted by arrows). The highest pull-off forces of about 200 μN, 65 μN, and 48 μN were received for L5T-S, anionic L-S2, and cationic L-5T, respectively.

In addition, the three other amphoteric samples (L3T-S, LS-3T, and LS-5T in Fig. S4.7 in supplementary materials) depicted a higher adhesion force compared to the single ionic ones (Fig. 4.7). The higher adhesion force of amphoteric polymer than anionic one reveals that the amphoteric lignin could interact more than the anionic one with the water droplet due to the anionic and cationic groups on its surface.

On the other hand, the anionic lignin showed a slightly higher adhesion force to water droplet than did the cationic sample, which was the result of its higher GR and hydrophilic sulfonate functional group attached to its surface. These results are in agreement with the wettability analysis in which the weaker attraction of water droplet was observed for the anionic L-S2 and cationic L-5T samples ($\theta_{W/O}$ values of 55° and 76°, respectively) than for the amphoteric L5T-S ($\theta_{W/O}$ 19°) (Fig. 4.6).
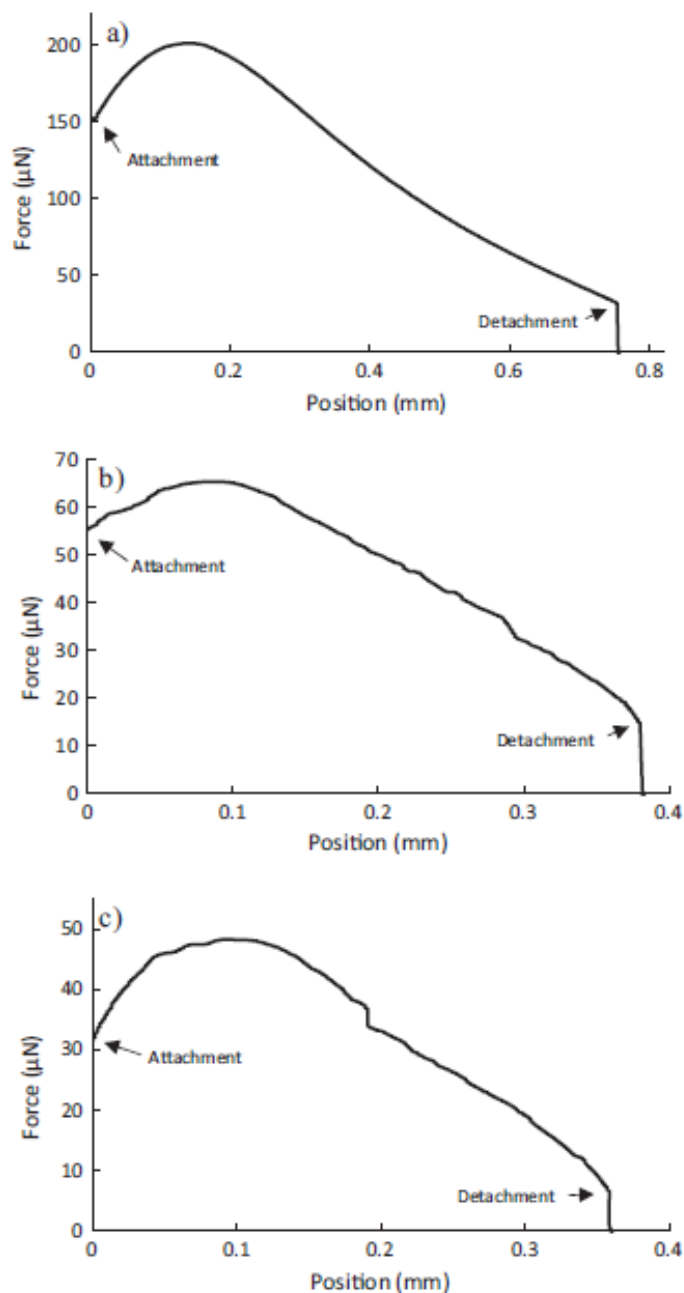
Fig. 4.7. Measured adhesion force curves among a water droplet and glass coated with polymers of a) amphoteric L5T-S, b) anionic L-S2, and c) cationic L-5T in oil medium.

Fig. 4.8 indicates the measured interaction force between an oil droplet and amphoteric L5T-S, anionic L-S2, and cationic L-5Tcoated surface in water media. Although the chains of three polymers could all be hydrated well in the water, they showed distinct interaction forces and behaviors with oil droplet. For anionic L-S2and amphoteric L5T-S, no attachment of the oil droplet was observed (as a negative force and a lack of peak were found), which could be related to high

170

underwater oil repellency and large $\theta_{O/W}$ (>120°) raised from the durable hydrophilic nature of the surface coated with the anionic lignin polymer. In other words, this oil repellency in water could be associated with the electrostatic double-layer interaction between L-S2 or L5T-S and oil droplet in water.[75] This is in agreement with the zeta potential analysis in which L-S2 and L5T-S had a negative zeta potential of -14.5 mV, and -9.2 mV, respectively, with a reported zeta potential of -35 mV for oil (toluene),[75,76] resulting in electrostatic repulsion. Also, the extended polyelectrolyte chain in amphoteric L5T-S and anionic L-S2 may also play a role in hindering the attachment of oil droplet in the water medium by developing a steric repulsion.

In contrast, the force profile of cationic L-5T surface and the oil droplet in water depicted an attachment. By considering the zeta potentials of the oil droplet (-35 mV) and the cationic L-5T (14 mV), the electrostatic attraction between these substrates is predicted to be the reason for the attachment. This phenomenon is observed in Fig. 4.6 by the relatively low $\theta_{O/W}$ (90°) of cationic L-5T.

The relatively higher adhesion force of L-5T to water than to oil droplet in oil or water medium, respectively, was also observed, and this showed its higher wettability with water compared to that with the oil droplet. This would be due to the presence of positively charged groups on L-5T, facilitating its interaction with water molecules.
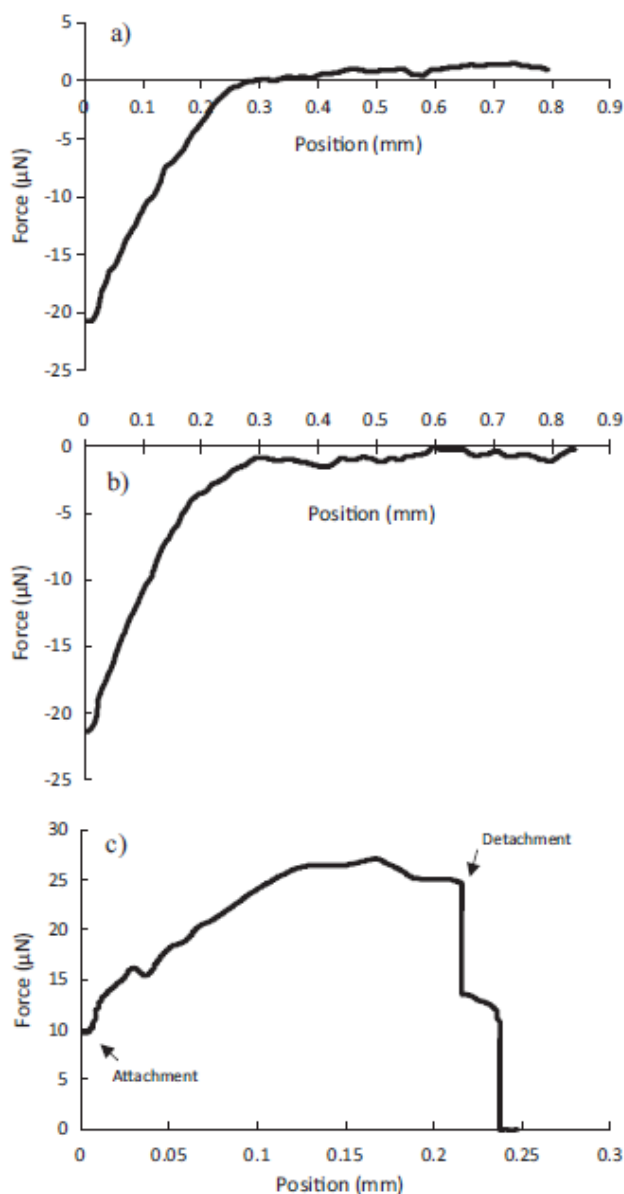
Fig. 4.8. Measured adhesion force curves among an oil droplet and glass coated with polymers of a) amphoteric L5T-S, b) anionic L-S2, and c) cationic L-5T in a water medium.

4.4.2.5 Behavior of anionic, cationic and amphoteric lignin polymers in different media

Fig. 4.9 and 4.10 show the proposed configuration of amphoteric L5T-S, anionic L-S2, and cationic L-5T polymers adsorbed on different interfaces. Under $\theta_{O/A}$ condition (Fig. 4.9, left column), polymers would have a flattened configuration on surfaces. In this case, the hydrophobic part of lignin would interact with oil and wet thoroughly by the oil droplet while its charge groups would have the minimum interaction with their surroundings leading to a reduction in hydrophilicity. By immersing polymers in water (Fig. 4.9, right column), some water molecules would be trapped

within the structure of lignin derivatives. Meanwhile, polymers would adopt a tail and loop configuration and expose their charged parts to the surface of the water. In this case, the surface charge density would be maximized, leading to high surface hydration and strong oil repellency. The less lipophobic behavior observed for L-5Tcompared to amphoteric and anionic polymers (Fig. 4.8) could be attributed to the cationic charged groups on lignin.[58] Considering the negative zeta potential of oil, a charge interaction would occur among the droplet and the L-5T polymer, begetting a higher adhesion and thus, a lower $\theta_{O/A}$.[22]
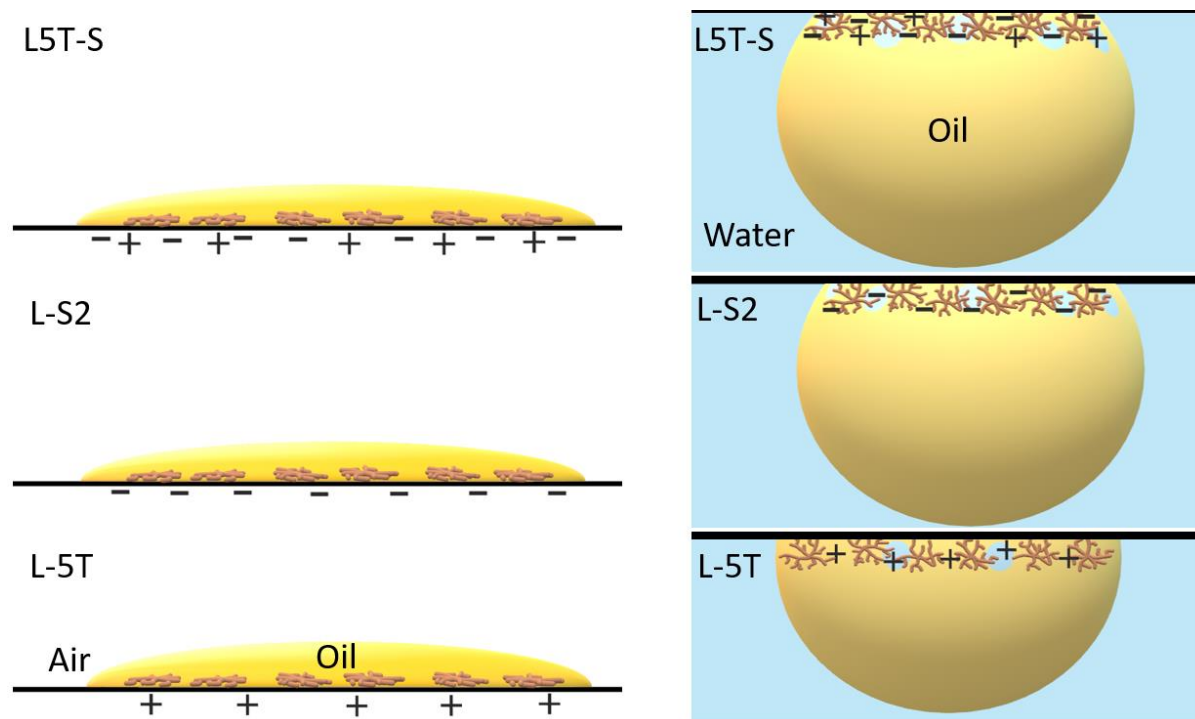
Fig. 4.9. Schematic demonstration of the configuration of amphoteric L5T-S, anionic L-S2, and cationic L-5T polymers in oil-air ($\theta_{O/A}$), and oil in water ($\theta_{O/W}$) interface. The charge signs plotted in the left column are to depict that the charged parts of polymers are configurated parallel to the surface plane.

Under $\theta_{W/A}$ condition (Fig. 4.10, left column), polymers would have a tail and lop configuration due to the hydrophilic nature of their surface functional groups, leading to a water wettability. By immersing the coated surface in the oil medium (Fig. 4.10, right column), oil molecules would be interacted with the hydrophobic parts of lignin and cause less water wettability. A higher $\theta_{W/O}$ of L-5T could be due to its cationic groups, which captures more oil molecules resulting from the charge interaction of its cationic group with the oil molecules. The amphoteric L5T-S would

interact more with water and result in the lowest $\theta_{W/O}$ than L-S2 via having both sulfonate and amine groups on its surface.

Therefore, the orientation of hydrophilic and hydrophobic parts of modified lignin, as well as its functional groups, would profoundly impact the behavior of these polymers in different interfaces.
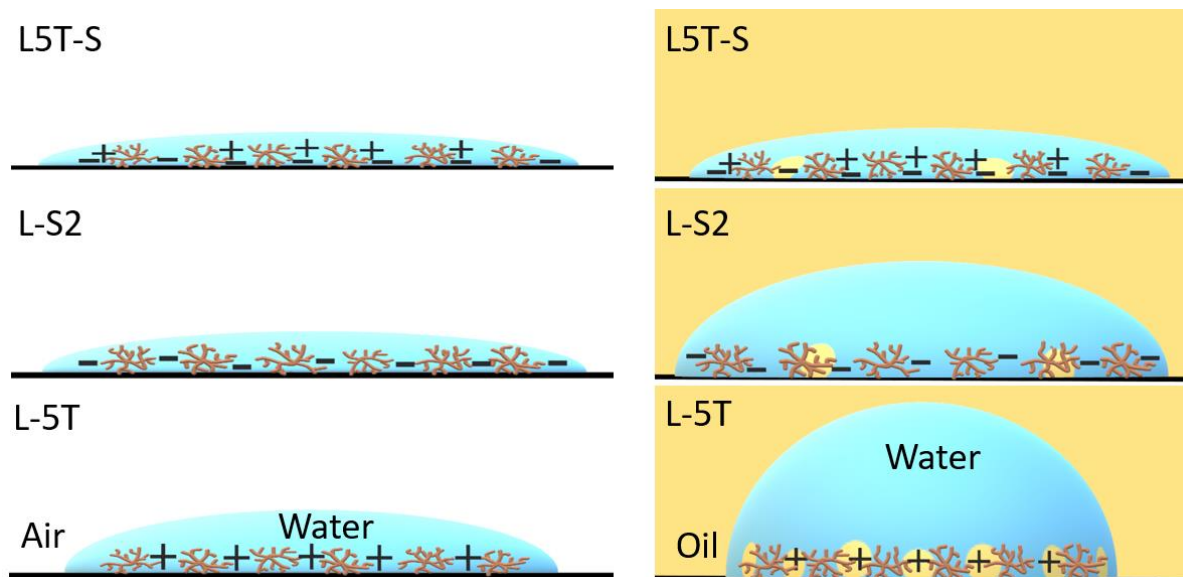
Fig. 4.10. Schematic demonstration of the configuration of amphoteric L5T-S, anionic L-S2, and cationic L-5T polymers in water-air ($\theta_{W/A}$), and water in oil ($\theta_{W/O}$) interface.

4.5 Conclusions

This study successfully exploited the production of amphoteric lignin-based derivatives in a semi-dry aqueous condition by grafting cationic reagent of propyl trimethylammonium bromide or pentyl trimethylammonium bromide and anionic polymerization of 3-sulfopropyl methacrylate monomer onto lignin. Our work proved the hypothesis that the order of the reactions was critical on the substitution of the functional groups of lignin due to the selectivity of the reaction chemistry of the hydroxy groups on lignin. Compared to the knowledge available in the literature,[1,4,48,52] our work proved that lengthening the carbon chain of a reagent increased the degree of substitution of lignin and impacted the behavior of amphoteric lignin in various media. At the water/air interface, the cationic (L-5T) polymer showed the least hydrophilicity compared to the amphoteric and anionic lignin. At the oil/air interface, good lipophilicity was observed for all three polymers on the surface. In water, amphoteric and anionic lignin samples depicted no lipophilicity, while the cationic sample showed some tendency to attach to the oil droplet. In oil, both cationic and anionic lignin polymers were barely wetted by water, whereas the amphoteric lignin depicted some

hydrophilicity. This analysis proves that polymer behavior in the wetting performance of the oil/water mixture depends on the phases and functional groups. Therefore, amphoteric lignin with different characteristics can be designed experimentally for different oil and water applications. In future, research may be conducted to correlate the characteristics of amphoteric lignin with its behavior in other multiphases for developing novel applications.

4.6 References

1) J. Zhu, G. Zhang and J. Li, J. Appl. Polym. Sci., 2011, 120, 518-523.

2) Q. Chu and L. Lin, RSC Adv., 2011, 9, 8608-8619.

3) S. Gao, J. Sun, P. Liu, F. Zhang, W. Zhang, S. Yuan and J. Jin, Adv. Mater., 2016, 28, 5307-5314.

4) L. Jia, J. Ma, D. Gao, B. Lyu and J. Zhang, J. Clean. Prod., 2016, 139, 788-795.

5) A.E. Kazzaz, Z.H. Feizi and P. Fatehi, Green chem. (2019), DOI: 10.1039/c9gc02598g.

6) J. Chen, A.E. Kazzaz, N. AlipoorMazandarani, Z.H. Feizi and P. Fatehi, Molecules, 2018, 23, 868.

7) S.H. Ghaffar and M. Fan, Biomass bioenergy, 2013, 57, 264-279.

8) A.M. Nada, N.F. Kassem and S.H. Mohamed, BioRes., 2008, 3, 538-548.

9) X. Liu, H. Zhu, C. Qin, J. Zhou, J.R. Zhao and S. Wang, BioRes., 2013, 8, 2257-2269.

10) J. Tian, S. Ren, G. Fang, Y. Ma and Q. Ai, BioRes., 2014, 9, 6290-6303.

11) L.H. Gan, M.S. Zhou and X.Q. Qiu, Adv. Mater. Res., 2012, 550, 1293-1298.

12) A.E. Kazzaz, Z.H. Feizi and P. Fatehi, Colloid Polym. Sci., 2018, 296, 1867-1878.

13) H. Kono and R. Kusumoto, React. Funct. Polym., 2014, 82, 111-119.

14) C. Dong, W. Chen and C. Liu, Bioresour. Technol., 2014, 170, 239-247.

15) C. Cai, Y. Bao, X. Zhan, X. Lin, H. Lou, Y. Pang, Y. Qian and X. Qiu, Green Chem., 2019, 21, 1141-1151.

16) C. Cai, X. Zhan, H. Lou, Q. Li, Y. Pang, Y. Qian, H. Zhou and X. Qiu, ACS Sustainable Chem. Eng., 2018, 6, 10679-10686.

17) R. De Oliveira Pedro, M. Takaki, T.C.C. Gorayeb, V.L. Del Bianchi, J.C. Thomeo, M.J. Tiera and V.A. de Oliveira Tiera, Microbiol. Res., 2013, 168, 50-55.

18) K. Bahrpaima and P. Fatehi, ChemSusChem, 2018, 11, 2967-2980.

19) Y. Xue, X. Qiu, Y. Wu, Y. Qian, M. Zhou, Y. Deng and Y. Li, Polym. Chem., 2016, 7, 3502-3508.

20) C. Huang, J. Ma, W. Zhang, G. Huang and G. Yong, Polymers, 2018, 10, 10, 841.

21) C. Roland-Swanson, J.P. Besse and F. Leroux, Chem. Mater., 2004, 16, 5512-5517.

22) C. Shi, B. Yan, L. Xie, L. Zhang, J. Wang, A. Takahara and H. Zeng, Chem. Int. Ed., 2016, 55, 15017-15021.

23) A. Natarajan, J. Xie, S. Wang, Q. Liu, J. Masliyah, H. Zeng and Z. Xu, J. Phys. Chem. C., 2011, 115, 16043-16051.

24) E.G. Schutt, D.H. Klein, R.M. Mattrey and J.G. Riess, Angew. Chem. Int. Ed., 2003, 42, 3218-3235.

25) I.U. Vakarelski, R. Manica, X. Tang, S.J. O'Shea, G.W. Stevens, F. Grieser and D.Y. Chan, Proc. Natl. Acad. Sci., 2010, 107, 11177-11182.

26) F. Kong, K. Parhiala, S. Wang and P. Fatehi, Eur. Polym. J., 2015, 67, 335-345.

27) M.I. Khalil, M.K. Beliakova and A.A. Aly, Carbohydr. Polym., 2011, 46, 217-226.

28) M.J. Sumner, W.L. Harrison, R.M. Weyers, Y.S. Kim, J.E. McGrath, J.S. Riffle and M.H. Brink, J. Membr. Sci.. 2004, 239, 199-211.

29) N. Joly, R. Granet, P. Branland, B. Verneuil and P. Krausz, J. Appl. Polym. Sci., 2005, 97, 1266-1278.

30) S. Y. Lin, 1982, US Pat. 4 332 589.

31) A.E. Kazzaz, Z.H. Feizi, F. Kong and P. Fatehi, Colloid Surf. A., 2018, 556, 218-226.

32) M.K. Konduri, F. Kong and P. Fatehi, Eur. Polym. J., 2015, 70, 371-383.

33) Y. Kawata, S. Kozuka and S.I. Yusa, Langmuir, 2018, 35, 1458-1464.

34) J. Cravillon, R. Nayuk, S. Springer, A. Feldhoff, K. Huber and M. Wiebcke, Chem. Mater., 2011, 23, 2130-2141.

35) B.H. Zimm, J. Chem Phys., 1956, 24, 269-278.

36) M. Kaszuba, D. McKnight, M.T. Connah, F.K. McNeil-Watson and U. Nobbmann, J. Nanopart. Res., 2008, 10, 823-829.

37) B. Zhang, S. Wang, L. Fu, J. Zhao and L. Zhang, J. Water Air Soil Pollut., 2018, 229, 199.

38) Z.H. Feizi, A.E. Kazzaz, F. Kong and P. Fatehi, Sep. Purif. Technol., 2019, 222, 254-263.

39) P. Maes, Y.B. Monakhova, T. Kuballa, H. Reusch and D.W. Lachenmeier, J. Agric. Food Chem., 2012, 60, 2778-2784.

40) Y. Ma, Z. Li, H. Wang and H. Li, J. Colloid Interface Sci., 2019, 534, 469-479.

41) X. Wen, X. Lu, K. Xiang, L. Xiao, H. Liao, W. Chen and H. Chen, J. Colloid Interface Sci., 2019, 554, 711-721.

42) G. Viswanadam and G.G. Chase, J. Colloid Interface Sci., 2012, 367, 472-477.

43) Y.C. Jung and B. Bhushan, Langmuir, 2012, 25, 14165-14173.

44) O. Ozkan and H.Y. Erbil, Surf. Topogr. Metrol. Prop., 2017, 5, 024002.

45) L. Heng, J. Su, J. Zhai, Q. Langmuir, 2011, 27, 12466-12471.

46) A.T.W.M. Hendriks and G. Zeeman, Bioresour. Technol., 2009, 100, 10-18.

47) D.K. Setua, M.K. Shukla, V. Nigam, H. Singh and G.N. Mathur, Polym. Compos., 2000, 21, 988-995.

48) H. Homma, S. Kubo, T. Yamada, Y. Matsushita and Y. Uraki, J. Wood Chem. Technol., 2008, 28, 270-282.

49) T. Aso, K. Koda, S. Kubo, T. Yamada, I. Nakajima and Y. Uraki, J. Wood Chem. Technol., 2013, 33, 286-298.

50) Y. Jiao, Z. Xu, W. Qiao and Z. Li, Energy Sources, Part A, 2007, 29, 1425-1432.

51) J. Yanhua, Q. Weihong, L. Zongshi and C. Lubai, Energy Sources, 2004, 26, 409-414.

52) Z. Yang, H. Wu, B. Yuan, M. Huang, H. Yang, A. Li, R. Cheng and Cheng, R. Chem. Eng. J., 2014, 244, 209-217.

53) T.M. Garver and P.T. Callaghan, Macromolecules, 1991, 24, 420-430.

54) G. Gilardi and A.E. Cass, Langmuir, 1993, 9, 1721-1726.

55) S. Wang, F. Kong, W. Gao and P. Fatehi, Ind. Eng. Chem. Res., 2018, 57, 6595-6608.

56) R. Simha, J. Phys. Chem., 1940, 44, 25-34.

57) P.S.S.K. Bhattacharya, S.K. Saha, A. Yadav, P.E. Phelan and R.S. Prasher, J. Appl. Phys., 2004, 95, 6492-6494.

58) Malvern Instruments, Inform White Paper: Dynamic light scattering, http://www.biophysics.bioc.cam.ac.uk/wp-content/uploads/2011/02/ DLS_Terms_defined_Malvern.pdf, (accessed July 2019).

59) H. Song, D. Wu, R.Q. Zhang, L.Y. Qiao, S.H. Zhang, S. Lin and J. Ye, Carbohydr. Polym. 2009, 78, 253-257.

60) P.C. Parvathy and A.N. Jyothi, J. Appl. Polym. Sci., 2014, 131, 40368.

61) Y.C. Sun, J.L. Wen, F. Xu and R.C. Sun, Sci. Res. Essays, 2010, 5, 3850-3864.

62) A. Hasan and P. Fatehi, J. Appl. Polym. Sci., 2018, 135, 46338.

63) N.E. El Mansouri, Q. Yuan and F. Huang, BioRes., 2011, 6, 2647-2662.

64) H. Mainka, O. Täger, E. Körner, L. Hilfert, S. Busse, F.T. Edelmann and A.S. Herrmann, J. Mater. Res. Technol., 2015, 4, 283-296.

65) T. Rashid, C.F. Kait, I. Regupathi and T. Murugesan, Ind. Crops Prod., 2016, 84, 284-293.

66) Z. Abdollahi, M. Frounchi and S. Dadbin, J. Ind. Eng. Chem., 2011, 17, 580-586.

67) D. Chen, X. Liu, Y. Yue, W. Zhang and P. Wang, Eur. Polym. J., 2006, 42, 1284-1297.

68) Y. Xu, A. Walther and A.H. Müller, Macromol. Rapid Commun., 2010, 31, 1462-1466.

69) G. Masci, D. Bontempo, N. Tiso, M. Diociaiuti, L. Mannina, D. Capitani and V. Crescenzi, Macromolecules, 2004, 37, 4464-4473.

70) D.R. Lide, Boca Raton FL 2008.

71) K. Tajima, T.T. sutsui and H. Murata, Bull. Chem. Soc. Jpn., 1980, 53, 1165-1166.

72) P. Liu, H. Wang, T. Yan, J. Zhang, L. Shi and D. Zhang, J. Mater. Chem. A., 2016, 4, 5303-5313.

73) X. Liu, C. Leng, L. Yu, K. He, L.J. Brown, Z. Chen and D. Wang, Angew. Chem., Int. Ed., 2015, 54, 4851-4856.

74) R. Scheu, Y. Chen, H.B. de Aguiar, B.M. Rankin, D. Ben-Amotz and S. Roke, J. Am. Chem. Soc., 2014, 136, 2040-2047.

75) C. Shi, L. Zhang, L. Xie, X. Lu, Q. Liu, C.A. Mantilla and H. Zeng, Langmuir, 2016, 32, 2302-2310.

76) H.J. Busscher, B. Van de Belt-Gritter and H.C. Van der Mei, Colloids Surf., B., 1995, 5, 111-116.

4.7 Appendix A. Supplementary material

Supporting information

Fabrication and Characterization of Amphoteric Lignin and its Hydrophilicity/Oleophilicity at oil/water Interface

Armin Eraghi Kazzaz, Pedram Fatehi*

Green Processes Research Centre and Chemical Engineering Department, Lakehead University, 955 Oliver Road, Thunder Bay, ON, Canada, P7B5E1

* Corresponding author, email: pfatehi@lakeheadu.ca; tel: 807-343-8697; fax: 807-346-7943

Methylation of Lignin

2.0 g of lignin was dissolved in 30 mL NaOH (0.7 mol/L) solution at room temperature by stirring at 200 rpm for 30 min. Then a 2.5 mmol of dimethyl sulfate was added per each mmol of total phenolic hydroxy groups of lignin (defined according to the method used by Kong et al.),[1] and the solution was mixed for 30 min at room temperature. The mixture was then heated to 80 °C for 2 h. During the reaction, the pH of the system was kept at 11-11.5 with continuous addition of 0.7 mol/L NaOH solution. After the reaction completion, the mixture was acidified to pH 2.5 by adding HCl (2 mol/L) solution, and the solid precipitate was washed with an excess amount of deionized water until neutral pH was obtained. The sample was then freeze-dried, and the final product was denoted as ML.

Reaction Optimization for Cationic Lignin-based Samples

A total of 16 runs of the reaction were conducted based on Taguchi orthogonal design (L16) to determine the optimum condition to produce L-3T and L-5T polymers (Table S4.1). In this reaction, the CD and grafting ratio (GR) parameters were chosen to be considered in determining the best L-3T, and L-5T polymers produced in the reaction under various conditions since the amine group attached to lignin directly affects the change in the CD and GR of lignin.

Table S4.1. Factors and levels in Taguchi design (L16) for L-3T, and L-5T.

Expt. No.	Control factors and their levels					L-3T polymer		L-5T polymer	
	Temperature	Time	3T or 5T/L	NaOH	Water content	CD	DS	CD	DS
	)C°(	)min(	mol/mol	Molar	%	(meq/g)	mol/mol	(meq/g)	mol/mol
1	80	120	1	1	50	0.67	0.13	1.09	0.24
2	80	30	1.5	2.5	40	0.15	0.04	1.00	0.22
3	60	30	0.5	1	30	0.14	0.04	0.54	0.11
4	60	90	1.5	2	50	0.22	0.07	0.46	0.17
5	80	90	0.5	1.5	92	-0.97	0.02	0.20	0.05
6	90	60	1.5	1	92	0.11	0.04	0.29	0.09
7	70	30	1	2	92	-0.89	0.03	-0.32	0.03
8	70	120	1.5	1.5	30	0.69	0.12	1.01	0.22
9	60	60	1	1.5	40	0.25	0.07	0.48	0.11
10	90	30	2	1.5	50	0.49	0.09	0.89	0.19
11	60	120	2	2.5	92	-0.56	0.03	-0.40	0.03
12	90	90	1	2.5	30	1.01	0.19	1.47	0.33
13	90	120	0.5	2	40	0.61	0.1	1.38	0.30
14	70	90	2	1	40	0.49	0.10	0.89	0.20
15	80	60	2	2	30	0.63	0.1	0.81	0.18
16	70	60	0.5	2.5	50	0.32	0.07	0.53	0.12
17	90	120	1.5	1	30	0.92	0.13	-	-
18	90	120	1.5	1	30	-	-	1.00	0.22

Reaction Optimization for polymerization with an Anionic Monomer

A total of 16 runs of the reaction were conducted based on Taguchi orthogonal design (L16) to determine the optimum condition for the production of anionic polymerized polymers (Table S4.2). In this reaction, CD and GR factors were chosen to be considered in determining the best L-S polymer produced in the reaction under various conditions, as the sulfonate group attached to L directly affected the change in the CD and GR of lignin. Thus, the polymer with the maximum CD and GR was considered the best-produced product.

Table S4.2. Factors and levels in Taguchi design (L16) for L-S.

Experiment number	Control factors and their levels					L-S polymer	
	Temperature)°C)	Time)min(	S/Lignin mol/mol	HCl %	Water content %	CD (-meq/g)	GR wt. %
1	60	60	1.5	14	50	2.15	95.0
2	90	30	1.5	10	92	1.80	82.3
3	70	60	2	10	40	2.33	95.7
4	80	60	0.5	12	92	1.60	68.4
5	60	10	0.5	10	30	1.90	87.4
6	70	10	1	14	92	1.65	77.9
7	80	120	1	10	50	2.45	107.2
8	90	10	2	12	50	1.83	89.0
9	80	10	1.5	16	40	2.04	99.8
10	80	30	2	14	30	2.56	124.7
11	60	30	1	12	40	2.61	115.0
12	90	60	1	16	30	2.55	116.4
13	60	120	2	16	92	1.60	72.7
14	70	30	0.5	16	50	2.25	108.1
15	70	120	1.5	12	30	2.21	105.5
16	90	120	0.5	14	40	2.24	103.9
17	80	30	1	14	30	2.88	137.0

Purification Steps for Produced Polymers

Upon completion, the reaction containers were cooled by soaking in cold water. The produced cationic lignin samples precipitated in the mixture of ethanol/water in the ratio of 80/20 v/v, and centrifuged at 3500 rpm for 10 min. For anionically polymerized samples, the level of the mixture's pH was adjusted to 2.0 by the addition of HCl and centrifuged at 3500 rpm for 10 min. UV spectroscopy (Genesys 10 s UV/Vis spectrophotometer, Thermo Scientific, Madison, USA) was used at λ =280 to monitor the concentration of cationic and anionic lignin in the supernatants. This way, the by-products (3T, 5T, and SM homopolymers), unreacted chemicals (3T, 5T, and SM), and NaOH or HCl remained in the supernatant and were separated from the cationic or anionic lignin products.[2-4]

Amphoteric Lignin Production

Table S4.3. The optimum reaction conditions for producing cationic, anionic, and amphoteric lignin as well as their control samples.

Samples name	Mass ratio (mol)				Optimum levels of different factors (µL)		Time (min)	Temperature (°C)
	Lignin	3T monomer	5T monomer	SM monomer	Cationization	Anionization		
L	1	-	-	-	-	-	-	-
L1	1	-	-	-	550 (NaOH), 900 H_2O	-	90	90
L-3T	1	1	-	-	550 (NaOH), 900 H_2O	-	90	90
L-5T	1	-	1	-	550 (NaOH), 900 H_2O	-	90	90
L2	1	-	-	-	-	760 H_2O, 550 Acid, 500 initiator	30	80
L3T-S[1]	1	1	-	1	550 (NaOH), 900 H_2O	760 H_2O, 550 Acid, 500 initiator	90, then 30	90, then 80
L5T-S[1]	1	-	1	1	550 (NaOH), 900 H_2O	760 H_2O, 550 Acid, 500 initiator	90, then 30	90, then 80
L3	1	-	-	-	550 (NaOH), 900 H_2O	760 H_2O, 550 Acid, 500 initiator	90, then 30	90, then 80
L-S	1	-	-	1	-	760 H_2O, 550 Acid, 500 initiator	30	80
LS-3T[2]	1	1	-	1	550 (NaOH), 900 H_2O	760 H_2O, 550 Acid, 500 initiator	30, then 90	80, then 90
LS-5T[2]	1	-	1	1	550 (NaOH), 900 H_2O	760 H_2O, 550 Acid, 500 initiator	30, then 60	80, then 90

[1]: cationization was carried out before anionization.

: anionization was carried out before cationization.

Weight-Average Molecular Weight (M_w) and Hydrodynamic Radius (R_h) Analysis

For molecular weight analysis, the produced lignin samples were prepared in five different concentrations of 0.4, 0.8, 1.2, 1.6 and 1.8 mg/mL in NaOH solution (20 mL, 0.5 mol/L). The He-Ne laser of the goniometer was operated at a wavelength of 637 nm with 20 % power at 25 °C. 12 scattering angles arranged in an angular regime of $15.0° \leq \theta \leq 155.0°$. The recording of the angular dependent curve completed after 2 ms. One thousand consecutive recordings were added to create a measurement requiring 2 s in total. The initiation of the concurrent measurements was at 10 s intervals. The solutions were filtered using 0.45 μm filters to eliminate any dust particles while transferring them to scattering cells. The scattering curves were analyzed as the Rayleigh ratio $\Delta R\theta$ at changing scattering angle θ. The scattering curves were approximated using BIC Zimm Plot.

For hydrodynamic analysis, solution samples were freshly prepared in 0.1 g/L concentrations and mixed with 1 mM NaCl at pH 7.0. Then, the DLS analysis was performed at 632 nm wavelength at a 90° scattering and 25.0 °C. Reported results are the mean values of the analysis carried out three times.

^{1}H NMR, 2D H COSY, and FTIR Spectroscopy

In this study, 50 mg of the samples were dissolved in 500 μL of D_2O, which contained TMSP (2 mg TMSP/500 μL D_2O) at 50 °C in a water bath shaker overnight at 150 rpm.

Moreover, 25-30 mg of methylated samples and 2 mg of TMSP were dissolved in a mixture of 9/1 v/v [D_6]DMSO/D_2O and incubated at 50 °C in the water bath shaker at 150 rpm overnight. A 458 pulseflipping angle, a 4.6 ms pulse width, a 2.05 s acquisition time, and a relaxation delay time of 1.00 s were considered in this experiment.

For the 2D ^{1}H COSY spectroscopy, the acquisition time was set to 3.983 s, and 16 scans with 128 increments and 1 second relaxation time delay were taken into account.

For the FTIR experiment, approximately 0.1 g of freeze-dried lignin and produced amphoteric samples were submitted to the Fourier-transform infrared spectroscopy (FTIR) spectrometer (Bruker Tensor 37, Germany, ATR accessory). The spectra of the samples were recorded in the

transmittance mode in the range of 600 and 4000 cm^{-1} with a 4 cm^{-1} resolution, and 32 scans per sample were performed.

Grafting Reaction Scheme

The by-products of grafting lignin with cationic monomers are (3-hydroxypropyl)trimethylammonium and (5-hydroxypentyl)trimethylammonium as shown in Figure S1b, which were removed by dialysis membrane in the purification step.
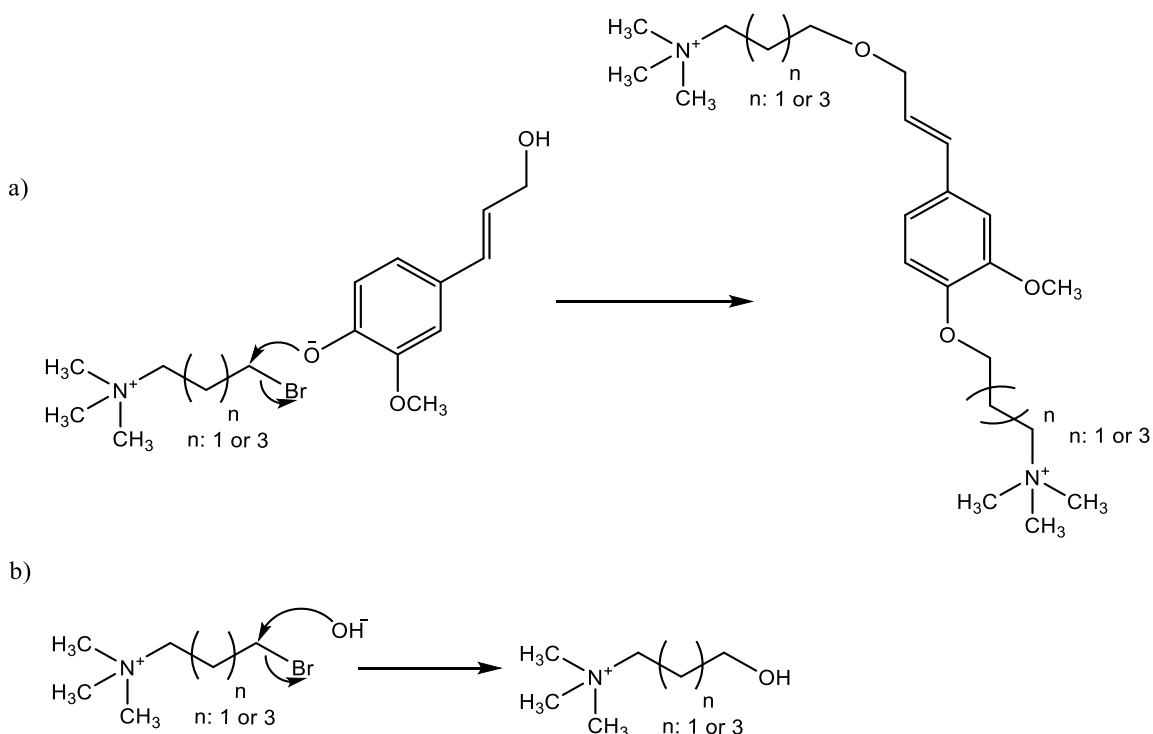
Fig. S4.1. Mechanism of a) grafting lignin with cationic monomers (3T = n:1, 5T= n:3), and b) the production of by-products in the side reaction.

Polymerization Scheme

Figure S2 presents the proposed polymerization scheme with lignin to produce L-S. Lignin is a guaiacyl lignin, which mainly consists of coniferyl alcohol units.[5] Thus, coniferyl alcohol was chosen to represent lignin in this figure. During the polymerization reaction, the sodium persulfate (Na$_2$S$_2$O$_8$) initially produces sulfate radicals (SO$_4^-$) in the reaction solution (Figure S2a), which can initiate the homopolymerization of vinyl monomers (Figure S2b). On the other hand, the

sulfate radicals can take the unstable hydrogen from the phenol group of lignin to generate phenoxyl radicals (Figure S2c), which can further propagate the polymerization reaction (Figure S1d).

a) $Na_2S_2O_8 \longrightarrow 2Na^+ + 2SO_4^{2-} \longrightarrow SO_4^{-\cdot}$

b)

Homopolymer

c)

d)
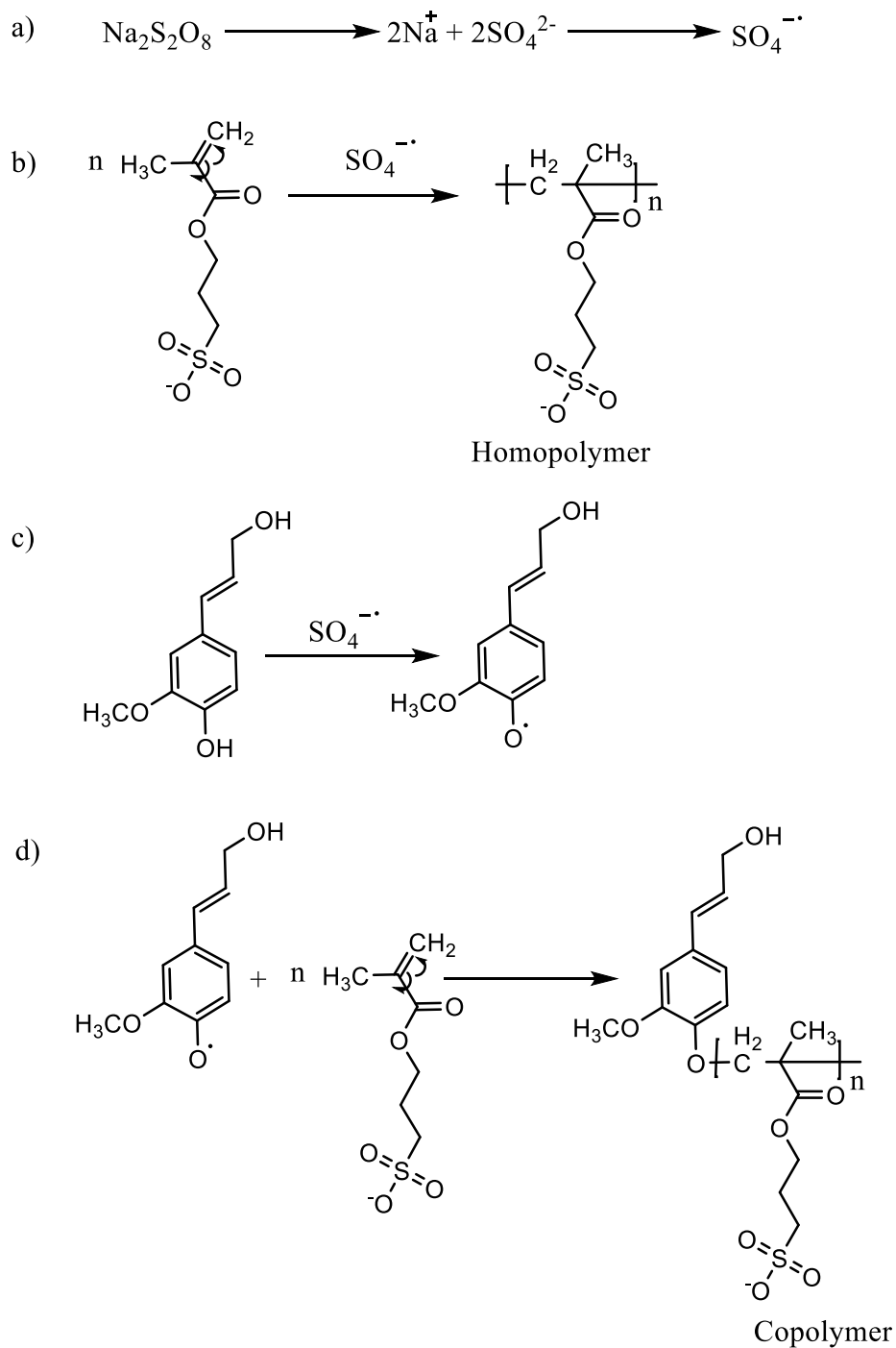
Copolymer

Fig. S4.2. Polymerization mechanism of L to produce L-S.

Factors Influencing Cationization Reaction

185

Statistical analysis was carried out to discover the significant levels of different factors affecting the CD and DS, as shown in Table S4. The K_i values for each factor were calculated from the mean of four sets of CD and DS results for each level listed in Table S4.1, in which i (1, 2, 3, and 4) is the number of levels. The range value (R) for each factor is determined from the difference between the maximum and minimum K_i values for that factor, and it depicts the effect of variables on the CD and DS results. The high R factor means that the factor has a strong effect on the results.[6] From the values of R, the significant sequence of affecting factors was identified. The optimal levels (Table S4.4) for each factor were water content (30%) > temperature (90 °C) > time (120 min) > monomer/lignin molar ratio (1.5 mol/mol) > NaOH (1 molar) for both L-3T and L-5T reactions. This condition for the reactions was not a set of conditions among 16 experimental options in the Taguchi design (Table S4.1). Therefore, two additional experiments, one for L-3T and one for L-5T, were conducted to track the influence on CD and DS. The products of this reaction were named as No.17 and No.18, and the results are shown in Table S4.1. According to the supplementary experiment (No. 17, and 18 in Table S4.1), no better results were obtained for CD and DS for the polymers and thus, the reaction conditions of experiment number 12 has been considered as the optimum for producing both cationic polymers of L-3T, and L-5T in this study.

Table S4.4a. Factors influence analysis on CD and DS of L-3T.

Factors	Temperature		Time		5T/Lignin mol		NaOH		Water content	
	CD (meq/g)	DS mol/mol	CD (meq/g)	DS mol/mol	CD (meq/g)	DS mol/mol	CD (meq/g)	DS mol/mol	CD (meq/g)	DS mol/mol
$K 1$	0.01	0.05	-0.03	0.05	0.03	0.06	0.35	0.08	0.62	0.11
$K 2$	0.15	0.08	0.05	0.07	0.26	0.11	0.12	0.08	0.38	0.08
$K 3$	0.12	0.07	0.19	0.10	0.29	0.07	0.14	0.08	0.43	0.09
$K 4$	0.56	0.11	0.35	0.10	0.26	0.08	0.23	0.08	-0.58	0.03
R (impact)	0.54	0.05	0.38	0.05	0.27	0.05	0.24	0.00	1.20	0.08

Table S4.4b. Factors influence analysis on CD and DS of L-5T.

Factors	Temperature		Time		5/Lignin mol		NaOH		Water content	
	CD (meq/g)	DS mol/mol	CD (meq/g)	DS mol/mol	CD (meq/g)	DS mol/mol	CD (meq/g)	DS mol/mol	CD (meq/g)	DS mol/mol
$K 1$	0.27	0.11	0.53	0.14	0.66	0.13	0.70	0.16	0.96	0.21
$K 2$	0.53	0.14	0.13	0.12	0.68	0.18	0.65	0.14	0.94	0.20
$K 3$	0.78	0.17	0.76	0.19	0.69	0.18	0.58	0.15	0.74	0.18
$K 4$	1.01	0.22	0.77	0.19	0.55	0.15	0.65	0.16	-0.06	0.05
R (impact)	0.74	0.11	0.65	0.07	0.14	0.05	0.12	0.02	1.02	0.17

Factors Affecting Anionic Polymerization

To understand the significant levels of factors on the CD and GR, the statistical analysis was performed, which is summarized in Table S4.5. The significant sequence of affecting factors was indicated based on K_i and R values. The optimal levels (Table S4.5) for each factor were water content (30%) > time (30 min) > monomer/lignin mol (1 mol/mol) > temperature (80 °C) > HCl (14 %) for L-S reaction. This condition for the reaction was not a set of conditions among 16 experimental options in the Taguchi design for anionic polymerized lignin (Table S4.2). Therefore, an additional experiment (No. 17) was performed to track the influence of the new condition on CD and GR. According to the supplementary experiment (No. 17 in Table S4.2), better results were obtained for CD and GR for the polymer. This can be attributed to the higher temperature and lower water content in which higher temperature may result in increasing the monomer movement and accessibility of monomers to lignin, and reduction in water content results in less hydrolysis of the monomer and the produced polymer.[7-9] Thus, the reaction condition of No. 17 has been considered as the optimum for producing anionic lignin polymers in this study and donated as L-S.

Table S4.5. Factors influence analysis on CD and GR of L-S.

Factors	Temperature		Time		S/lignin mol		HCl		Water content	
	CD (-meq/g)	GR wt. %	CD (-meq/g)	GR wt. %	CD (-meq/g)	GR wt. %	CD (-meq/g)	GR wt. %	CD (-meq/g)	GR wt. %
K 1	2.07	92.5	1.86	88.6	2.00	91.9	2.12	93.2	2.31	108.5
K 2	2.11	96.8	2.31	107.5	2.32	104.1	2.06	94.5	2.31	103.6
K 3	2.16	100.0	2.16	93.9	2.05	95.6	2.15	100.4	2.17	99.8
K 4	2.11	97.9	2.13	97.3	2.08	95.7	2.11	99.3	1.66	75.3
R (impact)	0.10	7.5	0.45	19.0	0.32	12.1	0.03	7.12	0.64	33.1

Factors affecting amphoteric lignin

For the cationic samples (Table S4.4), the optimal levels for each factor were water content (30%) > temperature (90 °C) > time (120 min) > monomer/lignin molar ratio (1.5 mol/mol) > NaOH (1 molar) for both L-3T and L-5T reactions. For the produced anionic polymers (Table S4.5), the optimal levels for each factor were water content (30%) > time (30 min) > monomer/lignin mol (1 mol/mol) > temperature (80 °C) > HCl (14 %) for L-S reaction. These conditions for the cationic samples and anionic polymers reactions were not a set of conditions mentioned among 16 experimental options in the Taguchi design (Table S4.2). Therefore, three additional experiments No.17 and No.18 (Table S4.1) for cationic modifications, and No.17 (Table S4.2) for anionic modification, were conducted to find the best results for CD and GR. According to these supplementary experiments, no better results were obtained for CD and GR for the cationic polymers. According to the supplementary experiment for produced anionic polymers, better results were obtained for CD and GR for the polymer. This can be attributed to the higher temperature and lower water content, in which higher temperature may result in increasing the monomer movement and accessibility of monomers to lignin, and reduction in water content results in the less hydrolysis of the monomer and the produced polymer.[7-9] Therefore, the reaction condition of L-3T, L-5T, and L-S experiment has been considered as the optimum for producing amphoteric lignin-based products in this study.

Mechanism of the Methylation Reaction

In lignin modifications, radicals are derived mainly from the phenolic hydroxy groups due to the high stability of phenoxyl radicals and the low stability of aliphatic alcohol radicals. Also, under alkaline condition, the ionization of aromatic hydroxy groups is more accessible than aliphatic hydroxy.[10] To testify whether the lignin anionization and cationization (by using S, 3T, 5T monomers) are performed on the aliphatic hydroxy groups, the L was methylated using dimethyl sulfate to selectively protect the phenolic hydroxy groups, by replacing with methoxy groups (ML).[1] In this case, only the aliphatic hydroxy groups would be accessible for reaction with cationic or anionic monomers. As seen in Figure S4.3, there is an intense peak caused by the methoxy group in the spectrum of L at 3.5-4.0 ppm in comparison with that in L (Figure 4.3).[1] Furthermore, the lack of any peak in the range of 8.00-9.35 ppm affirms that there were no phenolic groups left unreacted in ML.[6] The presence of the peak at 3.3 ppm corresponds to trimethylamine of cationic monomers which was absent in the spectrum of ML, proving the substitution of aliphatic hydroxy groups of lignin with cationic monomers. The absence of S peaks in ML-S indicates that S was unable to polymerize onto lignin in the absence of phenolic hydroxy groups.

189
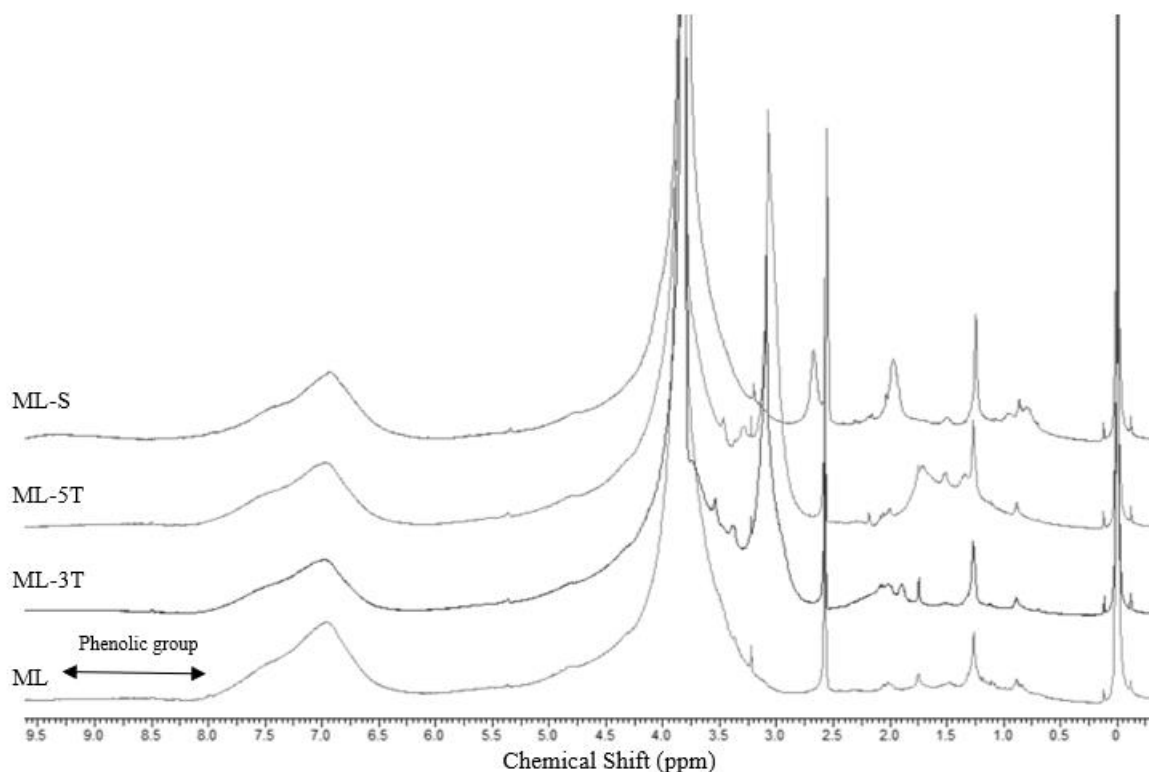
Fig. S4.3. ^{1}H NMR spectrum of ML, ML-S, ML-3T, and ML-5T in [D$_6$]DMSO/D$_2$O at 25 °C.

Efficiency of Purification Method in Cationization and Anionic Polymerization

For the cationic samples, the precipitated weight percentage of the homopolymer after centrifugation was measured to be 0.14 and 11.52 % in 80:20 v/v ethanol/water and pure ethanol, respectively. Hence, it was concluded that an ethanol/water (80:20, v/v) solution was more successful in retaining the homopolymer in the supernatant and thus, separate it from the precipitated products. For the anionic samples, the precipitated weight percentage of homopolymer by using HCl (decreasing the pH to 2.0), and ethanol/water (80:20, v/v) were 0.11 and 1.60 %, respectively. Apparently, by decreasing the pH to 2, the charged groups (i.e., sulfonate groups) became protonated, which further eliminated the charge effects on lignin solubility. Furthermore, in the polymerization reaction, the molecular weight enhanced, which made the uncharged polymerized lignin water insoluble. This facilitated the separation of L-S from solution and worked better than using ethanol/water (80:20, v/v). In the case of ethanol/water (80:20, v/v),[11,12] the phenomenon which separates lignin from the medium is the hindrance of polymer interaction (hydrogen bonding) with its surrounding, which is less effective than pH reduction in the sedimentation of polymerized polymer.

The UV analysis also revealed that the amount of L-3T, L-5T, and L-S products in the supernatant was less than 1 wt. %. Therefore, the presence of polar solvent (i.e., ethanol) in the solution facilitated the isolation of phenolic compounds for isolating cationic samples from the reaction mixture,[11,12] and acidifying was found to be the proper method for the isolation of anionic polymers from the reaction mixture. Therefore, for cationization, ethanol/water (80:20, v/v) was selected for purification, and acidification was chosen for anionic polymerization in this work, which was more successful in retaining the homopolymer in the supernatant.

Isoelectric Point
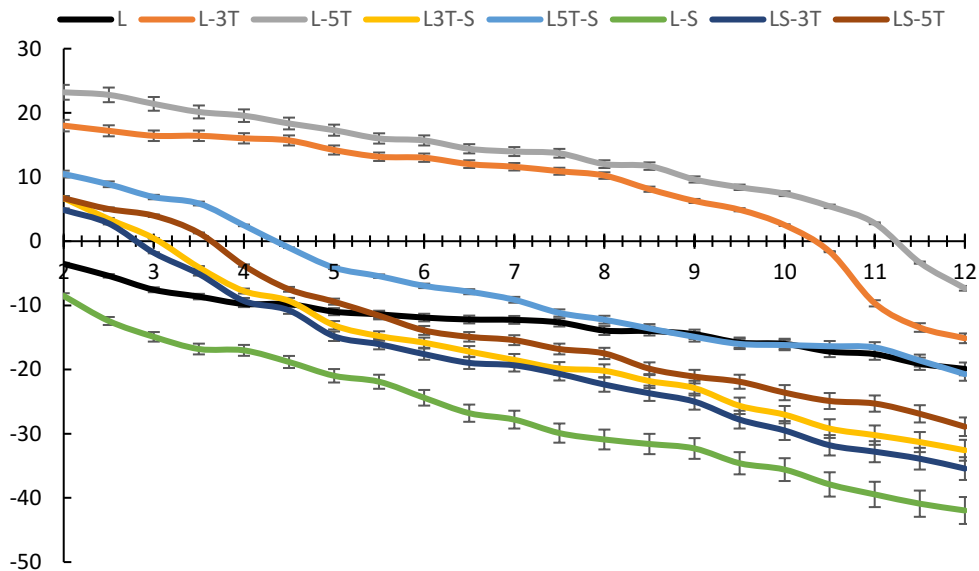
Fig. S4.4. The isoelectric point of unmodified and produced polymers under different pH at 25 °C.

FTIR Spectroscopy

FTIR spectra of lignin and produced amphoteric samples are presented in Figure S5, and the peak assignments are classified in Table S4.6. As depicted, both the unmodified and cationic lignin polymers show a broad band around 3400 cm^{-1} which is assigned to the O-H stretching absorption in the lignin phenolic and aliphatic parts. Peaks at 2960, 2897 and 1718 cm^{-1} are assigned to the C-H asymmetric, C-H symmetric and C=O of the conjugated ester stretching vibration in the S monomer, respectively, which is the sign of successful polymerization. The absorbance band at 1153 cm^{-1} is assigned to S=O stretch of sulfonate group of S, which is another sign of successful polymerization. The absorbance bands at 1261 cm^{-1} and 1140 cm^{-1} are assigned to the C-O and C-H stretch of the guaiacyl unit, respectively, which is a proof of softwood lignin. An increase in the intensity of the absorbance at 1032 cm^{-1} is related to the C-O-C bond, confirming the ether linkages between lignin and cationic/anionic monomer. In addition, new absorbance peaks at 1481 cm^{-1} and 966 cm^{-1}, which are assigned to the methyl group of propyltrimethylammonium and pentyltrimethylammonium monomers, are the signs of the successful grafting of 3T and 5T monomers on lignin.

Table S4.6. Assignment of the adsorption in FTIR spectra.

Entry	Band position (cm^{-1})	Assignment	References
1	966	methyl group	1,13
2	1032	C-O-C bond illustrating the ether linkages between lignin and cationic/anionic monomer	1,14
3	1140	The C-H stretch of guaiacyl unit	1,15,16
4	1261	The C-O stretch of guaiacyl unit	15,16
5	1140±20	The S=O stretch of the sulfonate group	17-20
6	1481-1466	C-H bending of trimethylammonium group	21,22
7	1750-1711	C=O stretch of ester	23,24
8	3000-2800	C-H stretching vibration of ester	24
9	3400	O-H stretching absorption in the phenolic and aliphatic parts of lignin	1
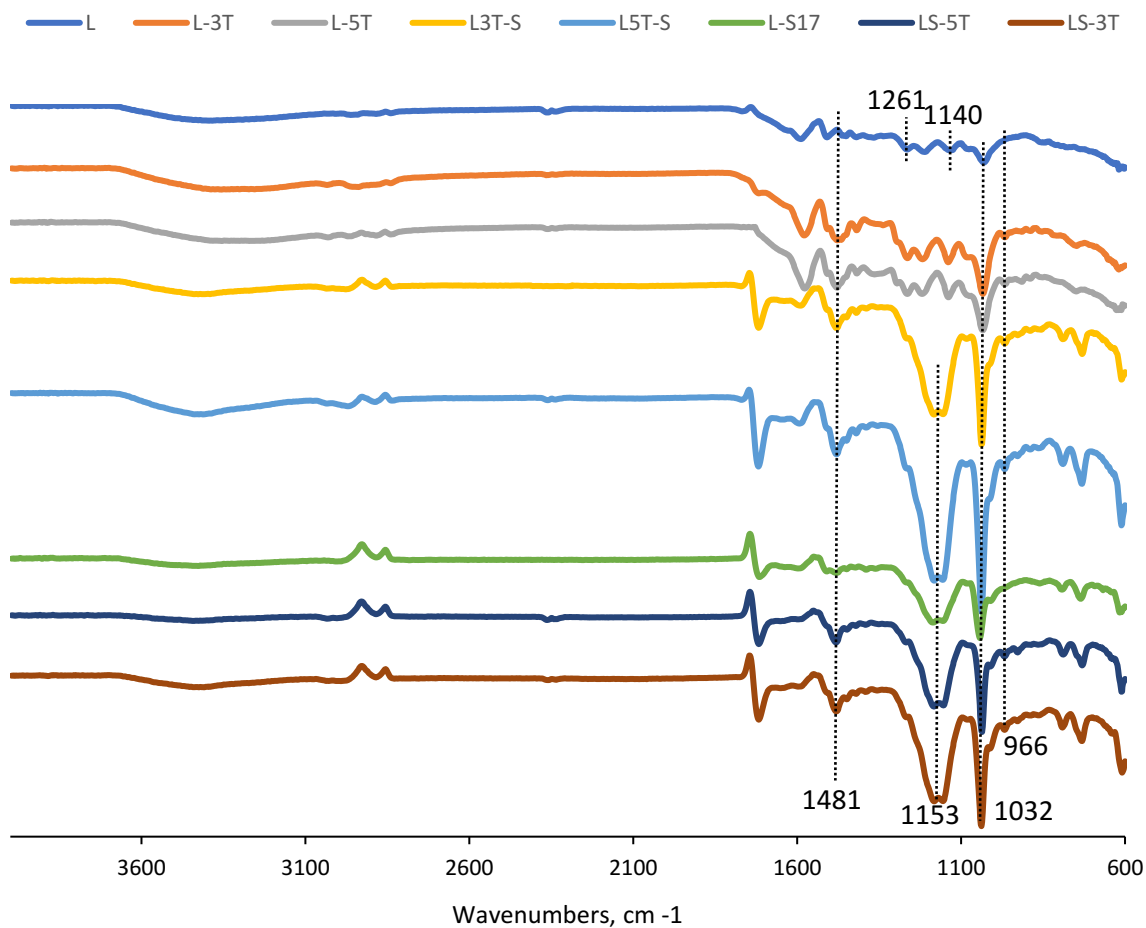
Fig. S4.5. FTIR spectra of lignin and produced amphoteric samples at 25 °C.
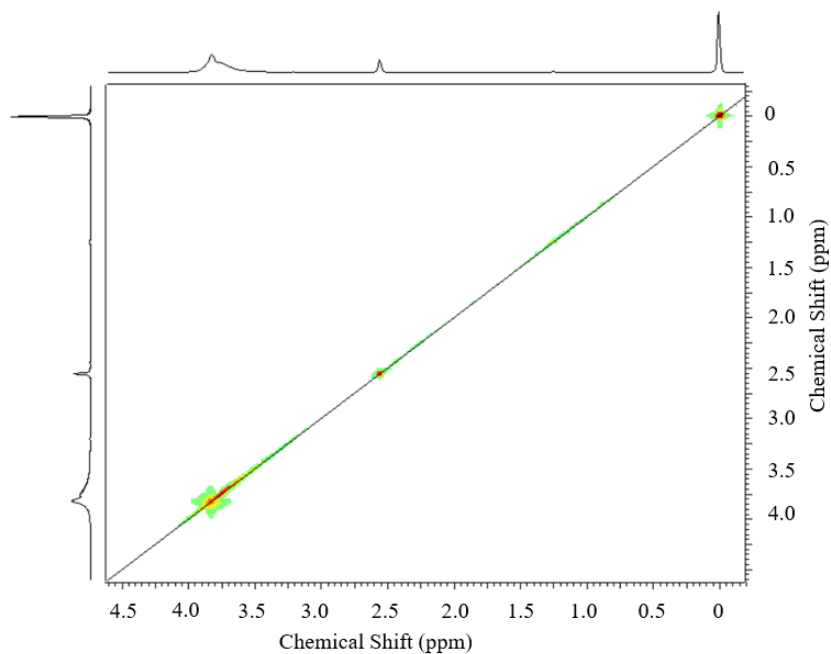
Fig. S4.6. 2D ^{1}H COSY spectroscopy of lignin (L) in DMSO[D$_6$]/D$_2$O.

Table S4.7. Wettability ($\theta_{W/A}$) of different produced polymers.

Samples name	L	L-3T	L-5T	L3T-S[1]	L5T-S[1]	L-S	LS-3T[2]	LS-5T[2]
Contact angle (°)	38 ± 1	28 ± 0.5	32 ± 0.5	<6	6 ± 1	15 ± 1	11 ± 1	12 ± 0.5

[1]: cationization was carried out prior to anionization.

[2]: anionization was carried out prior to cationization.

Adhesion Force
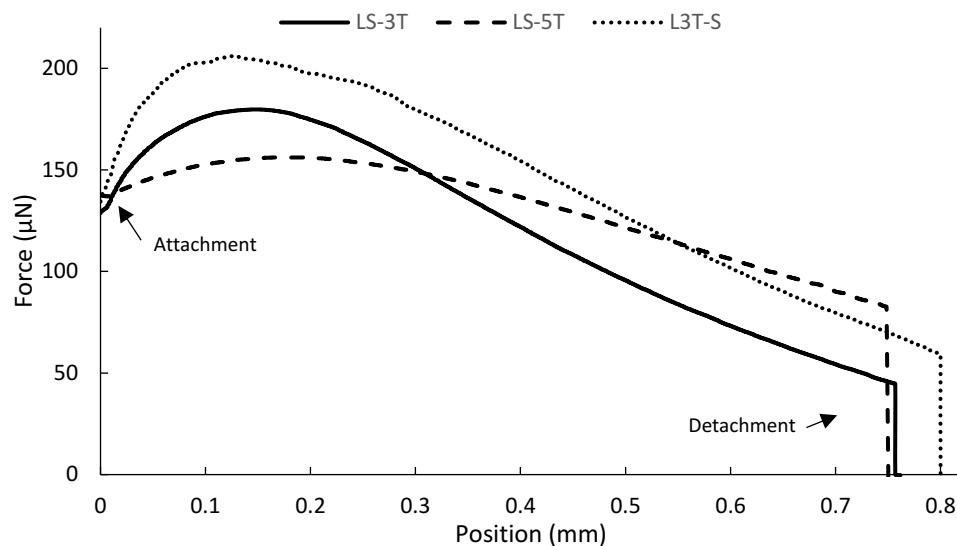
Fig. S4.7. Adhesion force curves between a water droplet and glass coated with amphoteric polymers of LS-3T, LS-5T, and L3T-S in oil medium.

References

1) F. Kong, K. Parhiala, S. Wang and P. Fatehi, Eur. Polym. J., 2015, 67, 335-345.

2) M.J. Sumner, W.L. Harrison, R.M. Weyers, Y.S. Kim, J.E. McGrath, J.S. Riffle and M.H. Brink, J. Membr. Sci., 2004, 239, 199-211.

3) N. Joly, R. Granet, P. Branland, B. Verneuil, P. Krausz, Joly, N., Granet, R., Branland, P., Verneuil and Krausz, P, J. Appl. Polym. Sci., 2005, 97, 1266-1278.

4) S.Y. Lin, 1982 US Pat. 4 332 589.

5) D.K. Setua, M.K. Shukla, V. Nigam, H. Singh and G.N. Mathur, Polym. Compos., 2000, 21, 988-995.

6) K. Bahrpaima and P. Fatehi, ChemSusChem, 2018, 11, 2967-2980.

7) M. Constantin, I. Mihalcea, I. Oanea, V. Harabagiu and G. Fundueanu, Carbohydr. Polym., 2011, 84, 926-932.

8) M.I. Khalil, M.K. Beliakova and A.A. Aly, Carbohydr. Polym. 2001, 46, 217-226.

9) M. Zaman, H. Xiao, F. Chibante and Y. Ni, Carbohydr. Polym. 2012, 89, 163-170.

10) X. Pan, J.F. Kadla, K. Ehara, N. Gilkes and J.N. Saddler, J. Agric. Food Chem., 2006, 54, 5806-5813.

11) B. Sultana, F. Anwar, M. Ashraf, Sultana, B., Anwar, F., and Ashraf, M, Molecules., 2009, 14,

2167-2180.

12) F.M. Abou-Elella and R.F. Mohammed Ali, Biochem. Anal. Biochem., 2014, 3, 1.

13) H. Ruihua, Y. Bingchao, D. Zheng and B. Wang, J. Mater. Sci., 2012, 47, 845-851.

14) A. Casas, M.V. Alonso, M. Oliet, E. Rojo and F. Rodríguez, J. Chem. Technol. Biotechnol.2012, 87, 472-480.

15) N.E. El Mansouri and J. Salvadó, Ind. Crops Prod. 2006, 24, 8-16.

16) S. Zhou, L. Liu, B. Wang, F. Xu and R. Sun, Process Biochem. 2012, 47, 1799-1806.

17) C.A. Barbosa, P.M. Dias, A.M.D.C. and Ferreira, V.R, Appl. Clay Sci., 2005, 28, 147-158.

18) M. Bouraada, M.S. Ouali and L.C. de Menorval, J. Saudi Chem. Soc., 2016, 20, 397-404.

19) A.E. Segneanu, I. Gozescu, A. Dabici, P. Sfirloaga and Z. Szabadai, InTech, 2012.

20) A.E. Hoshoudy, S. Desouky, A. Al-sabagh, M. El-kady, M. Betiha and S. Mahmoud, Int. J. Oil, Gas Coal Eng., 2015, 3, 43-55.

21) S. Sayin and M. Yilmaz, RSC Adv., 2017, 7, 10748-10756.

22) Z. Yang, H. Wu, B. Yuan, M. Huang, H. Yang, A. Li, R. Cheng and Cheng, R, Chem. Eng. J., 2014, 244, 209-217.

23) J. Coates, John Wiley and Sons Ltd, Chichester, 2000.

24) I. Rubinstein, S. Steinberg, Y. Tor, A. Shanzer and J. Sagiv, Nature, 1988, 332, 426.

Chapter 5. Production of reusable porous amphoteric lignin for water desalination

Armin Eraghi Kazzaz, Pedram Fatehi*

Biorefining Research Institute,
Green Processes Research Centre and Chemical Engineering Department,
Lakehead University,
955 Oliver Road,
Thunder Bay, ON P7B5E1, Canada

*Corresponding author

5.1 Abstract

With increasing world population and demand for desalinated water, feasible alternatives are urgently needed to address the global water crisis. In this work, insoluble amphoteric porous lignin (C-CM-AL) was synthesized by grafting carboxymethyl and tertiary amine groups to kraft lignin and then crosslinking the modified lignin by poly(ethylene glycol) diglycidyl ether, which all were confirmed by ^{1}H and ^{1}H-H COSY NMR analysis. The produced C-CM-AL polymer was found to possess the highest adsorption capacity of 1.25, 0.97, 0.71, and 0.62 mmol/g for KCl, NaCl, CaCl$_2$, and MgCl$_2$, respectively. Notably, C-CM-AL settled faster after adsorbing salts in solutions. In addition, by increasing the temperature (to 75 °C), the produced polymer released the adsorbed salts into the water due to the deprotonation and protonation of amine groups and carboxymethyl groups, respectively. The reusability analysis revealed that the C-CM-AL polymer maintained 70-80 % of its adsorption capacity after the 15th round of reusing the polymer. In the binary saline systems, C-CM-AL adsorbed more K$^+$ than Na$^+$ in KCl/NaCl, and more Na$^+$ in both NaCl/CaCl$_2$ and NaCl/MgCl$_2$ solutions. The adsorbed amount of Cl$^-$ on the polymer was higher for divalent salts, which indicates that divalent ions could bond to both cationic sites of the polymer and Cl$^-$. In the multicomponent saline systems, the XPS results revealed that the overall adsorption capacity of the polymer remains unchanged. Overall, the produced lignin-based polymer can be used as a highly efficient and environmentally friendly amphoteric adsorbent for desalination.

Keywords: thermoresponsive polymer, salt removal, amphoteric lignin, porous structure, desalination

5.2 Introduction

Water purification is a global challenge as it directly affects the environment and human health. By the year 2025, about 60% of the global population may suffer from water scarcity.[1] To address the high demand for drinkable or agricultural water, seawater (including oceans and seas) that consists of about 70% of the earth's surface could be a suitable resource.[2] To make the seawater drinkable or suitable for agriculture, the traditional routes of desalination, such as reverse-osmosis and evaporation, could be used.[3,4] These methods, however, need expensive infrastructure and operating investments.[5] Other methods, such as microorganism treatment, were also suggested for wastewater desalination.[6] However, microorganisms themselves could introduce secondary

197

pollution and release biochemicals, such as toxic enzymes, in water.[7] This method also suffers from slow effectiveness (i.e., long required treatment period).

Therefore, the need for a new desalination technology is still in high demand. Ion exchange polymers have found a wide range of applications in biomedical processings, sensors and actuators, non-linear optics,[8] energy storage and conversion,[9,10] and water purification, for instance.[11,12]

Various modifications have been conducted on natural polymers to valorize them.[13-15] Several studies have focused on introducing either anionic or cationic groups onto the natural polymers through chemical modification pathways.[15,16] However, the capability of these polymers is limited for capturing salts since these polymers could separate only anionic or cationic components. The other crucial problem related to anionic or cationic polymers is their high solubility, which complicates their separation from aqueous media after salt adsorption. On the other hand, amphoteric polymers made of lignin, chitosan and poly(vinyl alcohol) with the capability of interacting with both anionic and cationic compounds have been produced to be used in applications such as oil/water separation and composite filters.[18-19] However, they have not been used for desalination purposes.

Lignin is one of the most abundant phenolic polymers with unique potentials, such as renewability, nontoxicity, and biodegradability, which make it attractive to be used in the production of bio-based value-added products, such as adsorbents.[15,16,20-22] Over 50 million tons of lignin per year is estimated to be generated in the pulp and paper industry.[21] However, a large quantity of lignin is burned for generating energy, and only a small portion of the generated lignin is used in producing chemicals or high value-added materials currently.[16,23,24] Indeed, the combination of rich reactive groups, biodegradability, and low cost make lignin a promising candidate to be used as a raw material for producing adsorbents.[20-22] Although there are reports for the use of lignin as an adsorbent for removing color dyes or heavy metals,[25] limited efforts have been made to investigate the application of modified lignin polymers to remove salt from water. To the best of our knowledge, studies related to the generation of amphoteric insoluble lignin derived adsorbent for salts from crosslinking of soluble lignin polymers is limited.

The overall goal of this research is to utilize unique potentials of lignin for producing a tunable amphoteric polymer for separating multiple salts that exist in seawater (e.g., NaCl, KCl, CaCl$_2$, and MgCl$_2$).[26] The focus of this study is on the production of crosslinked amphoteric lignin through

the modification of lignin with grafting anionic and cationic monomers and crosslinking the charged lignin for the first time. Crosslinking would increase the surface area and porosity of lignin derivatives that further boosts the salt adsorption.[27,28] In other words, the produced polymer benefits from not only both anionic and cationic groups but also its crosslinked porous structure, which makes the adsorbent insoluble and thus, facilitating its separation/filtration from the water after the adsorption.

Although different studies have evaluated the adsorption performance of modified polymers, these polymers suffered from one-time usability.[15,29] To make natural-based polymers more industrially attractive, the recyclability and reusability of the produced polymers need to be studied. In this work, a bi-functional lignin derived polymer was produced by grafting anionic (i.e., carboxy) and cationic (i.e., amine) groups, which provide the reusability of the produced polymer, thanks to their thermoresponsive behavior.[30,31]

Herein, the insoluble crosslinked amphoteric lignin-based polymer was produced for the first time, and the performance of the produced polymer for desalination application in various saline systems is monitored as the second novelty. The advantage of using a lignin-based adsorbent for salt removal was discussed. Also, other crucial parameters, such as the reusability of the adsorbent, as well as its sedimentation/separation, were studied and discussed fundamentally, as the third novelty of this work.

5.3 Materials and methods

5.3.1 Materials

In this work, softwood kraft lignin (L) was received from a mill in Alberta, Canada. Sodium chloroacetate (SCA) (98 %), 2-Chloro-N,N-dimethylethylamine hydrochloride (DMA) (99 %), poly(ethylene glycol) diglycidyl ether (PEG) (M_n 500), potassium chloride (KCl) (>99 %), D$_2$O (with the isotopic purity of 99.8 %), magnesium chloride (MgCl$_2$) (≥98 %), 3-trimethylsilyl-(2,2,3,3-D$_4$)-propionic acid sodium salt (TMSP) (99.8 %), sodium hydroxide (99.0 %), sodium chloride (NaCl) (>99 %), hydrochloric acid (37 %), calcium chloride (CaCl$_2$) (≥99.9 %), methanol (99.8 %), dimethyl sulfoxide-d6 ([D$_6$]DMSO)(99.9 %), and cellulose acetate filters with a pore size of 0.2 μm were all obtained from Sigma-Aldrich Company. Dialysis membrane with the molecular weight cut-off of 1,000 g/mol was supplied from Thermo Fisher Scientific Inc., USA. All of the chemicals utilized in this work were of analytical grades.

5.3.2 Carboxymethylated lignin

Lignin (L) was carboxymethylated with sodium chloroacetate (SCA) based on the methodology described in a previous study.[13,32] Briefly, the reaction was conducted at a molar ratio of 2 SCA/L, 2 M NaOH, at 60 °C for 3 h. The produced polymer was precipitated by methanol and centrifuged at 3500 rpm for 10 min and then purified using membrane dialysis for three days. Produced carboxymethylated samples were freeze-dried and denoted as CML in this work.

5.3.3 Aminated lignin

Aminated lignin (AL) was prepared using 2-Chloro-N,N-dimethylethylamine hydrochloride (DMA). Lignin, L, was pretreated with NaOH (2 M) at pH 10.5 for 0.5 h to activate the hydroxy groups of lignin for the DMA grafting. Then, the reaction was conducted at a molar ratio of 2.5 DMA/L at 80 °C for 3 h. The produced sample was purified by methanol and centrifuged at 3500 rpm for 10 min. Membrane dialysis was used to further purify the sample for three days. The produced sample was freeze-dried and stored for further use.

5.3.4 Crosslinking reaction

The produced CML and AL samples were crosslinked by poly(ethylene glycol) diglycidyl ether (PEG). This reaction was carried out via adding the same mass of CML and AL into a 250 mL three-neck glass. The pH of the mixture was adjusted to 11.0 using NaOH (2 M) and left for stirring at 30 °C for 30 min. Then, PEG was added dropwise into the solution with a molar ratio of 0.5-3.0 PEG/(AL+CML) and reacted for 1-5 h. After the reaction, the mixture was centrifuged at 3500 rpm for 10 min, dialyzed by the membrane for 3 days, and freeze-dried.[33] According to its higher reaction yield, the produced crosslinked polymer (denoted as C-CM-AL) with a molar ratio of 2.0 PEG/(AL+CML), which reacted for 3 h was selected to be used in this study.

In another sets of reactions, L, CML, and AL were crosslinked with the PEG and considered as control samples. The reaction and purification were carried out following the same procedure described for C-CM-AL. The produced samples were freeze-dried and denoted as C-L, C-CML, and C-AL.

5.3.5 Solubility experiments

The solubility experiments were conducted by dissolving 5 g (M_1) of L, CML, AL, and CM-AL in 50 mL of pure water (100 g/L) and then stirred at 150 rpm for 24 h at 25 °C. The samples were then filtered using cellulose acetate filters (0.2 μm) allowing separation of the undissolved lignin from water.[34] The insoluble phase was left in the oven at 105 °C to reach constant weight (M_2).

The solubility yield was calculated based on the difference in the mass through equation 5.1.[35] The measurement was performed triplet and the mean value was reported.

Solubility yield (%) $= \frac{M_1 - M_2}{M_1} \times 100$ (5.1)

5.3.6 ^{1}H NMR, and ^{1}H-H COSY spectroscopy

The chemical structure of L, CML, AL, and C-CM-AL was analyzed by ^{1}H NMR (INOVA-500 MHz instrument, Varian, USA) using the spectroscopy with 32 scans in 128 increments. Samples were dissolved in D_2O or $[D_6]DMSO/D_2O$ (9:1 v/v) and stirred until fully dissolved (i.e., for 12 h). Trimethylsilyl propionic acid (TMSP) was used as the internal standard.[17,32] The detail of this experiment is available in the supporting information file. The ^{1}H-H COSY analysis of L, CML, AL, and C-CM-AL was carried out using the same instrument, solvent, and internal standard utilized for ^{1}H NMR.

5.3.7 Gel permeation chromatography (GPC)

The molecular weight of L, CML, AL, and C-CM-AL polymers was measured by a gel permeation chromatography, GPC, Malvern GPCmax VE2001 with multi-detectors (UV, RI, viscometer, low angle, and right-angle laser detectors).[17,36] More information about this experiment is available in the supporting information file.

5.3.8 Elemental analysis

The elemental analysis of the macromolecules was performed using an elemental analyzer (Vario EL Cube, Elemental Analyzer, Germany) as described in detail elsewhere.[37] The degree of substitution (DS) was then calculated based on the nitrogen content of the polymers. Further information about calculating the degree of substitution is available in the supporting information file.

5.3.9 Carboxylate group analysis

Carboxylate group analysis was performed by using an aqueous potentiometric titration instrument (Metrohm, 905 Titrado, Switzerland).[38] Based on the total carboxylate group content, the degree of substitution for this group was calculated. More details about this analysis can be found in the supporting information file.

5.3.10 Charge density analysis

The charge density of soluble samples was determined by using a Particle Charge Detector (PCD 04, BTG Mütek GmbH) with a 0.005 mol/L PVSK or PDADMAC solution as the titrant.[39] For insoluble polymers, the back-titration method was used to measure the charge density.[40]

5.3.11 Surface area analysis

The specific surface area (S_{BET}) of the samples were determined following the Brunauer-Emmett-Teller (BET) method by NOVA 2200e (Quantachrome Instruments) in the N_2 adsorption isotherm relative pressure range of $p/p_0 = 0.01$-0.99. Assuming their spherical shapes, the average pore size (d_p) of the samples was determined ($d_p = 4V_p/S_{BET}$). The total pore volume (V_p) was determined at $p/p_0 = 0.99$. The samples were degassed in a vacuum at 373 K for 12 h before conducting the measurement.[29,39,40]

5.3.12 Thermogravimetric analysis (TGA)

The thermal stability analysis of L, CML, AL, and C-CM-AL was assessed using a thermogravimetric analyzer, (TGA, i-1000 series, Instrument Specialist Inc.) as described elsewhere.[32] In this analysis, 7.5 mg of samples were heated from room temperature to 800 °C at the rate of 10 °C/min in nitrogen atmosphere at the flow rate of 35 mL/min.

5.3.13 Differential scanning calorimetry (DSC) analysis

To measure the Tg of the CML, L, AL, and C-CM-AL polymers, a modulated differential scanning calorimetry (MDSC), TA instrument (Q2000 DSC), was employed and the experiment was carried out as follows: equilibrate at 20 °C; modulate ± 0.64 °C every 40 seconds; isothermal for 5 min; ramp 3 °C/min to 220 °C; isothermal for 2 min; ramp 10 °C/min to 20 °C; isothermal for 2 min; ramp 3 °C/min to 220 °C; equilibrate at 40 °C. The analysis was conducted in the second round of heating.

5.3.14 Scanning electron microscopy

Scanning electron microscopy (SEM) analysis was conducted on the L and C-CM-AL samples using a Hitachi SU-70 (Hitachi Ltd., Japan) microscope at 15 kV voltage.[39] The samples were gold-coated before SEM analysis. The SEM image of C-CM-AL polymer was analyzed for circularity factor with ImageJ, version 1.53av.[42]

5.3.15 Adsorption

The adsorption of ions from NaCl, KCl, $CaCl_2$, and $MgCl_2$ aqueous environment onto C-CM-AL polymer was analyzed as a function of the polymer dosage. In this experiment, C-CM-AL with varied concentrations (10-200 g/L) were added to solutions containing different concentrations of salt (0.5-20 g/L), and the system was incubated for 1-2 h at 25 °C and 150 rpm. The adsorption kinetics was tested by mixing 1 g/L of mentioned salt solutions with 100 g/L of C-CM-AL polymer for 15 min to 4 h at 25 °C and 150 rpm. Also, to determine the best adsorption temperature, 1 g/L of different salt solutions were mixed with 100 g/L of C-CM-AL polymer for 2 h at 15-75 °C and 150 rpm.

Conductivity test was used to measure the salt concentration of the solution before and after the adsorption tests.[43-45] The calibration curve for the conductivity of the solution as a function of concentration was determined.[46] After conducting different adsorption experiments, the samples were centrifuged at 1000 rpm for 5 min to separate coagulated particles from the solution. The collected solutions were then tested for their conductivity. The conductivity of each salt solution was measured before and after adsorption with a conductivity meter (Orion Star A212, Thermo Scientific). The conductivity of pure water was determined to be below 1 µS/cm at 25 °C. The adsorption amount was then determined following equation 5.2:[47]

$$\text{Adsorption amount (mmol/g)} = \frac{VC}{M_w \times W} \quad (5.2)$$

where V (L) is the relevant salt solution volume, C (mg/L) is the concentration difference of salt before and after its adsorption, M_w (g/mol) is the salt molecular weight, and W (g) is the used C-CM-AL weight.

5.3.16 Desorption

The desorption of salts from C-CM-AL polymer was assessed by adding deionized water to the salt-loaded C-CM-AL polymer (2 mL/g). The sample was then incubated at different temperatures ranging 35-85 °C for 1 h and 150 rpm. Then, the C-CM-AL polymer was separated from the aqueous solution via centrifugation as stated above. The conductivity of the solution was measured to determine the concentration of salts in the solution before and after this experiment.

5.3.17 Sedimentation analysis

The sedimentation behavior of the C-CM-AL polymer in the absence or presence of salt was determined using the vertical scan analyzer (Turbiscan Lab Expert, Formulaction, France). In this experiment, 100 g/L of C-CM-AL was added to different salt solutions (1 g/L concentration) and stirred for 2 h at 25 °C and 150 rpm. Afterward, the samples were analyzed for their settlement. More information about this analysis could be found in the literature.[37,48] Upon submission of each sample to the instrument in cylindrical cells, an electroluminescent diode light with a wavelength of 880 nm scanned the cell from the bottom to the top with 40 µm height intervals. The scanning was conducted every 5 s and the experiment lasted for 30 min. In this experiment, a backscattering detector received light backscattered by the sample at 45° from the incident, and a transmission detector received light transmitted through the sample at 180° from the incident light. The data was collected as a function of the height of the sample and used for indicating the settling efficiency, settling velocity and sediment thickness.[39,40,48]

The Turbiscan Stability Index (TSI) was quantitively determined by following equation 5.3:[49]

$$TSI = \sqrt{\frac{\sum_{i-1}^{n}(x_i - x_{bs})^2}{n-1}} \quad (5.3)$$

where x_i, x_{bs}, and n refer to the average of the backscattered light intensity at the scanning time, average of x_i, and number of scans, respectively. In General, the lower the TSI, the higher the stability.[49]

The volume fraction of the C-CM-AL samples treated with salt was defined by gathering samples from the top part of the cell just after the C-CM-AL addition and after 30 min of settling. The collected samples were dried at 105 °C for 12 h to determine the concentration of the particles in the solution, which were then used to calculate the mass of the settled C-CM-AL sample. Considering this mass, the compactness (mass/volume) and the thickness of the sediment was determined for settled C-CM-AL sample.[40]

5.3.18 X-ray photoelectron spectroscopy (XPS)

The competitive adsorption of multi-salt solution (KCl, NaCl, $CaCl_2$, and $MgCl_2$) was studied by measuring the atomic concentration of adsorbed multi-salt components on the C-CM-AL polymer using X-ray photoelectron spectroscopy (XPS). The same amount of C-CM-AL polymer (100 g/L) and salt (1 g/L), and treatment period (2h) and temperature (25 °C) were considered in this adsorption analysis. Desorption results were conducted by treating the adsorbed C-CM-AL polymers at 75 °C for 1h. To define if any salt ions were detached from C-CM-AL after the 15th round of adsorption and desorption, the atomic concentration of the first and last rounds were compared by using this analysis. The XPS used in this analysis was a Kratos Axis Supra with a monochromatic Al Kα radiation (1486.6 eV) with 1mm spot diameter at a base pressure of about 3×10^{-10} mbar and 20 eV pass energy. Based on the surface plane, the take-off angle for the detected photoelectrons was adjusted at 60°. For energy referencing, spectra were calibrated to the C1 line peak at 284.6 eV.[50] Data analysis and peak fitting were performed using ESCApe software (V1.2.0.1325).

5.4 Results & Discussion

5.4.1 ^{1}H NMR, and ^{1}H-H COSY spectroscopy

Figure 5.1a indicates the ^{1}H NMR spectroscopy of produced C-CM-AL polymers. More information about ^{1}H NMR spectroscopy of AL and CML can be found in the supporting information in Figure S5.1. The peak appearing at 0.0, 2.5, 4.7 ppm are assigned to TMSP (3-trimethylsilyl-(2,2,3,3-D4)-propionic acid sodium salt), DMSO-d6, and D_2O, respectively.[51,52] The

spectrum of unmodified lignin (L) indicates the peak at 3.3-1.75 ppm, which is assigned to the aliphatic group of lignin, and the peak at 3.6-3.2 ppm is assigned to methylene protons in the β-β structure. The peak at 4.5-3.05 ppm is related to the proton of the methoxy group of lignin and the peak at 7.42-5.99 ppm is attributed to aromatic protons. The peak at 8.5 ppm is related to the unsubstituted phenolic protons of lignin (Figure 5.1a).

The successful conversion of lignin into crosslinked carboxymethylated-aminated lignin was confirmed by the appearance of new peaks in Figure 5.1a. The peak at 2.97 ppm corresponds to dimethylamine (-N(CH$_3$)$_2$) of the cationic group. The overlap peak at 3.4-4.0 ppm assigned to the methylene group connected to the ammonium group, carboxymethyl groups (anionic group), and PEG (-CH$_2$-OH, -CH$_2$-O-CH$_2$-) (crosslinked group).[32,53,54]

Due to the overlap among the methylene group of cationic, anionic, and crosslinked groups in the ^{1}H-NMR spectrum, the ^{1}H-H COSY NMR spectroscopy of produced C-CM-AL was obtained (Figure 5.1b). The ^{1}H-H COSY of L (prior to functionalization), AL, and CML can be found in the supporting information (Figure S5.2). The peak of DMSO was illustrated at F1=F2=2.5 ppm (Figure 5.1b). Four peaks at {F1=3.59, F2=3.59}, {F1=3.59, F2=3.97}, F1=F2=3.59, and F1=F2=3.97 ppm correspond to the methylene group connected to the diamine group (cationic monomer). The peaks at F1=F2=3.80, F1=F2=2.97, and F1=F2=3.41 ppm demonstrate that the methylene group is attached to the carboxymethyl group, ammonium group, and PEG. The ^{1}H-H COSY separates the overlapped peaks in ^{1}H-NMR by revealing distinct peaks and confirms the existence of dimethylamine (cationic), carboxymethyl (anionic), and PEG (crosslinked) groups in the produced amphoteric C-CM-AL polymer (Figure 5.1c).

R= H or OCH₃
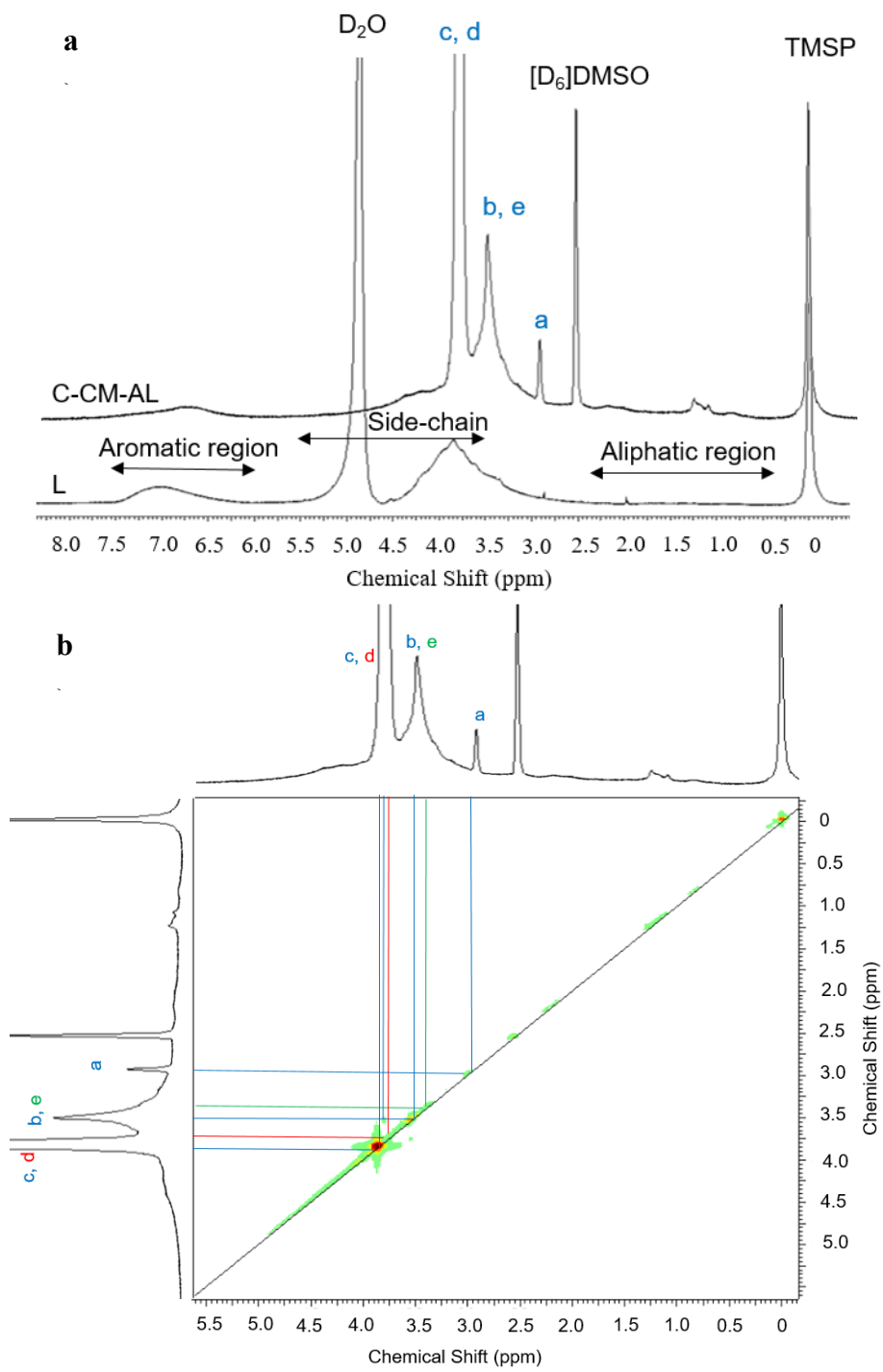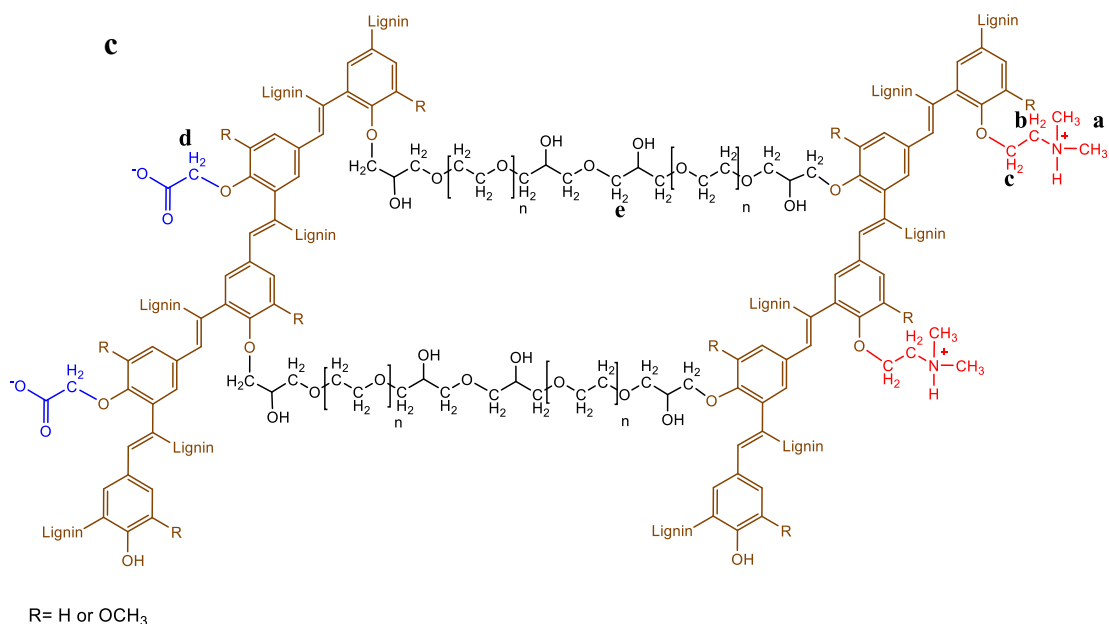
Figure 5.1. a) ¹H NMR, b) ¹H-H COSY spectra, and c) proposed structure of L and C-CM-AL in D₂O at 25 °C.

5.4.2 Characterization of produced polymers

The properties of polymers are presented in Table 5.1. Softwood kraft lignin (L) had a molecular weight of 18,030 g/mol and no traceable nitrogen (based on elemental analysis). The molecular weight of kraft lignin was reported to be <25,000 g/mol in the literature.[37,55] The titration method indicates 0.15 mmol/g of COOH group attached to L. Carboxymethylated lignin (CML) had the carboxylate content of 2.18 mmol/g with a molecular weight of 68,500 g/mol. The aminated lignin (AL) had the nitrogen content of 2.66 wt. % and molecular weight of 62,680 g/mol. The crosslinked carboxymethylated-aminated lignin (C-CM-AL) had the COOH degree of substitution of 0.39 mol/mol and 0.40 mol/mol for aminate and carboxylate groups, respectively. To identify the impact of crosslinking on carboxylate groups of CML and amine groups of AL, the content of carboxylate group and charge density of CML and C-CML, as well as the amine group content and the charge density of AL with C-AL were compared, and the result presented in Table S5.1 (supporting information). It is seen that the carboxylate group, amine group, and charge density of CML and AL did not change after crosslinking (i.e., C-CML generation). The overall reaction yield for produced polymers was 52, 55, and 43 % for CML, AL, and C-CM-AL, respectively. The lower yield of C-CM-AL than other lignin derivatives (CML, and AL) could be attributed to the less available hydroxy groups after carboxymethylation and amination of lignin for the crosslinking reaction.[16,17]

Table 5.1. Chemical properties of produced polymers.

Samples name	L	CML	AL	C-CM-AL
Nitrogen content[1] (wt. %)	<0.09[2]	<0.09[2]	2.66	1.98
COOH content[1] (mmol/g)	0.15	2.18	-	2.04
Charge density[1] (meq/g)	-1.31	-2.35	2.19	-
Nitrogen content degree of substitution (mol/mol)	<0.09[2]	<0.09[2]	0.39	0.39
COOH content degree of substitution (mol/mol)	-	0.43	-	0.40
M_w, (g/mol)	18,030	68,500	62,680	n.d.[3]
Reaction yield (%)	100	52	55	43
Solubility yield (%)	23	66	58	5
S_{BET} (m²/g)	1.7	-	-	771.2
d_p (nm)	18.1	-	-	17.8
V_p (cm³/g)	0.01	-	-	0.68

[1] Error was <0.05 %
[2] Method sensitivity <0.09
[3] Not detected

After crosslinking the produced CML and AL polymers, the bi-functional crosslinked C-CM-AL polymer was found to be insoluble in water. The BET surface area of L and C-CM-AL was calculated over a relative pressure (p/p_0) and found to be 1.7, and 771.2 m²/g, respectively.[29,56] As seen, the surface area was larger for C-CM-AL than L, which reflects the success of crosslinking. In the meantime, the average pore size of the materials was calculated using the density functional theory.[58] The average pore size (d_p) of C-CM-AL and L was in the range of 17.8-18.1 nm suggesting the presence of a mesoporous structure.[29] Moreover, C-CM-AL indicated a much larger total pore volume (V_p) (0.68 cm³/g) than L (0.01 cm³/g). The successful crosslinking of C-CM-AL increased the BET surface area and total pore volume, which would be beneficial for the adsorption of salts from aqueous solution using this polymer.

SEM micrographs showed that L had a smooth surface (Figures 5.2a, b, and c), whereas C-CM-AL contained a considerable porous surface (Figures 5.2d, e, and f). This is attributed to the grafting of crosslinked PEG which intensified the branched structure of lignin and improved the surface area of C-CM-AL.
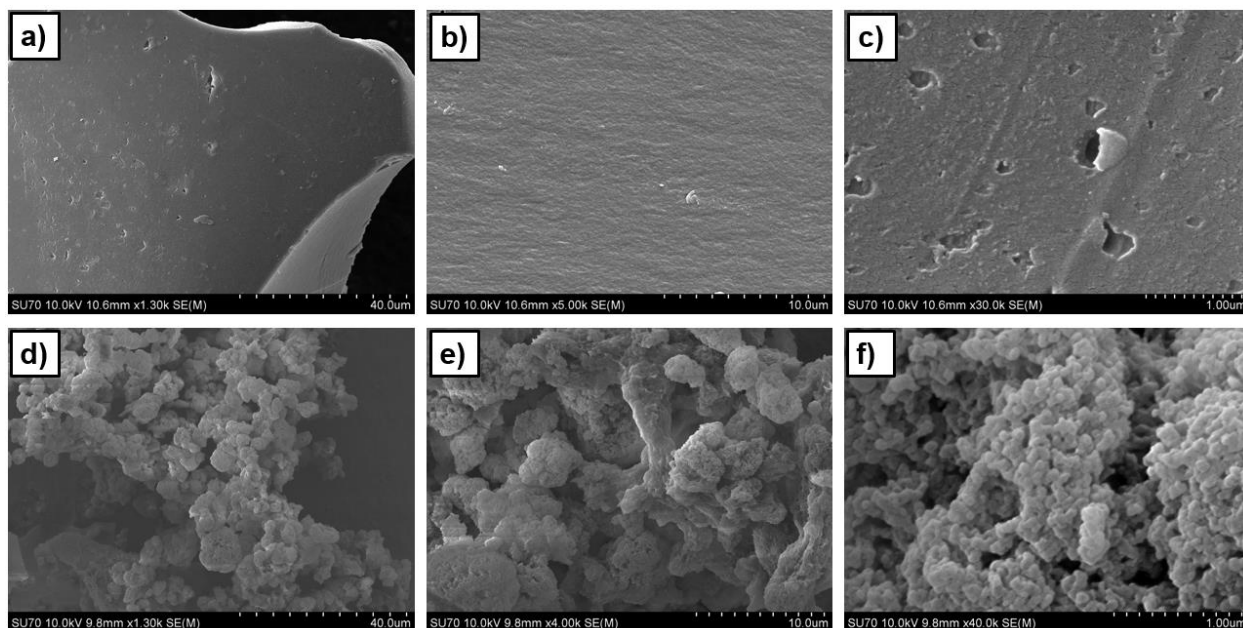
Figure 5.2. SEM images of a, b, and c) unmodified lignin (L), and c, d, and f) produced amphoteric crosslinked C-CM-AL polymer, with different scale bare of a, d) 40 μm, b, e) 10 μm, and c, f) 1 μm.

5.4.3 TGA and DSC analyses

The effect of chemical modifications on the thermal behavior of crosslinked bi-function lignin-based polymer of C-CM-AL was conducted using TGA, dTGA (differentiate thermogravimetric analysis) and DSC, and the results were compared with that of L, CML, and AL polymers. The detailed discussion Figures S5.3 are presented in the supplementary material. The thermal degradation occurred around 250-500 °C is attributed to the carboxy, amine, and methyl groups attached to the lignin backbone,[32,58] which indicates the successful grafting of the above-mentioned groups on lignin and C-CM-AL.[59,60] In addition, the graphs related to the modulated differential scanning calorimetry (MDSC) conducted for all samples are displayed in Figure S5.4. It was observed that the Tg point did not change significantly by the modifications, which reveals that the lignin backbone was remained intact.[61]

5.4.4 Adsorption kinetics

The adsorption of salts to the amphoteric C-AM-AL polymer was studied under different conditions (Figure 5.3). Based on the information provided in Tables S5.2 and S5.3, which reveal the salinity level of different water sources, as well as the composition of seawater salt, KCl, NaCl, $CaCl_2$, and $MgCl_2$, were chosen to be analyzed for their adsorption in this study.[6,12,26,47] Figure 5.3a shows the adsorption of different monovalent and divalent salts at different C-CM-AL

concentration. The results reveal that, by increasing the concentration of C-CM-AL polymer, the adsorption of all four salts was increased upon increasing the polymer concentration to 100 g/mol (Figure 5.3a). The salt adsorption was reduced when the polymer was concentrated more in the solution. This could be due to the aggregation of the polymer at a high C-CM-AL concentration, which diminished the total surface area of the polymer for adsorption.[62,53] The adsorption kinetic of amphoteric C-CM-AL is demonstrated in Figure 5.3b. The results indicate that a period of two hours is required to attain adsorption equilibrium. While, electrostatic interaction is considered a fast adsorption mechanism, the diffusion of salts into the porous structure of C-CM-AL could be more time-consuming.

Figure 5.3C shows the effect of temperature on the salt adsorption on the C-CM-AL polymer. The highest adsorption amount was obtained when the temperature of the solution was at 25 °C. As stated earlier, the produced amphoteric C-CM-AL contains both carboxy and amine groups, which could adsorb both cations and anions. The carboxy and tertiary amine groups exist in their deprotonated (COO^-) and protonated form (R_3NH^+), respectively, when the temperature is below 30 °C.[30,31] The reason for this behavior is related to the pKa of carboxy and tertiary amine groups. The pKa for the carboxy group lowers, while the pKa of the tertiary amine group increases, when the temperature drops to below 30 °C.[30,31,64] This further enhances the adsorption capacity of the amphoteric polymer for the salt adsorption. Conversely, when the temperature increases, the amphoteric C-CM-AL polymer loses its charges due to the protonation and deprotonation of carboxy ($COOH$) and tertiary amine groups (R_3N), respectively. [30,31,47,64] Thus, the charge interaction of the cation and anion sites in this polymer causes a reduction in the adsorption amount for both anions and cations from the solution.

Based on the results, the treatment conditions of 100 g/L of C-CM-AL concentration, 2h, and 25 °C were selected for the adsorption analysis.
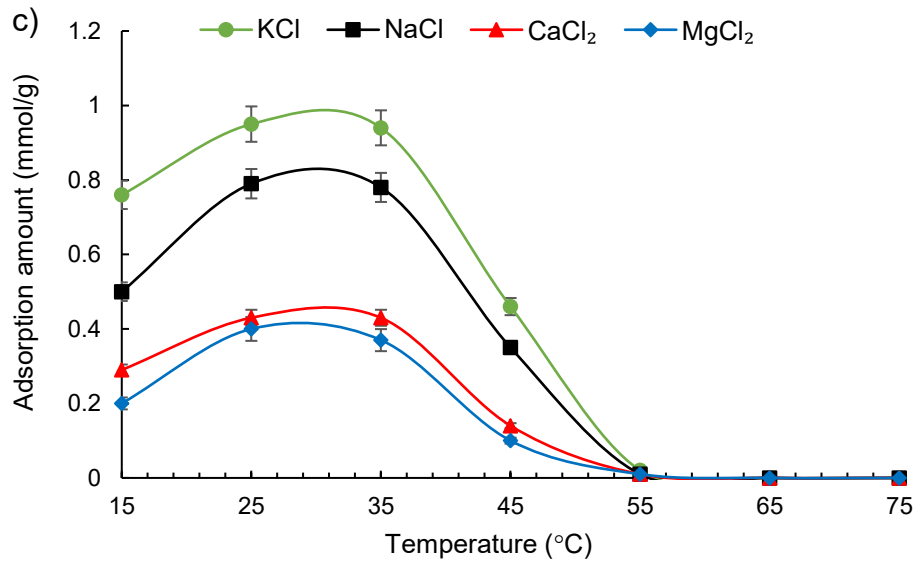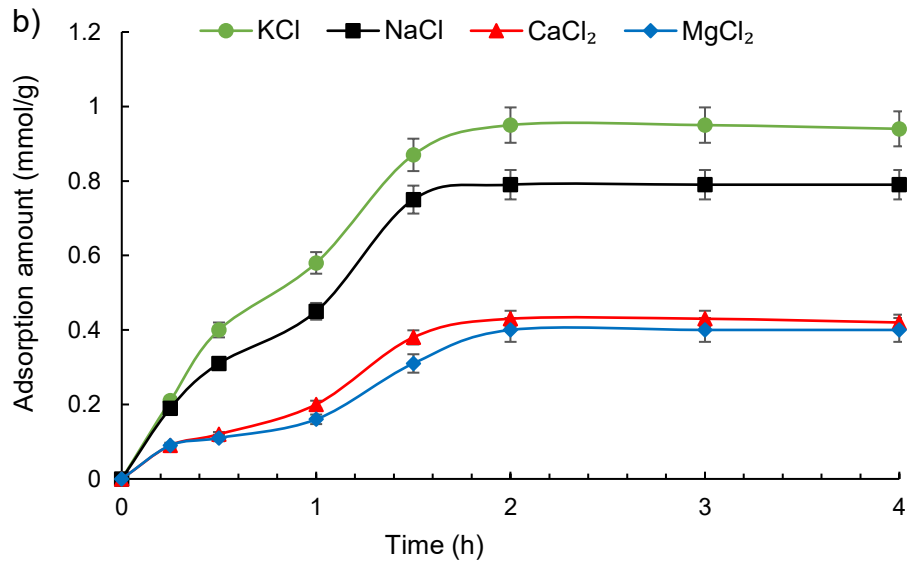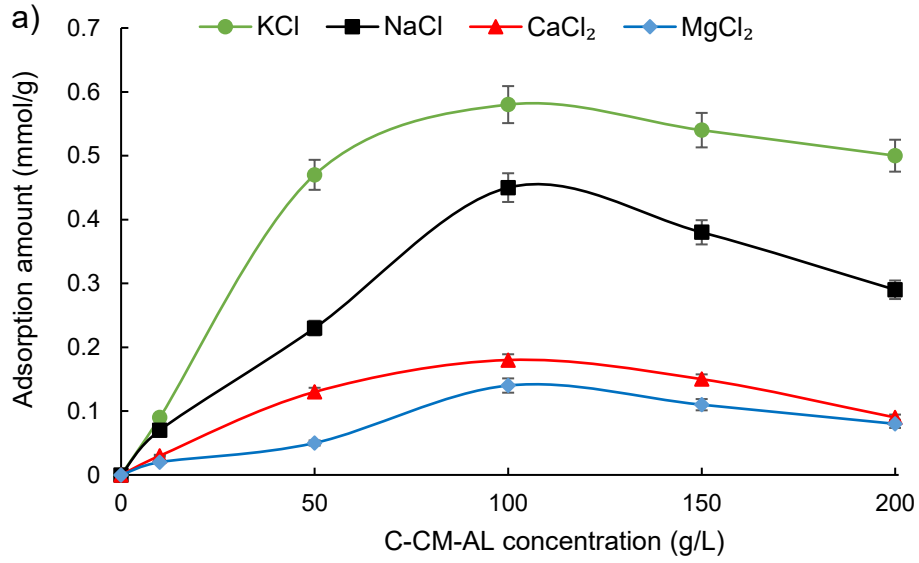
Figure 5.3. Salt adsorption of on C-CM-AL with respect to a) polymer concentration (1 g/L salt, 1 h, and 25 °C), b) time (1 g/L salt, 100 g/L C-CM-AL, and 25 °C), and c) temperature (1 g/L salt, 100 g/L C-CM-AL, and 2 h).

Moreover, the adsorption performance of produced control samples of C-L, C-CML, and C-AL polymers were analyzed under the same conditions (Figure 5.4). The results indicate that all these control samples have much lower adsorption capacity (Figure 5.4) compared to amphoteric C-CM-AL polymer. The crosslinked lignin (C-L), crosslinked anionic lignin (C-CML), and crosslinked cationic lignin (C-AL) polymers demonstrated the maximum adsorption capacity of 0.05, 0.1, and 0.11 mmol/g, respectively.

The adsorption of the monovalent salts on all of the mentioned polymers was observed to be higher than the divalent ones. Also, by comparing the results obtained from the crosslinked bi-functional polymer (C-CM-AL) (Figure 5.3) with control samples (C-L, C-CML, and C-AL), it can be concluded that the crosslinked and multi charge structure of the C-CM-AL polymer yields a high adsorption capacity for this polymer compared to others. This implies the successful application of C-CM-AL for salt adsorption and desalination.
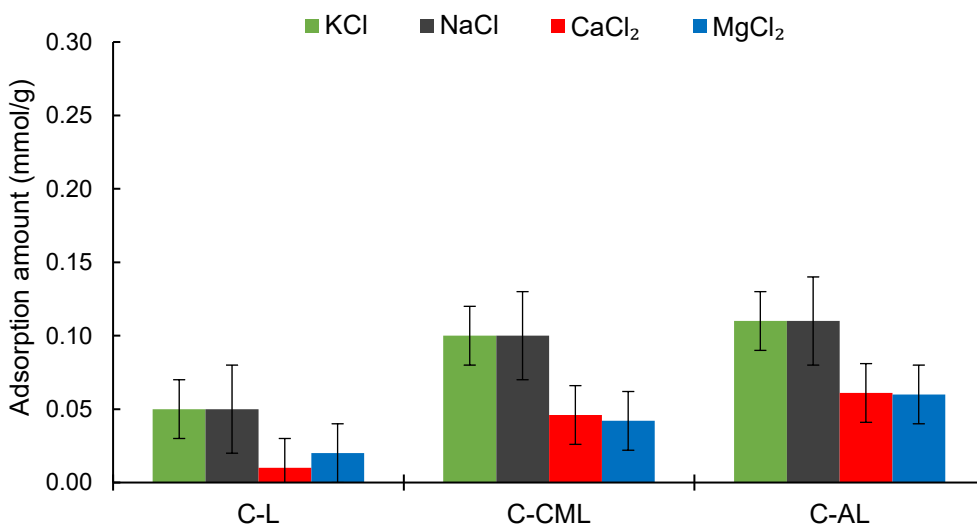
Figure 5.4. Salt adsorption of C-L, C-CML-, and C-AL polymers as control samples at 1 g/L salt, 100 g/L polymers, 2 h, at 25 °C.

5.4.5 Adsorption analysis under different salt concentrations
Figure 5.5a demonstrates the adsorption of C-CM-AL at different salt concentrations. As seen, the salt adsorption on the C-CM-AL is dependent on the salt concentration. Upon increasing the salt dosage, the adsorption amount of C-CM-AL was enhanced and reached equilibrium at 10 g/L

concentration for KCl, and NaCl and at 15 g/L concentration for $CaCl_2$, and $MgCl_2$. The equilibrium adsorption amount for KCl, NaCl, $CaCl_2$, and $MgCl_2$ was 1.25, 0.97, 0.71, and 0.62 mmol/g. The lower adsorption of the divalent salts than that of the monovalent ones could be related to their hydrated radius in solution (Table S5.4).[65,66] Since K^+ and Na^+ are smaller, they could more easily reach the pores and voids of C-CM-AL polymer, and thus fill them at a lower concentration (10 g/L). However, Mg^{2+}, and Ca^{2+}, by having a higher hydrated radius, would have more difficulties in reaching the pores of the polymer. At a higher concentration (15 g/L), they had stronger driving force (i.e., concentration gradient between the bulk and pores of polymers) for diffusing the pores of C-CM-AL even though they could reach a saturation level that was similar to that of monovalent salts.

By considering the carboxy (2.04 mmol/g) and tertiary amine group contents (1.41 mmol/g) (Table 5.1), and the highest salt adsorption amount (1.25 mmol/g) (Figure 5a), it could be revealed that the adsorption amount of salt was lower than the total cationic and anionic content (about 2.45 mmol/g). This could convey that not all adsorption sites are accessible to ions which could be due to (i) salts clogging the structure of the polymer, and/or (ii) nonstoichiometrical interaction of salts and charged groups of C-CM-AL and/or (iii) the charge-charge interaction of the cationic groups with the anionic ones.[67-69]

Ionic characteristics such as hydrated radius, ionic radius, and hydration free energy (presented in Table S5.4) were discussed in relation to the ability of ions to transfer through the crosslinked structure of C-CM-AL. Generally, the larger the hydrated radius, the farther the cationic center of charge would be from the surface, which leads to a weaker electrostatic interaction of the solid-cation. The hydration free energy includes the hydrated ion's stability in relation to the stability of its unhydrated form. This energy is exothermic as it includes weak bonding between the ions and the water molecules forming a hydration shell. Energy is released when the bonding occurs. Thus, energy is required to remove water molecules existed in the hydration shell. Also, a lower hydration free energy leads to ions diminish the number of water molecules that exist in their hydration shells, and thus, a higher likelihood to permeate.[70] By comparing the adsorption of monovalent and divalent ions (Figure 5.5a), it is seen that the adsorption sequence was KCl> NaCl> $CaCl_2$> $MgCl_2$. Although the ionic radius is K^+> Na^+> Ca^{2+}> Mg^{2+} (Table S5.4), the hydrated radius and absolute Gibbs free energy of hydration are Mg^{2+}> Ca^{2+}> Na^+> K^+ (Table

S5.4).[65,66] Thus, the higher adsorption of K^+ over Na^+ and Ca^{2+} over Mg^{2+} would be due to the easier penetration of these ions into the pores.

Another reason for such behavior could be related to the monovalent or divalent charges of ions (Figure 5.5b). Divalent ions (Mg^{2+}, Ca^2) have higher charge compared to monovalent ones (Na^+, K^+).[71] These charges interact with more available adsorption sites (COO^-) of the polymer and hinders the interaction of polymer's functional groups with the remaining divalent ions (Figure 5.5b (i)). Moreover, the divalent ion bond to the polymer would still have the ability to interact with another ion (Figure 5.5b (ii)) which could possibly fill the voids with fewer cations and reduce the overall salt adsorption.[72,73]
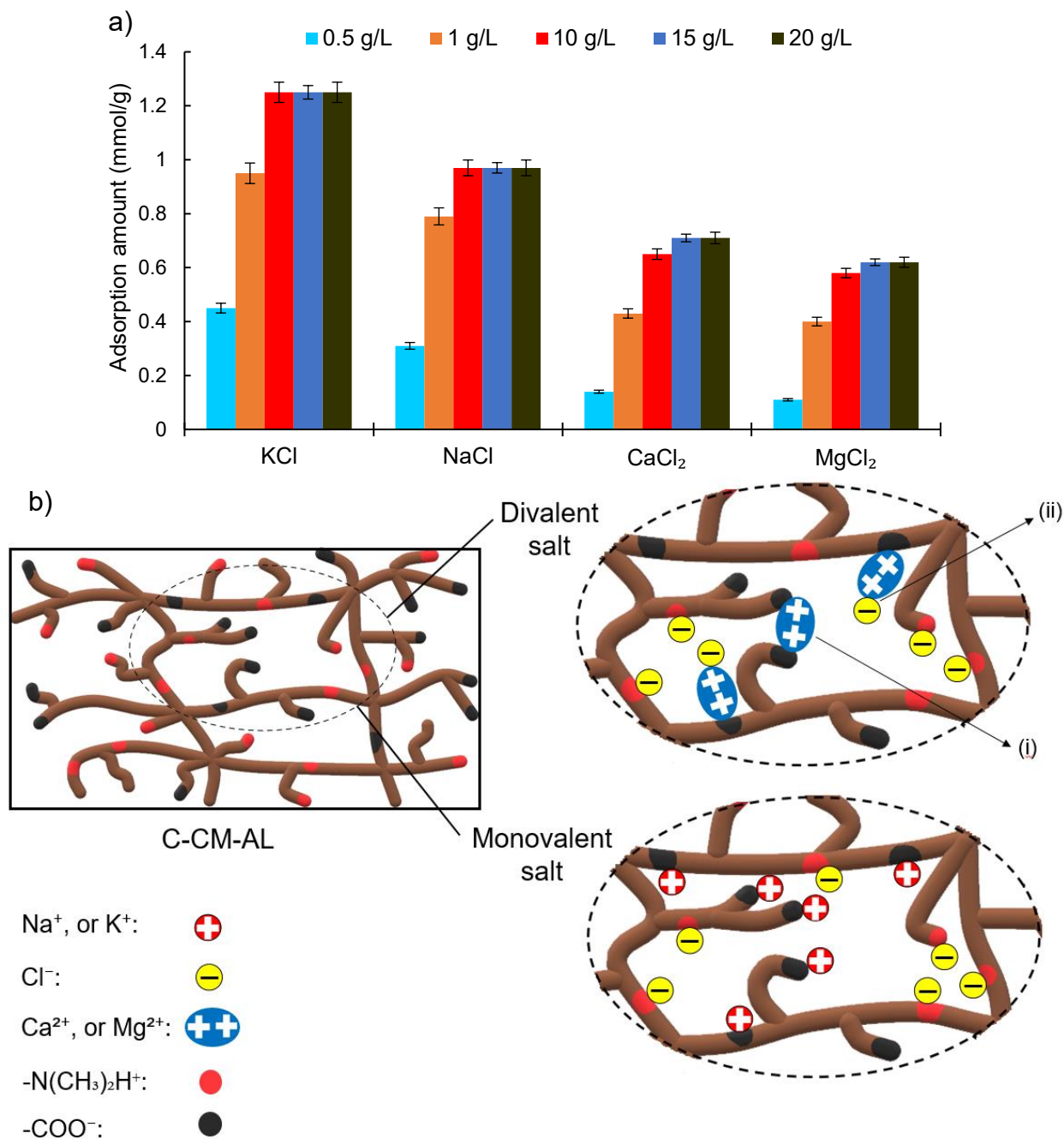
Figure 5.5. a) Salt adsorption of amphoteric C-CM-AL concerning the salt concentration performed under 100 g/L C-CM-AL, 2 h, and 25 °C, and b) the adsorption difference using monovalent and divalent salt in regards to the crosslinked structure of C-CM-AL polymer.

5.4.6. Desorption analysis

The salt desorption test was conducted by adding deionized water to the salt-loaded C-CM-AL polymer (2 mL/g) and increasing temperature from 35 to 85 °C (Figure 5.6a). Based on the results, no significant deionization occurred below 45 °C. However, by increasing the temperature, the

desorption amount started to augment for all salts. Interestingly, the maximum desalination of around 89-95 % was observed for all salts at 75 °C within one hour (Figure 5.6a), raised by the thermoresponsive behavior of tertiary amine and carboxylic acid groups.[30,31]

The desorption analysis of control samples (C-L, C-CM, and C-AL) was also conducted, and their desorption amount (Figure 5.6b) was compared to their adsorption capacity (Figure 5.4). Crosslinked lignin polymer (C-L) showed a maximum desorption amount of 0.01 mmol/g for KCl and NaCl salts, which accounts for only 20 % of its adsorbed amount (Figure 5.4). The anionic crosslinked polymer (C-CML) demonstrated a maximum desorption amount of 0.07 and 0.03 mmol/g for KCl and NaCl as well as for $CaCl_2$ and $MgCl_2$, respectively, which accounts for about 70 % of its adsorption amount. Also, the crosslinked cationic polymer (C-AL) showed 0.09 mmol/g of desorption for KCl, and NaCl, and about 0.05 mmol/g for $CaCl_2$ and $MgCl_2$, which accounts for about 80 % of its adsorption amount. These results indicated a desorption ability for anionically and cationically modified polymers while an insignificant desorption capacity was observed for the C-L sample (Figure 5.6b). Therefore, it could be concluded that the desorption ability of the amphoteric C-CM-AL polymer is raised from its carboxy and amine groups grafted to its structure, which will be discussed further in more detail.

The schematic thermoresponsive adsorption and desorption mechanism of C-CM-AL is presented in Figure 5.6c. The produced C-CM-AL, by having both anionic and cationic sites, could simultaneously adsorb both anions and cations at 25 °C. At this temperature, the amine and carboxy groups exist in their protonated ($-N(CH_3)_2H^+$) and deprotonated form (COO^-), respectively. Thus, this polymer was observed to have the affinity to adsorb salt, e.g., KCl, from the aqueous solution and form -COOK, and $-N(CH_3)_2HCl$ (Figure 5.6c).

The thermoresponsive behavior of the produced C-CM-AL provides the advantage of reusability, which could decrease the operating expenses and environmental impacts while introducing a novel application for lignin-based polymers. By using the excess heat released from operational facilities or solar thermal energy, the heat required for the desorption process could be provided, leading to an environmentally friendly desalination operation. Moreover, the adsorbed and released salt in this process could be used in many applications, such as food, textiles, tanneries, livestock, agriculture, deicing and microorganism production.[74-76]

It is worth mentioning that the faster desorption of salt (within one hour) (Figure 5.5a) than its adsorption (within two hours) (Figure 5.6a) could be due to the structural expansion of C-CM-AL

216

polymer in higher temperatures (75 °C).[50] In this case, lignin expansion would facilitate the salt desorption in water. The salt desorption could also be accelerated by the osmotic pressure, in which salts would have the tendency to desorb from the polymer and enter the aqueous medium where the salt concentration is minimal.

a)

b)
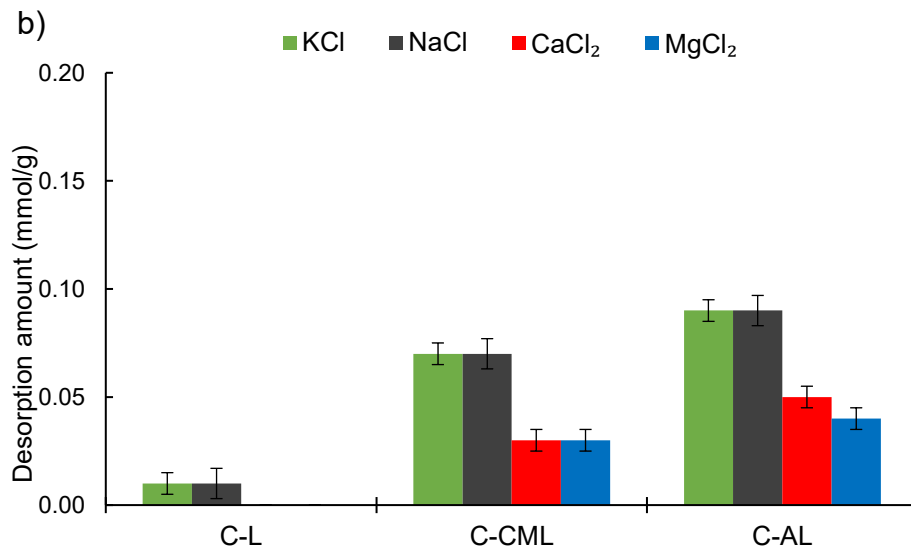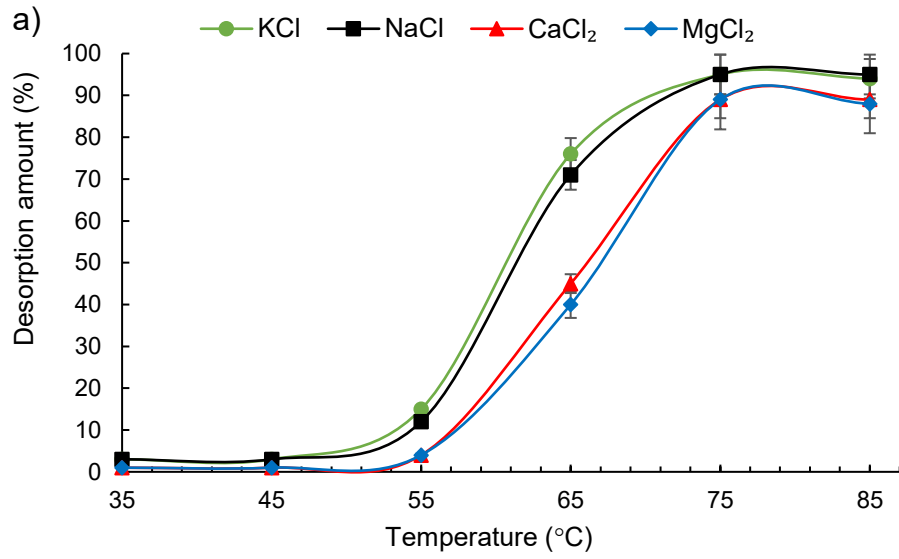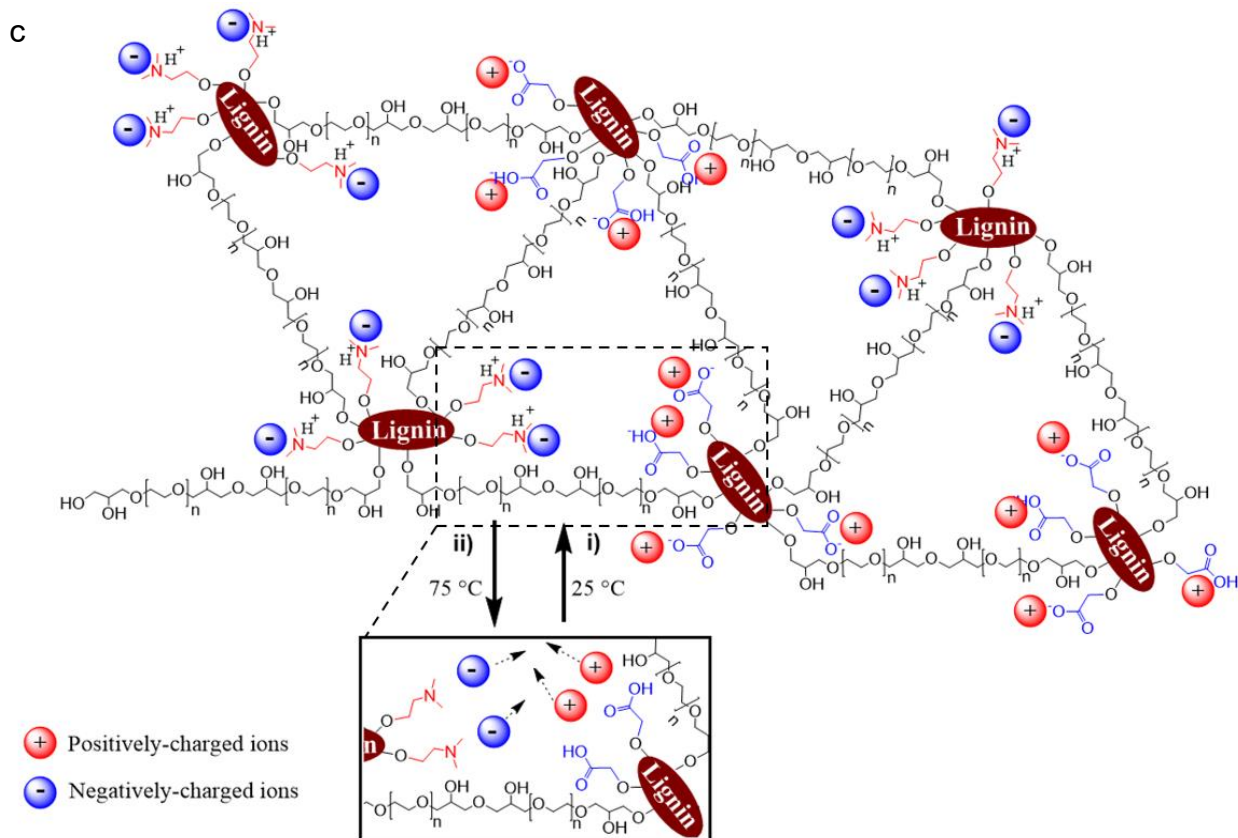
Figure 5.6. a) Salt desorption of amphoteric C-CM-AL at different temperatures conducted for 1 h, b) Salt desorption of C-L, C-CML, and C-AL polymers as control samples treated at 75 °C and c) Schematic illustration of amphoteric-functionalized C-CM-AL i) adsorption at 25 °C, and ii) desorption (thermoresponsive behavior) at 75 °C.

5.4.7. Reusability analysis

The results in Figures 5.4 and 5.6b shows that C-CM-AL polymer could be a more promising adsorbent than C-CML and C-AL for different salts among all polymers as it had much better adsorption and desorption performance. Therefore, the reusability test was conducted for C-CM-AL polymer as shown in Figure 5.7. The adsorption and desorption rounds were conducted at 25, and 75 °C, respectively. After the first cycle, the adsorption capacity decreased to approximately 95 % for KCl and NaCl, and to 89 % for $CaCl_2$ and $MgCl_2$. By 12 more rounds of reusing and recycling, the adsorption capacity reached about 70-80 % of the first adsorption capacity. The decrease in the overall adsorption capacity of C-CM-AL by further reusing and recycling could be due to the salt ions physically trapping and clogging some crosslinked structures of the polymer.[67-69]
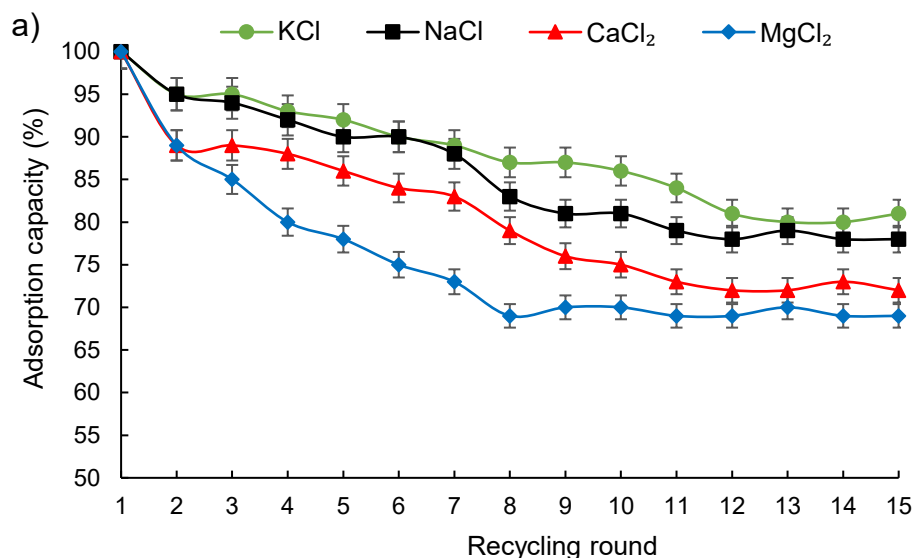
Figure 5.7. Reusability of C-CM-AL polymer in salt adsorption performed up to 15 rounds.

Table 5.2 includes the XPS data from the first and last rounds of adsorption/desorption. The increase in the atomic concentration of salts in the last round reveals that more salt components have remained in the polymer structure after the adsorption/desorption rounds, which could lead to a decrease in the adsorption affinity. Also, to reveal whether the increase in the atomic concentration of salts is raised from the adsorption or the desorption process, the amount of salt components in the 12th round of adsorption/desorption is also included in Table 5.2. The similar results obtained from the remained salt components in the 12th and 15th rounds (Table 5.2) indicate that the adsorption affinity reached equilibrium (Figure 5.7).

Table 5.2. The atomic concentration of cations from the first and last round of adsorption and then desorption obtained from XPS

Salt	Components	1st round (atomic concentration %)[1]	12th round (atomic concentration %)[1]	15th round (atomic concentration %)[1]
KCl	K 2p	0.02	0.18	0.19
	Cl 2p	0.04	0.11	0.11
NaCl	Na 1s	0.04	0.23	0.22
	Cl 2p	0.03	0.11	0.10
CaCl$_2$	Ca 2p	0.06	0.29	0.29
	Cl 2p	0.05	0.11	0.12
MgCl$_2$	Mg 1s	0.07	0.35	0.34
	Cl 2p	0.06	0.12	0.13

[1] Standard deviation was <0.02

Moreover, the high-resolution scan XPS spectra of C 1s of C-CM-AL of 1st and 15th rounds of adsorption/desorption are shown in Figures 5.8a, and 5.8b, respectively, while the area of each peak is included in Table S5.5. As shown in Figure 5.8, the main peak at 284.6 eV is attributed to the C-C bond.[77,78] The peaks at 286.3 eV, 287.1 eV, and 288.8 eV are attributed to C-O, C-N, and O=C-O and/or C=O bonds, respectively.[79,80] The results in Figure 5.8 and Table S5.5 indicate that the anionic (carboxy) and cationic (amine) groups in C-CM-AL were not affected after the 15th round of desorption and adsorption. Therefore, the decrease in the adsorption efficiency could be due to the decrease in the salt desorption affinity of the C-CM-AL polymer, which subsequently hampers the adsorption in the next round. The reduced desorption capacity might be due to the clogging of the pores or difficulties in movement of the adsorbed ions from the pores to the bulk solution in the desorption process.

Moreover, as seen in Figure 5.7, the adsorption capacity of the polymer for $CaCl_2$ and $MgCl_2$ was reduced more greatly than that for KCl and NaCl (as seen as a higher atomic concentration for Ca^{2+} and Mg^{2+} than K^+ and Na in Table 5.3). This could be ascribed to the fact that Ca^{2+} and Mg^{2+} ions associate with two carboxyl groups (Figure 5.5b (i)), which hampers the desorption affinity of these ions from the polymer.[72,73]
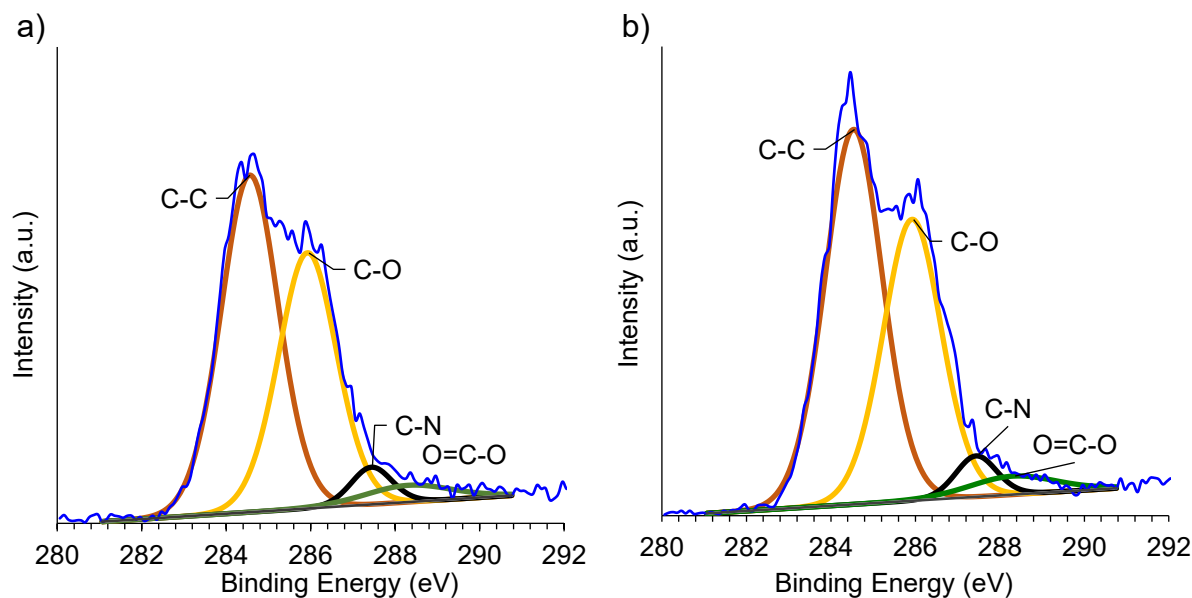
Figure 5.8. XPS high-resolution spectra of C1s for C-CM-AL polymer after a) 1st and b) 15th round of adsorption/desorption.

5.4.8. Sedimentation performance

Figure 5.9 illustrates the variation in the gravitational stability index (TSI) values of the C-CM-AL sample in the absence (control sample) and presence of KCl in the first and last round of adsorption/desorption. The TSI results for the first round of adsorption/desorption for NaCl, $MgCl_2$, and $CaCl_2$ are shown in Figure S5.5 for more comparison. Through time, the particles in the control sample started to settle, which made a clear and transparent layer on the top, and this increased the transmission of the sample to be 74.6 after 30 min. The TSI values increased to be around 94.7-99.4 for C-CM-AL after adsorbing salt (KCl, NaCl, $MgCl_2$, and $CaCl_2$) (Figures 5.9 and S5.5). These results indicate that C-CM-AL was settled faster after the salt adsorption, which would be due to the neutralization of its anionic and cationic groups by salts, leading to a decrease in the electrostatic attraction/repulsion between the C-CM-AL polymers, and thus faster settlement.[50,81] The faster settling rate of C-CM-AL with different salts would also facilitate its separation which would be beneficial from the industrial perspective. In addition, the TSI value of C-CM-AL after the 15th round of adsorption/desorption of KCl salt indicates that the settling rate of C-CM-AL polymer was not changed significantly after the 15th round of adsorption and desorption, revealing the successful reusability of the produced C-CM-AL polymer.

222
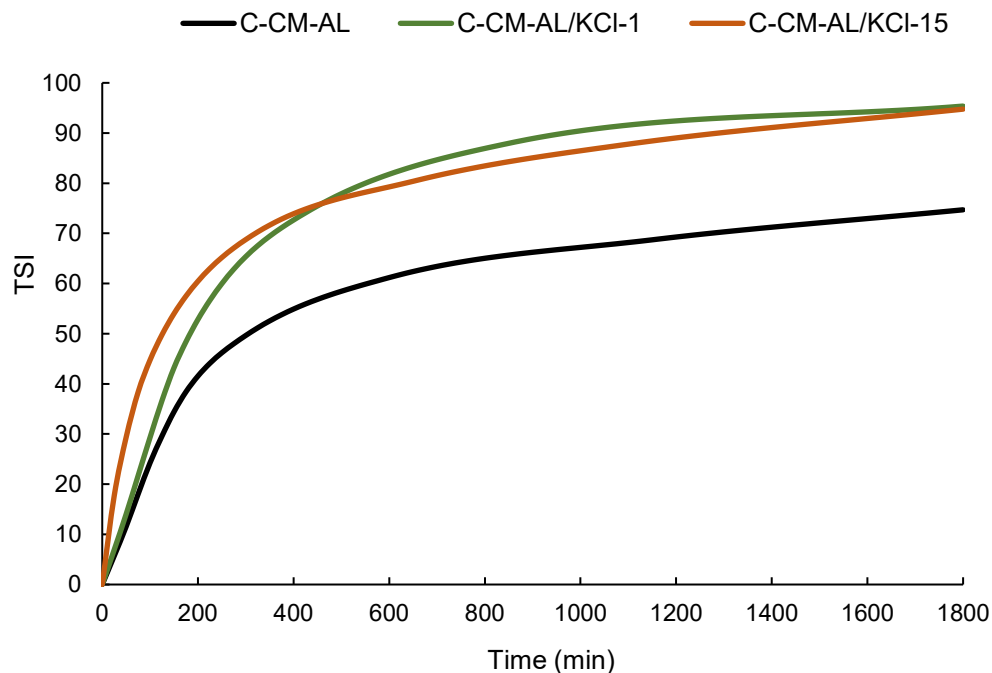
Figure 5.9. TSI variations as a function of time (C-CM-AL concentration of 100 g/L at 25 °C, scanning time of 30 min). C-CM-AL/KCl-1 indicates the system of the first round of adsorption/desorption and C-CM-AL/KCl-15 indicates the system of the 15th round of adsorption/desorption.

The settling velocity was also characterized as the increase rate of the sediment thickness.[82] The C-CM-AL polymer, as a control sample, had a settling velocity of about 65 mm/h. By adding salts, the settling velocity increased and reached the maximum amount of around 198 mm/h for $MgCl_2$. The settling velocity and the compactness of sediments after 30 min of settling are listed in Table 5.3. As observed, the control sample (C-CM-AL without salts) had the sediment compactness of 685 g/L. The addition of salts makes the sediment bulkier with the compactness of 450 g/L suggesting that treating C-CM-AL with different salts would create looser structures. This implies that the screening of the charges of C-CM-AL would create the polymer with a looser structure.[81]

Table 5.3. Sediment compactness and settling velocity of C-CM-AL after 30 min.

Label	Sediment compactness (g/L)	Settling velocity (mm/h)
C-CM-AL without salt (Control)	685 ± 4.1	65 ± 2.1
C-CM-AL with KCl[1]	460 ± 3.4	139 ± 3.5
C-CM-AL with KCl[2]	458 ± 5.6	143 ± 4.5
C-CM-AL with NaCl[1]	453 ± 5.3	185 ± 3.2
C-CM-AL with $CaCl_2$[1]	441 ± 7.3	189 ± 2.8
C-CM-AL with $MgCl_2$[1]	428 ± 2.8	198 ± 3.5

[1] 1st round of adsorption
[2] 15th round of desorption/desorption

5.4.9. Competitive adsorption analysis

The competitive adsorption analysis was conducted by mixing salts together in one medium for adsorption analysis, and the results are tabulated in Table 5.4. For the binary systems, the amphoteric C-CM-AL adsorbed more K^+ than Na^+ in KCl/NaCl solution, while it adsorbed more Na^+ in both $NaCl/CaCl_2$, and $NaCl/MgCl_2$ solutions. In addition, it was seen that in solutions where a divalent salt exists, the adsorbed amount of Cl^- was increased. This further indicates that divalent ions could bond to both cationic sites of the polymer as well as Cl^-, simultaneously, leading to an increase in the Cl^- adsorption amount, as discussed and shown in Figure 5.5b (ii). In the salt solutions, where all the monovalent and divalent salts co-exist, the overall adsorption was not changed. Although in the single salt system (Table S5.6), the cations indicated a higher adsorption amount compared to the binary and multi salt systems (Table 5.4), the overall adsorption capacity

of the polymer remains unchanged in the mixed salt solutions. Meanwhile, the produced C-CM-AL was also observed to successfully adsorb both monovalent and divalent salts concurrently.

Table 5.4. Competitive adsorption of mixed salt for C-CM-AL polymer obtained from XPS analysis.

Salt mixtures	Components (atomic concentration %)[1]				
	K 2p	Na 1s	Ca 2p	Mg 1s	Cl 2p
KCl, and NaCl	4.00	1.95	-	-	4.87
CaCl$_2$, and MgCl$_2$	-	-	1.04	0.74	5.36
KCl, and CaCl$_2$	3.78	-	1.12	-	5.18
KCl, and MgCl$_2$	3.68	-	-	0.88	5.12
NaCl, and CaCl$_2$	-	3.65	0.91	-	5.08
NaCl, and MgCl$_2$	-	3.54	-	0.71	5.05
KCl, NaCl, CaCl$_2$, and MgCl$_2$	1.95	1.01	0.89	0.58	5.14

[1] Standard deviation was <0.02

5.5 Conclusions

In this work, multi-charged crosslinked polymer (C-CM-AL) has been fabricated by crosslinking the produced anionic (carboxy) and cationic (tertiary amine) lignin. All modifications were confirmed by ^{1}H and ^{1}H-H COSY NMR. The produced amphoteric C-CM-AL polymer showed a higher desalination performance compared to the anionic or cationic ones (C-CM and C-AL). The highest adsorption capacity for the produced C-CM-AL was observed to be 1.25, 0.97, 0.71, and 0.62 mmol/g for KCl, NaCl, CaCl$_2$, and MgCl$_2$, respectively. Also, the reusability of this polymer was tested for 15 rounds. The XPS results of the last reusability test indicated that the desorption affinity decreased due to the salt ions trapping in the structure of C-CM-AL which led to a decreased adsorption capacity up to around 20-30%. However, the adsorption affinity did not change since the amount of anionic and cationic groups on the polymer did not decrease. By comparing the salt adsorption in binary and multicomponent systems, the overall adsorption capacity remained the same. Also, the sedimentation, settling velocity, and the compactness evaluations indicated that the C-CM-AL settled faster after adsorbing salts while creates a polymer with a looser structure in the sediment. Overall, the produced C-CM-AL polymer is expected to be a promising polymer for the development of reusable and efficient desalination applications.

5.6 References

1) S. Kumar, In Vital signs., 2013, Island Press, Washington, DC.

2) D. J. Smith, Power Eng., 2001, 105, 91-95.

3) T. M. Missimer and R. G. Maliva, Desalination, 2018, 434, 198-215.

4) D. H. Kim, Desalination, 2011, 270, 1-8.

5) A. Nasu, U.S. Patent No. 4,956,157., 1990, Washington, DC: U.S. Patent and Trademark Office.

6) S. I. Abou-Elela, M. M. Kamel and M. E. Fawzy, Desalination, 2010, 250, 1-5.

7) V. L. Taylor, A. D. Fitzpatrick, Z. Islam and K. L. Maxwell, In Advances in Virus Research, 2019, (Vol. 103, pp. 1-31). Academic Press.

8) F. Xuan and J. Liu, Polymer International, 2009, 58, 1350-1361.

9) J. Jagur-Grodzinski, Polym. Adv. Technol., 2007, 18, 785-799.

10) K. D. Kreuer, S. J. Paddison, E. Spohr and M. Schuster, Chem. Rev., 2004, 104, 4637-4678.

11) M. S. Jyothi, V. Nayak, M. Padaki, R. G. Balakrishna and K. Soontarapa, Chem. Eng. J., 2016, 283, 1494-1505.

12) M. D. Afonso and M. N. de Pinho, J. Membr. Sci., 2000, 179, 137-154.

13) Z. H. Feizi and P. Fatehi, Cellulose, 2020, 1-14.

14) Z. H. Feizi and P. Fatehi, Carbohydr. Polym., Accepted, 2021.

15) J. Chen, A. E. Kazzaz, N. AlipoorMazandarani, Z. H. Feizi and P. Fatehi, Molecules, 2018, 23, 868.

16) A. E. Kazzaz, Z. H. Feizi and P. Fatehi, Green Chem., 2019, 21, 5714-5752.

17) A. E. Kazzaz and P. Fatehi, J. Colloid Interface Sci., 2020, 561, 231-243.

18) J. Miao, g. H. J., Chen and C. J. Gao, Desalination, 2005, 181, 173-183.

19) Z. Zhao, Z. Wang, N. Ye and S. Wang, Desalination, 2002, 144, 35-39.

20) C. Jiang, X. Wang, D. Qin, W. Da, B. Hou, C. Hao and J. Wu, J. Hazard. Mater., 2019, 369, 50-61.

21) C. Huang, X. Shi, C. Wang, L. Guo, M. Dong, G. Hu and Z. Guo, Int. J. Biol. Macromol., 2019, 140, 1167-1174.

22) E. Zong, G. Huang, X. Liu, W. Lei, S. Jiang, Z. Ma and P. Song, J. Mater. Chem. A, 2018, 6, 9971-9983.

23) B. Wang, J. L. Wen, S. L. Sun, H. M. Wang, S. F. Wang, Q. Y. Liu and R. C. Sun, Ind. Crops Prod., 2017, 108, 72-80.

24) J. Zhang, H. Asakura, J. van Rijn, J. Yang, P. Duchesne, B. Zhang and N. Yan, Green Chem., 2014, 16, 2432-2437.

25) M. Yan and Z. Li, Mater. Lett., 2016, 170, 135-138.

26) M. J. Atkinson and C. Bingman, J. Aquaric. Aquat. Sci., 1997, 8, 39-43.

27) F. Chen, S. I. S. Shahabadi, D. Zhou, W. Liu, J. Kong, J. Xu and X. Lu, React. Funct. Polym., 2019, 143, 104336.

28) T. Pielhop, G. O. Larrazábal, M. H. Studer, S. Brethauer, C. M. Seidel and P. R. von Rohr, Green Chem., 2015, 17, 3521-3532.

29) Z. Li, D. Xiao, Y. Ge and S. Koehler, ACS Appl. Mater. Interfaces, 2015, 7, 15000-15009.

30) J. K. Saib, Am. J. Anal. Chem., 2015, 6, 429.

31) T. Matsui, H. C. Ko, and L. G. Hepler, Can. J. Chem., 1974, 52, 2912-2918.

32) M. K. Konduri, F. Kong and P. Fatehi, Eur. Polym. J., 2015, 70, 371-383.

33) E. Cortes-Trivino, C. Valencia, M. Delgado and J. Franco, Polymers, 2018, 10, 670.

34) M. Borrega, S. Päärnilä, L. G. Greca, A. S. Jääskeläinen, T. Ohra-Aho, O. J. Rojas and T. Tamminen, Langmuir, 2020, 36, 9675-9684.

35) W. C. Ribeiro, P. F. M. Martinez and V. Lobosco, BioResources, 2020, 15, 8577-8600.

36) Z. H. Feizi, A. E. Kazzaz, F. Kong and P. Fatehi, Sep. Purif. Technol., 2019, 222, 254-263.

37) A. E. Kazzaz and P. Fatehi, Ind. Crops Prod., 2020, 154, 112732.

38) S. N. Chien, T. E. Amidon and Y. Z. Lai, TAPPI JOURNAL, 2012, 11, 29-37.

39) A. E. Kazzaz, Z. H. Feizi F. Kong and P. Fatehi, Colloids Surf., A, 2018, 556, 218-226.

40) A. E. Kazzaz, Z. H. Feizi and P. Fatehi, Colloid Polym. Sci., 2018, 296(11), 1867-1878.

41) W. Gao, J. P. Inwood and P. Fatehi, J. Wood Chem. Technol., 2019, 1-17.

42) C. A. Schneider, W. S. Rasband and K. W. Eliceiri, Nat. methods, 2012, 9(7), 671-675.

43) H. Ray, D. Saetta and T. H. Boyer, Environ. Sci.: Water Res. Technol., 2018, 4, 87-98.

44) A. Criscuoli and M. C. Carnevale, Desalination, 2015, 365, 213-219.

45) A. Panday, S. Mullin, E. D. Gomez, N. Wanakule, V. L. Chen, A. Hexemer and N. P. Balsara, Macromolecules, 2009, 42, 4632-4637.

46) Orion Star, Thermo Scientific Orion Star A212 Benchtop Conductivity Meter, 2020, http://www.geotechenv.com/Manuals/Thermo_Scientific_Manuals/Orion_Star-A212-A222-A322.pdf (Access date Sep, 2020).

47) R. Ou, H. Zhang, J. Wei, S. Kim, L. Wan, N. S. Nguyen and H. Wang,   Adv.   Mater., 2018, 30, 1802767.

48) Y. Zhang, W. Gao and P. Fatehi, Sep. Purif. Technol., 2019, 215, 115-124.

49) S. Gharehkhani, N. Ghavidel and P. Fatehi, ACS Sustainable Chem. Eng., 2018, 7, 2370-2379.

50) A. E. Kazzaz and P. Fatehi, RSC Adv., 2020, 10, 36778-36793.

51) X. Liu, H. Zhang, C. Wu, Z. Liu, Y. Chen, B. Yu and Z. Liu, J. Chem., 2018, 42, 1223-1227.

52) Y. C. Sun, J. L. Wen, F. Xu and R. C. Sun, Sci. Res. Essays, 2010, 5, 3850-3864.

53) C. Chen, M. Zhu, M. Li, Y. Fan and R. C. Sun, Biotechnol. Biofuels, 2016, 9, 1-15.

54) R. Malet, M. Moreno-Mañas, T. Parella and R. Pleixats, The Journal of organic chemistry, 1996, 61, 758-763.

55) A. Tribot, G. Amer, M. A. Alio, H. de Baynast, C. Delattre, A. Pons and C. G. Dussap, Eur. Polym. J., 2019, 112, 228-240.

56) O. Y. Abdelaziz and C. P. Hulteberg, Waste Biomass Valorization, 2017, 8(3), 859-869.

57) J. P. Olivier, W. B. V. Conklin and M. V. Szombathely, In Studies in Surface Science and Catalysis, 1994 (Vol. 87, pp. 81-89). Elsevier.

58) J. M. Cervantes-Uc, J. V. Cauich-Rodriguez, W. A. Herrera-Kao, H. Vazquez-Torres, A. Marcos-Fernandez, Polym. Degrad. Stab., 2008, 93, 1891-1900.

59) P. Janarthanan, W. M. Z. W. Yunus and M. B. Ahmad, J. Appl. Polym. Sci., 2003, 90, 2053-2058.

60) J. Yi, Q. Xu, X. Zhang and H. Zhang, Cellulose, 2009, 16(6), 989-997.

61) J. Florio, R. Ravichandran, D. Switala and B. Hsieh, Eur Coat J, 2016, 2, 48-54.

62) L. Wang, C. Shi, L. Pan, X. Zhang and J. J. Zou, Nanoscale, 2020, 12, 4790-4815.

63) M. M. Rao, G. C. Rao, K. Seshaiah, N. V. Choudary and M. C. Wang, Waste Manage., 2008, 28, 849-858.

64) E. S. Hamborg and G. F. Versteeg, J. Chem. Eng. Data, 2009, 54, 1318-1328.

65) Y. Marcus, Biophys. Chem., 1994, 51, 111-127.

66) E. R. Nightingale Jr, The Journal of Physical Chemistry, 1959, 63, 1381-1387.

67) M. Ugurlu, I. Kula, M. H. Karaoğlu and Y. Arslan, Environ. Prog. Sustainable Energy, 2009, 28, 547-557.

68) J. H. Xu, Y. Zhou, J. J. Wen, Z. Y. Wu, C. F. Zhou and J. H. Zhu, Asia-Pacific Journal of Chemical Engineering, 2008, 3, 481-488.

69) G. M. Lu and D. D. Lau, Gas Sep. Purif., 1996, 10, 103-111.

70) B. Tansel, Sep. Purif. Technol., 2012, 86, 119-126.

71) S. Adapa and A. Malani, Sci. Rep., 2018, 8, 1-12.

72) A. L. Liu, Advances in planar lipid bilayers and liposomes. Elsevier, 2011.

73) A. Kundagrami and M. Muthukumar, The Journal of chemical physics, 2008, 128, 244901.

74) S. R. Feldman, Kirk-Othmer Encyclopedia of Chemical Technology, 2009, 1-27.

75) Z. H. Feizi and H. K. Guvenmez, J. Biotechnol., 2017, 256, S63.

76) A. E. Kazzaz, Z. H. Feizi and H. K. Guvenmez, Int. J. Appl. Biol. Pharm., 2015, 6, 63-73.

77) M. Ghanadpour, F. Carosio, P. T. Larsson and L. Wågberg, Biomacromolecules, 2015, 16, 3399-3410.

78) M. Bozic, P. Liu, A. P. Mathew and V. Kokol, Cellulose, 2014, 21, 2713-2726.

79) S. Migneault, A. Koubaa, P. Perré and B. Riedl, Appl. Surf. Sci., 2015, 343, 11-18.

80) X. Yan, T. Xu, G. Chen, S. Yang, H. Liu and Q. Xue, Journal of Physics D: Appl. Phys., 2004, 37(6), 907.

81) L. Alfhaid, N. H. Williams and M. Geoghegan, J. Appl. Polym. Sci., 2020, 49130.

82) P. Tong and B. J. Phys. Rev. E., 1998, 58, R6931.

5.7 Electronic supplementary material

Production of reusable porous amphoteric lignin for water desalination

Armin Eraghi Kazzaz, Pedram Fatehi*

Biorefining Research Institute, Green Processes Research Centre and Chemical Engineering Department, Lakehead University, 955 Oliver Road, Thunder Bay, ON, Canada, P7B5E1

*Corresponding author: email: pfatehi@lakeheadu.ca; tel: 807-343-8697; fax: 807-346-7943

Supporting experimental section

^{1}H NMR, and ^{1}H-H COSY spectroscopy

In this study, 50 mg of the samples were dissolved in 500 µL of D_2O or 9/1 v/v $[D_6]DMSO/D_2O$ which contained TMSP (2 mg TMSP/500 µL D_2O) at 50 °C in a water bath shaker overnight at 150 rpm. A 458 pulseflipping angle, a 4.6 ms pulse width, a 2.05 s acquisition time, and a relaxation delay time of 1.00 s were considered in this experiment.

^{1}H-H COSY spectroscopy was performed by conducting 32 scans with 128 increments and 1 second relaxation time delay. The acquisition time was set to 3.983 s.

Gel Permeation Chromatography (GPC)

For analyzing the molecular weight of unmodified lignin (L) and CML the organic columns of PolyAnalytic PAS106M, PAS103 and PAS102.5 were used, and tetrahydrofuran (THF) with HPLC-grade was used as both the eluent and solvent. For the cationic lignin sample, PolyAnalytic PAA206 and PAA203 columns were used and a 0.1 mol/L $NaNO_3$ solution was used as eluent and solvent. 0.2 µm nylon filter was used to filter samples before conducting the molecular weight analysis. The flow rate was set at 0.7 mL/min. The refractometer (RI) and differential pressure (DP) detectors were used to determine the molecular weight of the samples. All measurements were conducted with respect to standard polyethylene oxide.[1]

Nitrogen Content degree of substitution

The degree of substitution (DS) was calculated based on the equation:

$$\text{Degree of substitution (DS) (mol/mol)} = \frac{180 \times N}{1400 - R \times N}$$

where 180 is the molecular weight (g/mol) unit of lignin, R is the molar mass of N,N-dimethylethylamine group which is 72.13 g/mol, and 1400 stands for 100 times of the nitrogen atomic mass.

Carboxylate group analysis

1 g of unmodified and carboxymethylated lignin (CML) samples were added to 100 mL of distilled water and the solution pH was set to 10.5. Then the solution was titrated with a cationic polymer, TEGO trant A100, to measure carboxylate group content. The degree of substitution (DS) was determined using the equation:

$$\text{Degree of substitution (DS) (mol/mol)} = \frac{M \times C}{1 - 0.081 \times C}$$

where M is the mass of the basic unit of lignin (g/mmol),[2] C is the total carboxylate group content (mmol/g), and 0.081 (g/mmol) is the net increase in mass for each sodium carboxymethyl group attached to lignin.

Supporting information results

¹H NMR spectroscopy

230
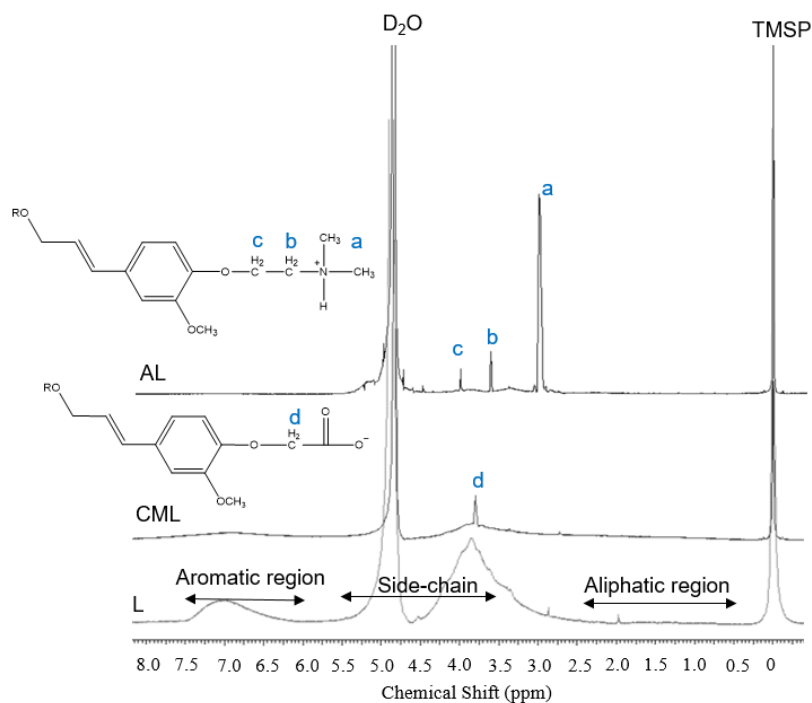
Figure S5.1. ^{1}H NMR spectrum of L, CML, AL, and CCM-AL, at 25 °C.
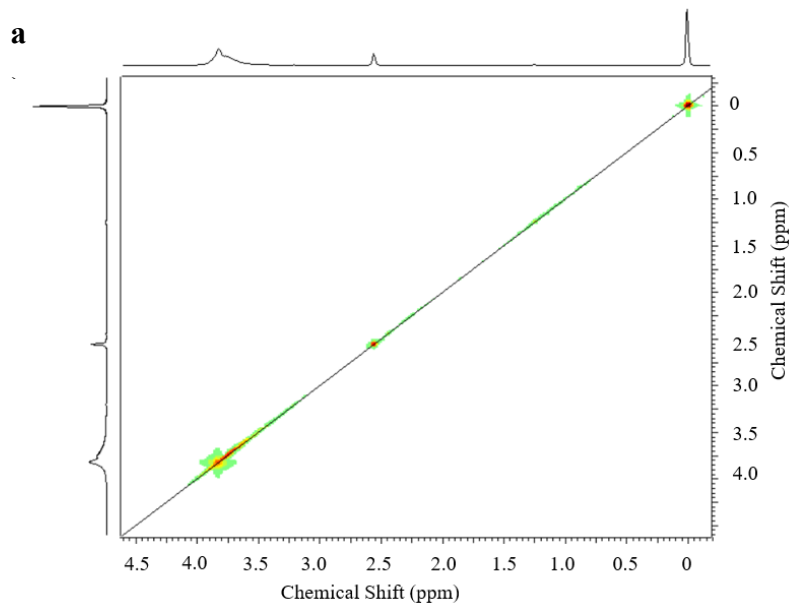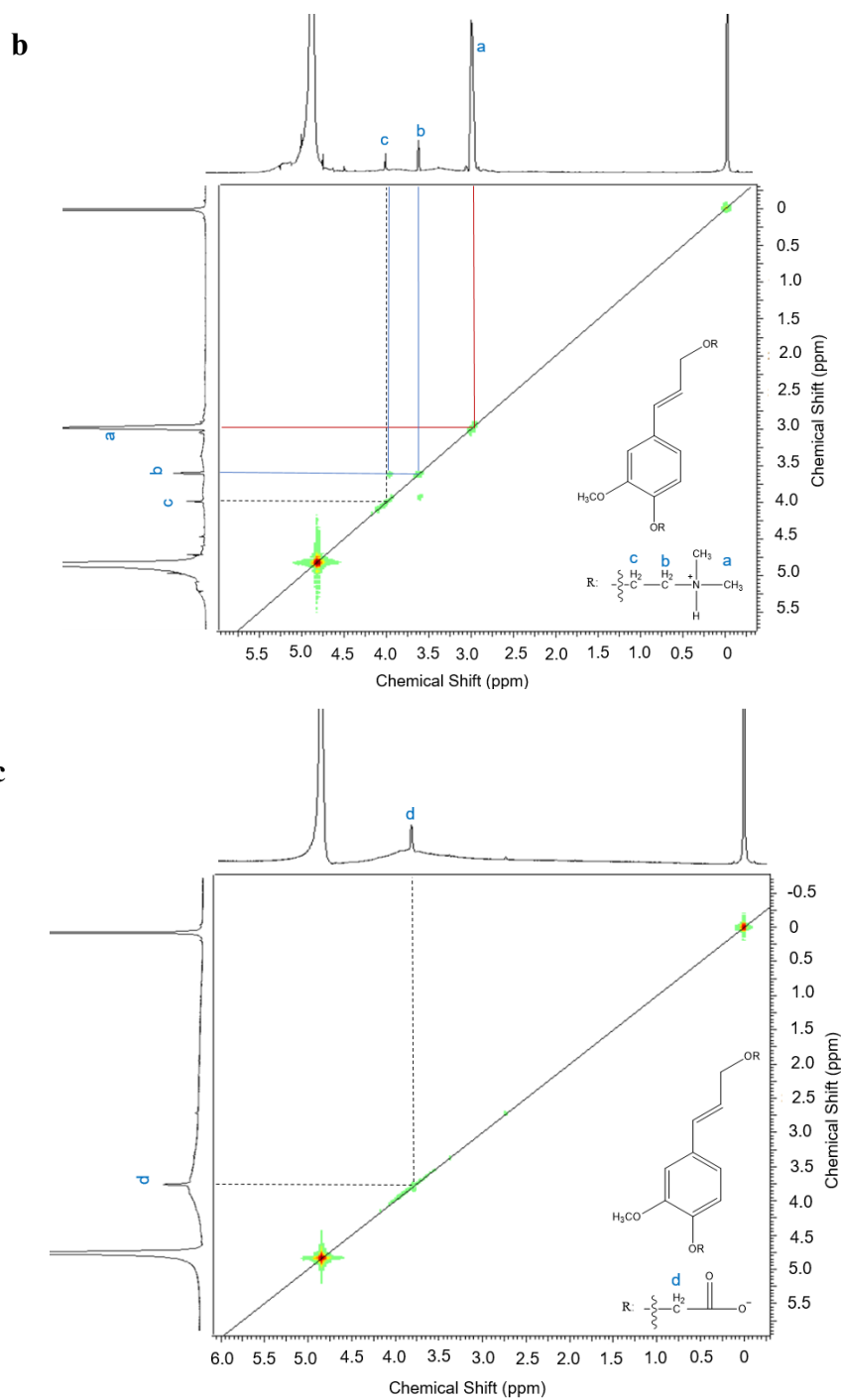
Figure S5.2. ^{1}H-H COSY spectroscopy of a) L, b) AL, and c) CML, at 25 °C.

Table S5.1. Chemical properties of produced crosslinked polymers as a control sample.

Samples name	C-L	C-CML	C-AL
Nitrogen content[1] wt. %	<0.09[1]	<0.09[1]	2.64
COOH content[1] (mmol/g)	0.09	2.04	-

Charge density (meq/g)	-1.28	-2.32	2.17
Nitrogen content degree of substitution (mol/mol)	<0.09[1]	<0.09[1]	0.39
COOH content degree of substitution (mol/mol)	-	0.40	-
Reaction Yield %	58	48	51

[1] Method sensitivity <0.09

TGA analysis

The TGA and dTGA (differentiate thermogravimetric analysis) profiles of L, CML, AL, C-CM-AL are presented in Figures S5.3a, and b, respectively. It can be seen that when the temperature was lower than 200 °C, the higher mass CML was lost compared to other polymers (Figure S5.3a), which is reported in the literature.[3] By increasing the temperature, the degradation of the lignin (L) polymer backbone occurred. About 10 % of the weight loss was seen when the temperature further elevated (in the range of 260-400 °C), which happened due to the thermal-cracking (chain scission) of between C-O-C and C-C bonds of L polymer. By augmenting the temperature from 420 °C to around 600 °C, about 55 % of weight loss was observed for the L, which might be due to the thermal cracking reaction of the aromatic ring.[4] The thermograph analysis of C-CM-AL indicates three distinct stages of thermal degradation at above 200 °C; i) the first stage happens in the range of 220-380 °C with 38 % of weight loss, ii) the second stage occurs in the range of 400-500 °C with 34.5 % of weight loss, and iii) the third stage happened in the range of 510-560 °C with 9.5 % of weight loss.
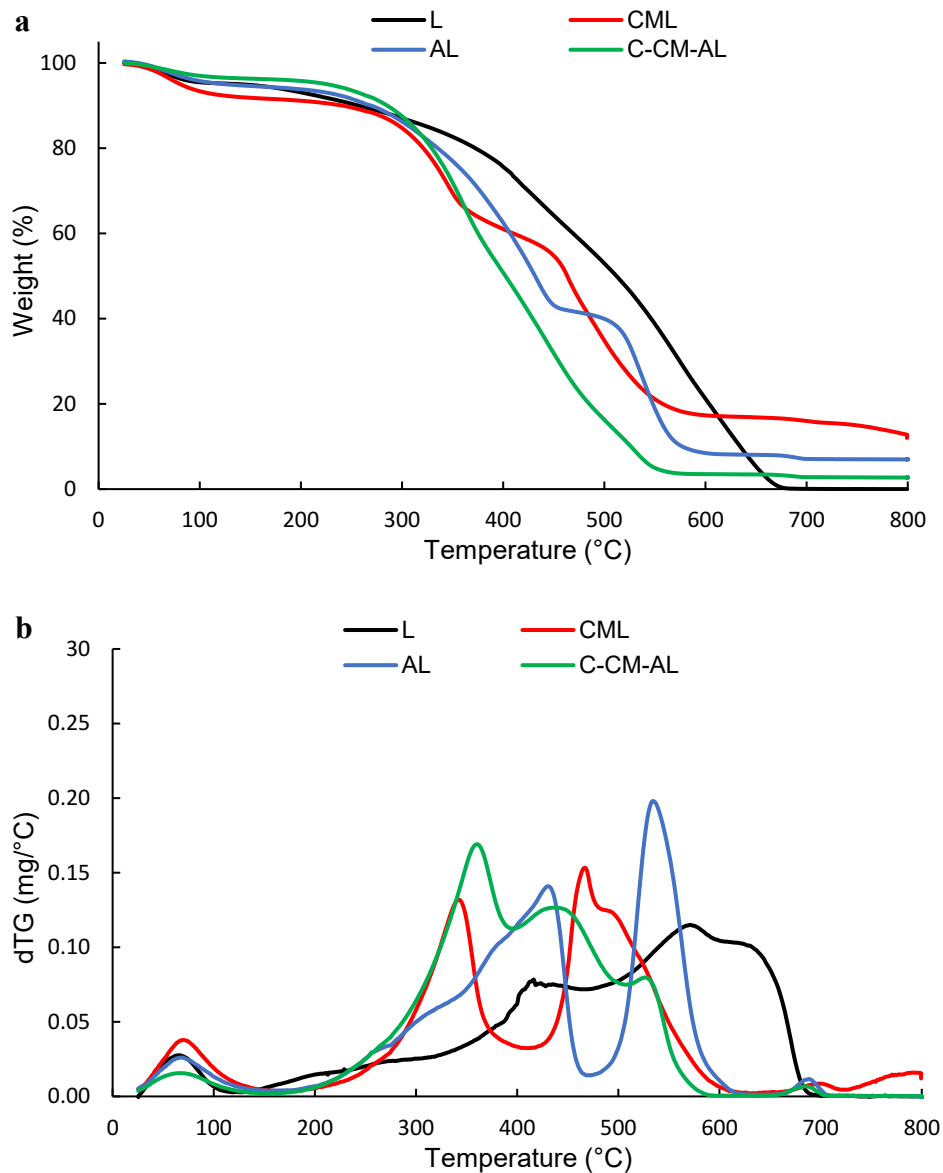
Figure S5.3. a) TGA, and b) dTG graphs of L, and C-CM-AL at a rate of 10 °C/min.

Thermogravimetric analysis

CML polymers indicate three-stage of thermal degradation at above 200 °C; i) the first stage occurs in the range of 220-370 °C with 25 % of weight loss, ii) the second stage takes place in the range of 450-480 °C with 13 % of weight loss, and iii) the third stage happened in the range of 490-550 °C with 23 % of weight loss. AL polymer demonstrates two distinct stages of thermal degradation at above 200 °C; i) the first stage occurs in the range of 220-460 °C with 51 % of weight loss, and ii) the second stage takes place in the range of 480-590 °C with weight loss of about 32 %.
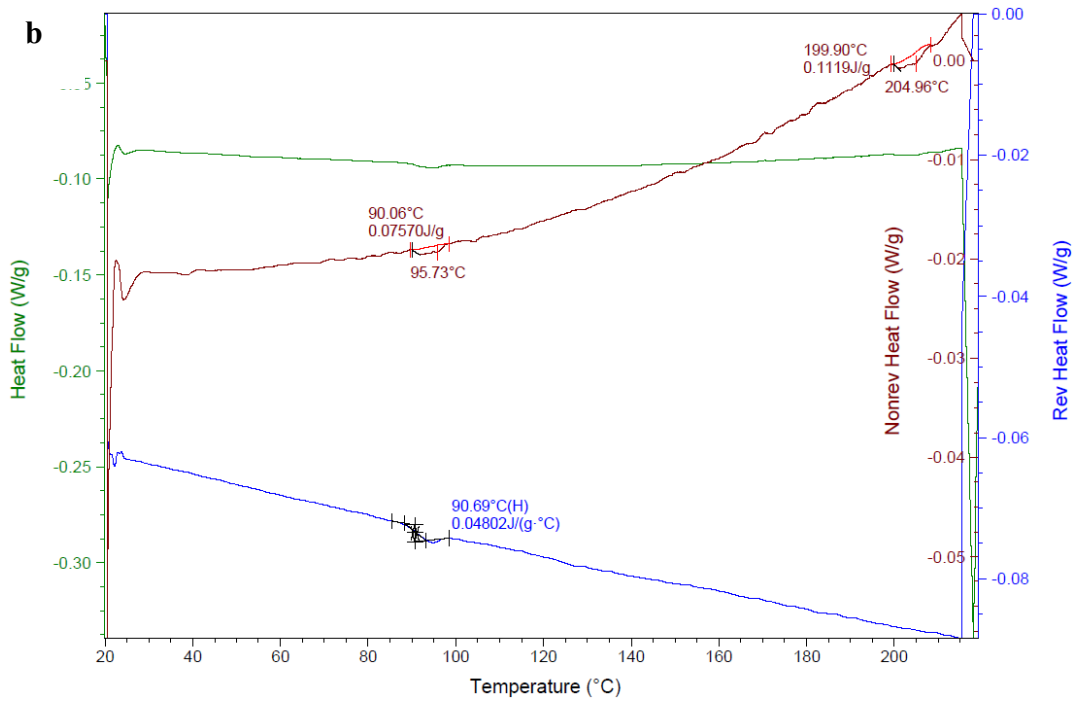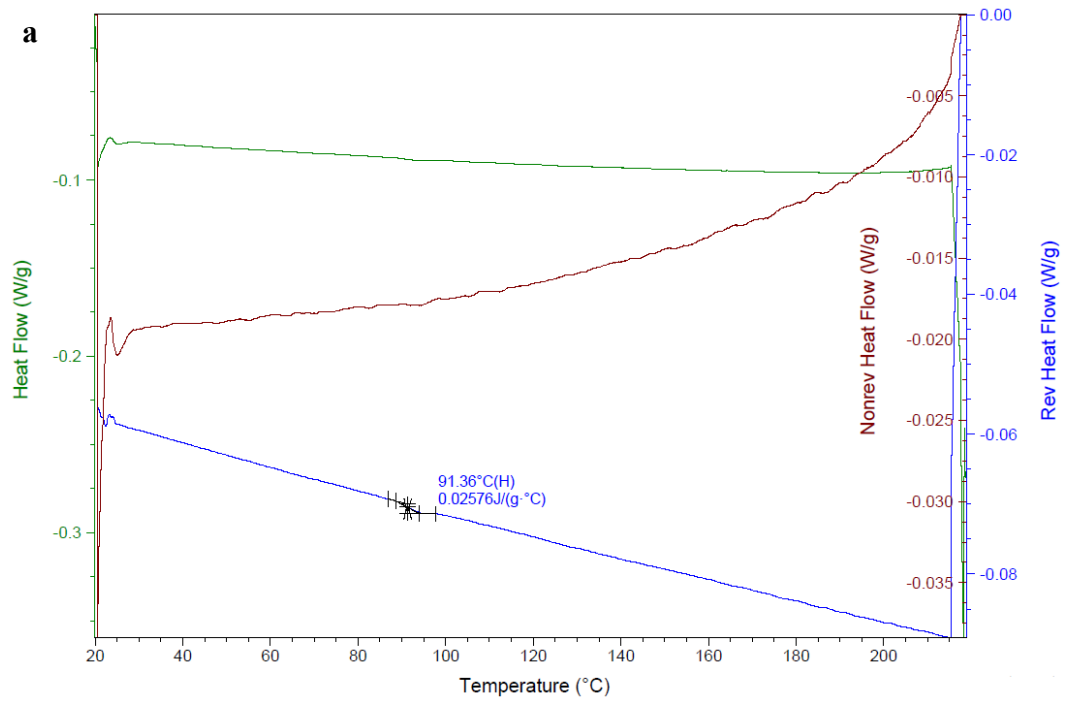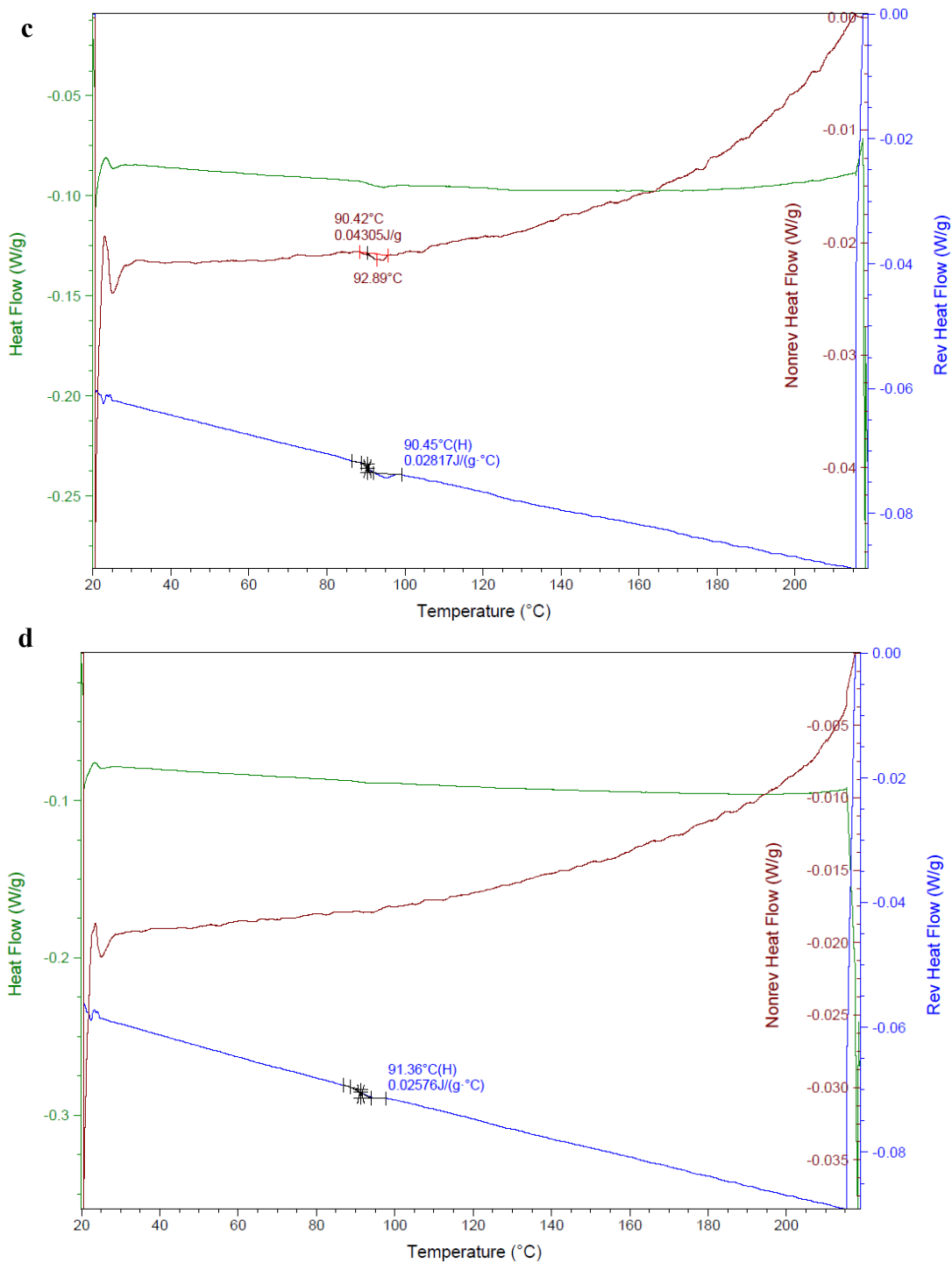
Figure S5.4. MDSC graphs for a) L, b) CML, c) AL, and d) C-CM-AL obtained from second heating and cooling cycles.

Table S5.2. Salinity amount of different water sources.[5]

Water source	Amount (ppm)

Freshwater, typical city water in the US	< 100
Water supply restriction	500
Freshwater, drinking water limitation in the US	1,000
Agriculture irrigation limitation	2,000
Brackish water, mildly	1,000-5,000
Brackish water, moderately	5,000-15,000
Brackish water, heavily	15,000-35,000
Seawater	30,000-50,000

Table S5.3. Composition of seawater.[6]

Component	Concentration (mg/L)	Total salt (%)
Chloride	18,980	55.04
Sodium	10,556	30.61
Sulfate	2,649	7.68
Magnesium	1,272	3.69
Calcium	400	1.16
Potassium	280	1.10
Bicarbonate	140	0.41
Bromide	65	0.19

Table S5.4. The ionic radius, hydrated radius, solubility, and hydration free energy of the cations.[7,8]

Cation	Ionic radius (Å)	Hydrated radius (Å)	Gibbs free energy of hydration (kJ/mol)	Enthalpy of hydration (kJ/mol)
K^+	1.38	3.31	-295	-330
Na^+	1.02	3.58	-365	-415
Ca^{2+}	1.00	4.12	-1505	-1600
Mg^{2+}	0.72	4.28	-1830	-1945

Table S5.5. Relative chemical bonds of C-CM-AL after 1st and 15th round of adsorption and desorption.

Sample	C 1s peak area (%)			
	C-C	C-O	C-N	O=C-O
1st round of adsorption/desorption	52.04	40.01	4.08	3.88
15st round of adsorption/desorption	52.31	39.78	4.06	3.86
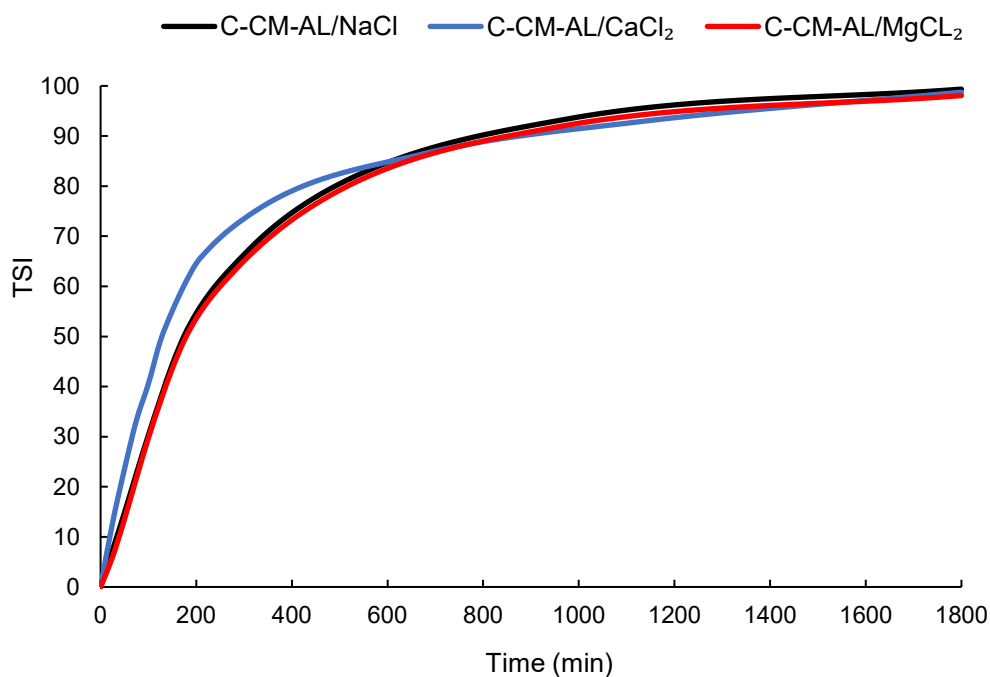
Figure S5.5. TSI variations as a function of time for the first round of adsorption/desorption (C-CM-AL concentration of 100 g/L at 25 °C, scanning time of 30 min).

Table S5.6. Adsorption of single salt for C-CM-AL polymer obtained from XPS analysis.

Salt	Components (atomic concentration %)[1]				
	K 2p	Na 1s	Ca 2p	Mg 1s	Cl 2p
KCl	6.10	-	-	-	4.75
NaCl	-	4.78	-	-	4.74
CaCl$_2$	-	-	3.14	-	5.15
MgCl$_2$	-	-	-	2.79	5.18

[1] Standard deviation was <0.02

References

1) F. Kong, K. Parhiala, S. Wang and P. Fatehi, Eur. Polym. J., 2015, 67, 335-345.

2) A. E. Kazzaz and P. Fatehi, J. Colloid Interface Sci., 2020, 561, 231-243.

3) M. K. Konduri, F. Kong and P. Fatehi, Eur. Polym. J., 2015, 70, 371-383.

4) N. Zhang, S. Wang, M. E. Gibril and F. Kong, Eur. Polym. J., 2020, 123, 109411.

5) The Engineering ToolBox, 2020. https://www.engineeringtoolbox.com/water-salinity-d_1251.html (30, July, 2020)

6) L. Ali, I. A. Girba, A. Pruiu and D. Marasescu, Naval Academy Scientific Bulletin, 2015, 19, 139-146.

7) E. R. Nightingale Jr, The Journal of Physical Chemistry, 1959, 63, 1381-1387.

8) Y. Marcus, Biophys. Chem., 1994, 51, 111-127.

Chapter 6. Interaction of sulfomethylated lignin and aluminum oxide

Adopted from: Armin Eraghi Kazzaz, Zahra Hosseinpour Feizi, Pedram Fatehi[*]

Department of Chemical Engineering,
Lakehead University,
955 Oliver Road,
Thunder Bay, ON P7B 5E1, Canada

* Corresponding author

6.1 Abstract

In this work, oxidized and sulfomethylated lignin was used as a flocculant for aluminum oxide suspension. The oxidized sulfomethylated lignin (OSML) samples had a similar charge density ($-$ 3.5 µeq/g) but varied molecular weights (between 26 and 46 kg/mol). The performance of the produced flocculants was evaluated in altering the relative turbidity and zeta potential of the aluminum oxide suspension. The chord length of particles was increased the most in the suspension by adsorbing OSML with the highest molecular weight. The flocs strength analysis revealed that the flocculation process was reversible. Flocculation analysis depicted that the molecular weight of OSML could influence the turbidity of the suspension dramatically. The settling velocity of the flocs was increased, and the sediment compactness was reduced as the flocs enlarged. The charge neutralization and patching mechanisms were estimated to be dominant for coagulating the particles.

Keywords: Aluminum oxide, Sulfomethylated lignin, Flocculation, Organic chemistry, Sedimentation, Colloidal stability

6.2 Introduction

Lignin is one of the most abundant phenolic polymers in the world,[1,2] which is produced vastly in pulping processes. It has a three-dimensional structure with subunits of phenol, guaiacol, and *p*-coumaryl alcohol.[3] However, most of the produced lignin is used as a fuel source, implying that lignin is under-utilized currently. Its renewability, nontoxicity, and biodegradability make it attractive to be used in the production of bio-based value-added products.[4] Lignin has previously been modified and used as a pesticide/dye/cement dispersant [5] and asphalt emulsifier.[6] It can also be converted to flocculants for treating wastewater.[7-10] In the past, the use of cationic modified lignin for removing anionic dyes and kaolin was studied.[4-11]

The flocculation efficiency of polymers in the colloidal suspensions is significantly affected by the polymer adsorption and polymer properties.[12,13] The impact of functional groups and charge density of linear polymers in flocculation processes has been documented.[5,14] However, these results cannot be extended to lignin-based flocculants, since lignin has a more complicated and three-dimensional structure. Lignin-based flocculants can have different charge densities and molecular weights. Konduri and Fatehi have studied the impact of lignin's charge density on the dispersion of kaolin particles.[15] In another study, the impact of charge density of sulfomethylated

241

lignin on the dispersion of cement particles was studied.[16] Likewise, the impact of charge density of sulfomethylated lignin on the flocculation of cationic dyes was investigated.[5] However, the impact of the molecular weight of sulfomethylated lignin on its flocculation performance is rather unclear, which is the primary objective of the current work.

Flocs induced by flocculation are irregular in structure.[17] The floc structure, e.g., porosity and density, was reported to impact the flocculation process.[18-20] In general, elongated flocs are more prone to settle with their long axis in parallel to the settling direction.[21] Also, the floc's density and porosity have direct effects on the floc size, as denser flocs are smaller in size while porous flocs are larger.[21] Furthermore, flocs with distortions on their surfaces have been observed to settle slower than the rounded ones.[22] Factors, such as turbidity and shear rate, were also reported to impact the flocs' shape and structure.[23] The second objective of this work was to explore the influence of properties of the produced flocs on their flocculation efficiency and sedimentation.

Aluminum oxide has a high surface area, thermal stability, mechanical strength, and low solubility.[24] These characteristics make this material widely utilized in different industries, such as mineral and ceramic processes.[24,25] Presumably, the wastewater produced in these industries contain aluminum oxide particles that need to be treated. In this work, the aluminum oxide suspension has been used as a model colloidal system to monitor the flocculation performance of sulfomethylated lignin having different molecular weights.[26] The changes in the physicochemical properties of the suspension, as well as the properties of the formed flocs, were monitored and correlated. The primary novelty of this work was the evaluation on the impact of sulfomethylated lignin's molecular weight on the flocculation of aluminum oxide particles.

6.3 Experimental section

6.3.1 Materials

Aluminum oxide (Al_2O_3) was purchased from Beta Diamond Products Inc., Yorba Linda, CA, USA. Aluminum oxide suspensions were prepared by dispersing aluminum oxide powders in deionized water to make a 25 g/L concentration, and the pH was adjusted to 6. The suspensions were gently stirred for 2 days to achieve complete hydration of the aluminum oxide surfaces before use. Softwood kraft lignin (SKL) with the molecular weight (Mw) of 9670 g/mol and negligible charge density (approximately zero) was received from FPInnovations, which was produced by the LignoForce™ technology. Nitric acid solution (65 wt%) was obtained from Caledon laboratory chemicals, Canada. Sodium metabisulfite ($Na_2S_2O_5$), polydiallyldimethylammonium chloride

(PDADMAC, 100–200 kg/mol), sodium hydroxide (NaOH, 97%), sulfuric acid (H_2SO_4, 98%), potassium chloride (KCl, 99%), polyacrylic acids (PAA) (35 wt% in H_2O, molecular weight of 15 kg/mol), and sodium nitrate ($NaNO_3$, 99%) were all purchased from Sigma-Aldrich company. Polyvinylsulfate potassium (PVSK) with a molecular weight of 170 kg/mol was purchased from Wako Chemicals Ltd., Japan. Formaldehyde (CH_2O) at 37 wt% concentration was also purchased from Sigma-Aldrich. Dialysis membrane of cellulose acetate (molecular weight cut-off of 1000 g/mol) was purchased from Spectrum Labs. Different molecular weights of poly (ethylene oxide) standards were purchased from Malvern Instruments Ltd. and used for the calibration of the instrument for the molecular weight analysis. Tetrafluoroethylene and silicon oil were received from Formulaction, and they were used as standards for calibrating a vertical scan analyzer.

6.3.2 Production of oxidized sulfomethylated lignin

The oxidized sulfometylated lignin (OSML) was produced using the method described by He and Fatehi.[16] The oxidation reaction was conducted by mixing 5 g of SKL with 40 wt% of nitric acid at 60 °C and 100 °C for 1 h at 500 rpm. Upon completion, the reaction mixtures were cooled to room temperature, and their pH was adjusted to 7. Generated products were then dialyzed with the membrane for several days while changing water in 12-h intervals and the product was then dried at 105 °C. The sulfomethylation reaction was carried out under the conditions of 4 wt% sodium hydroxide concentration to SKL, 1/1 mol/mol formaldehyde/SKL, and 0.5 mol/mol $Na_2S_2O_5$/SKL at 100 °C in 40, 60, and 180 min (as shown in Table 6.1). Samples were then neutralized, dialyzed, and dried as stated previously.[16] The product of this process was denoted as oxidized sulfomethylated lignin (OSML). The detail of these analyses is available in an earlier publication.[16]

Table 6.1. Oxidation and sulfomethylation of softwood kraft lignin

Name	Lignin (g)	Water (mL)	HNO_3 (40%)	Oxidation time (min)	Oxidation temperature (°C)	The molar ratio of CH_2O/SKL	The molar ratio of $Na_2S_2O_5$/SKL	Sulfomethylation temperature (°C)	Sulfomethylation time (min)	Yield (%)
OSML-1	25	100	100	60	100	1	0.5	100	60	33.2
OSML-2	25	100	100	60	100	1	0.5	100	40	32.4
OSML-3	25	100	100	60	100	1	0.5	100	180	28.8
OSML-4	5	30	10	60	60	1	0.5	100	180	38.0

6.3.3 Charge density analysis

The charge density of OSML samples and PAA were determined at pH 7 by a Particle Charge Detector (PCD 04, BTG Mütek GmbH) using a 0.005 mol/L PDADMAC solution as the titrant as

explained elsewhere.[27] The surface charge density of aluminum oxide particles was determined via following a back-titration method with the PCD as also detailed elsewhere.[27]

6.3.4 Surface area analysis

The surface area of aluminum oxide particle was measured by a surface area and pore size analyzer (NOVA 2200e, Quantachrome Instruments). In this experiment, approximately 0.05 g of the particle was kept at 105 °C overnight to remove any moisture. The specific surface area was then analyzed according to Brunauer-Emmett-Teller (BET) method via adsorption-desorption isotherms using nitrogen gas at −180 °C within the relative pressure range of 0.01 to 0.99.[28]

6.3.5 Molecular weight analysis

The molecular weight of OSMLs was measured via a gel permeation chromatography (GPC, Malvern GPCmax VE2001 Module + Viscotek TDA305 with multi-detectors) with columns of PolyAnalytic 206 and PAA203, using 0.1 mol/L $NaNO_3$ as solvent and eluent. OSMLs were dissolved in a solution of 0.1 mol/L $NaNO_3$ to produce samples at 5 g/L concentration and left under stirring at 150 rpm overnight. Afterward, the samples were filtered by 0.2-μm nylon filters, and then the filtrates were collected for molecular weight analysis. The measurements were performed at 35 °C with the eluent flow rate of 0.70 mL/min. The reflective index (RI) and intrinsic viscosity-differential pressure (IV-DP) signals were used for molecular weight analysis, and the results were determined against the results of standard poly (ethylene oxide) polymers.

6.3.6 Hydrodynamic diameter (d_h) measurement

A dynamic light scattering (DLS) instrument (Brookhaven BI200, USA) was used to measure the hydrodynamic diameter of OSML samples and PAA pursuant to the literature.[29,30] In this set of experiments, freshly prepared 0.1 g/L solutions were mixed with 1 mM NaCl at pH 6. DLS analysis was conducted at 90° scattering angle at 632 nm wavelength to measure the hydrodynamic diameter of lignin-based polymers in the solutions at 25 °C. Reported results are the mean values of the analysis conducted three times.

6.3.7 Adsorption analysis

The adsorption of OSML samples onto aluminum oxide particles was studied as a function of polymer dosage at two different temperatures (25 °C and 55 °C). In this experiment, different dosages of 2 mg/L and 128 mg/L of OSML were added to aluminum oxide suspension (25 g/L). The mixtures were incubated at 25 °C for 1 h and 150 rpm. Afterwards, the mixtures were centrifuged at 4500 rpm for 10 min and then filtered using nylon filters with the size of 0.45 μm

to separate the aluminum oxide particles from the suspensions. The concentration of OSML in the samples before and after the adsorption experiment was measured using UV-Vis spectrophotometer at a wavelength of 280 nm (Genesys 10S UV-Vis, Thermo Scientific).[31]

6.3.8 Zeta potential analysis

The zeta potential analysis of aluminum oxide suspensions was determined using a NanoB rook Zeta PALS (Brookhaven Instruments Corp, USA). In this experiment, different dosages of OSMLs (1 g/L) were added to aluminum oxide suspensions (25 g/L). The mixtures were incubated at 25 °C for 1 h and 150 rpm. Upon completion, samples were dispersed by ultrasonic for 1 min, and then 400 µL of them were transferred into 20 mL of 1 mM potassium chloride (KCl) solution (pH 6), which was initially filtered by a 0.2-µm nylon filter to make a solution with 0.5 g/L concentration. The experiments were performed three times, and the average values were reported in this study.[32,33]

6.3.9 Relative turbidity analysis

In this experiment, 450 mL of deionized water was added to the container of a dynamic drainage jar (DDJ) and passed through a 3-mm diameter plastic tube with the flow rate of 20 mL/min. The sample was circulated to the DDJ with the help of a peristaltic pump. The plastic tube was connected to a particle dispersion analyzer (PDA 3000, Rank Brothers Ltd) to track the changes in the relative turbidity of the suspension passing through the tube. Five hundred milliliters of a 25 g/L aluminum oxide suspension was added to the container of the DDJ at 300 rpm agitation and allowed to circulate through PDA. Different dosages of OSML (1 g/L) were added to the aluminum oxide suspension in the DDJ, and the turbidity of the suspensions was determined according to the literature.[34]

To investigate the flocs' strength, aluminum oxide suspension (25 g/L) was poured into DDJ and stirred at 300 rpm. After 100 s, OSML samples were added to the suspension, and the flocs started to form. After 500 s, the intensity of agitation was immediately enhanced to 3000 rpm and kept for 100 s, when flocs would break. Afterwards, the agitation intensity was reduced to 300 rpm and kept for 500 s to allow the flocs reformation and regrowth. This procedure repeated twice, and the flocculation behavior was evaluated. Flocculation index (FI), the ratio of the mean square root (RMS) to the direct (DC) voltage measured by PDA, was used to monitor the breakage and re-flocculation degree of the flocs.[14]

6.3.10 Flocculation analysis under dynamic conditions

The flocculation of OSML and aluminum oxide particles in suspensions was assessed using a focused beam reflectance measurement (FBRM, Mettler-Toledo E25). In this set of experiments, the chord length (i.e., the distance between the two edges of floc or a particle) was determined by the instrument. The data was acquired using 90 log-channels over the range of 1–1000 μm by the iC-FBRM software (version 4.4.29).[35,36] In this set of experiments, the laser probe having a diameter of 25 mm was placed in 200 mL of aluminum oxide suspension (25 g/L) stirring at 200 rpm. The beam was rotated around the axis of the probe at the scan speed of 2 m/s with the scan diameter of 5 mm. The focal point was set to −20 μm (as default) and scan duration was set at 3 s. In the FBRM analysis, two dosages of 3 and 15 mg/g of OSML polymers were added to the suspension, and the analysis was conducted for 30 min after adding OSML samples. The number-weighted median chord length (NW-Med-CL) and the square-weighted median chord length (SW-Med-CL) were evaluated as defined by iC-FBRM software (version 4.4.29).

6.3.11 Sedimentation analysis

A vertical scan analyzer, Turbiscan Lab Expert, Formulaction, France, was used for investigating the sedimentation behavior of the aluminum oxide particles in the absence or presence of OSML samples. The transmission and backscattering affinity of the suspensions were determined by Turbisoft 2.1 software. In this analysis, different dosages of OSML (1 g/L) samples were added to aluminum oxide suspensions (25 g/L), and the suspensions were stirred at 300 rpm for 2 min. Afterwards, the mixtures (20 mL) were transferred to the cylindrical glass cells of the instrument, and electroluminescent diode light with a wavelength of 880 nm started to scan the height of the cell every 25 s at 25 °C for 1 h.

The coagulation resulting from the interaction of OSML polymers and aluminum oxide particles leads the flocs to settle at the bottom of the cell as sediment while creating a clear layer on top of the cell. This settlement happens at different rates. The flocculation efficiency of OSML polymers was evaluated from the transmission data gathered from the top layer, while sedimentation thickness data was gathered from the backscattering results from the bottom layer. The sediment compactness was assessed from the ratio of the mass to volume for settled flocs after 1 h of experiments. Samples were gathered from the top part of the cell right after the addition of OSML and after 1 h of settling. These samples were then dried at 105 °C overnight to determine the concentration of the particles in the samples. These concentrations were used for assessing the

mass of the settled flocs. By considering the mass of settled flocs, the thickness of the sediment and cross-section area of the cell, the compactness of the settled particles was determined.

6.3.12 Scanning electron microscopy (SEM)-energy dispersive X-ray (EDX) spectroscopy

The scanning electron microscopy (SEM) analysis was carried out on the aluminum oxide particles with or without treating with OSML by a Hitachi SU-70 (Hitachi Ltd., Chiyoda, Tokyo, Japan) microscope at 10 kV. In this experiment, aluminum oxide was mixed with water and hydrated at pH 6 overnight to be used as a blank sample. In addition, OSMLs and aluminum oxide were mixed together at 150 rpm and 3 mg/g dosage of OSML/particles in Erlenmeyer flasks at 25 °C for 1 h. The samples were then collected without filtration, freeze-dried, and then were carbon-coated for SEM analysis.[37] The elements of C, O, and Al on the surface of particles were detected using an energy dispersive X-ray EDX spectroscopy (Oxford Aztec 80 mm/124 ev) that was attached to the SEM instrument.

6.4 Results and discussion

6.4.1 Properties of aluminum oxide suspension and OSML polymers

The hydrodynamic diameter (d_h) of aluminum oxide particles in the suspension was 1.54 μm. The specific surface area of aluminum oxide particle was 100.3 m^2/g with the average pore size of 4 nm and the total pore volume of 0.2 mL/g. The zeta potential of the aluminum oxide suspension was + 26 mV at pH 6. The properties of OSMLs were presented in Table 6.2. The charge density of the three OSML polymers was similar (3.5 ± 0.1 μeq/g). However, a notable difference was observed in their molecular weight. The results also showed that the polydispersity of the samples was slightly different, which was ascribed to different severity of oxidation reactions for OSML production (Table 6.1). It was reported that polyacrylic acid (PAA), a linear polymer with the molecular weight of 296 kg/mol, had a dh of 16.6 nm,[38] while lignin used in this study with a molecular weight of 26 kg/mol had a d_h of 27.07 nm. Polydiallyldimethylammonium chloride (PDADMAC) with the molecular weight of 44.6 kg/mol was reported to have a d_h of 27.5 nm and mean diffusion coefficient of 1.76×10^{-7} cm^2/s [39]. Mean diffusion coefficients of particles were calculated following Stokes-Einstein equation, which provided information about the average mobility of the polymers.[40-42] OSML-4 with the highest molecular weight had the smallest diffusion coefficient. The lower diffusion and higher dh of lignin than PDADMAC may provide evidence for the three-dimensional structure of OSML.

Table 6.2. Properties of OSML polymers

Label	OSML-1	OSML-2	OSML-3	OSML-4
Charge density (µeq/g)	$-3.5 (\pm 0.1)$	$-3.5 (\pm 0.1)$	$-3.4 (\pm 0.1)$	$-3.5 (\pm 0.1)$
Mw (kg/mol)	26	29	34	46
Mn (kg/mol)	14	17	20	31
Mw/Mn	1.83	1.68	1.72	1.48
Hydrodynamic diameter (nm)	27.07	31.20	35.95	41.43
Mean diffusion coefficient (cm^2/s) $\times 10^{-7}$	1.84	1.60	1.39	1.20

6.4.2 Adsorption of OSMLs on aluminum oxide

The adsorption isotherms of OSML polymers on aluminum oxide particles at 25 °C is demonstrated in Fig. 6.1. The OSML adsorption amounts were enhanced by increasing the OSML dosages and reached plateau with the OSML dosages higher than 32 mg/L. The results also suggest that OSML-4 had higher adsorption, which may be due to its higher molecular weight supporting the interaction of this polymer with the aluminum oxide particles.[43]

The particles' surface charge density (without polymer) was experimentally measured to be + 3.1 µeq/g as explained in the experimental section. Considering the charge density of OSMLs, their adsorption levels and surface charge density of the particles, the surface charge density of particles can be estimated after polymer adsorption. The surface charge density of aluminum oxide particles was neutralized when the adsorption amount was 0.86 mg/g and became anionic at higher adsorption dosages. This indicates that the adsorption amount of 0.86 mg/g was sufficient to cover all the positive charges on the aluminum oxide particles.
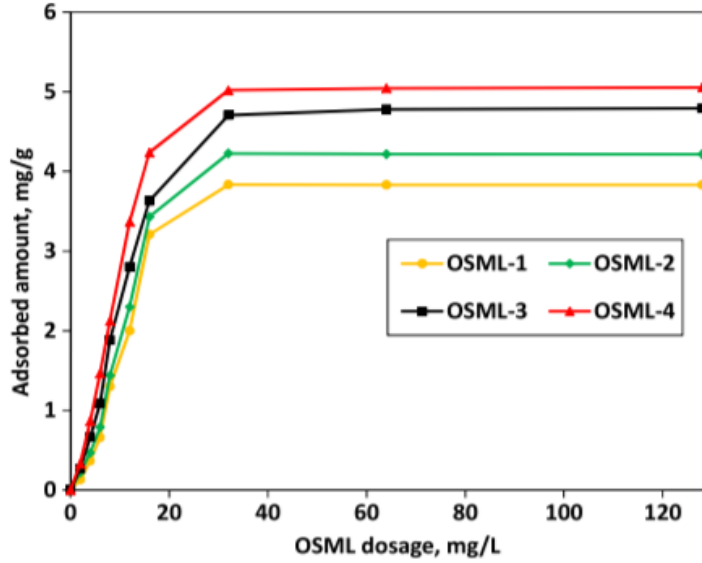
Fig. 6.1. Adsorption isotherm of OSML on aluminum oxide particles.

For elucidating the adsorption mechanism of the OSML polymers on the aluminum oxide particles, the results in Fig. 6.1 were fitted into adsorption isotherm models of Langmuir and Freundlich (Eq. (6.1) and (6.2), respectively), and the correlation functions were listed in Table 6.3.

Langmuir: $\frac{C_e}{Q_e} = \frac{1}{k_a Q_{max}} + \frac{C_e}{Q_{max}}$ (6.1)

Freundlich: $\log Q_e = \log k_f + \left(\frac{1}{n_f}\right) \log C_e$ (6.2)

In these equations, C_e is the concentration of unadsorbed OSLMs in the suspension (mg/L), Q_e is the corresponding adsorbed amount of polymer on the particle's surface (mg/ g), Q_{max} is the maximum adsorption of OSMLs on the particles (mg/g), k_a is the constant of the Langmuir isotherm (L/mg), k_f is the constant of the Freundlich isotherm (L$^{1/n}$ mg$^{(1-1/n)}$/g), and $1/n$ is the Freundlich exponent. The Langmuir model is assumed a saturated monolayer adsorption while there is no interaction between the adsorbed polymers, and all the adsorption sites are identical on the surface for adsorption (i.e., adsorption sites have the same energy of adsorption). The Freundlich model, on the other hand, is assumed a multi-layer adsorption mechanism, in which adsorption amount enhances with the increment of the concentration of the polymers.[44-47]

It can be inferred from Table 6.3 that OSML adsorption was fitted into Langmuir adsorption model better than into Freundlich model, indicating the saturated monolayer adsorption of the polymers on the aluminum oxide surface. These results are consistent with the literature reports, in which

the Langmuir model fitted into the adsorption of the PAA polymer with the molecular weight ranging from 2 to 120 kg/mol on the aluminum oxide particles.[24]

These results suggest that the three-dimensional structure of lignin did not affect its adsorption pattern, and similar to linear polymers, e.g., PAA, OSML had a monolayer adsorption configuration.

Table 6.3. Parameters of isotherm models obtained via fitting data of Fig. 6.1 into Eqs. 6.1 and 6.2

Models	Parameters	OSML-1	OSML-2	OSML-3	OSML-4
Langmuir	Q_{max}	3.83	4.22	4.79	5.05
	k_a	1.35	1.24	1.19	1.15
	R^2	0.78	0.91	0.94	0.96
Freundlich	n_f	1.26	1.41	1.51	1.65
	k_f	0.17	0.26	0.36	0.48
	R^2	0.75	0.79	0.79	0.77

6.4.3 Effect of OSML on zeta potential

Figure 6.2 shows the zeta potential of aluminum oxide suspension as a function of adsorbed OSML polymers. The zeta potential of aluminum oxide suspension without OSML was measured to be + 26 mV at pH 6. By adsorbing anionic OSML polymers on aluminum oxide particles, the zeta potential of the aluminum oxide suspension dropped, regardless of the OSML molecular weight. OSML-4 adsorbed more than other OSMLs on the particles, which led to more reduction in the zeta potential at a lower dosage (Fig. 6.2). These results are supported by those reported in the literature in that concentrating poly (diallyldimethylammonium chloride) (PDADMAC) and polyacrylamide polymer from 0.16 to 3.2 mg/L raised the zeta potential of the clay suspension from − 37.5 to + 42.1 mV.[48]

250
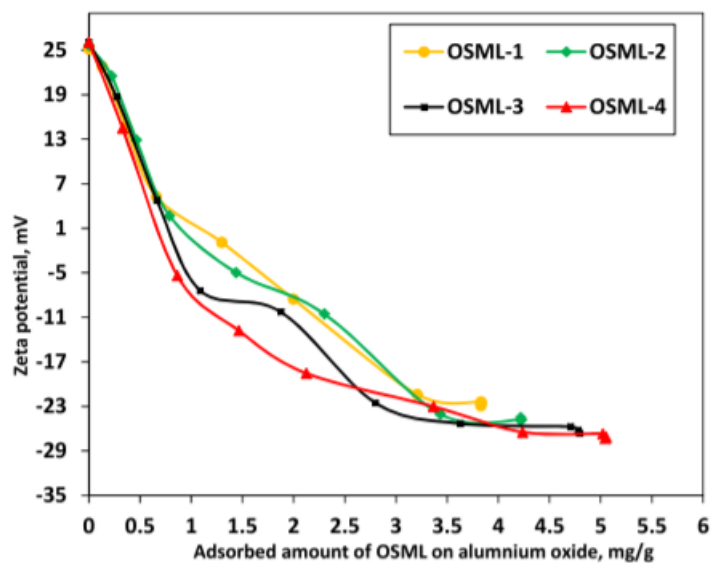
Fig. 6.2. Effect of adsorbed OSML on the zeta potential of aluminum oxide suspension, which was carried out under the conditions of pH 6, 1 h, 25 °C, and 25 g/L of aluminum oxide concentration

Figure S6.1 in the Supplementary materials includes the results of the changes in the zeta potential of the suspension as a function of the theoretical surface charge density of the particles. The theoretical surface charge density is the calculated surface charge of the particles, while zeta potential is the potential of a diffused double layer on the particles. The surface charge density of aluminum oxide particles was + 3.1 μeq/g when the zeta potential of the suspension was + 26 mV. The zeta potential of the suspension became neutral when the surface charge density of particles was between + 1 and − 1.5 μeq/g. This implies that the charge neutralization played a role in the flocculation. By increasing the OSML adsorbed amount, the particle's surface charge density and the zeta potential were rendered cationic, illustrating a direct relationship between the suspension's zeta potential and the theoretical surface charge density. Also, OSML-4 with a higher molecular weight was observed to affect the charge density of the particles more than that of lower molecular weight ones because of its higher adsorption.

6.4.4 Relative turbidity

To assess the flocculation efficiency of OSML on aluminum oxide particles under the dynamic condition, the relative turbidity of OSML/aluminum oxide suspension was investigated. Figure 6.3 shows the relative turbidity of the suspension as a function of adsorbed OSML on the aluminum oxide particles. With the addition and adsorption of the OSML polymers, the relative turbidity of the suspension dropped for all four samples. This decline in turbidity was more pronounced for

the OSML-4 than for the others, which may stem from its higher adsorption on the particles (Fig. 6.1). The 3 mg/g adsorption of the polymers seemed to be sufficient for the maximum reduction in the suspension's turbidity and thus was chosen as an optimum dosage for the polymers. By adsorbing more of the OSML polymers, the electrostatic repulsion was enhanced among the aluminum oxide particles leading to the restabilization of the particles in the suspension and cloudiness of the suspension. In one study, PAA with the molecular weight ranging from 2 to 50 kg/mol was used as a flocculant for aluminum oxide suspension. It was revealed that, by increasing the molecular weight of the PAA, the flocculation efficiency of the suspension was improved by about 25 %.[26]
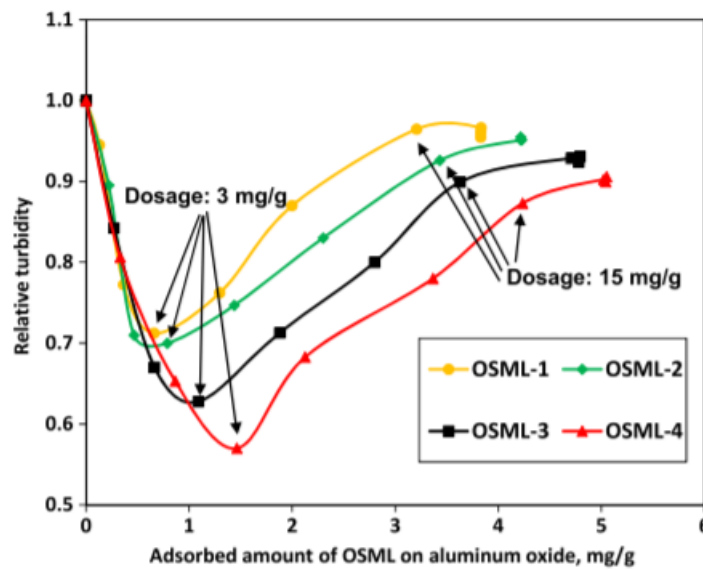
Fig. 6.3. Effect of the adsorbed OSML polymers on the relative turbidity of the aluminum oxide suspension conducted at 300 rpm, pH 6, 25 °C, and 25 g/L of aluminum oxide concentration

6.4.5 The relationship between the zeta potential and relative turbidity

Figure 6.4 shows the relative turbidity of aluminum oxide suspension as a function of zeta potential. This figure was plotted to evaluate the dominant flocculation mechanism in the suspension. As seen, the minimum relative turbidity of aluminum oxide suspension was occurred at around − 5 mV of zeta potential for the samples of OSML-1 and OSML-2, which reveals that the charge neutralization may be the dominant flocculation mechanism (Fig. 6.5). For the OSML-3 and OSML-4 with higher molecular weights, it can be seen that the lowest suspension turbidity occurred when the zeta potential was reversed (around − 12 mV). This may reveal that aside from

the charge neutralization, patching mechanism may have played a role in the flocculation as shown in Fig. 6.5.[49]
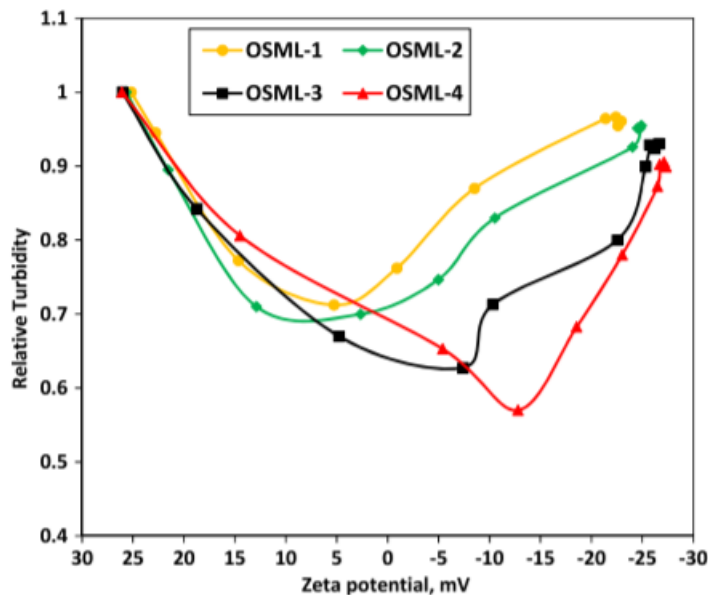
Fig. 6.4. Relationship between the relative turbidity and zeta potential of aluminum oxide suspension (25 g/L aluminum oxide suspension, pH 6)

Figure S6.2 in the Supplementary materials indicates the relative turbidity of aluminum oxide suspension as a function of the theoretical surface charge density of the particles. A maximum suspension clearness was observed when the theoretical surface charge density of the aluminum oxide particles was 0.8, 0.3, − 0.6, and – 2 µeq/g for OSML-1, OSML-2, OSML-3, and OSML,4, respectively. Herein, the patching mechanism was proved to be the flocculation mechanism for OSML-4 since the lowest relative turbidity was achieved when the surface charge density of the particles was reversed to around − 2 µeq/g. In one study, the xylan-METAC (2-(methacryloyloxy) ethyl trimethylammonium chloride) polymer was used to remove kaolin particles. The bridging and patching mechanism was revealed to be dominant for the flocculation since the maximum reduction in relative turbidity was observed while the theoretical particle surface charge density was around 12 µeq/g and the suspension's zeta potential was around 60 mV.[14]
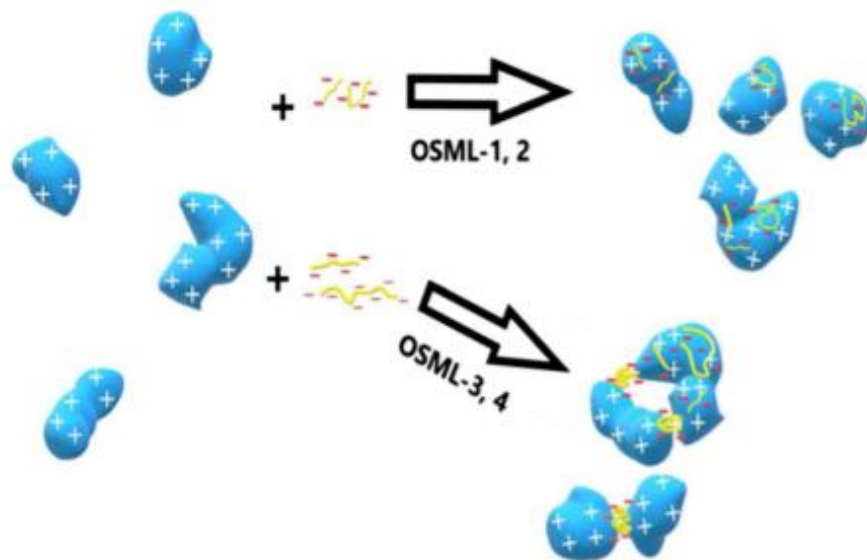
Fig. 6.5. Flocculation mechanism based on charge neutralization for OSML-1 and OSML-2 and charge neutralization associated with patching for OSML-3 and OSML-4

6.4.6 Floc strength under different mixings

The flocculation index of aluminum oxide suspension was studied under various mixing rates (Fig. 6.6) to explore the strength and regrowth of the produced flocs. As stated earlier, flocculation index, the ratio of RMS/DC, is the indirect representation of the floc size in the suspension.[50] By adding 3 mg/L of OSML samples to the aluminum oxide suspension at 300 rpm, the flocculation index rose to around 1 for OSML-3 and OSML-4 and around 0.7 for OSML-1 and OSML-2. By increasing the shear rate from 300 to 3000 rpm and keeping this shear rate for 100 s, the flocculation index dropped for all OSML polymers, presenting the floc breakage via intensifying the shear rate. By reducing the shear rate, the flocs were reformed, and the particle size was increased in the suspension. This demonstrates a relatively reversible process and implies that the charge neutralization and patching may be the dominant flocculation mechanisms since the broken flocs were able to regrowth at 300 rpm.[51,52] By repeating this cycle, flocculation index behaved similarly but each time, a lower flocculation index was obtained, which reveals that the chance of the flocculation suppressed by breaking the flocs each time. Wang and coworkers used xylan-METAC polymer to flocculate kaolin and bentonite particles.[14] As reported, irreversible flocculation was observed for bentonite particles after the first breakage of the flocs due to the low

254

adsorption of the polymer onto the particle surface. While, relatively reversible, flocculation was observed for the kaolin particles even after the second breakage.[14]
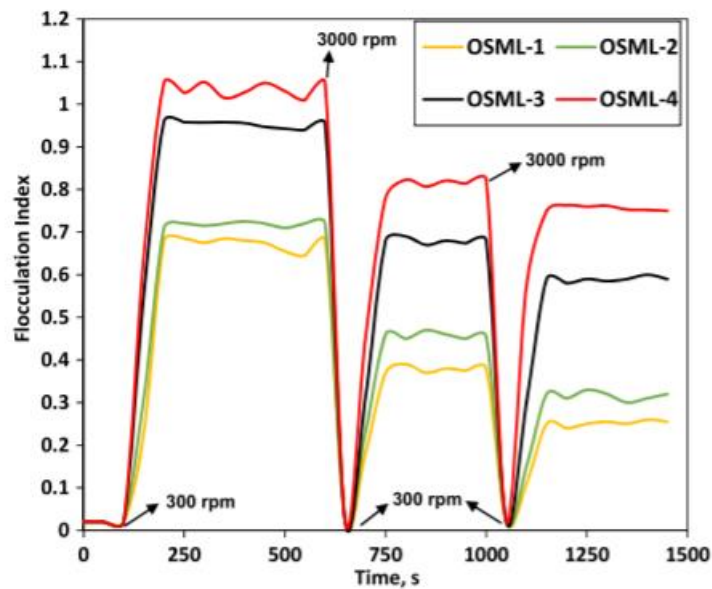
Fig. 6.6. The strength of the flocs produced by the adsorption of 3 mg/g OSML polymers on aluminum oxide particles (25 g/L) at different shear rates performed at 25 °C

6.4.7 Flocs characterization

Characteristics of the flocs in flocculation are critical in monitoring the efficiency of the flocculation process. The unweighted chord length distribution of flocs formed between OSML and aluminum oxide particles at different dosages of 3 and 15 mg/g of OSML polymers in the aluminum oxide suspension is shown in Fig. 6.7.

As can be seen, aluminum oxide particles had around 2020 counts with the mean size of 10 μm. By adding 3 mg/g of the polymers, the chord length was ramped up, and the number of the particles in the suspension diminished. This momentous change provides evidence for flocculation of the aluminum oxide particles with OSML polymers.[39] Furthermore, OSML-1 with a lower molecular weight showed the minimum, and OSML-3 and OSML-4 with higher molecular weights showed the maximum flocculation performance via increasing the chord length distribution and reducing the particle's concentration. It is also evident that at the dosage of 15 mg/g, the number of smaller flocs boosted in the suspension, which indirectly depicts that the flocs became disintegrated at this dosage.[53]
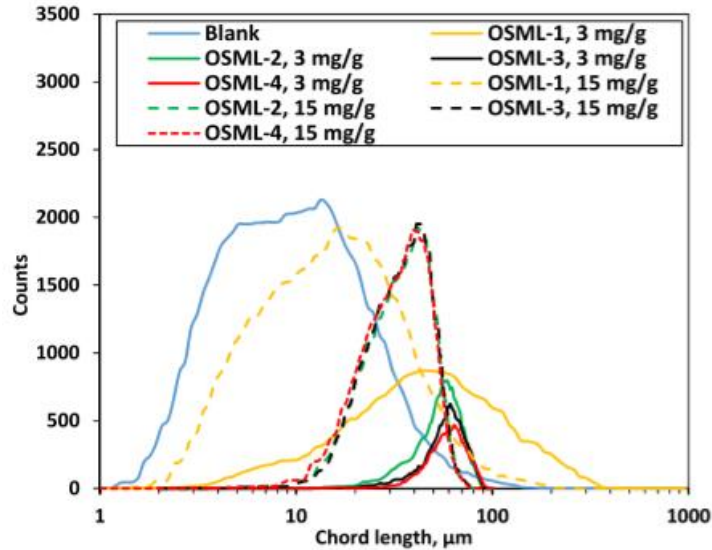
Fig. 6.7. Unweighted chord length distribution of aluminum oxide flocs formed under the treatments of OSMLs (dosages of 3 mg/g and 15 mg/g)

6.4.8 Settling efficiency

Figure 8 depicts the transmission of the suspension as a function of time. As can be seen, clearer supernatant was obtained with settling time for all the samples in 3 mg/g dosage. The transmission of the blank sample (25 g/L) suspension was slightly exceeded to around 6.8% in 1 h of analysis. OSML-4 showed the best performance among the samples with 31% transmission at 3 mg/g dosage in 1 h. It is seen that OSML-4 led to a high supernatant transmission implying a faster settlement at this dosage.[52] However, the higher dosage of 15 mg/g hampered the sedimentation of the particles, which is due to re-stabilization of the flocs and particles in the suspension at this dosage. These results can be correlated with the data in Fig. 6.6 as the maximum transmission in the samples was achieved when the suspension zeta potential was fairly neutral. It is also evident that the system's zeta potential was raised to − 20 mV with 15 mg/g addition of the polymers, which raised the suspension turbidity (Fig. 6.3) and thus reduced the transmission of the suspension.

Fig. 6.8. Supernatant transmission of aluminum oxide suspension as a function of time (aluminum oxide concentration 25 g/L, 1 h of scanning time)

Analyzing the sedimentation kinetics is essential for monitoring the flocculant performance in a non-stirring state. In this work, the flocs' settling velocity and the compactness of the sediment were evaluated at different dosages, and the results are depicted in Table 6.4. As seen, the sediment compactness of the aluminum oxide sample reduced by adding 3 mg/g of OSML polymers. The most compact sediment was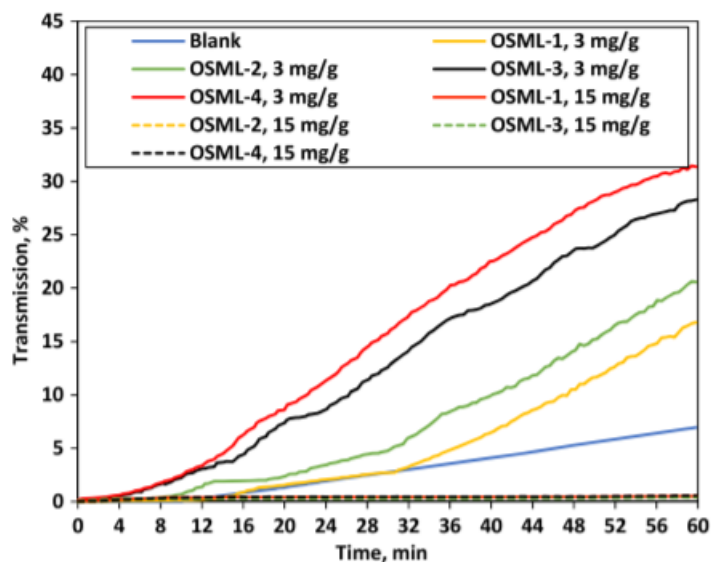 obtained using OSML-1, and the loosest was observed using OSML-4. The reason may be attributed to the molecular weight of the polymers as OSML-1 with a lower molecular weight produced smaller and more compact flocs than OSML-4 with a higher molecular weight, which produced larger and more complex but looser flocs.[54] By dosing 15 mg/g OSML in the suspension, the sediment became more porous. The reason may stem from the repulsion force between the particles and the reversal in the suspension's zeta potential (Fig. 6.4), which hinders the sedimentation of the aluminum oxide particles (Fig. 8). In one study, the polyethyleneimine flocculant dosage upsurging from 0.004 to 0.4 g in the kaolin suspension led to suspension of particles due to the elevated repulsion force, achieving a sediment with lower compactness.[55]

The settling velocity of the aluminum oxide particles was enhanced with OSML polymers (3 mg/g) from around 82 to around 137, 140, 183, and 203 mm/h for OSML-1, OSML-2, OSML-3, and OSML-4, respectively. This reveals the size enlargement by agglomeration of the particles (Fig. 6.7) accelerated the sedimentation velocity of the particles (Fig. 8). The polymer dosage in the suspension (15 mg/g) hampered the flocculation, as observed in Figs. 3 and 7, and thus suppressed

257

the particles' settling velocity. In one study, goethite particles were flocculated using ammonium polyacrylate and observed that larger flocs were settled faster than the smaller ones.[56]

Table 6.4. Settling velocity and compactness of the formed flocs after 1 h of treatment

Models	Dosage, mg/g	Sediment compactness (g/L)	Settling velocity (mm/h)
Blank	–	118 ± 2.8	82.54 ± 3.7
OSML-1	3	96 ± 3.1	137.75 ± 2.8
OSML-2	3	91 ± 1.8	140.23 ± 7.5
OSML-3	3	87 ± 5.1	183.45 ± 5.4
OSML-4	3	80.3 ± 2.8	203.7 ± 8.1
OSML-1	15	94.7 ± 5.1	45.6 ± 4.5
OSML-2	15	71 ± 4.2	63.15 ± 6.15
OSML-3	15	56 ± 3.3	59.5 ± 2.4
OSML-4	15	38.1 ± 6.5	55.4 ± 4.4

6.4.9 SEM analysis

Figure 9 displays the SEM analysis of aluminum oxide particles with and without treating by OSMLs. As observed, the blank sample (aluminum oxide particles without any OSML) consists of Al and O. The small peak of C in this sample comes from the coating of the sample with carbon for SEM analysis. By adding different OSML polymers, the carbon content of the particles was increased, which confirms the adsorption of OSMLs on the aluminum oxide particles. The SEM images also show larger size of OSML-treated particles than blank particles.
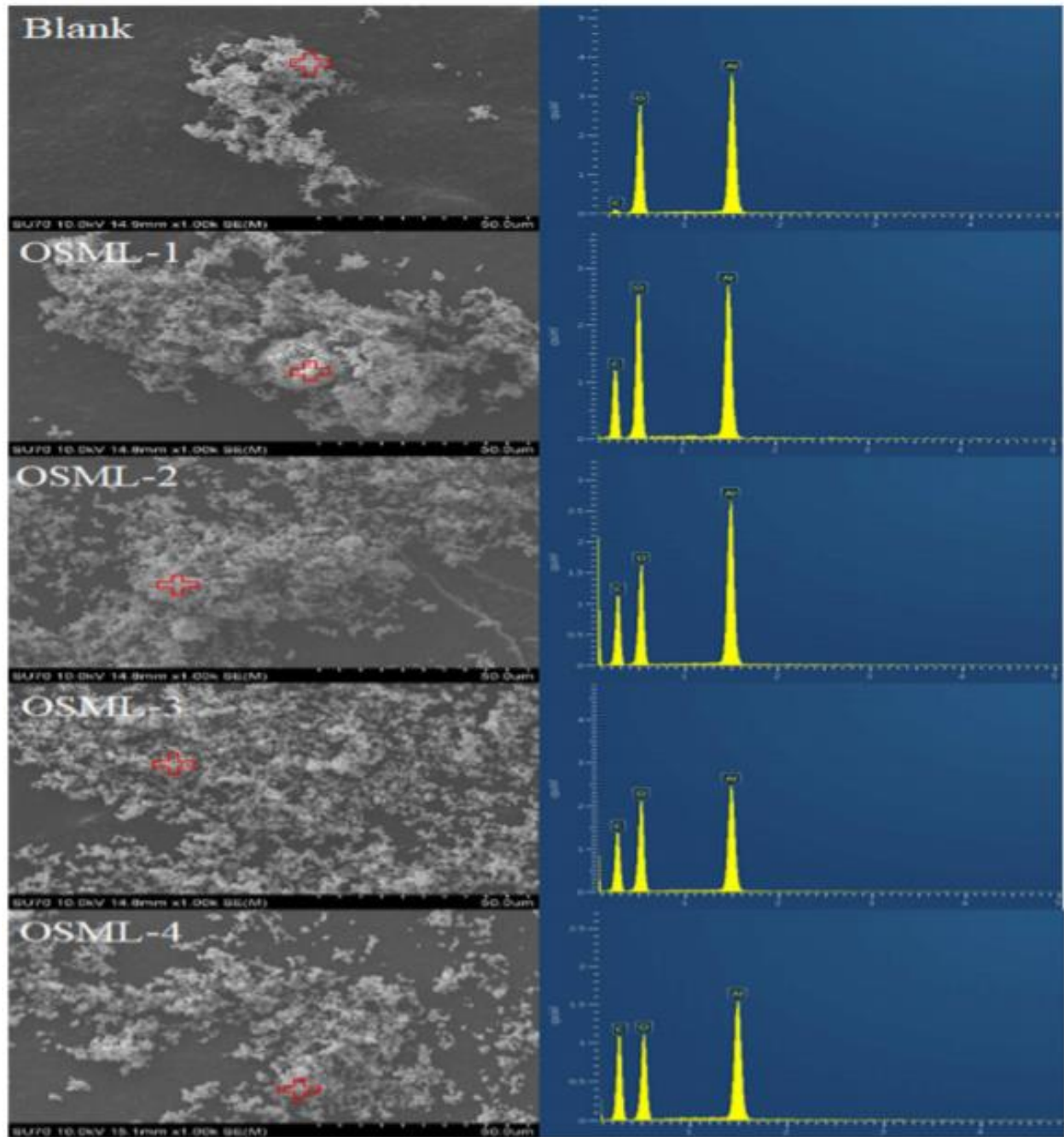
Fig. 6.9. SEM and EDX image of Blank, OSML-1, OSML-2, OSML-3, and OSML4 (with magnification of × 1000)

6.4.10 OSML flocculation functionality and the 3D structure impact

The produced OSML samples were performed well as a flocculant for aluminum oxide suspension. The adsorption of the polymers on the particles (Fig. 6.1) paved the way to accelerate the

flocculation by producing large size flocs (Fig. 6.7) and clarifying the suspension (Figs. 3 and 8) at lower dosages.

As highlighted in the literature,[57] the flocculant structure is critical in flocs' formation. For example, linear polymers were observed to form pliable coils in solutions while branched polymers with complex structures were reported to produce more compact structures.[58] In using linear polymers as flocculants, the inter and intramolecular bonds in coiled polymers suppress their interaction with the other particles, leading to a lower flocculation performance. As illustrated in Table 6.2, OSMLs had larger dh than linear polymers, such as PDADMAC and PAA, which confirmed the three-dimensional structure of the lignin-based polymers. This phenomenon ultimately helps with its flocculation as it may be able to interact with more colloidal particles in suspensions. However, further studies need to be performed to confirm this phenomenon.[59]

6.5 Conclusions

In this work, the flocculation performance of OSML polyelectrolytes having a similar charge density of 3.5 µeq/g, but various molecular weights, on oppositely charged aluminum oxide particles was assessed. OSML-4 with the highest molecular weight of 46 kg/mol had the maximum adsorption of 5 mg/g and changed the zeta potential of the suspension to neutral more greatly than the other OSMLs. The suspension's relative turbidity dropped the most (to 0.5) by OSML-4 ascribing to higher adsorption of OSML on the aluminum oxide particles. OSML had monolayer adsorption characteristics on the particles. By extending the flocculant's molecular weight, the chord length and counts of the produced flocs were raised and dropped, respectively. A relatively reversible flocculation mechanism was observed in using OSML polymers when exposing the flocs to different shear rates. By analyzing the flocculation performance under static conditions, the suspension became clearer for OSML with the higher molecular weight. The results reveal charge neutralization and patching mechanisms for the flocculation of the aluminum oxide suspension with the OSML polymers. The results also confirmed that the higher dosage of 15 mg/g induced repulsion force between particles that prevented their flocculation and settling.

6.6 References

1) R. Kaur and S. K. Uppal, Colloid Polym. Sci., 2015, 293, 2585–2592.

2) J. Chen J, A. E. Kazzaz, N. AlipoorMazandarani, Z. H. Feizi and P. Fatehi, Molecules, 2018, 23, 868.

3) E. M. De Oliveira, S. D. A. Sanchez, M. H. Bettega, A. P. Natalense, M. A. Lima and M. T. D. N. Varella, Phys. Rev. A, 2012, 86, 020701.

4) F. Kong, K. Parhiala, S. Wang and P. Fatehi, Eur. Polym. J., 2015 67, 335–345.

5) W. He, Y. Zhang and P. Fatehi, Colloids Surf. A Physicochem. Eng. Asp., 2016, 503, 19–27.

6) L. I. Tolosa, A. J. Rodríguez-Malaver, A. M. González and O. J. Rojas, J. Colloid Interface Sci., 2006, 294, 182–186.

7) D. Yang, L. X. Zhong, T. Q. Yuan, X. W. Peng and R. C. Sun, Ind. Crop Prod., 2013, 43, 141–149.

8) H. A. Aziz, S. Alias, M. N. Adlan, A. H. Asaari and M. S. Zahari, Bioresour. Technol., 2007, 98, 218–220.

9) J. Wei, B. Gao, Q. Yue and Y. Wang, Chem. Eng. J., 2009, 151, 176–182.

10) A. Szyguła, E. Guibal, M. A. Palacín, M. Ruiz and A. M. Sastre, J. Environ. Manag. 2009, 90, 2979–2986.

11) R. Fang, X. Cheng and X. Xu, Bioresour. Technol., 2010, 101, 7323–7329.

12) Y. I. Chang and K. H. Liu, Colloid Polym, Sci., 2010, 288, 223–231.

13) D. J. Walsh and J. Anderson, Colloid Polym. Sci., 1980, 258, 883–890.

14) S. Wang, M. K. Konduri, Q. Hou and P. Fatehi, RSC Adv. 2016, 6, 40258–40269.

15) M. K. Konduri and P. Fatehi, Colloids Surf. A Physicochem. Eng. Asp., 2018, 538, 639–650.

16) W. He and P. Fatehi, RSC Adv., 2015, 5, 47031–47039.

17) J. C. Flesch, P. T. Spicer and S. E. Pratsinis, AICHE J., 1999, 45, 1114– 1124.

18) P. T. Spicer and S. E. Pratsinis, Water Res., 1996, 30, 1049–1056.

19) J. Gregory, The role of floc density in solid-liquid separation, Filtr. Sep., 1998, 35, 367–371.

20) S. A. Lee, A. G. Fane, R. Amal and T. D. Waite, Sep. Sci. Technol., 2003, 38, 869–887.

21) I. G. Droppo, D. E. Walling and E. D. Ongley, IAHS Publ., 1998, 249

22) B. Camenen, J. Hydraul. Eng., 2007, 133, 229–233.

23) F. Xiao, P. X. R. Yi, X. R. Pan, B. J. Zhang and C. Lee, Desalination, 2010, 250, 902–907.

24) M. Wisniewska, S. Chibowski and T. Urban, J. Colloid Interface Sci., 2009, 334, 146–152.

25) T. K. Sheel, P. Poddar, A. B. M. W. Murad, A. J. M. T. Neger and A. M. S. Chowdhury, J Adv. Chem. Eng., 2016, 6, 1000152.

26) K. K. Das and P. Somasundaran, Colloids Surf. A Physicochem. Eng. Asp., 2003, 223, 17–25.

27) M. K. Konduri, F. Kong and P. Fatehi, Eur. Polym. J., 2015 70, 371–383.

28) M. Dashtban, A. Gilbert and P. Fatehi, Bioresour. Technol., 2014, 159, 373–379.

29) W. Li, Q. Wang, S. W. Cui, X. Huang and Y. Kakuda, Food Hydrocoll., 2006 20, 361–368

30) H. Jia, C. Zhong, F. Huang, C. Wang, L. Jia, H. Zhou and P. Wei, ChemPlusChem, 2013, 78, 451–458.

31) D. Fengel and G. Wegener,Walter de Gruyter, Berlin and New York, 1984, p 613

32) A. Saeed and P. Fatehi, Y. Ni, Carbohydr. Polym., 2011, 86, 1630–1636.

33) L. Klapiszewski, T. J. Szalaty, B. Kurc, M. Stanisz, B. Zawadzki, A. Skrzypczak and T. Jesionowski, ChemPlusChem, 2018, 83, 361–374.

34) H. Xiao, Z. Liu and N. Wiseman, J Colloid Interface Sci., 1999, 216, 409–417.

35) H. G. Merkus, Particle size measurements: fundamentals, practice, quality, Vol. 17. Springer, Pijnacker, 2009, p 539

36) C. Negro, A. Blanco and J. Tijero, AICHE J., 2005, 51, 1022–1031.

37) A. E. Kazzaz, Z. H. Feizi, F. Kong and P. Fatehi, Colloids Surf. A Physicochem. Eng. Asp., 2018, 556, 218–226

38) D. Reith, B. Müller, F. Müller-Plathe and S. Wiegand, J. Chem. Phys., 2002, 116, 9100–9106.

39) Y. Sun, Z. Liu and P. Fatehi, J. Environ. Manag., 2017 200, 275–282.

40) B. H. Zimm, J. Chem. Phys., 1956, 24,269–278.

41) M. Kaszuba, D. McKnight, M. T. Connah, F. K. McNeil-Watson and U. Nobbmann, J. Nanopart. Res., 2008, 10, 823–829.

42) S. Viel, D. Capitani, L. Mannina and A. Segre, Biomacromolecules, 2003, 4, 1843–1847.

43) J. A. Davis and R. Gloor, Environ. Sci. Technol., 1981, 15, 1223–1229.

44) P. C. Hiemenz and R. Rajagopalan, Principles of colloid and surface chemistry. CRC press, Boca Raton, 1997.

45) T. E. Cosgrove, Colloid science: principles, methods and applications, Vol 2. Wiley, Bristol, 2010, p 374.

46) H. K. Chung, W. H. Kim, J. Park, J. Cho, T. Y. Jeong and P. K. Park, J. Ind. Eng. Chem., 2015, 28, 241–246.

47) B. Chen, Z. Zhu, J. Ma, Y. Qiu and J. Chen, ChemPlusChem, 2015, 80, 740–748.

48) G. Petzold, M. Mende, K. Lunkwitz, S. Schwarz and H. M. Buchhammer, Colloids Surf. A Physicochem. Eng. Asp., 2003, 218, 47–57.

49) Z. Yang, H. Yang, K. Li, A. Li and R. Cheng, Water Res., 2013, 47, 3037–3046.

50) D. Chen and T. G. van de Ven, Colloids Surf. A Physicochem. Eng. Asp. 2016, 504, 11–17.

51) M. A. Yukselen and J. Gregory, Int. J. Miner Process, 2004, 73, 251–259.

52) Y. D. Yan, S. M. Glover, G. J. Jameson and S. Biggs, Int. J. Miner Process, 2004, 73, 161–175.

53) A. R. Heath, P. D. Fawell, P. A. Bahri and J. D. Swift, Part Part Syst. Charact., 2002, 19, 84–95.

54) H. Lu, Fundamental study on novel synthetic polymer systems for fine particles settling. Dissertation, University of Alberta, 2016.

55) L. Avadiar, Y. K. Leong and A. Fourie, Wellington, New Zealand, 1266. ISBN: 9781922107596, 2012.

56) G. Liang, W. Chen, A.V. Nguyen and T. A. Nguyen, J. Colloid Interface Sci., 2018, 517, 230–238.

57) E. Carissimi and J. Rubio, Miner Eng. 2015, 70, 20–25.

58) R. Rahmani, B. Shahmoradi and A. Maleki, RJET, 2015, 9, 261–267.

59) W. B. Wu, J. Gu, Y. Jing, X. F. Zhou and H. Q. Dai, Bioresources, 2012, 7, 4926–493.

6.7 Electronic supplementary material

Interaction of sulfomethylated lignin and aluminum oxide

Armin Eraghi Kazzaz, Zahra Hosseinpour Feizi , Pedram Fatehi*

Chemical Engineering Department, Lakehead University, 955 Oliver Road, Thunder Bay, Ontario P7B 5E1, Canada

* Corresponding author, email: pfatehi@lakeheadu.ca; tel: 807-343-8697; fax: 807-346-7943
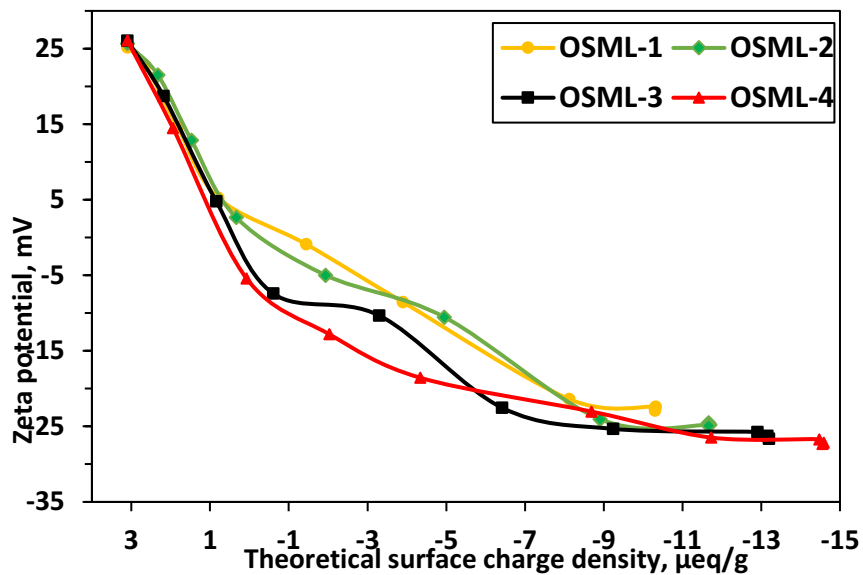
Fig. S6.1. Zeta potential of aluminum oxide suspensions as a function of the theoretical surface charge density of the particles, carried out under the conditions of pH 6, 1 h, 25 °C and 25 g/L of aluminum oxide concentration
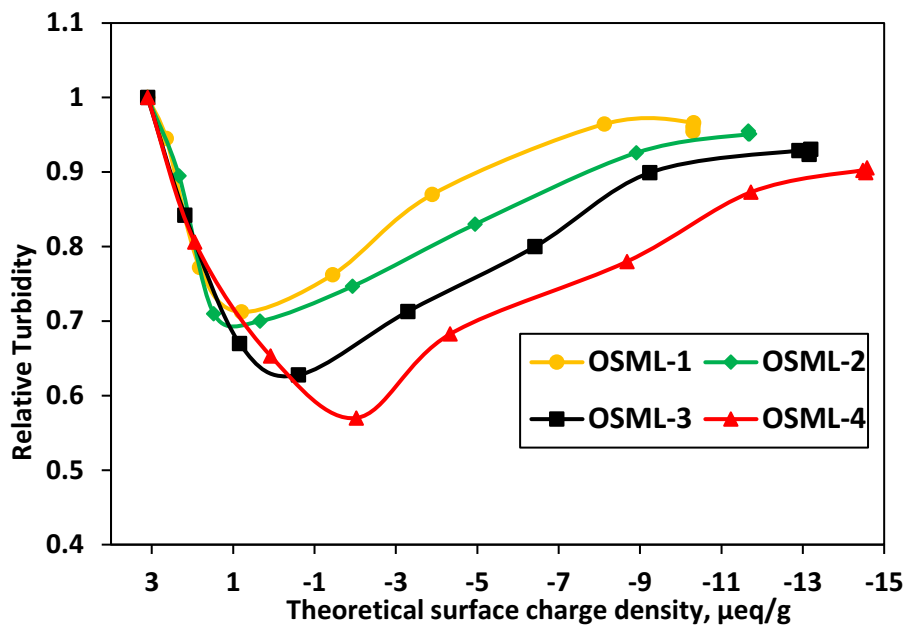
Fig. S6.2. Correlation between the relative turbidity and theoretical surface charge density (25 g/L aluminum oxide suspension, pH 6)

Chapter 7. Conclusion and Future directions

7.1 Summary of conclusions

In the review study, various modification routes of lignin were comprehensively reviewed while the pros and cons of each modification were highlighted. Distinguishing and knowing the precise manner of the modification occurring either on the aliphatic or aromatic part of lignin can facilitate the use of lignin in various processes. In conclusion, although many studies have covered the conduct of various modifications on lignin, there is still room for performing other modification methods to produce even more value-added products from lignin. Moreover, to expand the functionality of lignin, the biological application of lignin could also be studied more comprehensively.

In one of our research studies, two polymers of lignin-3-sulfopropyl methacrylate (L-S), and poly (vinyl alcohol-*co*-vinyl acetate)-3-sulfopropyl methacrylate (PVA-S), one a bio-based polymer and one a synthetic polymer, respectively, were produced with similar negative charge density and molecular weight. To reveal how each polymer could interact with specifically functionalized surfaces, the adsorption of these two polymers were studied on different surfaces and compared by using QCM with dissipation. PVA-S could adsorb more onto the -OH surface than L-S, which would indicate the limited hydrogen bonding affinity of the lignin-based polymer. However, temperature, pH, and salt showed an adverse impact on the adsorption of PVA-S onto this surface. On the -COOH surface, the adsorption was increased by increasing the salinity of the system for both PVA-S and L-S polymer. The PVA-S could adsorb more onto the -CH$_3$ surface than L-S, revealing the development of a better hydrophobic interaction of this polymer; Meanwhile, temperature increment was observed to improve the adsorption of L-S onto the -CH$_3$ surface, which could be attributed to the more exposure of the hydrophobic parts in L-S. L-S also was adsorbed less than PVA-S onto the -NH$_2$ surface, which could be due to its rigid structure and less solubility. Interestingly, the temperature and salinity increments of the system affected the L-S adsorption more significantly than PVA-S onto this surface. In conclusion, the maximum adsorption of PVA-S was observed on -CH$_3$ functionalized surface at pH 3.0 while the maximum adsorption of L-S (24.32 mg/m^2) was observed on -OH functionalized surface at 1000 mM salt.

To synthesize the amphoteric lignin, the cationic reagent of propyl trimethylammonium bromide or pentyl trimethylammonium bromide and the polymerized anionic 3-sulfopropyl methacrylate

monomer were grafted onto lignin in a semi-dry aqueous condition. In this study, the order of the reactions was found to be critical on the substitution of the functional groups on lignin. Also, it was found that lengthening the carbon chain of a reagent would affect not only the degree of substitution but also the behavior of the amphoteric lignin in various media. In comparing produced polymers, the cationic L-5T polymer showed less hydrophilicity compared to the anionic and amphoteric ones, while all three polymers depicted good lipophilicity at the oil/air interface. Moreover, the cationic polymer showed some tendency to attach to the oil droplet while the anionic and amphoteric ones indicated no lipophilicity. In the oil/water interface, amphoteric lignin showed some hydrophilicity whereas anionic and cationic ones were barely wetted by water. This study proved that the phase and functional groups have an important effect on the performance and behavior of the polymer in the oil/water mixture. Thus, based on oil and water applications, the amphoteric lignin with the required characteristics could be designed experimentally.

To produce a multi-charged crosslinked polymer (C-CM-AL) for desalination application, the produced anionic (carboxy) and cationic (tertiary amine) lignin polymers were crosslinked by poly(ethylene glycol) diglycidyl ether. All modifications were confirmed by ^{1}H and ^{1}H-H COSY NMR. The produced amphoteric C-CM-AL polymer showed a higher desalinating performance compared to the anionic (C-CM) or cationic (C-AL) one. The highest adsorption capacity of C-CM-AL was obtained for KCl, NaCl, $CaCl_2$, and $MgCl_2$ to be 1.25, 0.97, 0.71, and 0.62 mmol/g, respectively. The reusability of this polymer was tested and it was seen that the produced polymer could retain up to 70-80 % of its adsorption capacity after 15 rounds of adsorption and desorption. The XPS results from the last cycle of adsorption-desorption indicated that the decrease in the desorption affinity would be due to the salt ions trapping in the structure of the polymer. The results also revealed that the adsorption affinity did not change since the amount of cationic and anionic groups on the polymer did not decrease. Also, the overall adsorption capacity of the polymer remained unchanged in the multi salt systems. According to the sedimentation, settling velocity, and compactness analyses, the C-CM-AL polymer created a looser structure in the sediment and settled faster after adsorbing salts. Overall, the produced C-CM-AL polymer could serve as an effective polymer for the development of reusable and efficient bio-based polymers for desalination applications.

To reveal the effect of the polymer molecular weight on the flocculation of aluminum oxide particles, four oxidized-sulfomethylated lignin (OSML) polymers having a similar charge density

267

of 3.5 µeq/g, but various molecular weights were produced. OSML-4 with the highest molecular weight of 46 kg/mol showed the highest adsorption amount of 5 mg/g onto aluminum oxide particles and affected the zeta potential of the suspension more greatly than the other OSML polymers. The relative turbidity of the suspension dropped the most (to 0.5) when OSML-4 was used as the flocculant, which would be due to its higher adsorption onto the aluminum oxide particles. Also, OSML polymers indicated monolayer adsorption on aluminum oxide particles. The study of the chord length and counts of produced flocs revealed that OSML-4 was able to produce flocs with a higher chord length in lower counts compared to other OSML polymers with lower molecular weight, which directly indicates its better flocculation performance. By increasing the shear rate, the reversible flocculation mechanism was observed in all OSML polymers. Also, increasing the OSML dosage to 15 mg/g hampered the flocculation since the repulsion force developed between aluminum oxide particles prevented their flocculation and settling. Overall, the flocculation mechanism of aluminum oxide particles with produced OSML polymers was obtained to be charge neutralization and patching.

7.2 Recommendation for future work

In the review study, the grafting reactions performed on lignin were presented and existent reaction routes were discussed in deep. However, other reactions conducted on lignin such as polymerization, two-step depolymerization, redox-neutral, and photocatalysis would also need to be reviewed to could obtain more industrially and environmentally attractive methods for lignin valorization.

In addition, although the adsorption mechanisms of anionic softwood kraft lignin were compared with an anionic synthetic polymer (poly (vinyl alcohol-*co*-vinyl acetate)), different kinds of lignin such as hardwood lignin or other available technical lignin types could also be studied along with a modeling study to understand the interaction mechanisms of lignin even better.

In another research study, the amphoteric lignin was produced, and the interaction of this polymer was analyzed in the oil/water interface. In the future, research may also be conducted to correlate the characteristics of the amphoteric lignin with its behavior in other liquid-liquid/liquid-solid interfaces for developing novel applications, such as bio-active materials.

The produced cross-linked bi-functional lignin-based polymer was used to adsorb mono and divalent salts. The adsorption and interaction of the produced polymer could also be studied with

biological polymers having both anionic and cationic groups, such as antibiotics and other proteins, so that the amphoteric lignin could be used and introduced in applications where both its anionic and cationic groups would be essential and could play a key role. Also, systematic studies could be conducted on solid surfaces with different functional groups, porosity, and roughness in order to obtain a more comprehensive outcome for the interaction of lignin with solid surfaces.

Publication list

1) Kazzaz, A. E., & Fatehi, P. (2020). Interaction of synthetic and lignin-based sulfonated polymers with hydrophilic, hydrophobic, and charged self-assembled monolayers. *RSC Advances*, *10*(60), 36778-36793.

2) Kazzaz, A. E., & Fatehi, P. (2020). Technical lignin and its potential modification routes: A mini-review. *Industrial Crops and Products*, *154*, 112732.

3) Kazzaz, A. E., & Fatehi, P. (2020). Fabrication of amphoteric lignin and its hydrophilicity/oleophilicity at oil/water interface. *Journal of Colloid and Interface Science*, *561*, 231-243.

4) Feizi, Z. H., Kazzaz, A. E., Kong, F., & Fatehi, P. (2019). Evolving a flocculation process for isolating lignosulfonate from solution. *Separation and Purification Technology*, *222*, 254-263.

5) Kazzaz, A. E., Feizi, Z. H., & Fatehi, P. (2019). Grafting strategies for hydroxy groups of lignin for producing materials. *Green Chemistry*, *21*(21), 5714-5752.

6) Kazzaz, A. E., Feizi, Z. H., Kong, F., & Fatehi, P. (2018). Interaction of poly (acrylic acid) and aluminum oxide particles in suspension: particle size effect. *Colloids and Surfaces A: Physicochemical and Engineering Aspects*, *556*, 218-226.

7) Kazzaz, A. E., Feizi, Z. H., & Fatehi, P. (2018). Interaction of sulfomethylated lignin and aluminum oxide. *Colloid and Polymer Science*, *296*(11), 1867-1878.

8) Chen, J., Eraghi Kazzaz, A., AlipoorMazandarani, N., Hosseinpour Feizi, Z., & Fatehi, P. (2018). Production of flocculants, adsorbents, and dispersants from lignin. *Molecules*, *23*(4), 868.